WVMP SAR Reference 3-19

Response of High Performance to Fire Conditions: Review of Thermal Property Data and Measurement Techniques, NIST Report GCR 99-767, D. R. Flynn, March 1999.

NIST GCR 99-767

RESPONSE OF HIGH PERFORMANCE CONCRETE TO FIRE CONDITIONS: REVIEW OF THERMAL PROPERTY DATA AND MEASUREMENT TECHNIQUES

Daniel R. Flynn

MetSys Corporation
Millwood, VA 22646-0317

United States Department of Commerce
Technology Administration
National Institute of Standards and Technology

NIST GCR 99-767

RESPONSE OF HIGH PERFORMANCE CONCRETE TO FIRE CONDITIONS: REVIEW OF THERMAL PROPERTY DATA AND MEASUREMENT TECHNIQUES

Prepared for

U.S. Department of Commerce
Building and Fire Research Laboratory
National Institute of Standards and Technology
Gaithersburg, MD 20899

By

Daniel R. Flynn

MetSys Corporation
Millwood, VA 22646-0317

Final Report

December 1998
Issued March 1999

[redacted]

[redacted]

Notice

This report was prepared for the Building and Fire Research Laboratory of the National Institute of Standards and Technology under Contract number 43-NANB-809607. The statement and conclusions contained in this report are those of the authors and do not necessarily reflect the views of the National Institute of Standards and Technology or the Building and Fire Research Laboratory.

[redacted]

[redacted]

MetSys Report No. 98-01-101

December 1998

Response of High Performance Concrete to Fire Conditions:

Review of Thermal Property

Data and Measurement Techniques

by

Daniel R. Flynn

MetSys Corporation

Millwood VA 22646-0317

This report is based upon work supported by the Department of Commerce/National Institute of Standards and Technology (NIST) under contract No. 43-NANB-809607. Any opinions, findings, and conclusions or recommendations expressed in this publication are those of the author and do not necessarily reflect the views of the Department of Commerce/NIST.

Abstract

The NIST Building and Fire Research Laboratory (BFRL) has undertaken a project concerning the effect of fire on high strength concrete. Heating concrete to sufficiently high temperatures results in water of hydration being driven off, with a resultant irreversible loss of concrete strength. In addition, it has been observed that rapid heating of high strength concrete can result in spalling of the concrete. Computer models for prediction of temperature and pore pressure distributions in heated concrete typically include consideration of (1) mass transfer of air and water by diffusion and by forced convection, conversion of liquid water to vapor, and release of water of hydration and (2) heat transfer by conduction, mass diffusion, and forced convection. In order to make valid predictions, the computer models require reliable data as to the physical properties of the concrete. Mass transport properties are being investigated by the Building Materials Division. Thermal transport properties, the subject of this report, are being investigated by the Building Environment Division. The present report addresses (1) identification of material properties critical to prediction of heat and mass transfer in high strength concrete at high temperatures, (2) variation of the thermal properties with temperature, pressure, and thermal history, (3) examination of correlations between concrete composition and thermal properties, (4) identification of appropriate experimental techniques for determination of the thermal properties of high strength concrete, (5) identification of available equipment and testing services for carrying out such measurements, and (6) preliminary design of special equipment that needs to be constructed for measurement of the thermal conductivity of concrete.

[redacted]

Acknowledgements

The Principal Investigator thanks the following organizations for permission to reproduce copyrighted figures and tables:

American Society for Testing and Materials

NRC Research Press (National Research Council – Canada)

Pearson Education Limited (Longman Group Limited)

Portland Cement Association

The Principal Investigator also thanks Robert R. Zarr, the NIST Contracting Officer's Technical Representative for the contract under which this report was prepared, for his guidance and his review of earlier drafts of the report and James R. Lawson, of NIST, for assisting with the preparation of this report.

[redacted]

Table of Contents

List of Figures

List of Tables

Nomenclature

The nomenclature list below is limited to those symbols that are used in the main body of this report. The symbols used in Sections 2.1, 2.2, and 2.3 are not included, since the symbols used there, and defined there, are those of the various investigators whose work is being cited and they are not used elsewhere in this report. The symbols used for the various equations in Appendices A and B are not included since they are defined as they are used in those appendices.

A relative mass [kg/kg] = [1] of water that would fill voids

B bulk modulus [Pa]

C specific heat [J/kg·K] at constant pressure

$\bar{C}$ sensible heat contribution to the specific heat [J/kg·K]

D mass diffusivity [m^2/s]

f volume fraction [m^3/m^3] = [1]

H enthalpy [J/kg]

K permeability [m^2]

ℓ length [m]

m dimensionless constant used in the Bruggeman mixture rule (Eq. (55)

$\dot{m}$ mass flux [$kg/m^2 \cdot s$]

n index of summation

p partial pressure [Pa]

P pressure [Pa], porosity [m^3/m^3] = [1], or fraction of area or of length (Eq. (75))

q heat flux [W/m^2]

S source term [$kg/m^3 \cdot s$] for creation of liquid or vapor

t time [s]

T temperature [K]

v volume fraction [m^3/m^3] = [1]

V volume [m^3]

W mass [kg]

x coordinate axis [m]

Greek

α coefficient of linear thermal expansion [$m/m \cdot K$] = [K^{-1}]

β coefficient of volumetric thermal expansion [$m^{-3}/m^{-3} \cdot K$] = [K^{-1}]

γ dimensionless constant in Harmathy's form of Hamilton-Crosser mixture rule (Eqs. (58)-(59))

δ mass diffusivity [kg/m·s·Pa] when the partial pressure gradient is the driving force; this quantity is usually called "permeability" in the building research literature

ΔH_P heat of reaction, or latent heat contribution to the specific heat [J/kg·K]

ζ degree of conversion of a chemical reaction ($0 \leq \zeta \leq 1$)

η dimensionless constant used in the Hamilton-Crosser mixture rule (Eq. (57))

κ thermal diffusivity [m^2/s]

λ thermal conductivity [W/m·K]

μ viscosity [kg/m·s]

ξ moisture capacity [kg/kg] = [1]

π 3.14159265...

ρ density [kg/m^3]

ϕ a particular property of interest

ω mass fraction [kg/kg] = [1]

Subscripts

0 reference

1,2 component

c forced convection, cement, or continuous phase

d diffusion, or dispersed phase

i component

m mass

n non-evaporable water

P at constant pressure

s saturation

u energy

w water

1. Introduction

The NIST Building and Fire Research Laboratory (BFRL) has undertaken several projects concerned with the performance of high strength concrete. One of these projects concerns the effect of fire on high strength concrete. Heating concrete to sufficiently high temperatures results in water of hydration being driven off, with a resultant irreversible loss of concrete strength. In addition, it has been observed that rapid heating of high strength concrete can result in spalling of the concrete. The most common explanation for this phenomenon is that, because of the very low permeability of high strength concrete, the moisture freed during dehydration (release of chemically bound water) cannot escape quickly enough to prevent a large buildup in pore pressure, which "blows off" some of the concrete. Another possible explanation for the observed spalling is that it occurs due to the large thermal stresses encountered under fire conditions.

Several computer models have been developed to predict temperature and pore pressure distributions in concrete exposed to simulated fire conditions. It probably will be necessary to develop a companion computer program to predict spalling and strength loss. BFRL is examining such computer programs to ascertain how reliably they can predict the overall response of high strength concrete structures to fire conditions and, hopefully, can provide insights into possible spalling prevention procedures.

The computer models for prediction of temperature and pore pressure distributions utilize an analysis procedure that involves the strongly coupled heat and mass transfer within the concrete. Such models typically include consideration of **mass transfer** of air and water by diffusion and by forced convection, conversion of liquid water to vapor, and release of water of hydration and **heat transfer** by conduction, mass diffusion, and forced convection with inclusion of the effects of the heat of vaporization of water, the heat of dehydration, and the thermal capacity of the concrete. Regardless of how good the computer programs are, in order to make valid predictions, they require reliable data as to the physical properties of the concrete. Mass transport properties are being investigated by the Building Materials Division. Thermal transport properties, the subject of this report, are being investigated by the Building Environment Division.

The present report addresses (1) identification of material properties critical to prediction of heat and mass transfer in high strength concrete at high temperatures, (2) variation of these properties with temperature, pressure, and thermal history, (3) examination of correlations between concrete composition and thermal properties, (4) identification of appropriate experimental techniques for determination of the thermal properties of high strength concrete, (5) identification of available equipment and testing services for carrying out such measurements, and (6) preliminary design of special equipment that needs to be constructed for measurement of one or more thermal properties.

Section 2 of this report provides an overview of heat and mass transfer in porous media, identifies the properties that are required in mathematical modeling of heat and mass transfer, and provides the mass and energy conservation equations for several different models that have been previously developed. Section 3 provides an overview of the available data on thermal properties of normal and high strength concrete. Section 4 is a discussion of various correlations and procedures that might be useful in prediction of the thermal properties of concrete. In Section 5, various experimental

techniques for determination of the needed thermal properties are described. The current availability of apparatus and testing services, for these properties, is covered in Section 6, with the aim of determining whether NIST has the appropriate capabilities, should procure or build appropriate equipment, or should rely on testing at outside laboratories. It is concluded that no suitable equipment for high temperature thermal conductivity measurements is available and that NIST needs to develop such capability. Accordingly, Section 7 provides a preliminary design of the apparatus that is proposed to be built for high temperature thermal conductivity measurements.

2. Modeling of Simultaneous Heat and Mass Transfer in Porous Media

When moisture is present, a very complex analysis can be required to deal with the coupled heat and mass transfer that can occur, involving both liquid mass transfer and vapor mass transfer. In general, moisture transport may include air-vapor mixture flow due to forced convection, free convection, and infiltration through cracks and pores; vapor transport by diffusion; flow of liquid due to diffusion, capillary action, or gravity; and the further complications associated with phase changes due to condensation/evaporation, freezing/thawing, ablimation/sublimation, and adsorption/desorption. There is a vast literature concerned with moisture transfer in materials and with simultaneous heat and mass transfer. The literature concerning moisture flow in porous materials encompasses the development of analytical/mathematical models, experimental studies, combined experimental and analytical studies, field studies, and retrofit studies. Much theoretical and experimental work has been done on the development of the theory of heat and mass transfer, separately and together, in porous media. This work comes mainly from the fields of drying, chemical processing, and building research, as well as from geophysics. However, in general it is fair to state that consistent and universally reliable analytical approaches and test methods are yet to be achieved for predicting combined heat and moisture transfer through porous media.

While analytical approaches differ, in general it is customary to write a set of coupled equations in which there are three "currents," such as heat flow, liquid water flow, and water vapor flow. Each current has three components, driven by one of three "forces," the temperature gradient, the gradient in liquid water content, and the gradient in water vapor content. Thus there are nine coefficients corresponding to the nine "conductivities" or "diffusivities" relating the currents and the forces. The Onsager reciprocal relations reduce the number of independent coefficients to six. Depending upon the application and the investigator, the moisture contents may be written in a variety of ways (e.g., mass or volume or relative humidity of moisture per mass or volume of medium). There also is a variety of choices used for the currents and for the forces. A few of the approaches used are discussed below.

The "apparent" thermal conductivity can be thought of as the ratio of the heat flux to the temperature gradient, even though the heat flux is also affected by the gradients in liquid-phase and vapor-phase moisture content. If moisture is migrating slowly, it can appear as if the apparent thermal conductivity is constant. However as the local moisture content changes over time, the true thermal conductivity will change, the heat transport associated with the fluxes of liquid and vapor will change, and thus the apparent thermal conductivity will change.

Obviously, the extensive theoretical literature concerned with heat and mass transfer in porous media cannot be reviewed in this report. Rather the approach taken is to (1) provide an overview of what happens when a concrete wall is exposed to fire conditions (and define various terms), (2) use the principles of irreversible thermodynamics to derive the much simpler problem of diffusion of a single gas through a porous media, (3) summarize the theoretical results which three different investigations found for the mass flux densities and energy flux density of coupled heat and moisture transfer through a porous medium in the absence of convective mass transfer, and (4) summarize the equations used in the Ahmed model (which does include convection) for predicting temperatures and pore pressures in concrete exposed to fire conditions.

2.1 Overview of Heat and Mass Transfer in Concrete Exposed to Fire

For concrete, particularly at high temperature, one cannot predict heat transfer from just the traditional thermal properties: thermal conductivity and volumetric specific heat (or, under some conditions, one of these properties plus thermal diffusivity). Movement of air, water, and possibly carbon dioxide through the concrete is accompanied by significant energy transfer, particularly associated with the latent heat of water and the heats of hydration and dehydration. Because of the high pore pressures that result when high-strength concrete is exposed to a fire, it is necessary to consider forced convection as well as diffusion.

Consider a concrete slab that initially may have small temperature gradients, e.g., due to indoor-to-outdoor temperature differences. Further, the extent of hydration of the concrete may not be uniform throughout the structure. Because of the heat released during initial curing and drying out of the concrete near one or both surfaces, there may be a higher amount of hydration in the middle of the material than near the surfaces. The free moisture content also may vary throughout the concrete if the different surfaces have been exposed to different humidities.

At the beginning of a fire, the temperature of the exposed side of the concrete slab will rise rapidly. Free moisture, both liquid and vapor, will migrate toward the cold side of the concrete. Initially, this moisture movement occurs by diffusion processes, where the driving force may be considered to be the gradient in moisture content (commonly expressed as partial pressure, humidity, molar or mass fraction, or molar or mass density). As the temperature of the fire-exposed side increases, any free liquid water will boil off and migrate toward the colder side where some of it will condense. The latent heat required to boil the liquid water will retard the rate of temperature rise at that location. When water vapor is transported into a colder region, some of it is absorbed into the concrete, with a heat of sorption that is approximately equal to the latent heat associated with condensation of free water vapor into liquid, so that significant heat is released. As moisture moves into the slab and the interior temperature rises towards 100 °C, portions of the slab may experience additional hydration (conversion of free water to chemically bound water), with an attendant release of heat. When the temperature of any portion of the concrete slab exceeds (roughly) the boiling point of water (at the local pressure) some dehydration (release of chemically bound water) will begin to take place, with an attendant absorption of heat. The dehydration reactions continue to temperatures in excess of 800 °C, with the most pronounced reaction being the dehydration of calcium hydroxide between 400 and 600 °C. The free water introduced into the concrete tries to diffuse toward the cold side. However, high-strength concrete is not very permeable to water vapor and is even less permeable (by, say, roughly two orders of magnitude) to liquid water. Thus the moisture cannot escape as rapidly as it is being released and the pore pressure in the concrete will rise substantially. Eventually, liquid water may fill the concrete pores at a location ahead of the temperature front, creating a condition known as moisture clog, where the liquid water blocks the transfer of water vapor toward the cold side of the slab. Under such conditions, the pore pressure will result in forced convective mass transfer of superheated steam and air to the heated side of the slab.

For concrete with carbonate aggregates, the situation is further complicated. Between 660 and 980 °C, calcium carbonate breaks down into calcium oxide with the release of carbon dioxide. Magnesium carbonate is similarly decomposed between 740 and 840 °C. Both reactions are

endothermic, thus absorbing heat and delaying temperature rise in the concrete. Quartz undergoes a pronounced phase transformation, with an accompanying volume increase, at about 573 °C.

During temperature exposure of the concrete, its transport properties for both heat and mass can change quite significantly due to differential thermal expansion opening up microcracks and changes to the solid structure associated with chemical decomposition of the cement paste (dehydration) and of any carbonate aggregates (conversion to oxides), both processes leading to less dense material and thus lower thermal conductivity (and thermal diffusivity) and higher mass transport properties.

In the absence of mass transfer and chemical reactions, conductive heat transfer is described by

$$\rho_o C \frac{\partial T}{\partial t} = \frac{\partial}{\partial x}\left(\lambda \frac{\partial T}{\partial x}\right) \quad , \tag{1}$$

where T is temperature [K], t is time [s], ρ_o is the bulk **density** [kg/m^3] of the medium, C is **specific heat** [J/kg·K], and λ is **thermal conductivity** [W/m·K]. If there are no other mechanisms of heat transfer and if λ can be assumed to be constant, this equation can be replaced by

$$\frac{1}{\kappa}\frac{\partial T}{\partial t} = \frac{\partial^2 T}{\partial x^2} \quad , \tag{2}$$

where $\kappa = \lambda/\rho_o C$, the ratio of thermal conductivity to volumetric specific heat, is known as the **thermal diffusivity** [m^2/s]. For a boundary value problem with prescribed surface temperatures as functions of time, the interior temperatures versus time depend only on the thermal diffusivity and it is not necessary to know the thermal conductivity or the specific heat separately. (Correspondingly, in measuring thermal diffusivity it is only necessary to measure a geometrical factor and a temperature variation with time; no power or energy measurements are required.) For a boundary value problem with a prescribed heat flux or with a radiation boundary condition, the temperature variation with time depends upon both thermal conductivity and thermal diffusivity (or upon one of these properties plus the volumetric heat capacity).

When exothermic or endothermic chemical reactions, or phase changes in the solid concrete, take place, it is preferable to replace Eq. (1) with

$$\rho\left(\frac{\partial H}{\partial T}\right)_P \frac{\partial T}{\partial t} = \frac{\partial}{\partial x}\left(\lambda \frac{\partial T}{\partial x}\right) \quad , \tag{3}$$

where H is **enthalpy** [J/kg] and P is **pressure** [Pa]. If the **degree of conversion** from the reactants into the products is designated by ζ ($0 \le \zeta \le 1$), Eq. (3) can be rewritten as

$$\rho\left(\bar{C} + \Delta H_P \frac{\partial \zeta}{\partial T}\right)\frac{\partial T}{\partial t} = \frac{\partial}{\partial x}\left(\lambda \frac{\partial T}{\partial x}\right) \quad , \tag{4}$$

where $\bar{C}$ represents the **sensible heat** contribution to the specific heat at a given degree of conversion, and the term involving ΔH_P, the **heat of reaction**, is the latent heat contribution. Sometimes the latent heat term is written as a heat source/sink term.

Turning now to mass transfer, diffusion is first considered. Assuming that Fick's law for diffusion holds, the mass flux due to a gradient in the density of the diffusing fluid is simply

$$\dot{m}_d = -D \frac{\partial \rho}{\partial x} \quad , \tag{5}$$

where $\dot{m}_d$ is the mass flux [kg/m^2·s] due to diffusion, ρ is the density [kg/m^3] of the fluid, and D is the **mass diffusivity** [m^2/s]. In the building research literature, for moisture transfer this equation is often expressed in terms of partial pressures as

$$\dot{m}_d = -\delta \frac{\partial p}{\partial x} \quad , \tag{6}$$

where p is the partial pressure [Pa] and δ is usually called the "permeability" [kg/m·s·Pa] rather than being called a mass diffusivity. For diffusion of water vapor, a similar expression is often seen with the driving force being the gradient in the humidity.

For forced convection through a porous medium, the mass flux is given approximately by

$$\dot{m}_c = -K \frac{\rho}{\mu} \frac{\partial P}{\partial x} \quad , \tag{7}$$

where P is the total pressure [Pa], ρ is the density [kg/m^3] of the moving fluid, μ is the **viscosity** [kg/m·s] of the moving fluid, and K is the **permeability** [m^2] of the medium for the particular fluid. (Often experimental results will indicate that K is not really a constant but varies with the pressure gradient so that a more complex expression may be required.)

The energy transport (heat flux) associated with a mass flux is simply

$$q = \dot{m} H \quad , \tag{8}$$

where H is the enthalpy of the moving fluid. The net energy content per unit volume (i.e., the additional term to be included in the energy differential equation, Eq. (4)) is

$$\dot{m} \frac{\partial H}{\partial x} = \dot{m} \left(\frac{\partial H}{\partial T} \right)_P \frac{\partial T}{\partial x} = \dot{m} C \frac{\partial T}{\partial x} \quad , \tag{9}$$

where C is the heat capacity of the moving fluid. If, as is the case with water, a phase change and the associated latent heat are involved, it is necessary to deal appropriately with the step function in the enthalpy.

In the case of diffusion or forced convection of a gas, absorption and desorption by the medium (concrete) probably can be ignored. However, for moisture transfer at temperatures below the boiling point of water (at the local pressure), absorption effects are quite important and the mass storage of water, and the associated enthalpy storage, need to be considered. Absorption/desorption of water vapor is usually described in terms of **sorption isotherms**, curves which relate the equilibrium absorbed moisture content of a medium, at a specific temperature, to the moisture content (usually expressed as vapor pressure or humidity) to which it is exposed. At low humidities, absorption is mainly by adsorption, first in monomolecular layers and then in multimolecular layers. Above about 40 percent relative humidity, capillary condensation begins in the smallest micropores of the material and then, as the humidity increases, there is condensation in larger pores and cracks, due to the depression of vapor pressure over the curved menisci of the water-filled capillaries. Porous materials exhibit hysteresis, so that absorption isotherms differ from desorption isotherms. The **moisture capacity** of a material is defined as the slope of the sorption isotherm (analogous to the heat capacity being the slope of the enthalpy-versus-temperature curve). The moisture capacity increases markedly as the water vapor pressure increases toward the saturation vapor pressure. Above a relative humidity of about 97 percent, it is customary to treat the moisture as being a liquid. Here the moisture capacity of a material is related to the capillary suction pressure by what is known as a **suction curve**, which also exhibits hysteresis.

Consideration of the mass flux (e.g., Eq. (5) or (6)) and the moisture capacity results in a differential equation, for diffusive mass transfer, that is analogous to Eq. (1) for heat transfer. A source term is added to this differential equation to represent the mass of moisture that is created or annihilated by hydration or dehydration, respectively. If the driving potential is taken as the density of the water vapor, mass conservation plus Eq. (5) results in

$$\frac{1}{D}\frac{\partial \rho}{\partial t} = \frac{\partial^2 \rho}{\partial x^2} + \frac{S}{\rho} \quad , \tag{10}$$

where S is the source term [kg/m^3·s] included to deal with conversion of liquid to vapor, or vice versa, or with the creation of water by dehydration of the medium. Comparison of the form of Eq. (10) with that of Eq. (2) shows the analogy between mass diffusivity and thermal diffusivity. The form of Eq. (10) does not explicitly show the dependence upon moisture capacity. If partial pressure or, equivalently, relative humidity is used as the driving potential and Eq. (6) is used to obtain the mass flux, mass conservation yields

$$\frac{\rho_o \xi}{\delta p_s}\frac{\partial p}{\partial t} = \frac{\partial^2 p}{\partial x^2} + \frac{S}{\delta} \quad , \tag{11}$$

where ρ_o is the bulk density of the medium, p_s is the saturation pressure [Pa] at the local temperature of the medium, and ξ is the moisture capacity obtained as the slope of the sorption curve, plotted as mass of water vapor per unit mass of the medium versus relative humidity (so ξ is dimensionless).

Some investigators explicitly consider two moisture fluxes, one for vapor and one for liquid, while others use a single moisture flux, with the moisture capacity being used to deal with the change of phase, or the absorption and desorption, of the water. An equation analogous to Eq. (11) can be

derived for transfer of liquid water, with the moisture capacity being obtained from capillary suction curves.

Forced convection of moisture through the medium also requires consideration of the moisture capacity of the medium. For sufficiently small flows, one might assume that the moisture absorbed or desorbed can be predicted from the moisture capacity as determined from sorption curves or suction curves measured under steady-state conditions. In such a case, differential equations analogous to Eq. (11) could be written. However, for concrete under simulated fire conditions and high pore pressures, it is questionable whether there would be time for such equilibrium to be achieved.

2.1 Irreversible Thermodynamics Approach for Diffusion of a Gas

Before discussing the rather complex analysis of two-phase (liquid and vapor) flow of moisture through a porous solid, the more simple case of diffusion of a gas through a stationary medium is considered. This is done most conveniently by the methods of irreversible thermodynamics, applying the Onsager Reciprocal Relations [1-24]. A set of current densities is defined as

$$\mathbf{J}_i = \sum_j L_{ij} X_j \quad , \tag{12}$$

where X_j are the "conjugate forces," such that

$$R(S) = \sum_j \mathbf{J}_i \cdot X_i \quad , \tag{13}$$

where $R(S)$ is the rate of entropy production in the system. The Onsager Reciprocal Theorem states that

$$L_{ij} = L_{ji} \quad . \tag{14}$$

The rate of entropy production is uniquely defined by the system under consideration, but since $R(S)$ can be split into a sum of products in many ways, one is left with a choice of current densities and conjugate forces. We choose a mass current density $\mathbf{J}_m$, an internal energy current density $\mathbf{J}_u$, and an entropy current $\mathbf{S}$, so that the divergence of each of these current densities is the rate of change per unit volume of the corresponding thermodynamic variable. With these definitions for the current densities,

$$T\mathbf{S} = \mathbf{J}_u - \mu \mathbf{J}_m \quad , \tag{15}$$

where T is the absolute temperature and μ is the chemical potential of the diffusing gas. The rate of production of entropy is

$$R(S) = \nabla \cdot \mathbf{S} = \mathbf{J}_m \cdot \nabla \left(-\frac{\mu}{T} \right) + \mathbf{J}_u \cdot \nabla \left(\frac{1}{T} \right) \quad . \tag{16}$$

The current densities are

$$\mathbf{J}_m = L_{mm} \nabla \left(-\frac{\mu}{T} \right) + L_{mu} \nabla \left(\frac{1}{T} \right) \tag{17}$$

$$\mathbf{J}_u = L_{mu} \nabla \left(-\frac{\mu}{T} \right) + L_{uu} \nabla \left(\frac{1}{T} \right) \quad . \tag{18}$$

In order to put these expressions in terms of measurable gradients, it is noted that

$$\nabla \left(\frac{\mu}{T} \right) = \frac{v}{T} \nabla P - \frac{Ts + \mu}{T^2} \nabla T = \frac{v}{T} \nabla P - \frac{h}{T^2} \nabla T \quad , \tag{19}$$

where v is the specific volume, s is the specific entropy, and h is the specific enthalpy. Substitution of Eq. (19) into Eqs. (17) and (18) yields

$$\mathbf{J}_m = -\frac{L_{mm} v}{T} \nabla P + \frac{L_{mm} h - L_{mu}}{T^2} \nabla T \tag{20}$$

$$\mathbf{J}_u = -\frac{L_{mu} v}{T} \nabla P + \frac{L_{mu} h - L_{uu}}{T^2} \nabla T \quad . \tag{21}$$

Thermal conductivity is defined as

$$\lambda = \left[\frac{-\mathbf{Q}}{\nabla T} \right]_{\mathbf{J}_m = 0} = \left[\frac{-\mathbf{J}_u}{\nabla T} \right]_{\mathbf{J}_m = 0} \quad , \tag{22}$$

where $\mathbf{Q}$ is the heat current density, since when $\mathbf{J}_m = 0$, $\mathbf{J}_u = \mathbf{Q}$. Setting Eq. (20) equal to zero yields

$$\left(\frac{\nabla P}{\nabla T} \right)_{\mathbf{J}_m = 0} = \frac{h - L_{mu}/L_{mm}}{vT} \quad . \tag{23}$$

This ratio of the pressure gradient to the temperature gradient, when there is no mass flow, is called the thermomolecular pressure difference. Combining Eqs. (21)-(23) yields the following expression for the thermal conductivity in terms of the Onsager coefficients

$$\lambda = \frac{L_{uu} L_{mm} - L_{mu}^2}{T^2 L_{mm}} \quad . \tag{24}$$

When the system is isothermal, $\nabla T = 0$ and the two current densities are simply

$$\mathbf{J}_m = -\frac{L_{mm}v}{T}\nabla P \qquad \text{and} \qquad \mathbf{J}_u = -\frac{L_{mu}v}{T}\nabla P \quad , \tag{25}$$

Under such conditions, the two currents are related to each other by

$$\mathbf{J}_u = \frac{L_{mu}}{L_{mm}}\mathbf{J}_m = \alpha \mathbf{J}_m \quad , \tag{26}$$

where α is a quantity that can be determined experimentally by measuring both heat flow and mass flow for isothermal conditions. Permeability is defined as

$$\beta = \left[\frac{-\mathbf{J}_m}{\nabla P}\right]_{\nabla T=0} = \frac{L_{mm}}{\rho T} \quad , \tag{27}$$

where $\rho = 1/v$ is the density of the gas.

The Onsager coefficients can be expressed in terms of the measurable quantities λ, α, and β (other measurable quantities could have been selected of course):

$$L_{mm} = \beta T \qquad L_{mu} = \alpha\beta T \qquad L_{uu} = \lambda T^2 + \alpha^2\beta T \quad . \tag{28}$$

With these substitutions into Eqs. (20) and (21), the current densities become

$$\mathbf{J}_m = -\beta\nabla P + \frac{\beta(h-\alpha)}{T}\nabla T \tag{29}$$

$$\mathbf{J}_u = -\alpha\beta\nabla P - \left(\lambda - \frac{a\beta(h-\alpha)}{T}\right)\nabla T \quad . \tag{30}$$

Note that the use of the Onsager reciprocal relation results in only three measurable parameters being required, rather than four (h does not have to be measured since accurate data for the specific enthalpy are available for most gases and liquids of interest and certainly for water). Note that the quantity α requires thermal measurements even though it is defined under isothermal conditions.

Consider now the case of moisture transfer through a hygroscopic material. Even though there is no liquid water entering or leaving the specimen, there will be adsorbed water and, at moderately high humidities, liquid water inside the pores and capillaries. In general, proper understanding of simultaneous heat and mass transfer for such circumstances requires that both the vapor phase and

the liquid phase be explicitly considered. The current densities, analogous to those in Eqs. (17) and (18), are

$$\mathbf{J}_v = L_{vv}\nabla\left(-\frac{\mu_v}{T}\right) + L_{vl}\nabla\left(-\frac{\mu_l}{T}\right) + L_{vu}\nabla\left(\frac{1}{T}\right) \tag{31}$$

$$\mathbf{J}_l = L_{lv}\nabla\left(-\frac{\mu_v}{T}\right) + L_{ll}\nabla\left(-\frac{\mu_l}{T}\right) + L_{lu}\nabla\left(\frac{1}{T}\right) \tag{32}$$

$$\mathbf{J}_u = L_{uv}\nabla\left(-\frac{\mu_v}{T}\right) + L_{ul}\nabla\left(-\frac{\mu_l}{T}\right) + L_{uu}\nabla\left(\frac{1}{T}\right) \quad . \tag{33}$$

where $\mathbf{J}_v$ is the mass current density for water vapor, $\mathbf{J}_l$ corresponds to mass flow of liquid water and, as before, $\mathbf{J}_u$ is the current of internal energy. The nine coefficients can be reduced to six by invoking the Onsager reciprocal relations. Further reduction in the number in coefficients requires that certain assumptions be made, or other information be used, concerning the relationship between water vapor and liquid water. For example if the sorption isotherm curve is known for the specimen of interest, one can infer how much water will be adsorbed and/or absorbed in a specimen that is exposed to a particular temperature and relative humidity. The Kelvin equation can be used to relate hydraulic pressure inside a capillary to the relative humidity. Several workers have developed theories to describe simultaneous heat and mass transfer due to moisture migration in hygroscopic materials. Such derivations are quite complex and space and time do not permit showing the details in this report. Rather, the results obtained by several prominent workers in the field are given and differences and similarities are pointed out. There are many differences among these several developments in the definitions of terms and the symbols used; here the same nomenclature of the original workers is used so as not to add further confusion.

2.2 Heat Transfer and Diffusive Mass Transfer (no convection)

One comment is in order before proceeding to list the expressions which previous workers have obtained for the mass and heat fluxes associated with moisture transfer. In the derivation given above, a single gas was diffusing through a porous medium under the combined effects of a temperature gradient and a pressure gradient. In the case of moisture transfer, the water vapor pressure is normally very small compared to the total pressure of the moist air. Therefore in most derivations in the moisture literature it is assumed that the total pressure in the medium is uniform and that the water vapor diffuses under the combined influence of a concentration gradient (which may be expressed as a vapor pressure gradient or a humidity gradient) and a temperature gradient. If one wished to allow for the effects of a gradient in the total pressure, as is the case for concrete exposed to a fire, it would be necessary to add a convective term to the expressions given below. Similarly, the effects of gravitational forces are usually neglected in the case of moisture transfer through a hygroscopic medium.

Philip and de Vries [18-20] defined liquid flux density as

$$\mathbf{q}_l = -\rho_l (D_{\theta l} \nabla \theta_l + D_{Tl} \nabla T + K \mathbf{k}) \quad , \tag{34}$$

where

$$D_{\theta l} = K \partial \psi / \partial \theta_l \qquad \text{and} \qquad D_{Tl} = K \partial \psi / \partial T \quad . \tag{35}$$

In these equations ρ_l is liquid density, θ_l is volumetric liquid moisture content, $D_{\theta l}$ is macroscopic diffusivity for liquid transport due to $\nabla \theta_l$, T is temperature, D_{Tl} is macroscopic diffusivity for liquid transport due to ∇T, K is hydraulic conductivity, $\mathbf{k}$ is the unit vector in the z-direction, and ψ is moisture potential (see Eq. (39), below).

Philip and de Vries defined vapor flux density as

$$\mathbf{q}_v = -\rho_l (D_{\theta v} \nabla \theta_l + D_{Tv} \nabla T) \tag{36}$$

where

$$D_{\theta v} = f(a) D \frac{P}{P - p_v} \frac{Mg}{RT} \frac{\rho_v}{\rho_l} \frac{\partial \psi}{\partial \theta_l} \tag{37}$$

$$D_{Tv} = f(a) D \frac{P}{P - p_v} \frac{\rho_v}{\rho_l} \frac{\zeta}{p_{vs}} \frac{dp_{vs}}{dT} \tag{38}$$

$$p_v = h p_{vs} = p_{vs} \exp(Mg\psi / RT) \tag{39}$$

$$f(a) = a + \theta_l = S \quad , \qquad \text{for} \quad \theta_l \le \theta_{lk} \tag{40}$$

$$f(a) = a + a(S - a)/(S - \theta_{lk}) \quad , \qquad \text{for} \quad \theta_l > \theta_{lk} \tag{41}$$

$$\zeta = (\nabla T)_a / \nabla T \quad . \tag{42}$$

In these equations θ_v is volumetric moisture vapor content, $D_{\theta v}$ is macroscopic diffusivity for vapor transport due to $\nabla \theta_v$, D_{Tv} is macroscopic diffusivity for vapor transport due to ∇T, a is volumetric air content, D is the diffusion coefficient of water vapor in air, P is total gas pressure, M is molar mass, g is acceleration due to gravity, R is the universal gas constant, ρ_v is vapor density, p_{vs} is the partial pressure of water vapor at saturation, h is relative humidity, and S is porosity. They also define a total moisture flux density as

$$\mathbf{q}_m = \mathbf{q}_l + \mathbf{q}_v = -\rho_l (D_\theta \nabla \theta_l + D_T \nabla T + K \mathbf{k}) \quad . \tag{43}$$

Philip and de Vries defined the heat flux density as

$$\mathbf{q}_h = -\lambda^* \nabla T + c_l (T - T_o)\mathbf{q}_m - L\rho_l D_{\theta v} \nabla \theta_l \tag{44}$$

or

$$\mathbf{q}_h = -\lambda^+ \nabla T + c_l (T - T_o)\mathbf{q}_m - L\rho_l D_{\theta v} \nabla \theta_l \tag{45}$$

where λ^* is the (apparent) thermal conductivity associated with macroscopic inclusion of water vapor, λ^+ is the (apparent) thermal conductivity associated with microscopic inclusion of water vapor, c_l is specific heat of liquid water, T_o is a reference temperature, and L is the latent heat of evaporation. In this expression, the first term represents normal heat conduction, the second term represents the sensible heat transfer due to mass transfer, and the third term corresponds to the latent heat transfer due to mass transfer.

Fortes and Okos [21-22] derived the following heat and mass transfer equations, applicable to hygroscopic capillary-porous media:

Liquid mass flux:

$$\mathbf{j}_l = -K_l \left(\rho_l R_v \ln H \nabla T - \rho_l \frac{R_v T}{H} \frac{\partial H}{\partial M} \nabla M \right) \tag{46}$$

Vapor mass flux:

$$\mathbf{j}_v = -K_v \left[\left(\rho_{vo} \frac{\partial H}{\partial T} + H \frac{\mathrm{d}\rho_{vo}}{\mathrm{d}T} \right) \nabla T - \left(\rho_{vo} \frac{\partial H}{\partial M} \right) \nabla M \right] \tag{47}$$

Heat flux:

$$\mathbf{j}_q = -K_T \nabla T - \left[\rho_l K_l R_v \ln H + K_v \left(\rho_{vo} \frac{\partial H}{\partial T} + H \frac{\mathrm{d}\rho_{vo}}{\mathrm{d}T} \right) \right] \frac{R_v T^2}{H} \frac{\partial H}{\partial M} \nabla M \ . \tag{48}$$

In these equations K_l is "liquid conductivity," ρ_l is liquid density, R_v is the gas constant per unit mass of water vapor, H is relative humidity, M is moisture content expressed as mass of moisture per unit mass of dry medium, K_v is "vapor conductivity," ρ_{vo} is the saturation density of water vapor, and K_T is apparent thermal conductivity. Note that everywhere ∇M appears it is multiplied by $\partial H/\partial M$ so that the equations are effectively given in terms of the humidity gradient.

Luikov [23-24] combines the mass current density for water vapor and the mass current for liquid water into a single mass current density for moisture,

$$\mathbf{J}_m = -a_m \rho_o \nabla u - a_m \rho_o \delta \nabla T \ , \tag{49}$$

where u is moisture content, a_m is "moisture diffusivity," ρ_o is the density of the dry medium, and δ is the "thermogradient coefficient." The corresponding heat current density is

$$\mathbf{J}_u = -\lambda \nabla T - r \epsilon \mathbf{J}_m \quad , \tag{50}$$

where λ is thermal conductivity (Luikov put conductive heat transfer in terms of the thermal diffusivity $a = \rho_o c \lambda$, where c is the effective heat capacity of the moist medium), r is the latent heat of vaporization, and ϵ is the "phase conversion factor" of liquid into vapor.

The final expressions of Philip and de Vries, Fortes and Okos, and Luikov are all of the general form of Eqs. (31)-(33) but without some of the "cross" terms. For example, Philip and de Vries expressed the liquid flux density in terms of the gradient of liquid moisture content and the temperature gradient but did not have a term involving the gradient of moisture vapor content. Similarly, their expression for the vapor flux density involved the vapor concentration but not the liquid content. Fortes and Okos effectively used relative humidity, along with temperature, as the driving force for both liquid and vapor flow. Luikov combined liquid and vapor and only considered total moisture content (in his derivations this simplification was accomplished by using the sorption isotherm to infer liquid content from vapor concentration and vice versa).

2.3 Ahmed Model

Since the NIST parties involved with this project have access to the papers by Ahmed, *et al.*, describing the model used to simulate coupled heat and mass transfer in concrete slabs, only the three coupled differential equations which they use are shown here.

The differential equation for conservation of mass for water vapor is

$$\frac{\partial}{\partial t}\left(\rho_v \epsilon_g \phi\right) - \frac{\partial}{\partial x}\left(\rho_v \epsilon_g K_p \frac{\partial P}{\partial x} \phi\right) - \frac{\partial}{\partial x}\left(\rho_g \epsilon_g D \frac{\partial \phi}{\partial x}\right) = \Gamma \quad , \tag{51}$$

where ρ_v and ρ_g are the density [kg/m^3] of, respectively, the water vapor and the gaseous mixture of water vapor and air, ϵ_g is the volume fracture [m^3/m^3] of gaseous mixture in the porous medium, ϕ is the mole fraction [kmol/kmol] of water vapor in the gaseous mixture, K_p is the "coefficient of permeability" [m^3•s/kg], P is the pore pressure [Pa] of the gaseous mixture in the porous medium, D is the "modified diffusivity" [m^2/s] of the gaseous mixture, and Γ is the mass rate of evaporation of water per unit volume of porous medium [kg/m^3•s]. The coefficient of permeability, K_p, is defined as $K_p = K_g / g \rho_g \epsilon_g$, where K_g is the "permeability" [m/s] of the gaseous mixture and g is the acceleration [m/s^2] due to gravity. The modified diffusivity, D, [m^2/s] is $D = (M_v M_a / M^2) D'$, where M, M_a, and M_v are the molecular weights [kg/kmol] of, respectively, the gaseous mixture, the air in the gaseous mixture, and the water vapor in the gaseous mixture and D' is the diffusivity [m^2/s] of the gaseous mixture. Ahmed, *et al.* identify the four terms of Eq. (51) as the transient term, the convection term, the diffusion term, and the source term.

Ahmed, *et al.*, use a different definition for permeability than the one that is normally used. Apparently $K_g = (\rho g/\mu) \cdot K$, where ρ is density, μ is viscosity, and K is the permeability as normally defined (see Eq. (7), above).

The differential equation for conservation of mass of the mixture of water vapor and air is

$$\frac{\partial}{\partial t}\left(\rho_g \epsilon_g\right) - \frac{\partial}{\partial x}\left(\rho_g \epsilon_g K_p \frac{\partial P}{\partial x}\right) = \Gamma \quad , \tag{52}$$

where the three terms are the transient term, the convective term, and the source term. The differential equation for conservation of energy is

$$\rho C_p \frac{\partial T}{\partial t} - \rho_g \epsilon_g C_{p_g} \frac{\partial P}{\partial x} \frac{\partial T}{\partial x} - \left(\rho_g \epsilon_g (C_{p_v} - C_{p_a}) D \frac{\partial \phi}{\partial x}\right) \frac{\partial T}{\partial x} = \frac{\partial}{\partial x}\left(k \frac{\partial T}{\partial x}\right) - Q\Gamma \quad , \tag{53}$$

where C_p, C_{p_g}, C_{p_v}, and C_{p_a} are, respectively, the (total) effective heat capacity of the porous medium, the heat capacity of the gaseous mixture, the heat capacity of water vapor, and the heat capacity of air, k is the effective thermal conductivity of the medium, and the source term (evaporation/dehydration) is defined as

$$Q\Gamma = -\left(Q_\ell \frac{\partial \delta_{\ell f}}{\partial t} + (Q_\ell + Q_{dh}) \frac{\partial \delta_{\ell d}}{\partial t}\right) \quad , \tag{54}$$

where Q_ℓ is the latent heat of evaporation [J/kg] of free water vapor, Q_{dh} is the heat of hydration [J/kg] of chemically bound water in the porous medium, $\delta_{\ell f}$ is the mass concentration of free liquid water in the pores per unit volume of porous medium [kg/m^3], and $\delta_{\ell d}$ is the mass concentration of chemically bound water (in the cement paste) per unit volume of porous medium [kg/m^3]. The five terms in Eq. (53) represent the transient term, the convection term, the diffusion term, the conduction term, and the source term, respectively.

3. Existing Data on Thermal Properties of Concrete and Its Constituents

Since the data available for the properties of high strength concrete are quite limited and since most of the thermal properties of high strength concrete are not expected to differ considerably from the properties of normal concrete, this section addresses data available for both normal and high strength concrete.

The most important references, over the past thirty years, that contain data on the thermal properties of concrete, mortar, or cement paste over extended temperature ranges include [25-50]; these references in turn refer to many other publications. The vast majority of data on thermal properties of concrete correspond to temperatures close to normal room temperature. Reference [51] contains an extensive compendium of data on rocks and minerals, including materials that can be used as fine and coarse aggregates in Portland cement concrete. Although this reference has a 1989 copyright date, it was originally written in the late 1970's and all of the references are to publications dated 1978 or earlier, with very few references for 1977 or 1978. Other references relevant to the thermal properties of rocks include [52-59].

3.1 Mass, Volume, and Density

The density of concrete and its constituents is needed to compute volumetric heat capacity, which is needed for the various theoretical models used to predict heat transport in fire-exposed concrete; however, since the density does not vary by much over the temperature range of interest, only relatively small corrections to the room temperature density are required.

In addition, the variation of mass with time and temperature is an important indicator of the degree of conversion from the reactants to the products in a chemical reaction, such as dehydration or loss of carbon dioxide. Accordingly, information as to mass variation is important in determining the enthalpy of a specimen. Similarly, since a material may expand or contract when a chemical reaction takes place, thermal expansion data can be useful in determining the degree of conversion for a chemical reaction.

Thermal expansion data also will be needed to predict thermal stresses that might contribute to spalling. In addition, post-test measurements of thermal expansion would provide sensitive indicators of the degree of dehydration due to the temperature-time exposure that took place during a real or simulated fire.

Figure 1 shown the mass loss and the thermal expansion of a particular cement paste as functions of temperature when the specimen is heated at a nominally uniform rate from room temperature to 1000 °C. At 1000 °C, the one-dimensional length change is about 3.3 percent so that the volumetric contraction is approximately 10 percent. Since the same type of cement paste lost 15 percent of its mass, the bulk density would decrease by a rather small percentage between room temperature and 1000 °C (see Figure 16, below).

Figure 2 shows mass loss and temperature change for a sample of Portland cement paste that was heated to 260 °C over a period of 4.75 h, held at 260 °C for 44 h, and then allowed to cool to room temperature.

Curves A and C in Figure 3 show mass loss versus temperature for, respectively, a calcareous aggregate, containing carbonate (lime or limestone), and a siliceous aggregate, containing silica. The much greater mass loss for the carbonate aggregate is due to the dissociation of the carbonate and the attendant release of carbon dioxide. Curves B and D correspond to concretes made with the two types of aggregate. Figure 4 shows mass loss for various concretes, including measurements by two different investigators on limestone concrete. Another set of data for carbonate concrete is shown in Figure 5, with this concrete having the composition indicated in column 2 of Table 1 (the other two specimens for which data are shown in Figure 4 contained reinforcing steel fibers, which would not be expected to change the mass loss versus temperature curve significantly).

Table 2 shown the constituents of five high-strength concretes recently studied by investigators at the Portland Cement Association. The mass loss versus temperature for these specimens are shown in Figures 6, 7, and 8, corresponding to the different heating rates listed at the bottom of each figure.

Figure 9 shows how the amount of silica fume in a high-strength concrete affects the loss of mass with increasing temperature.

As mentioned above, in addition to mass loss, Figures 1 and 2 showed thermal expansion versus temperature for Portland cement paste. Additional thermal expansion data for cement paste are shown in Figure 10.

With regard to potential aggregates, Figure 11 shows thermal expansion data on the ten different types of rocks that are listed in Table 3. The data for limestone are shown by the curve labeled LI.

Thermal expansion versus temperature for several different types of concrete are shown in Figures 12, 13, and 14. Each of these figures includes data for a limestone-aggregate concrete. Figure 15 indicates how the room-temperature thermal expansion coefficient for concretes is related to the thermal expansion coefficient of the aggregate.

Figure 1 presented information on the mass loss and thermal expansion of a particular cement paste. Figure 16, shows, for that same paste, how the true density, the bulk density, and the porosity are believed to change with increasing temperature.

Figures 17 and 18 show the effect of temperature on the density of concretes with different types of aggregate. The data in Figure 17 correspond to limestone-aggregate concrete, which loses considerable density when the carbonate disassociates. Figure 19 shows the density versus temperature curves used in the version of the Ahmed model (see Section 2.3, above) that is currently available at NIST. Type 1 refers to carbonate aggregate concrete and Type 2 to siliceous concrete.

(Text continued on p. 32)

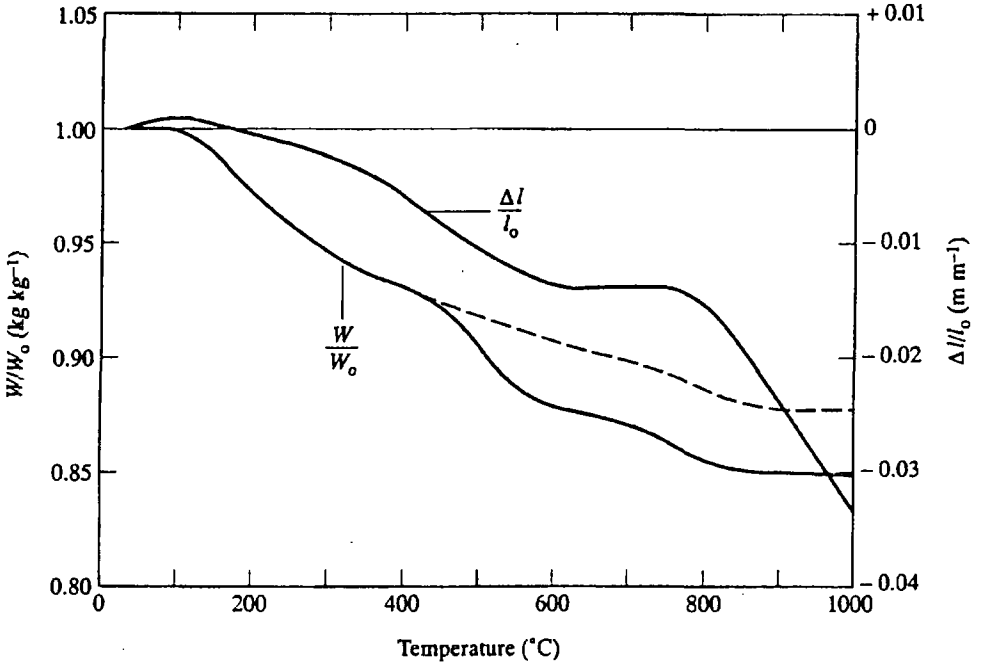

Figure 1. Thermogravimetric and dilatometric curves for Cement Paste C [27,41].

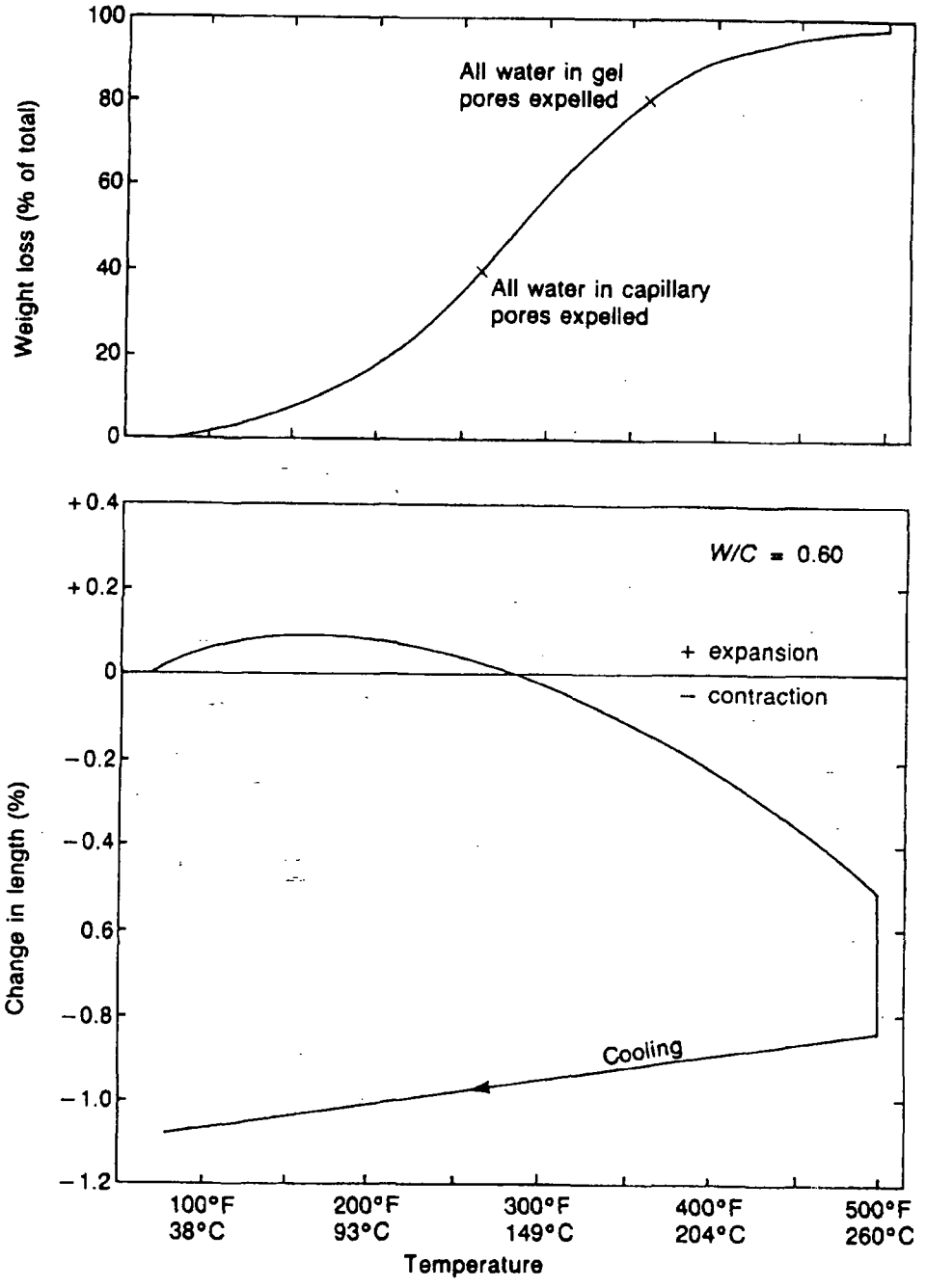

Figure 2. Typical relationships between weight loss, corresponding length change, and temperature for Portland cement paste: + expansion; − contraction [45].

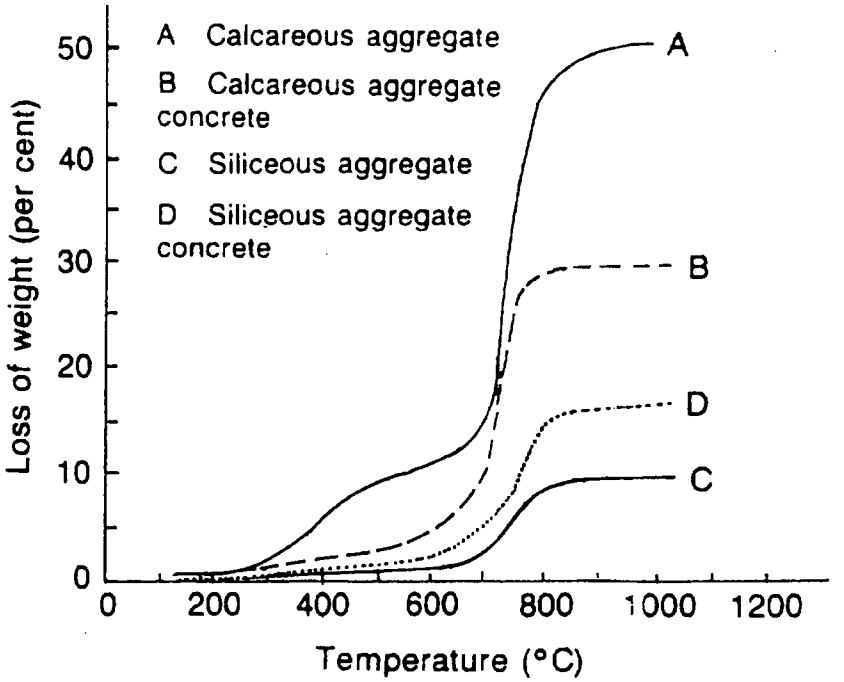

Figure 3. Weight loss of calcareous and siliceous aggregates and concretes caused by heating [45].

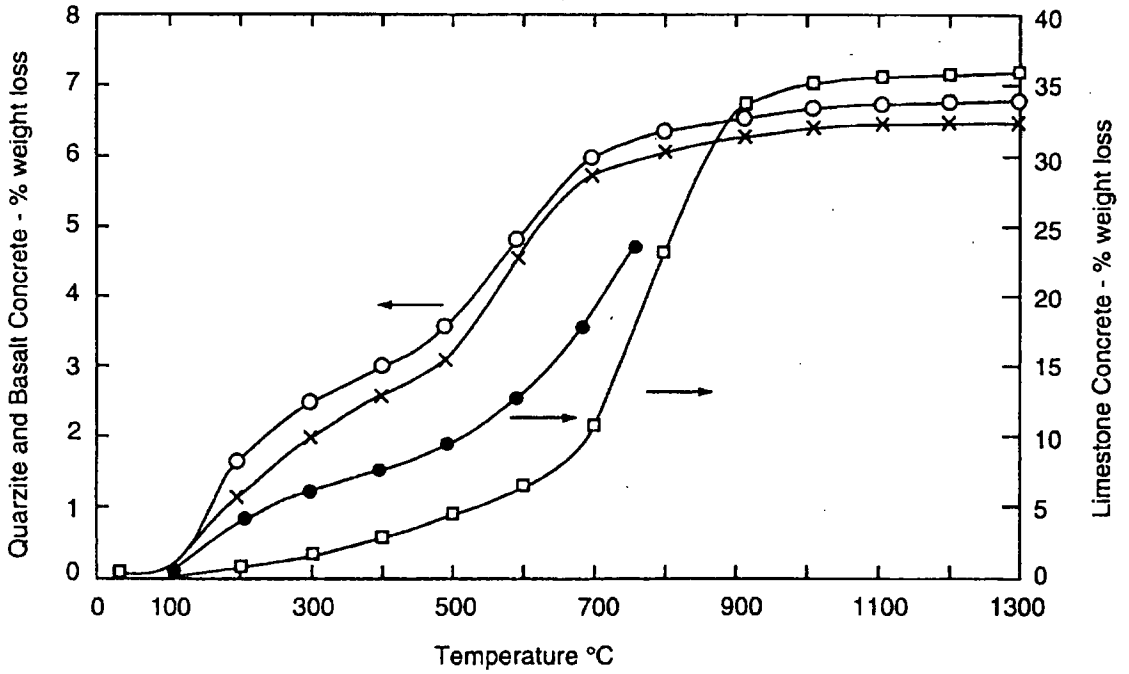

Figure 4. Weight loss as a percentage of initial weight for various concretes caused by heating (Kühl, 1958; Schneider, 1982): quartzite concrete (○); basalt concrete (×); limestone concrete (□) (all by Schneider, 1982); limestone concrete (●) – Philleo (1958) [45].

Property	Batch (specimen type)		
	1 (NRC1)	2 (NRC2)	3 (NRC3)
Cement content (kg/m^3)	380	439	439
Fine aggregate (kg/m^3)	673	621	621
Coarse aggregate (kg/m^3)			
19 mm	678	788	788
9.5 mm	438	340	340
Total	1162	1128	1128
Aggregate type	Siliceous	Carbonate	Carbonate
Water (kg/m^3)	167	161	161
Water–cement ratio	0.44	0.37	0.37
Retarding admixture (mL/m^3)	745	—	—
Superplasticizer (mL/m^3)	2500	300	1200
Steel fibre (kg/m^3)	42	—	42
28-day compressive strength (MPa)	39.9	32.6	43.2
Compressive strength at test date (MPa)	40.9	37.1	43.3

Table 1. Batch quantities and properties of concrete mix [44].

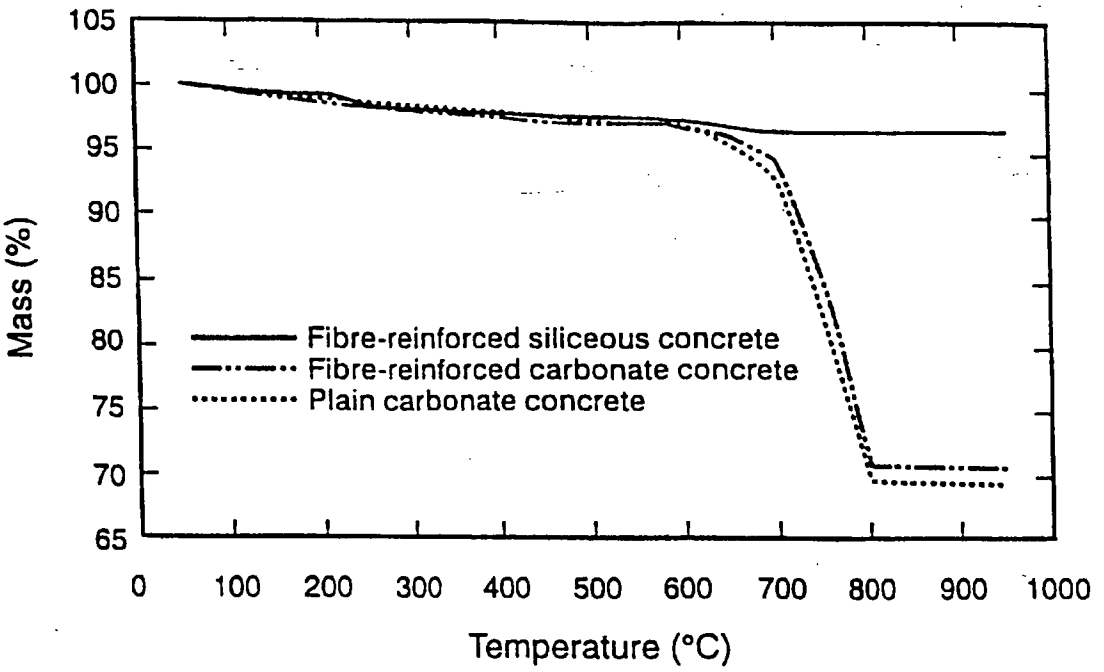

Figure 5. Mass loss of various concrete types as a function of temperature [44].

Parameter Units per cubic meter	Number identifying type of mix				
	1	2	3	4	5
Cement Type I, kg	564	475	487	564	475
Silica Fume, kg (1)	-	24	47	89	74
Fly Ash, kg	-	59	-	-	104
Coarse Agg. SSD, kg. (2)	1068	1068	1068	1068	1068
Fine Agg. SSD, kg.	647	659	676	593	593
HRWR Type F, liter	11.60	11.60	11.22	20.11	16.44
HRWR Type G, liter	-	-	-	-	-
Retarder Type D, liter	1.12	1.05	0.97	1.46	1.50
Total Water, kg. (3)	158	160	155	144	151
Water/Cement Ratio	0.281	0.338	0.320	0.255	0.318
Water/Cementitious Ratio	0.281	0.287	0.291	0.220	0.321

Note: As reported by ready-mix supplier
(1) Dry weight
(2) Maximum aggregate size: 12 mm
(3) Weight of total water in mix including admixtures

Table 2. Composition of concrete mixtures [47-48].

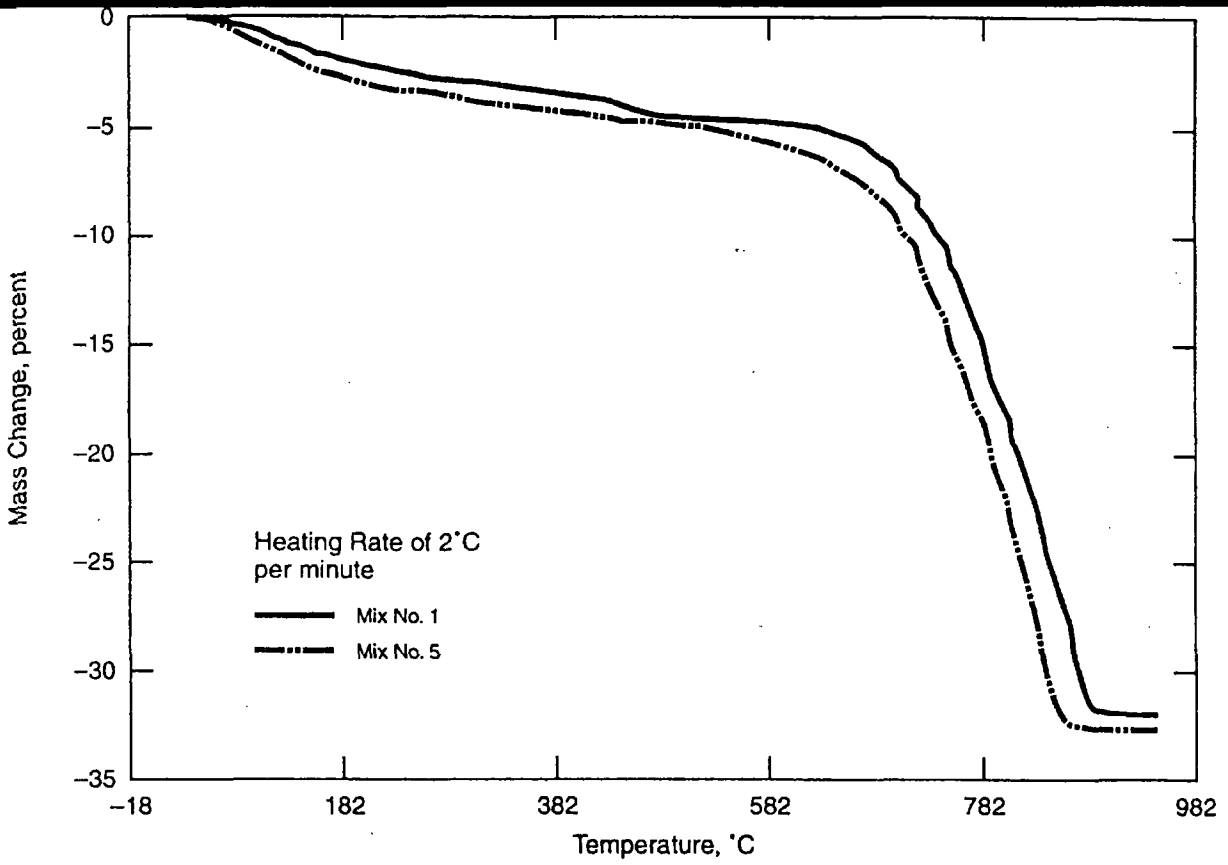

Figure 6. Mass loss of high strength concrete at elevated temperatures [47-48]

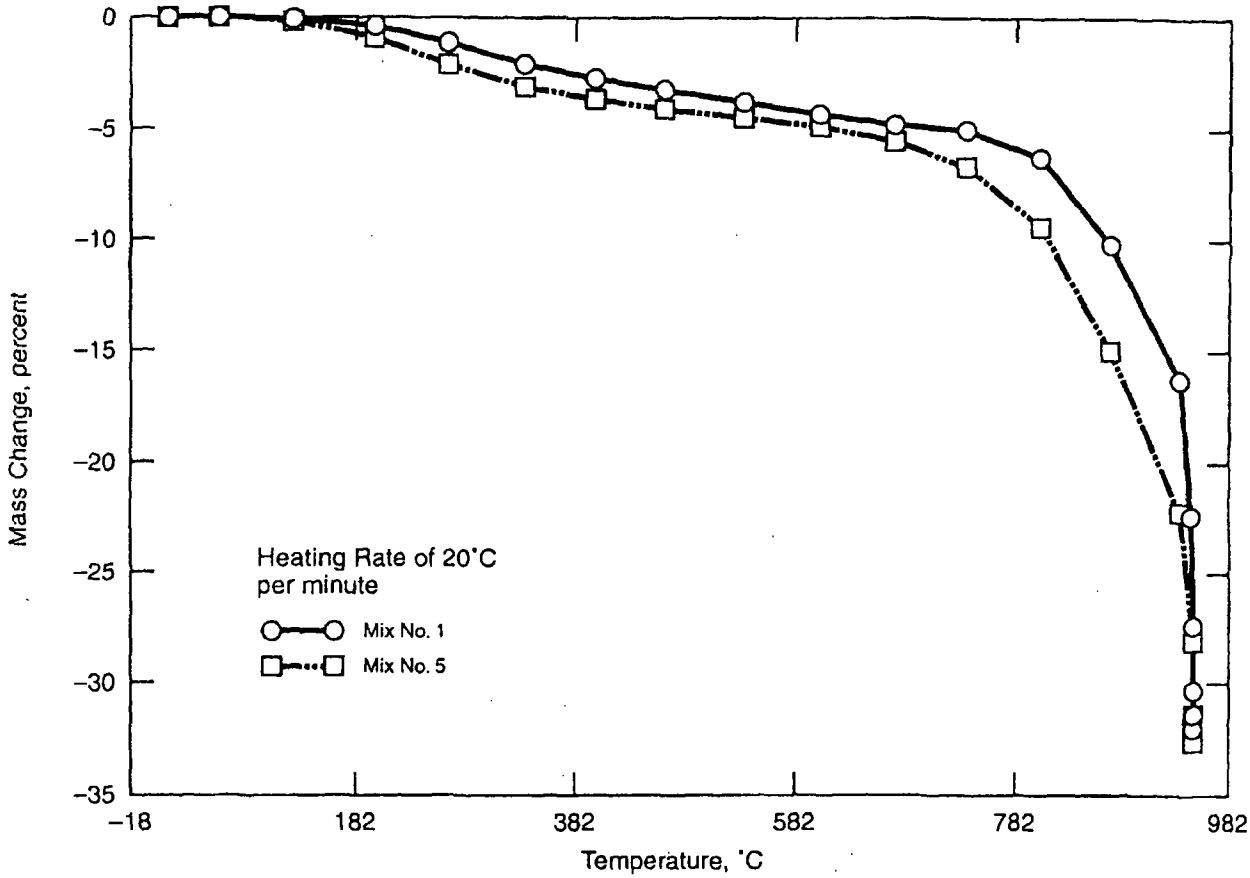

Figure 7. Mass loss of high strength concrete at elevated temperatures [47-48]

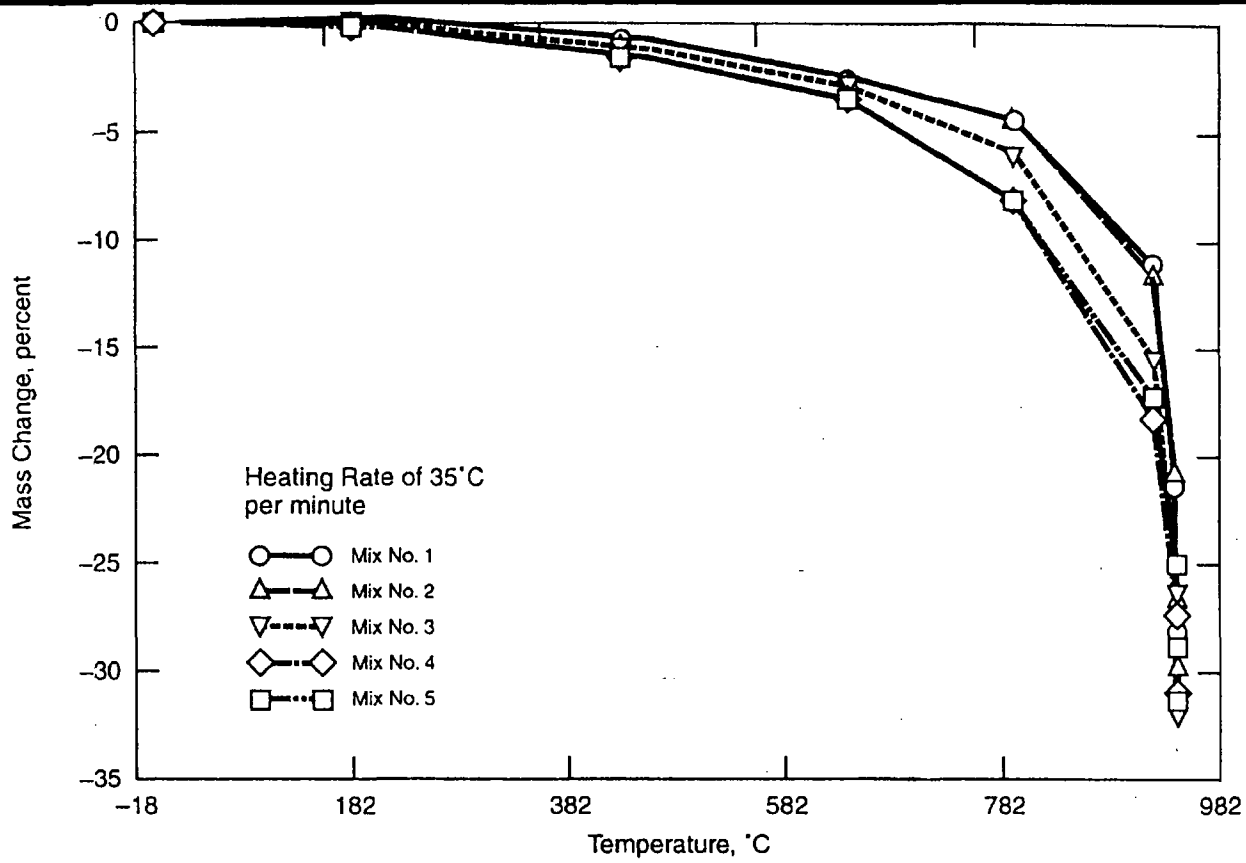

Figure 8. Mass loss of high strength concrete at elevated temperatures [47-48]

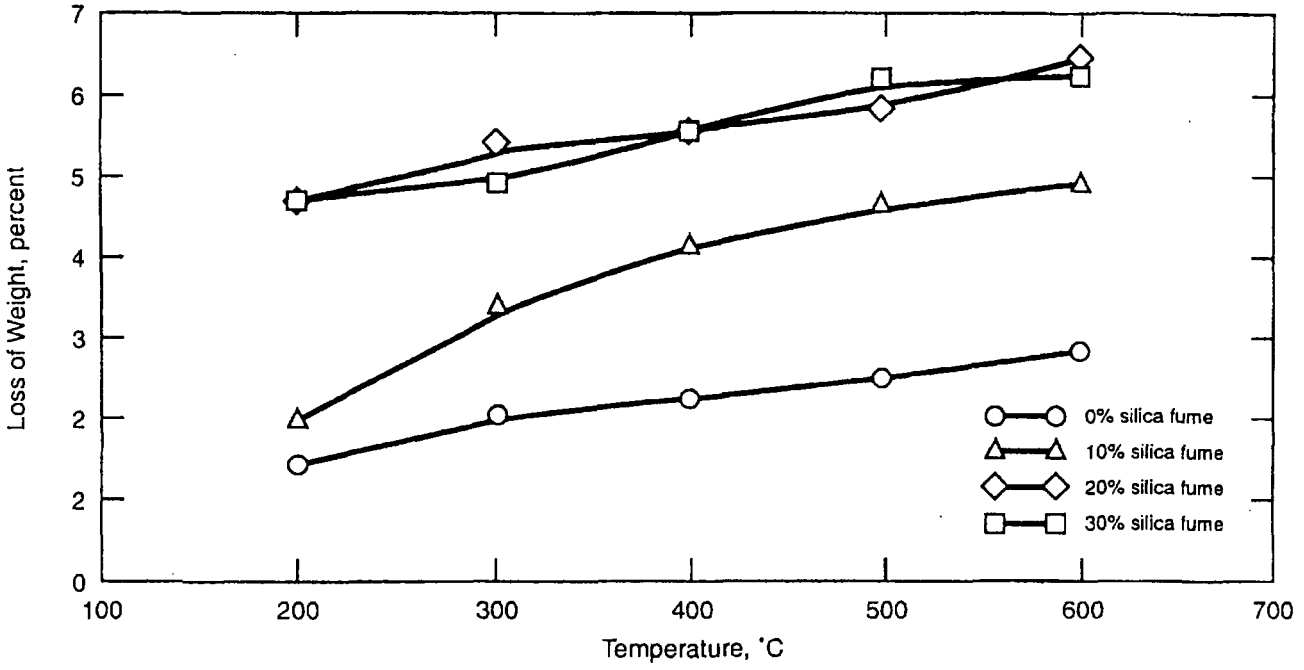

Figure 9. Change of weight with temperature of concrete containing silica fume [46].

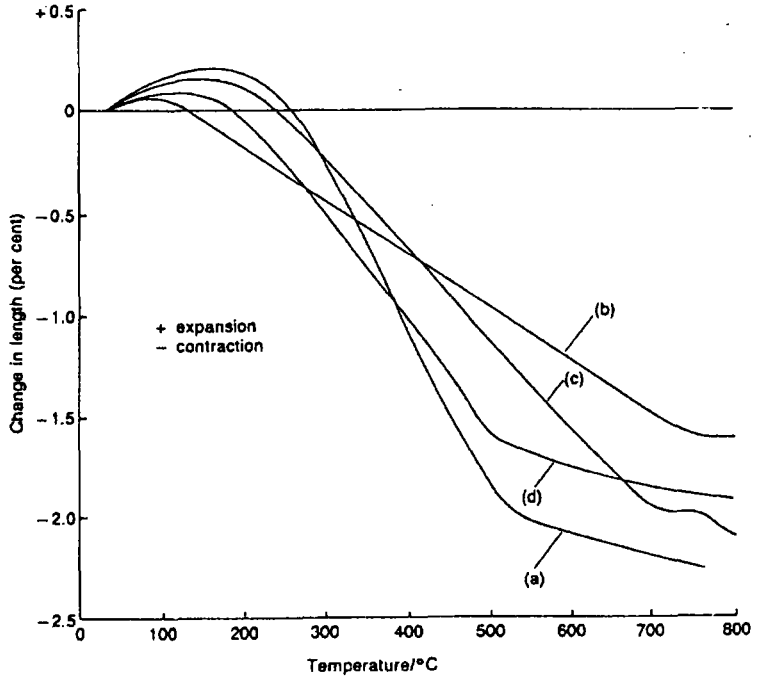

Figure 10. Length change of Portland cement paste specimens at various temperatures: (a) Philleo (1958); (b) Harada *et al.* (1972); Cruz and Gillen (1980); (d) Crowley (1956) [45].

Name	Symbol	Geological Origin	Composition	Density (kg/m^3)	Grain size (mm)
Anorthosite	AN	Igneous	Almost all plagioclase feldspars	2770	0.05-20
Basalt	BA	Igneous	Mainly epidotes, pyroxenes and plagioclase feldspars	3040	0.005-0.08
Dolomite	DO	Sedimentary	Almost all dolomite	2490	0.1-7
Granodiorite	GD	Igneous	Plagioclase feldspars, quartz amphiboles and micas	2750	0.05-4
Granite	GR	Igneous	Mainly potash and plagioclase-feldspars, quartz	2620	0.05-5
Limestone	LI	Sedimentary	Mainly calcite	2700	0.002-2
Quartz Monzonite	QM	Igneous	Mainly potash and plagioclase-feldspars and quartz	2645	0.5-7
Quartz	QR	Igneous	All quartz	2650	0.2-10
Rhyolite	RH	Igneous	Mainly potash and plagioclase-feldspars, and quartz	2640	0.05-3
Syenite	SY	Igneous	Mainly potash and plagioclase-feldspars, and amphiboles	2715	0.1-10

Table 3. Some characteristics of the ten rocks whose dilatometric curves are shown in Figure 11 (Geller, *et al.* 1962) [41].

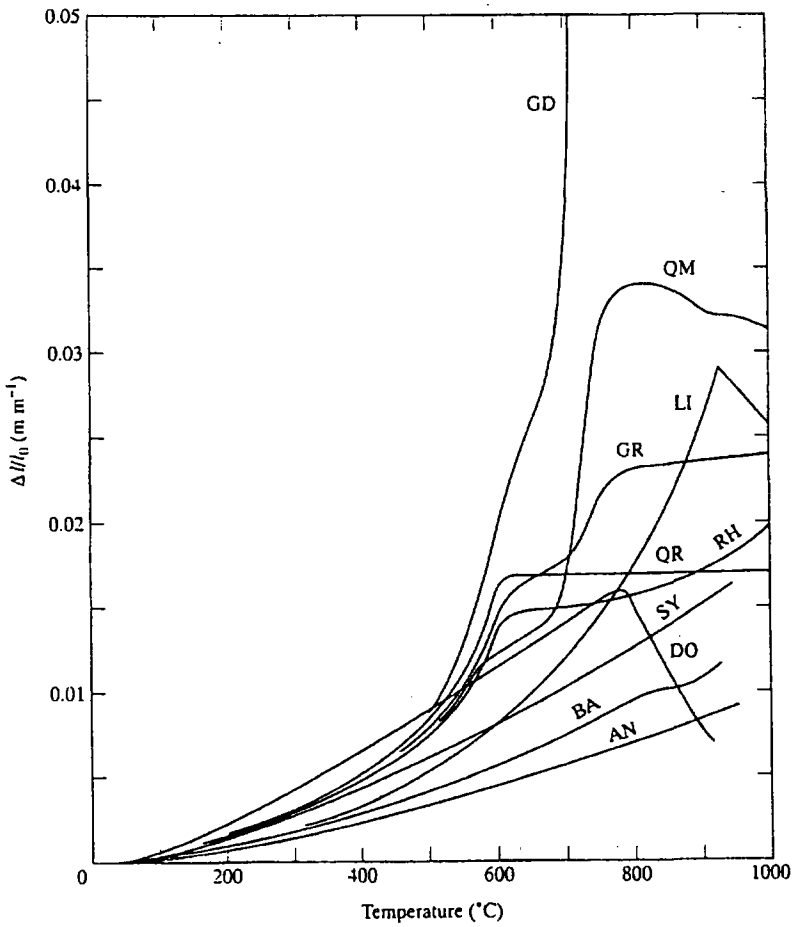

Figure 11. Dilatometric curves for the ten rocks described in Table 3 (Geller, *et al.* 1962) [41].

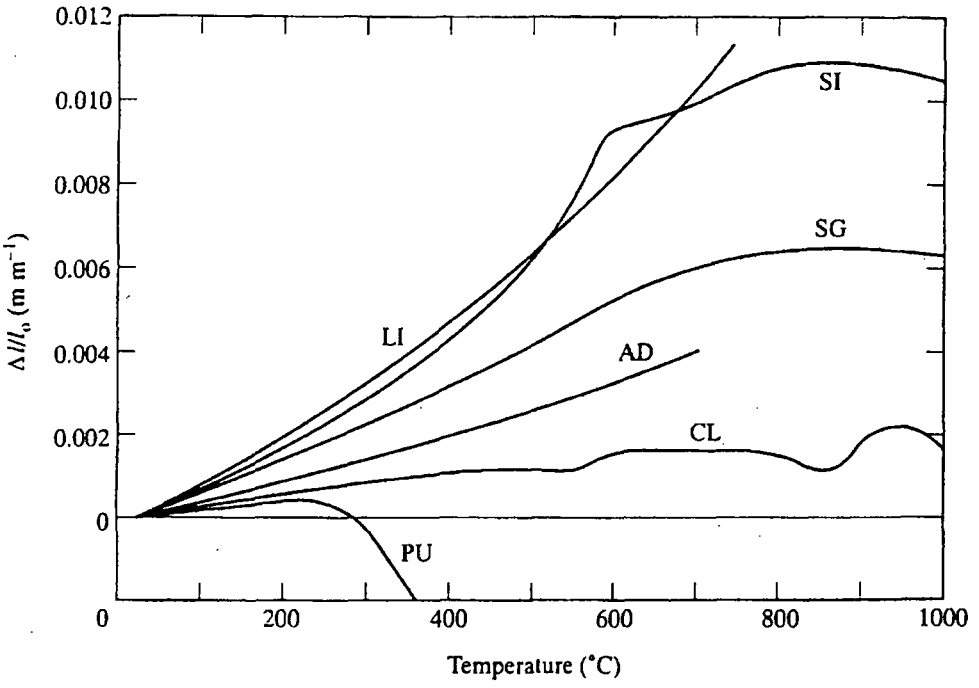

Figure 12. Dilatometric curves for three normal-weight concretes and three lightweight concretes. Aggregates: LI, limestone; SI siliceous rock; AD, andesite; SG, expanded shale; CL, expanded clay; PU, pumice (Harada, *et al.* 1972; Harmathy and Allen 1973) [41].

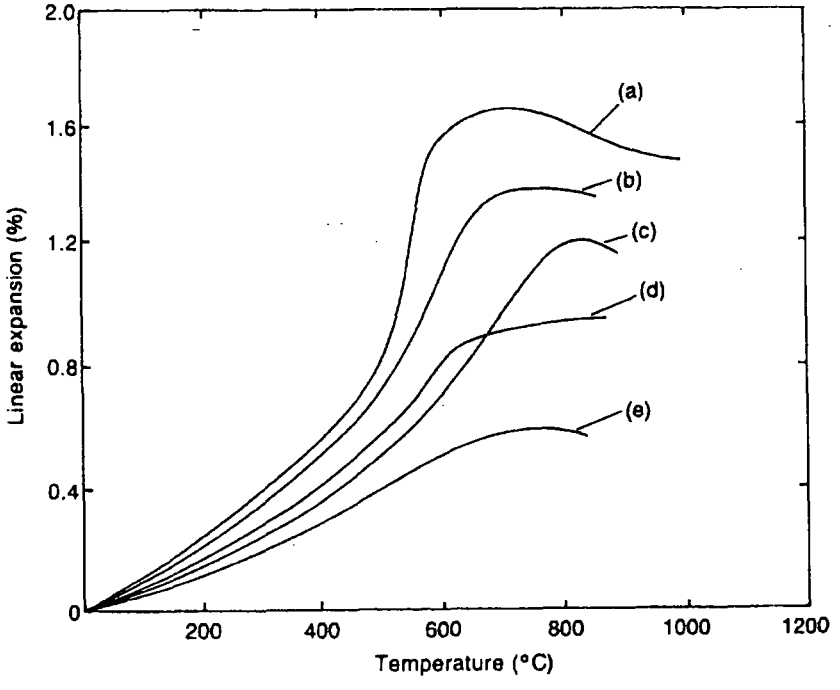

Figure 13. Linear thermal expansion of concretes made with various conventional aggregates, as a function of temperature (adapted from Schneider (1982)): (a) quartzite; (b) sandstone; (c) limestone; (d) basalt; (e) expanded slag [45].

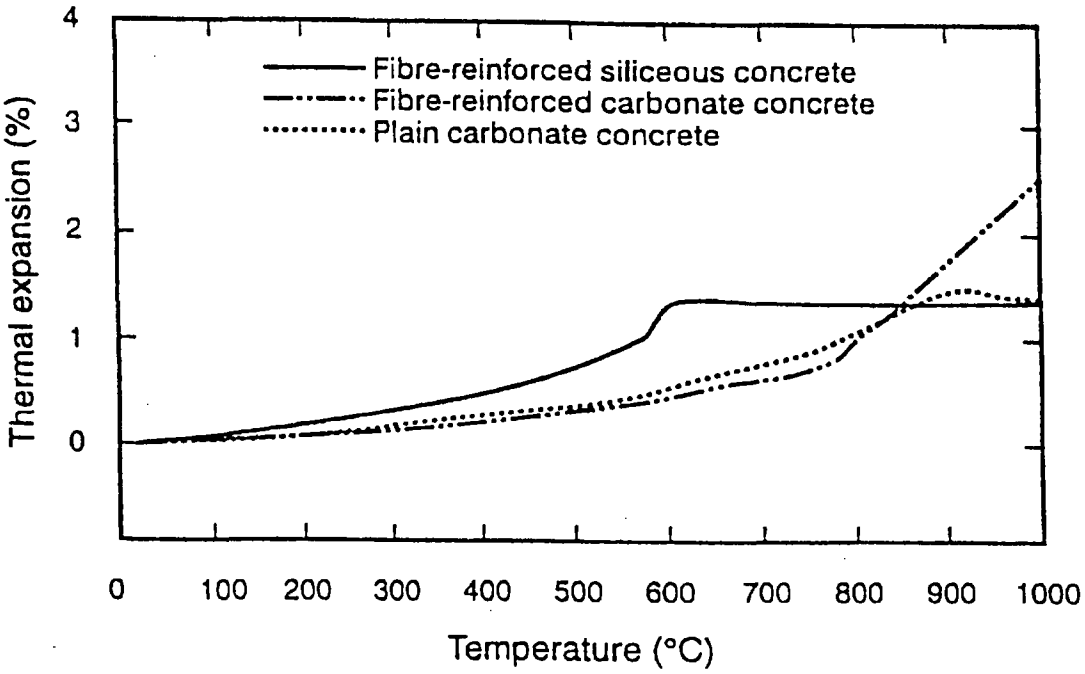

Figure 14. Thermal expansion, as a function of temperature, of the three concrete types described in Table 1 [44].

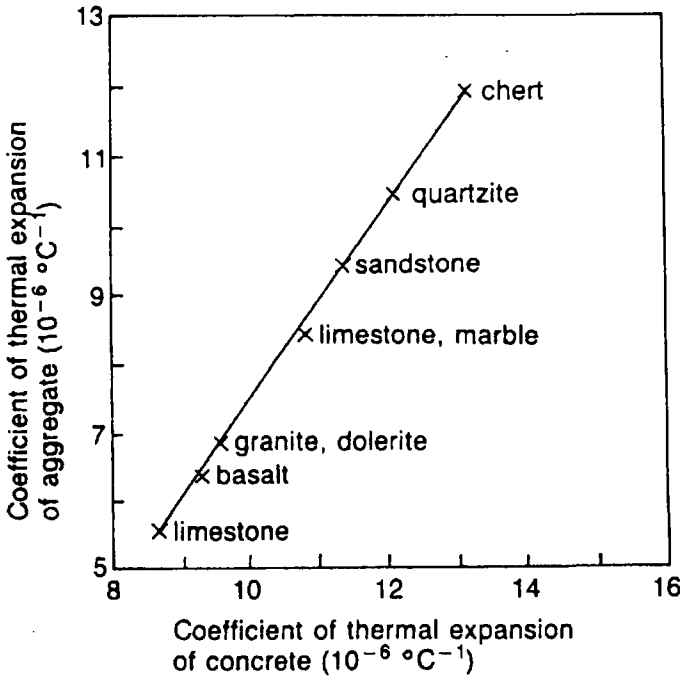

Figure 15. Correlation between the coefficient of thermal expansion of the aggregate and that of the concrete [45].

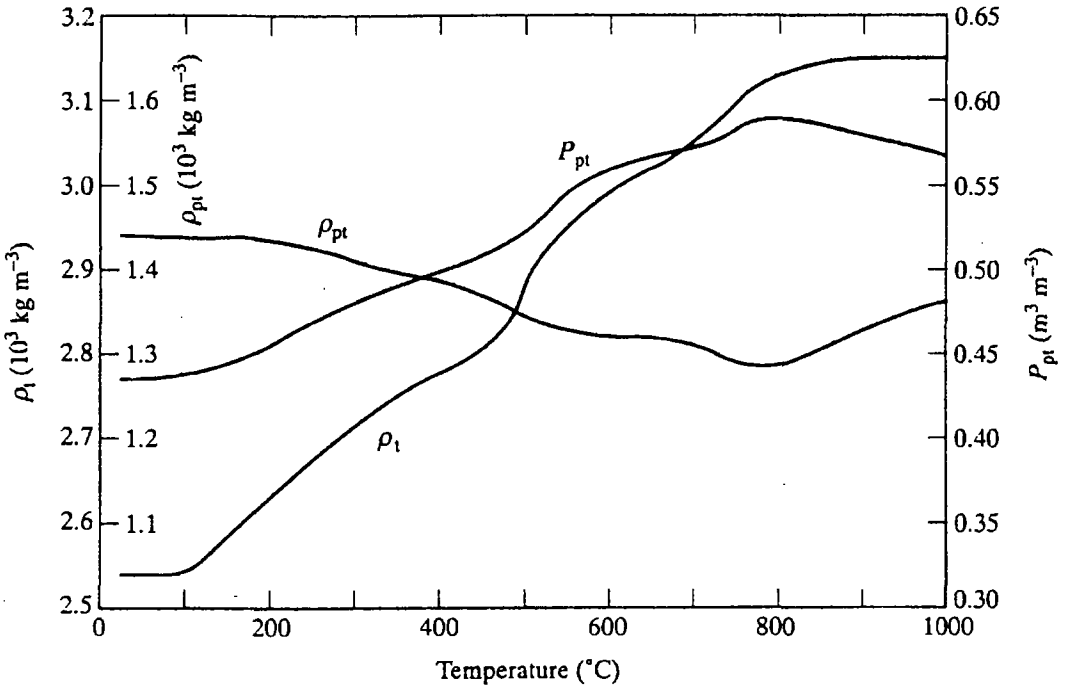

Figure 16. True density (ρ_t), bulk density (ρ_{pt}), and porosity (P_{pt}) of Cement Paste C (calculated): note the different scales for the three properties [27,41].

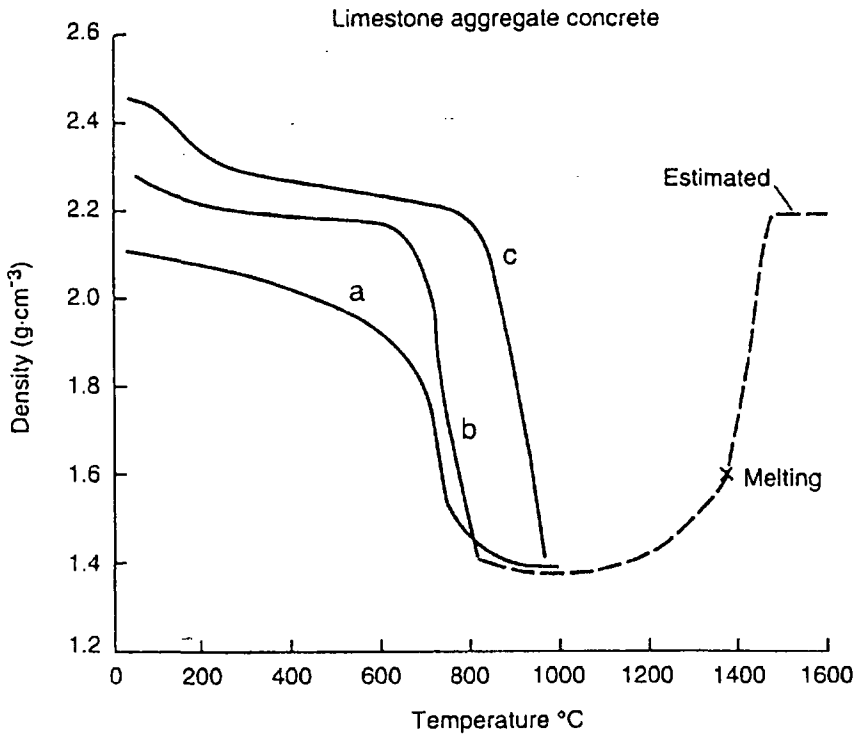

Figure 17. Effect of temperature on density of concrete made with limestone aggregate (Schneider, 1982): (a) Harmathy and Allen (1973); (b) cured at 20 °C and 65 percent RH (Schneider, 1982); (c) water cured (Schneider, 1982) [45].

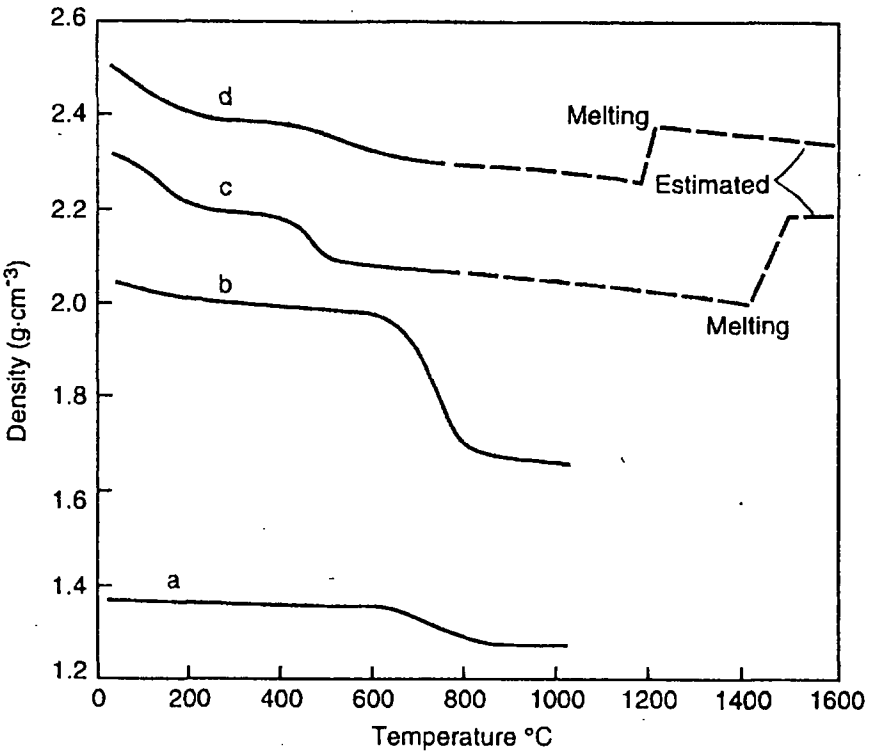

Figure 18. Effect of temperature on mass density of concretes made with quartzite, bauxite, and expanded shell aggregates: (a) expanded shale aggregate concrete (Harmathy and Allen, 1973); (b) siliceous aggregate concrete (Harmathy and Allen, 1973); (c) quartzite aggregate concrete (Schneider, 1982); (d) basalt aggregate concrete (Schneider, 1982) [45].

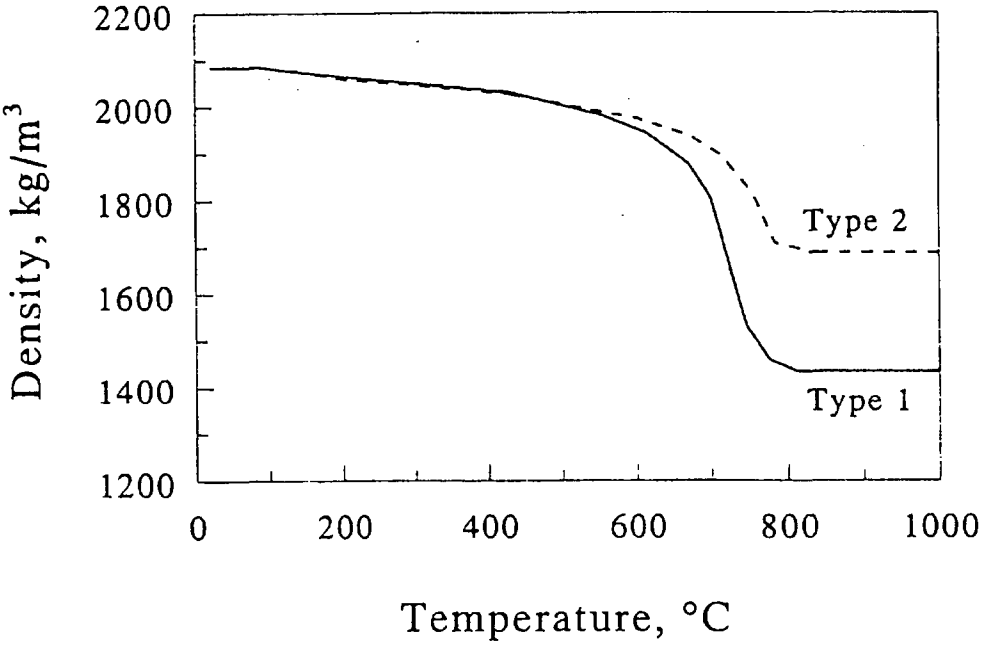

Figure 19. Density versus temperature curves used in the Ahmed model (see text).

3.2 Enthalpy, Specific Heat, and Heats of Reaction

The enthalpy or the specific heat, the derivative of enthalpy with respect to temperature, and the heats of reaction of any chemical reaction are required for modeling heat and mass transfer through concrete. These quantities are briefly discussed on pp. 5-6 of this report. Their inclusion in various models is indicated in Section 2.

Harmathy [27,41] has developed detailed procedures, which are briefly addressed in Section 4.2 of this report, for predicting the specific heat of cement paste and of concrete. Figure 20 shows his predicted specific heats for three different cement pastes; Figure 21 shows his later experimental results for those same cement pastes. The large peaks near 500 °C correspond to the release of bound water. The width and height of such peaks will depend significantly on the heating rate; the area under the curve represents the total energy absorption or release associated with a chemical reaction and thus will be much less dependent upon the heating rate. Some the models for predicting heat and mass transfer through concrete or other materials do not include the latent heat of reaction in the specific heat of the material but treat it separately. Thus, one must be careful to select the "proper" specific heat for use in a particular model.

Fu and Chung [50] recently published room temperature values of the specific heat of cement paste with various admixtures. For a plain cement paste with a water/cement ratio of 0.45, the density was 1.99 g/cm^3 and the specific heat was 0.703 J/g•K, corresponding to a volumetric heat capacity of 1.40 J/cm^3•K. A cement paste with 15 percent (by weight of cement) silica fume, 3 percent (by weight of cement) water reducing agent, and a water cement ratio of 0.35 had a density of 1.72 g/cm^3 and a specific heat of 0.765 J/g•K, corresponding to a volumetric heat capacity of 1.32 J/cm^3•K.

Figure 22 shows the volumetric specific heats that Harmathy [27,41] computed for four hypothetical concretes that he believed were "limiting cases," at least with regard to thermal conductivity. It is seen that the computed volumetric specific heats are very nearly identical for the two normal-weight concretes, one of which (Concrete 1) had crystalline quartz aggregate while the other one had crystalline anorthosite aggregate.

Figures 23 and 24 show the specific heat (per unit mass) of various types of Portland cement concrete as functions of temperature. Curve 6 in Figure 23 appears questionably low at higher temperatures. The curve for plain carbonate concrete in Figure 24 clearly shows the heat absorbed at high temperatures when the carbonate converts to the oxide with carbon dioxide being released. Note also, in this figure, that the specific heat is significantly lower at temperatures above this transition than it is at temperatures just below the carbonate decomposition temperature. Figure 25 shows the specific heat versus temperature curves used in the version of the Ahmed model that is currently available at NIST. As stated on p. 17, Type 1 concrete has a carbonate aggregate and Type 2 a siliceous aggregate. Both of these curves appear to be in error at high temperatures. For the Type 1 concrete, the specific heat should drop drastically from the peak at temperatures near 800 °C, in a manner similar to that seen for carbonate concrete in Figure 24. For the Type 2 concrete, there is no apparent reason to expect a high-temperature peak at all.

(Text continued on p. 37)

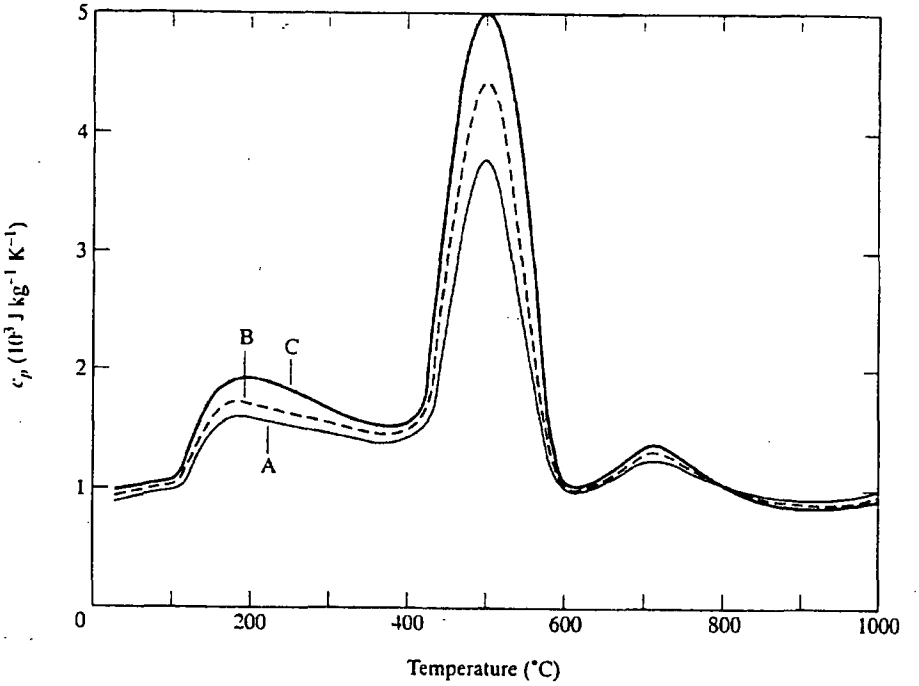

Figure 20. Computed specific heat of Model Pastes A, B, and C [27,41].

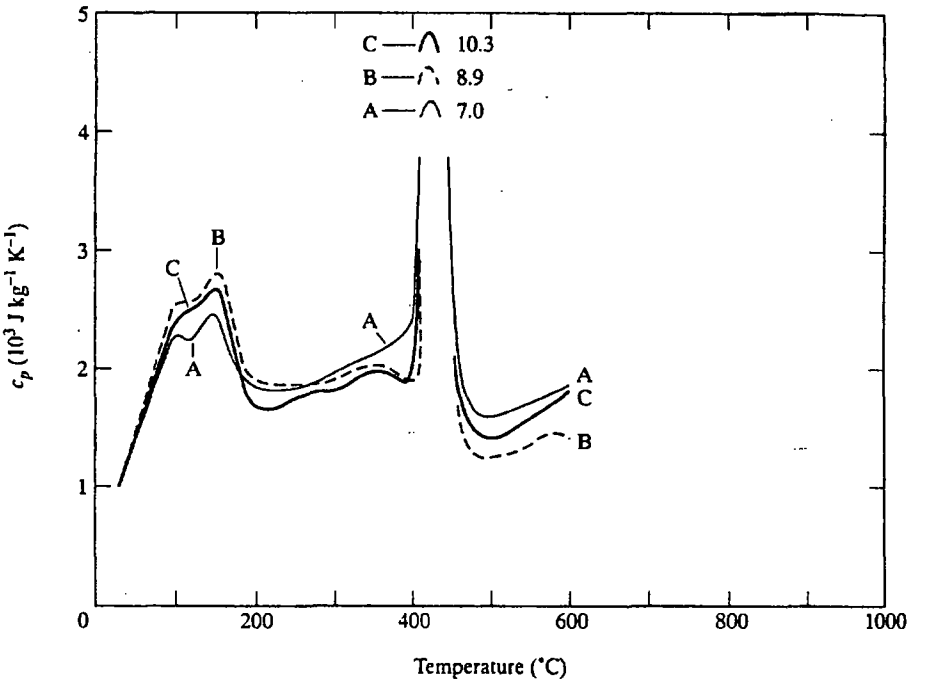

Figure 21. Measured specific heat of Cement Pastes A, B, and C [41].

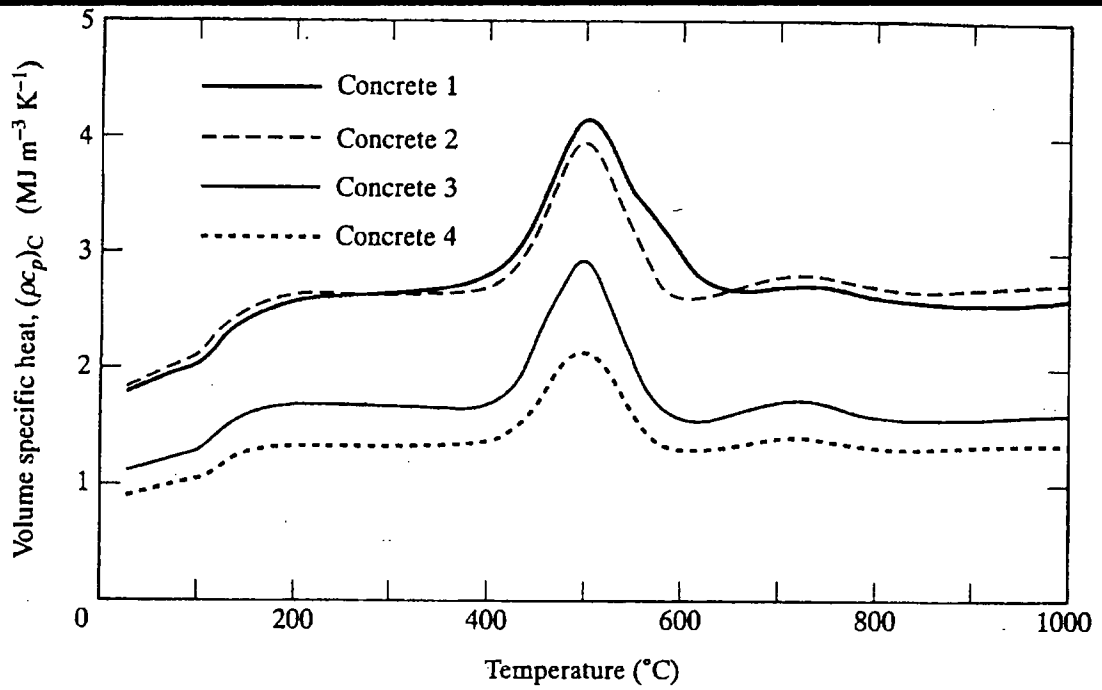

Figure 22. Volumetric specific heats (computed) for four hypothetical concretes: normal-weight, Concretes 1 and 2; lightweight, Concretes 3 and 4 [27,41].

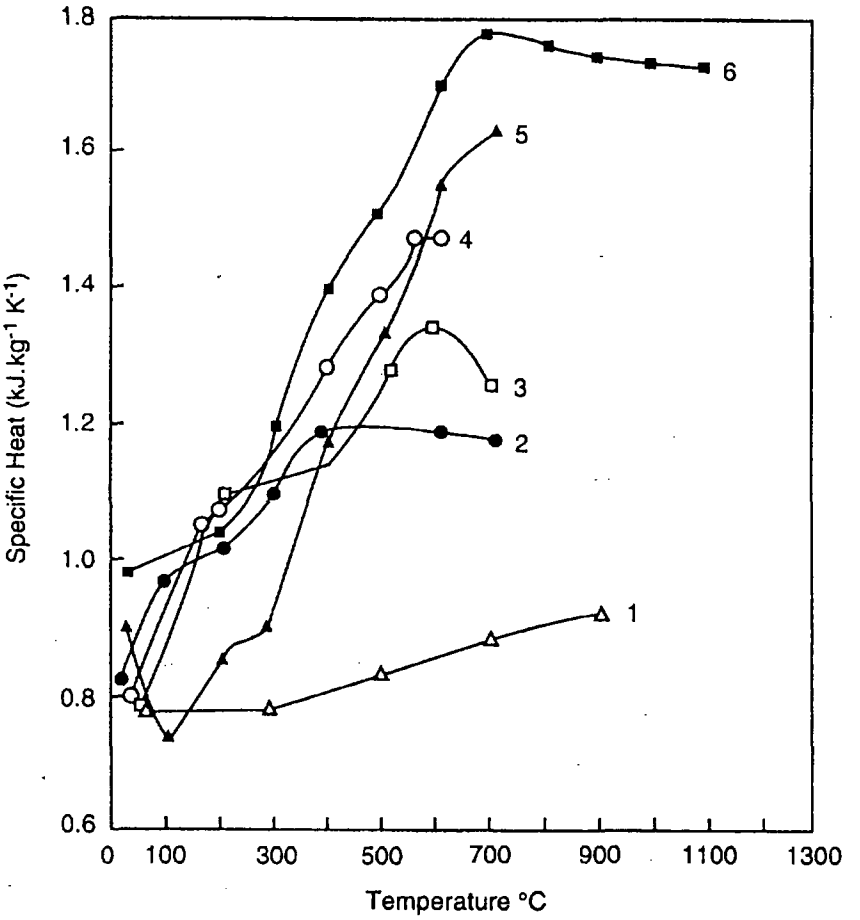

Figure 23. Effects of temperature on measured specific heats of various concretes: (1) granite aggregate concrete (Ödeen, 1968); (2) limestone aggregate concrete (Collet and Tavernier, 1976); (3) limestone aggregate concrete (Harmathy and Allen, 1973); (4) siliceous aggregate concrete (Harmathy and Allen, 1973); (5) limestone aggregate concrete (Hildenbrand, *et al.*, 1978); (6) siliceous aggregate concrete (Hildenbrand, *et al.*, 1978) [45].

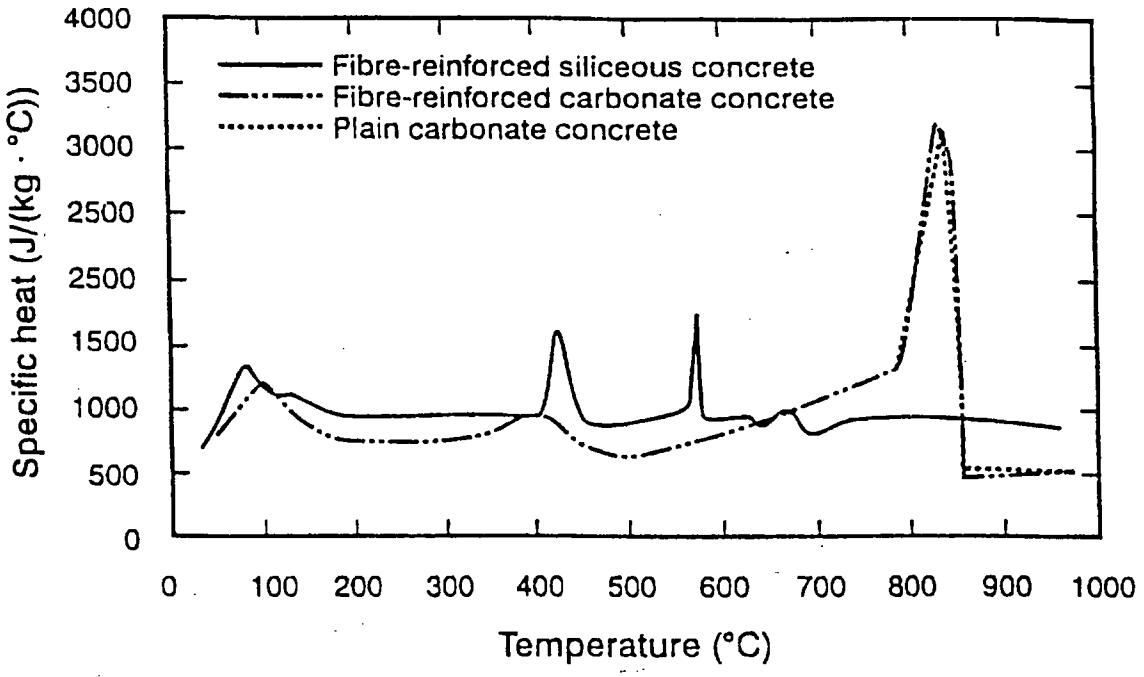

Figure 24. Specific heat, as a function of temperature, of the three concrete types described in Table 1 [44].

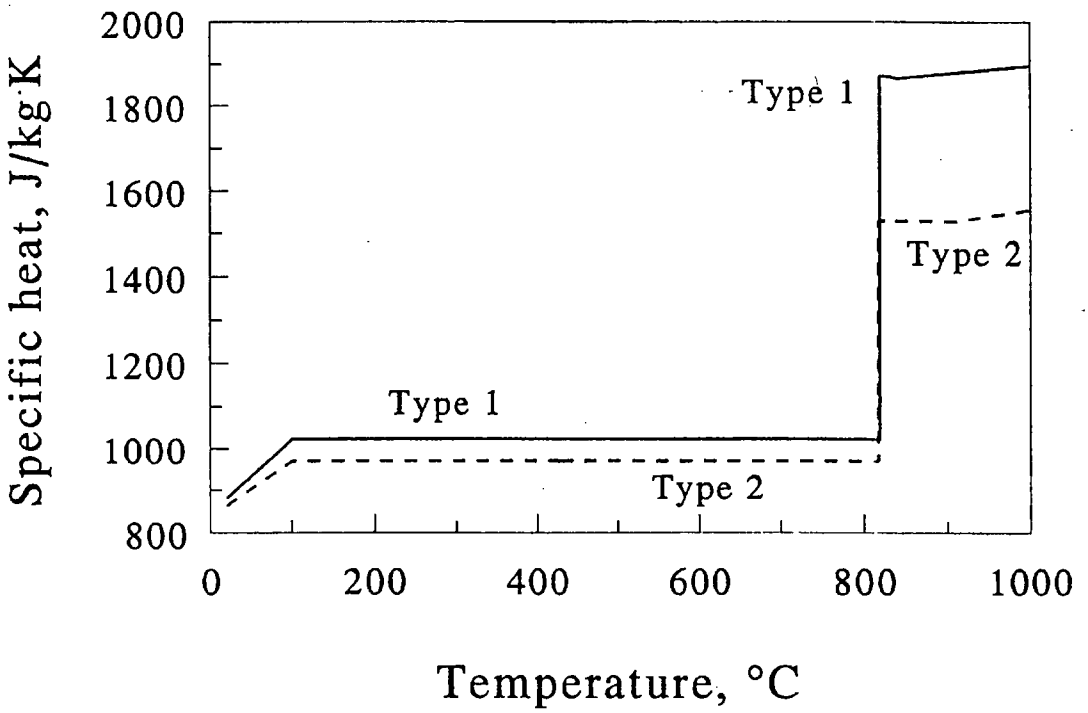

Figure 25. Specific heat versus temperature curves used in the Ahmed model (see text).

3.3 Thermal Conductivity and Thermal Diffusivity

Thermal conductivity is a key thermal property in predicting heat and mass transport in concrete exposed to fire conditions. As mentioned on p. 5, thermal diffusivity can be used if there are no mechanisms of heat transfer other than conduction and if the thermal conductivity can be considered to be constant. For modeling simultaneous heat and mass transfer, thermal diffusivity, in general, should not be used. However, rather than to measure thermal conductivity directly, many investigators have chosen to measure thermal diffusivity and then compute thermal conductivity from the thermal diffusivity and the specific heat.

Harmathy determined the thermal conductivities of several cement pastes, which have significant porosity and cracks, over a wide temperature range and then extrapolated these results to obtain an estimate of the thermal conductivity of a hypothetical pore-less cement paste, as shown in Figure 26. This curve can then be used to estimated the thermal conductivity of pastes of various porosities.

Fu and Chung measured the room-temperature specific heat, thermal diffusivity, and density of a plain cement paste and one containing silica fume (see p. 32 of this report for compositions) and then computed the thermal conductivity. The measured thermal diffusivities of the plain cement paste and the silica fume cement paste were 0.37 mm^2/s and 0.27 mm^2/s, respectively. The corresponding thermal conductivities were 0.52 W/m•K and 0.36 W/m•K, respectively, indicating that the higher porosity of the silica fume cement paste resulted in the room-temperature thermal conductivity being lowered by about 30 percent.

Figure 27 shows the thermal conductivity of 15 rocks and minerals at temperatures up to 300 °C; these materials are described in Table 4. Harmathy based his "limiting cases," discussed briefly on p. 32 of this report, for the thermal conductivity of concrete by selecting Curve QS (quartzitic sandstone) and Curve AN (anorthosite) as the thermal conductivity of the aggregates. The thermal conductivity of rocks and minerals can vary widely depending upon the source and the porosity. Touloukian, *et al.* [51] provide extensive data on the thermophysical properties of rocks, taken from the literature through the mid-1970s. They comment that because the properties of rocks and minerals can vary widely over relatively small distances and because the specimens used for thermophysical property measurements are relatively small, the measured properties can vary widely on specimens taken from nominally the same location. Figure 28 is a histogram showing the variation in the room-temperature thermal conductivity of limestone samples taken from two locations. It is clear that tests on numerous samples would be required to obtain statistically significant results.

Figure 29 shows the thermal conductivity of limestone, versus temperature, as measured by three different investigators. The two curves on samples taken in Nazareth, Pa., were from the same study as the curves shown in Figure 27.

Figure 30 shows the measured roon-temperature thermal conductivity of several different types of concrete, plotted versus the moisture content. These data were taken using a hot-wire method that allows measurements to be completed before the moisture has time to migrate significantly. It is seem that 10 percent moisture content can cause the thermal conductivity to be roughly doubled.

Obviously, this effect would be much smaller at higher temperatures. However, as pointed out by Thompson [60] many years ago, and as is known by competent workers in the field of thermal conductivity, it is very difficult to obtain values of thermal conductivity without some moisture movement and/or drying out occurring.

The thermal conductivity of concrete will depend upon the porosity of the cement paste and upon the type, quantity, and porosity of aggregates. Figure 31 shows one set of data indicating how the thermal conductivity of different types of concrete varies with porosity.

The thermal conductivity of concrete is known to show considerable hysteresis, although there appear to have been very few quantitative studies of this effect. Figure 32 indicates one set of data indicating how the thermal conductivity of a concrete changes due to the loss of moisture of hydration.

There has been considerable variation in thermal conductivity values reported by different investigators on nominally similar concretes. Part of the variations seen may be attributed to sample differences but it appears quite likely that large experimental errors have occurred in some cases. Figures 33 and 34 shown the thermal conductivity of, respectively, limestone-aggregate concrete and siliceous aggregate concrete.

Figures 35-37 show the thermal conductivity of different types of normal-strength concrete as functions of temperature.

In Section 3.1 curves were shown of the mass loss versus temperature of five high-strength concretes studied by investigators at the Portland Cement Association (PCA). The constituents of these materials were shown in Table 2. Figure 38 shows the thermal conductivity values obtained for these materials using a guarded hot plate apparatus. Thermal conductivity data on these materials were also obtained, by a different testing laboratory, using a hot-wire method (ASTM C1113). In addition, thermal diffusivity data were obtained by the same testing laboratory using a radial heat flow method and then thermal conductivity values were computed, apparently using specific heat values computed from the specific heats of the several components of the concrete. For one of these high-strength concretes, the three sets of thermal conductivity values are shown plotted in Figure 39. The differences are rather startling.

Figure 40 shows the thermal conductivity versus temperature curves used in the version of the Ahmed model that is currently available at NIST (one obvious typo in the program was corrected).

Turning to thermal diffusivity, Figure 41 shows the range of values for the thermal diffusivity of limestone from three different investigations.

Figures 42-46 show thermal diffusivity versus temperature for a number of types of normal-strength concrete. Figure 47 shows thermal diffusivity data obtained at PCA on the five high-strength concretes described in Table 2; these data were obtained in their guarded hot plate apparatus, run in a transient mode with the hot plate removed. For one of these samples, these data are shown in Figure 48 along with data obtained elsewhere by the radial heat flow method mentioned above.

(Text continued on p. 55)

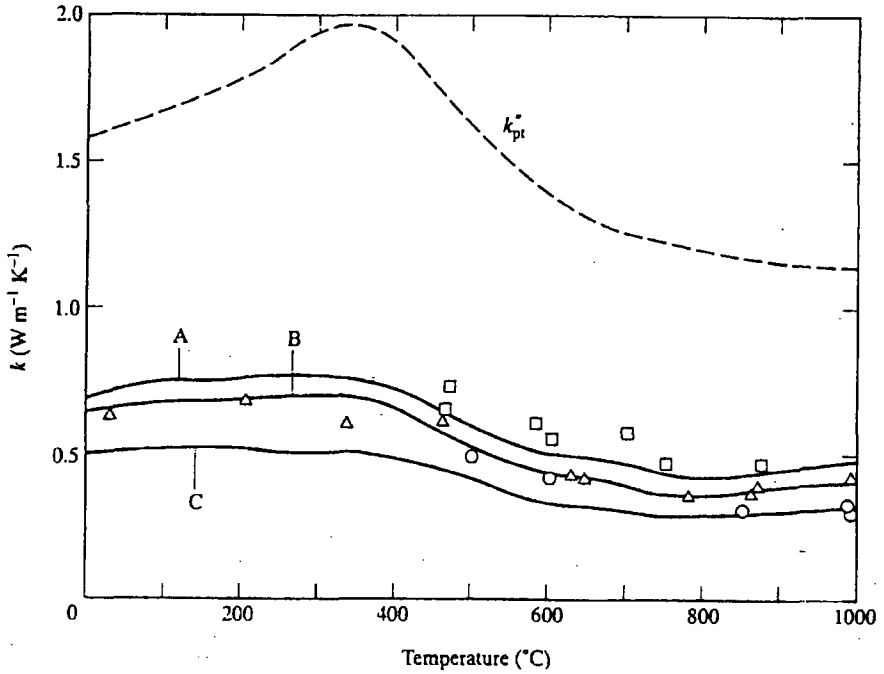

Figure 26. Thermal conductivities of Cement Pastes A, B, and C (points and solid-line curves), and thermal conductivity of a hypothetical pore-less cement paste (broken-line curve): □, Paste A; open triangle, Paste B; O, Paste C [27,41].

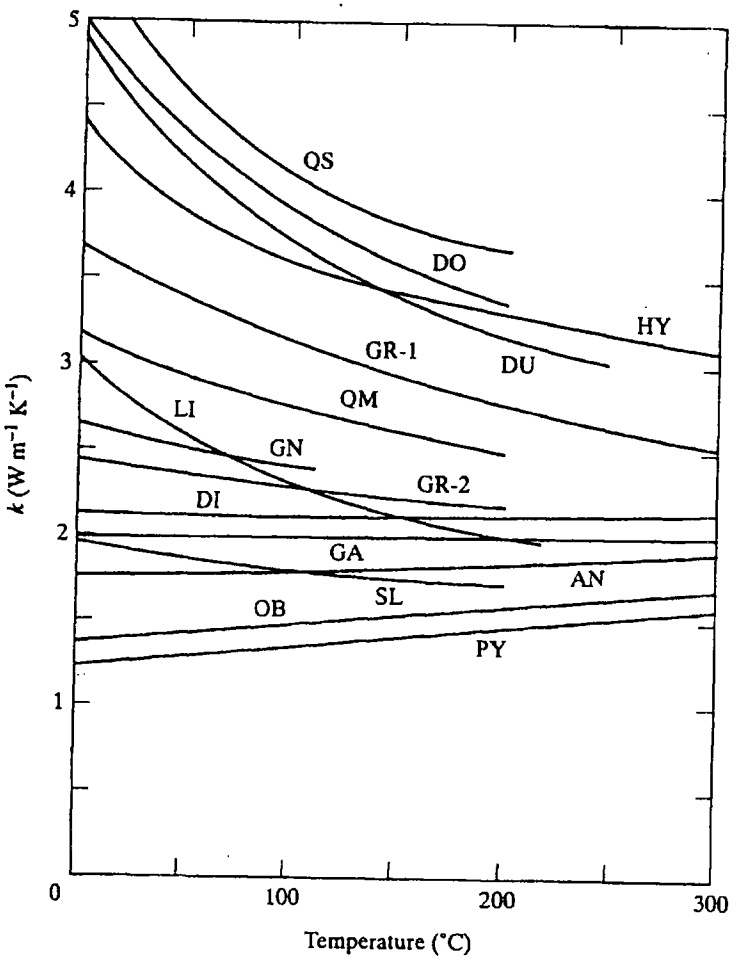

Figure 27. Thermal conductivity of 15 materials (rocks, minerals, glass) described in Table 4 (Birch and Clark 1940) [41].

Name	Symbol	Geological origin	Composition	Density (kg/m^3)	Mean grain size (mm)
Anorthosite	AN	Igneous	Almost all plagioclase feldspars	2700	0.5
Diabase	DI	Igneous	Mainly plagioclase feldspars and pyroxenes	2960	0.5
Dolomite	DO	Sedimentary	Carbonate group	2830	0.01
Dunite	DU	Igneous	Almost all olivines	3250-3270	1.0
Gabbro	GA	Igneous	Mainly plagioclase feldspars, pyroxenes and olivines	2860-2880	3.0
Gneiss	GN	Metamorphic	Layered mineral, mainly feldspar and quartz	2640	0.2
Granite-1	GR-1	Igneous	Mainly potash feldspars and quartz	2610	1.5-2.0
Granite-2	GR-2	Igneous	Mainly potash and plagioclase-feldspars, quartz	2640	0.5
Hypersthenite	HY	Igneous	Pyroxene group	3290	2.0
Limestone	LI	Sedimentary	Carbonate group, mainly calcite	2610	0.001-0.01
Obsidian	OB	Igneous	Glassy potash feldspar and quartz	2440	
Pyrex	PY	Artificial		2230	
Quartz monzonite	QM	Igneous	Mainly potash and plagioclase-feldspars and quartz	2640	1.0
Quartzitic sandstone	QS	Sedimentary	Mainly quartz	2640-2650	0.3
Slate	SL	Metamorphic	Layered clay minerals	2760	

Table 4. Some characteristics of the 15 materials (rocks, minerals, glass) whose thermal conductivity are plotted in Figure 27 (Birch and Clark, 1940) [41].

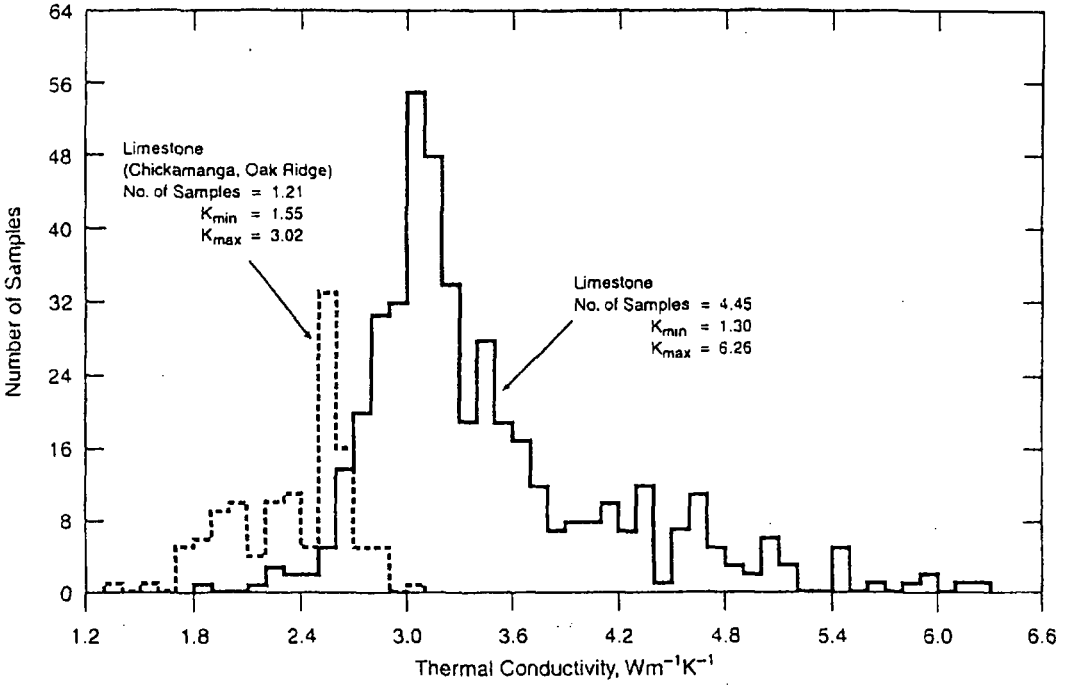

Figure 28. Histogram of the thermal conductivity of limestones [51].

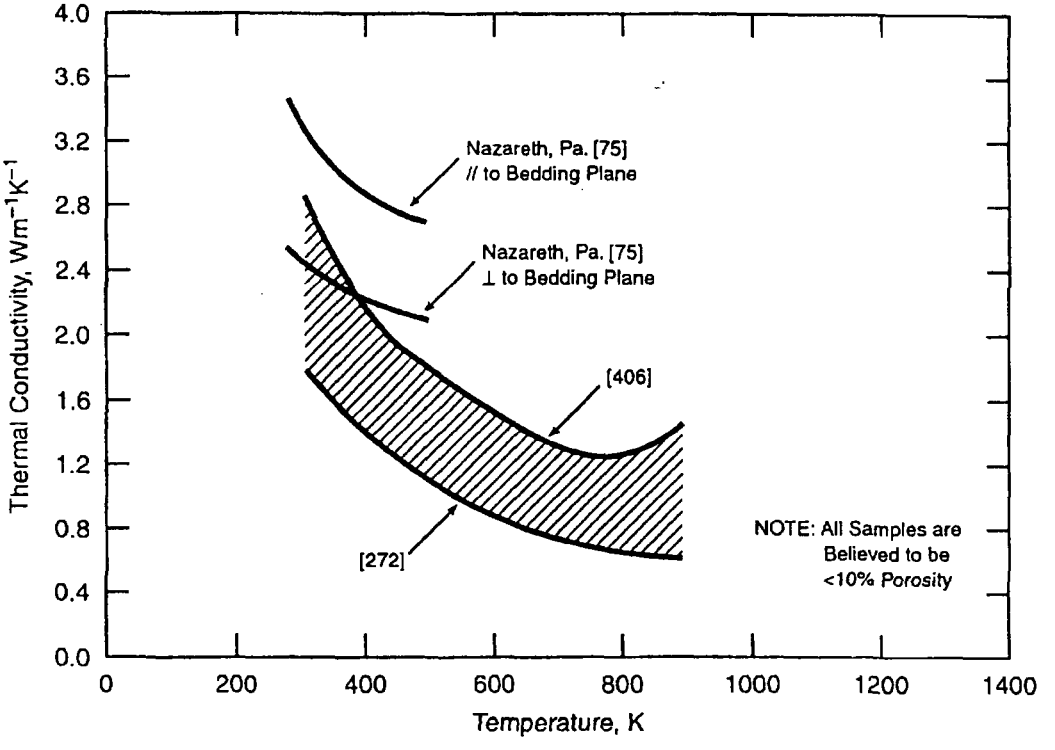

Figure 29. Thermal conductivity of limestones [51].

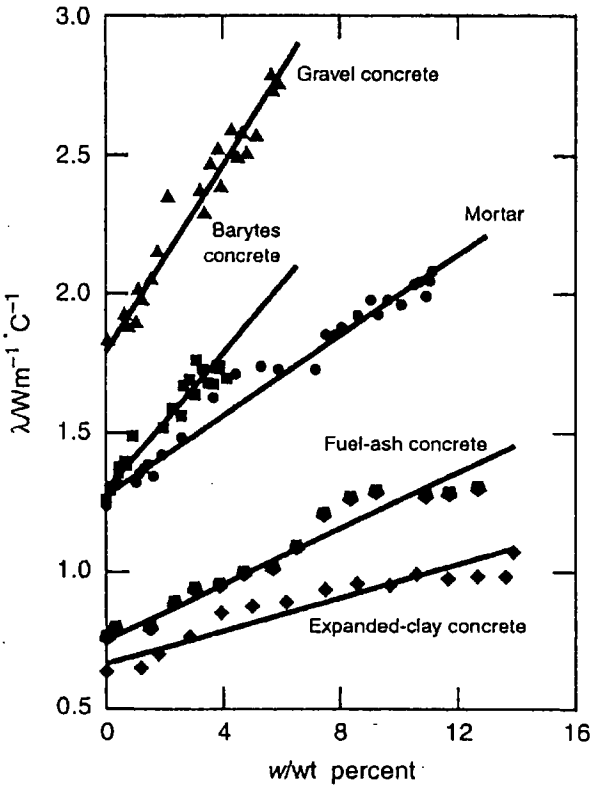

Figure 30. Plot of thermal conductivity against the moisture content of concrete [40].

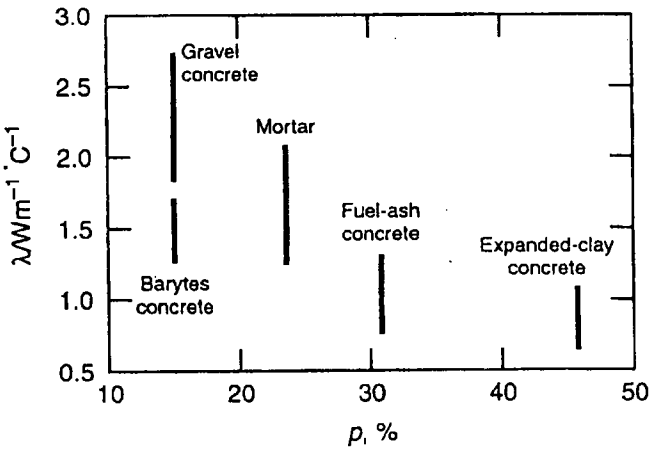

Figure 31. Variation range of thermal conductivity of concretes, plotted against the porosity [40].

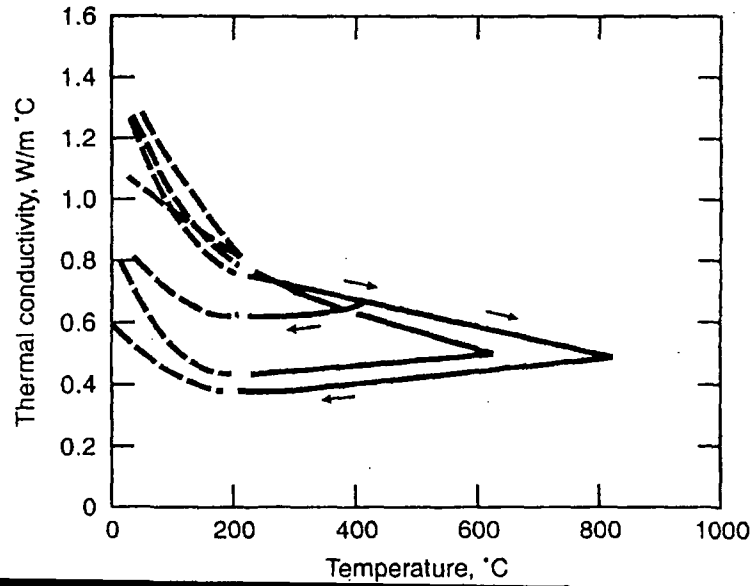

Figure 32. Thermal conductivity of granite-aggregate concrete as a function of temperature under heating and subsequent cooling [32].

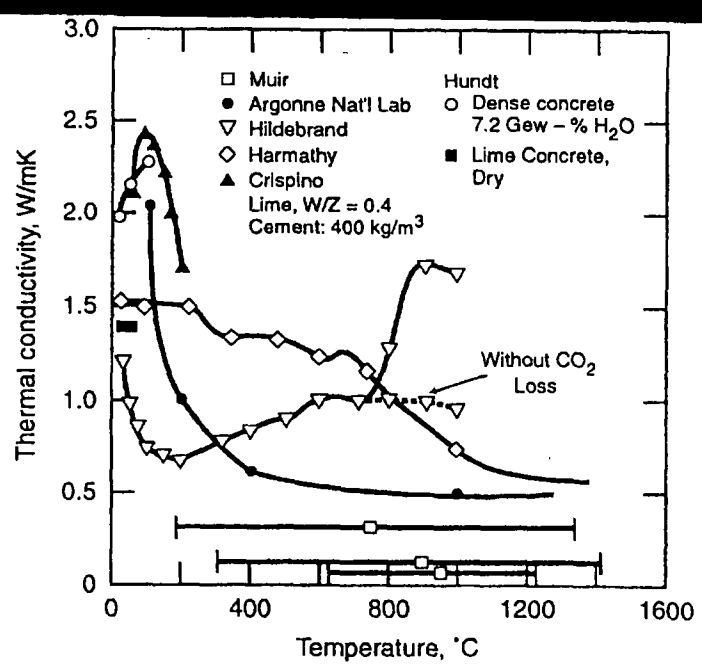

Figure 33. Thermal conductivity of limestone-aggregate concretes [35].

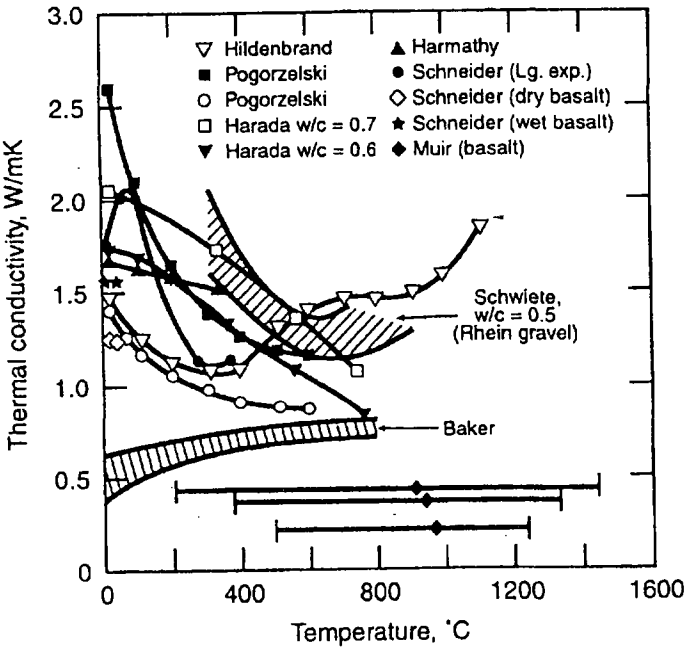

Figure 34. Thermal conductivity of siliceous-aggregate concretes [35].

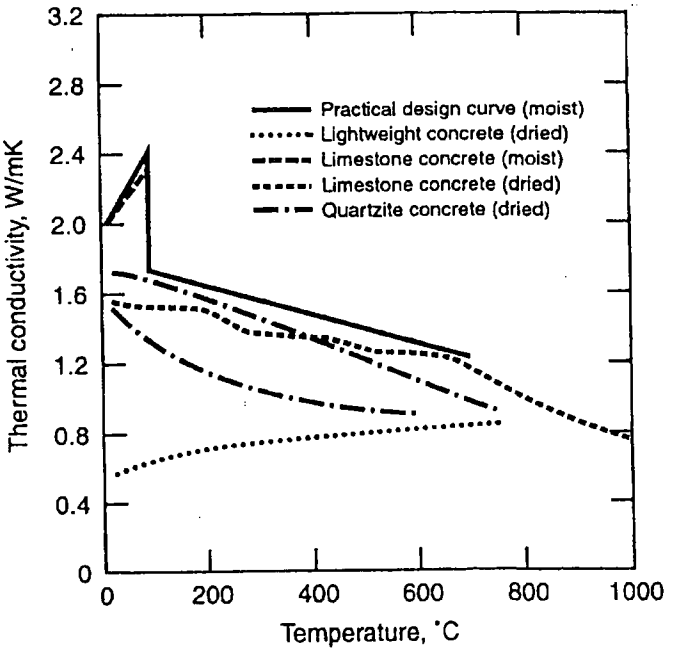

Figure 35. Thermal conductivity of different structural concretes [38].

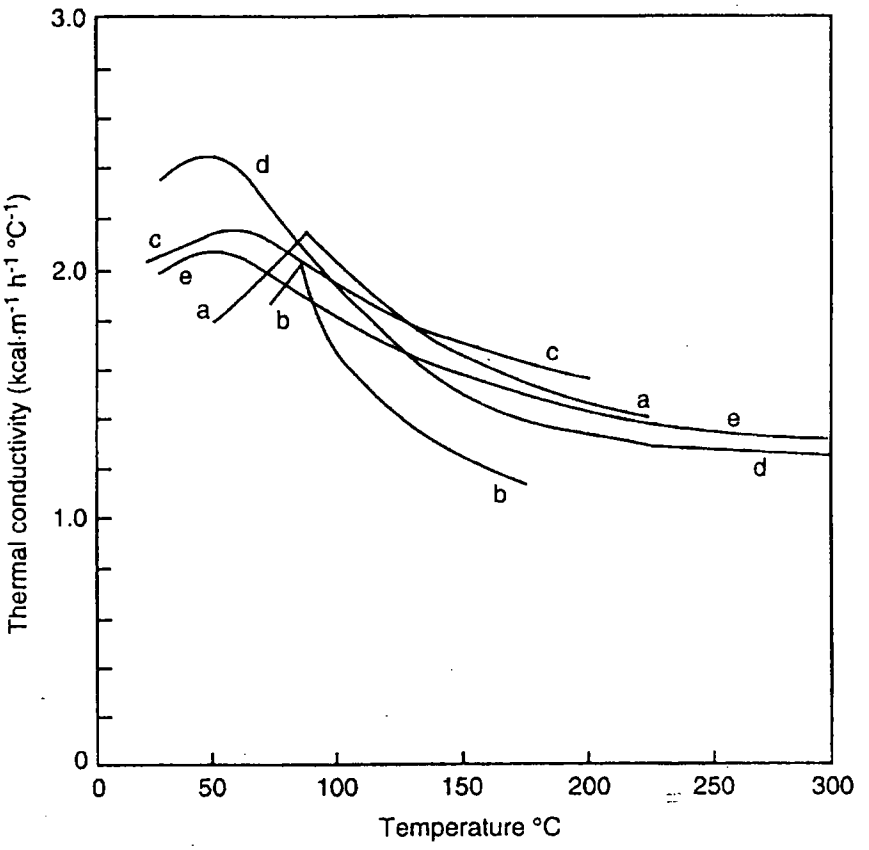

Figure 36. Thermal conductivity of various concretes that were not oven-dried before test, as a function of temperature: (a) limestone aggregate concrete (Crispino, 1972); (b) barytes aggregate concrete (Crispino, 1972); (c) gravel aggregate concrete (Abe, *et al.*, 1972); (d) quartzite aggregate concrete (Maréchal, 1972); (e) quartzite aggregate concrete (Maréchal, 1972) (1 kcal m^{-1} h^{-1} $°C^{-1}$ = 1.16 W/m•K) [45].

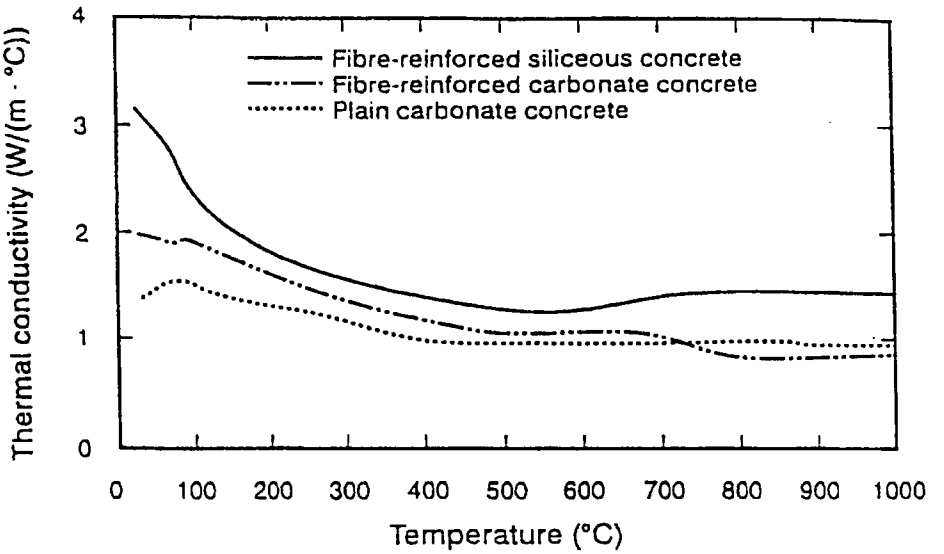

Figure 37. Thermal conductivity, as a function of temperature, of the three concrete types described in Table 1 [44].

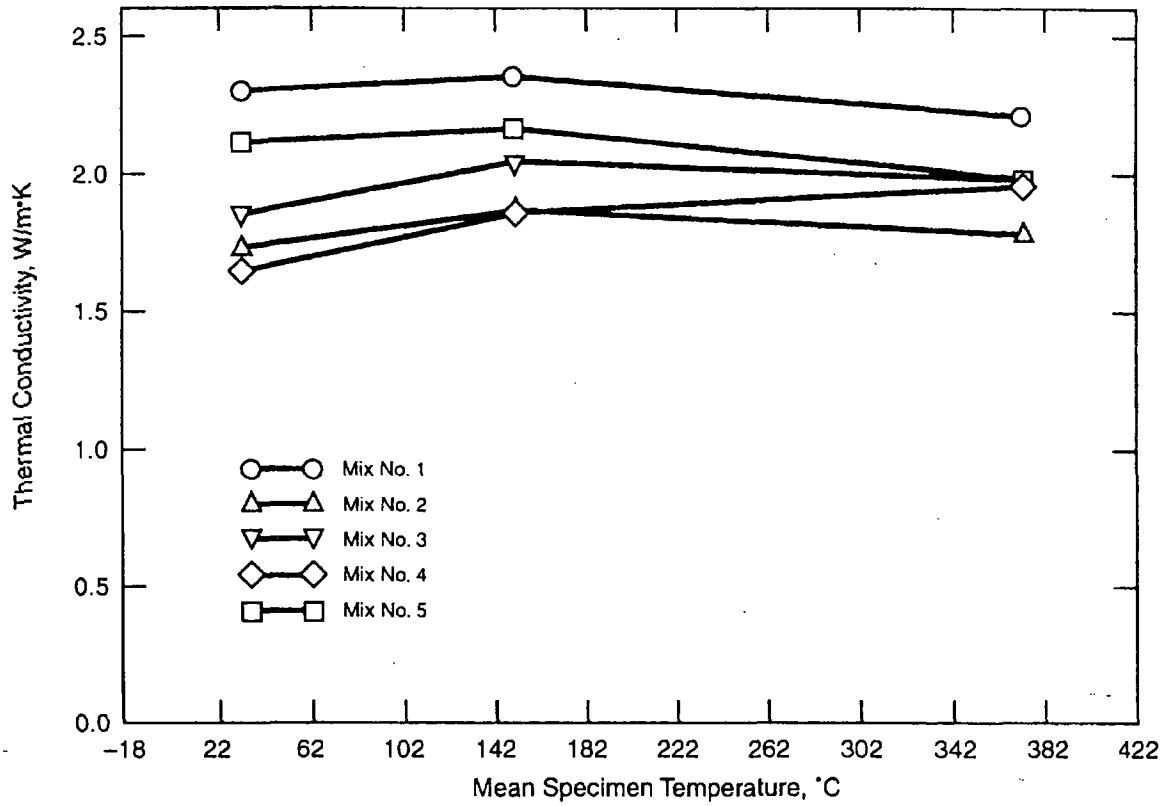

Figure 38. Thermal conductivity versus temperature for the five high strength concretes described in Table 2 [47-48]

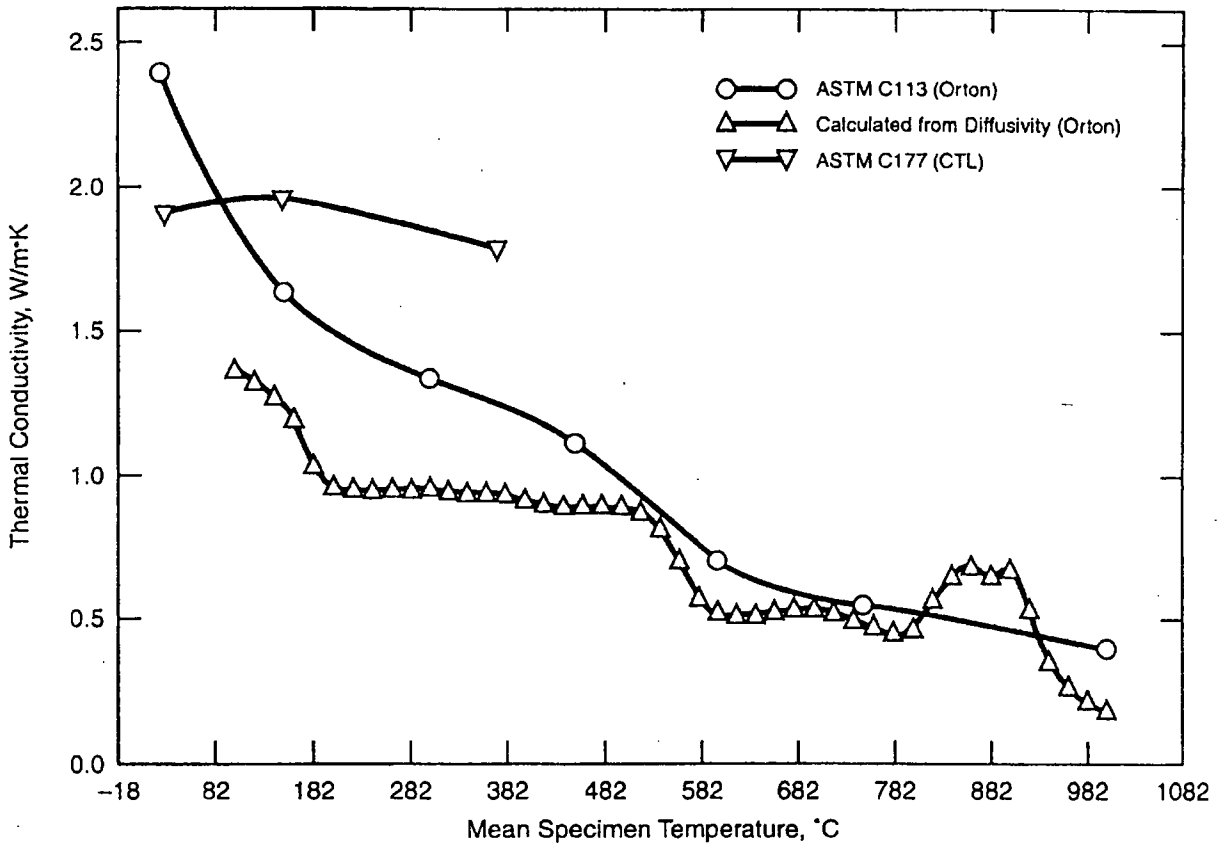

Figure 39. Thermal conductivity of oven-dried high-strength concrete mix No. 5, as determined by three different techniques [47-48]

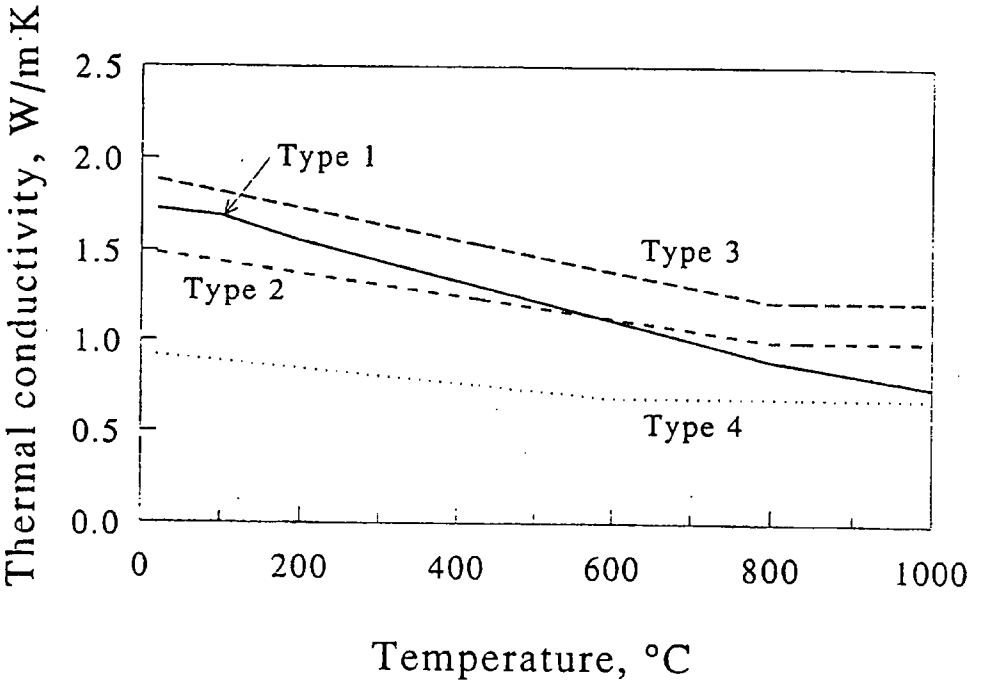

Figure 40. Thermal conductivity versus temperature curves used in the Ahmed model (see text).

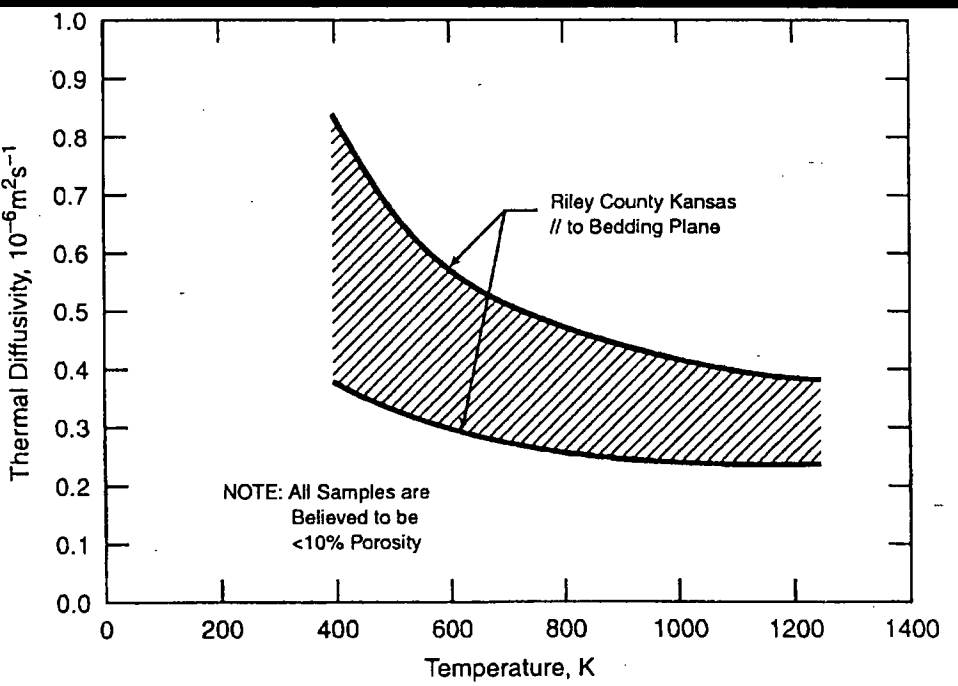

Figure 41. Thermal diffusivity of limestones [51].

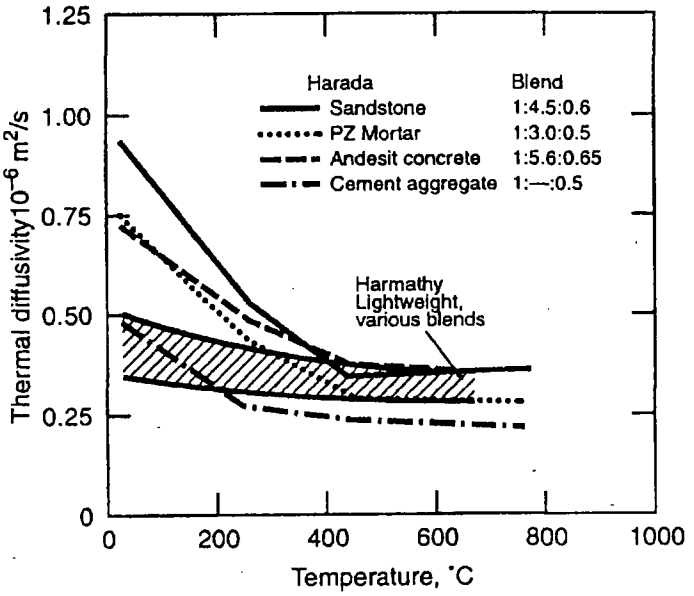

Figure 42. Thermal diffusivity of normal and lightweight concrete, mortar, and cement stone [35].

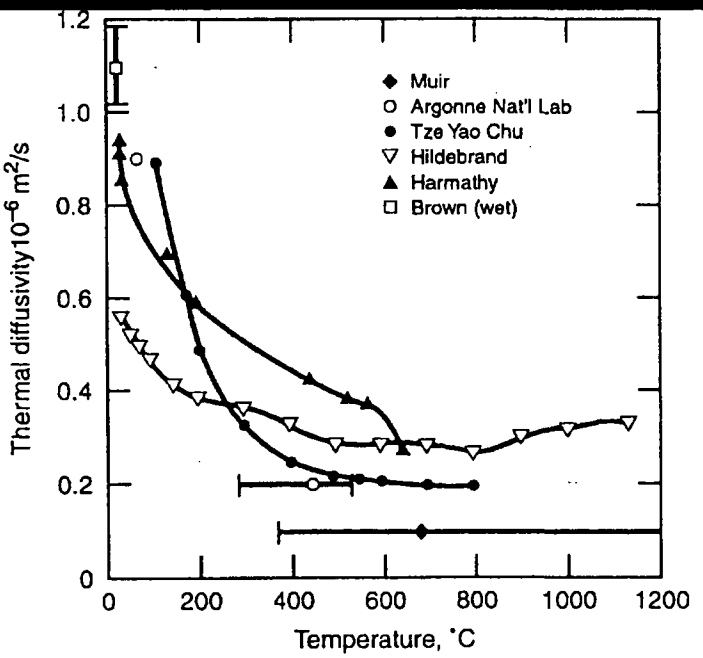

Figure 43. Thermal diffusivity of limestone concrete [35].

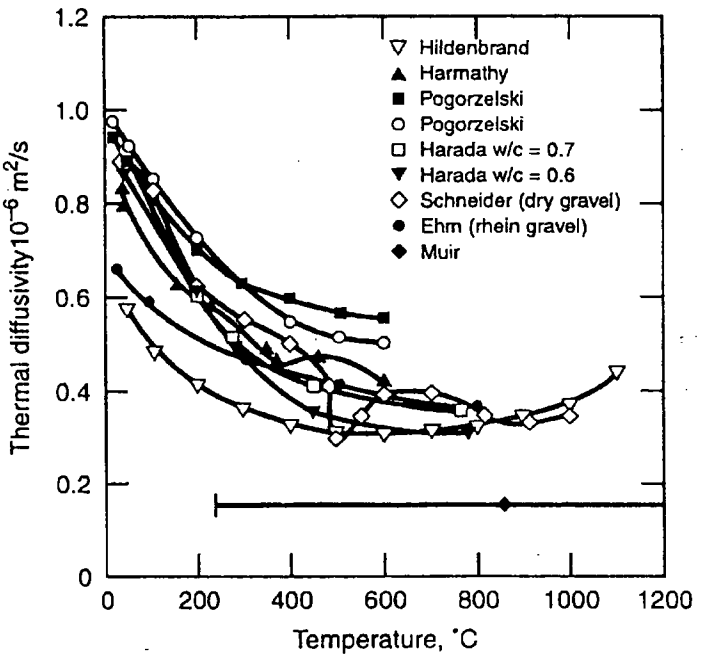

Figure 44. Thermal diffusivity of siliceous concrete [35].

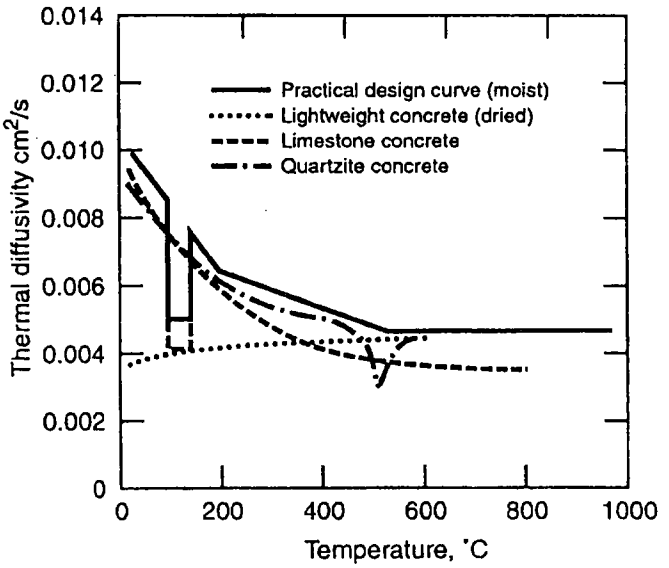

Figure 45. Thermal diffusivity of different concretes [38].

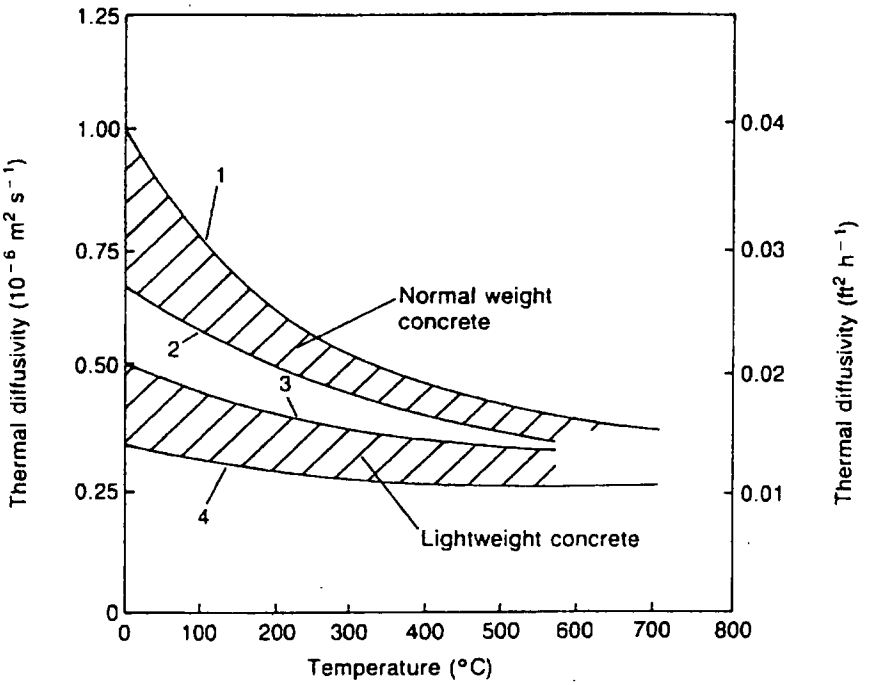

Figure 46. Effect of temperature on thermal diffusivity of concrete made with siliceous and calcareous aggregates and with lightweight aggregates [45].

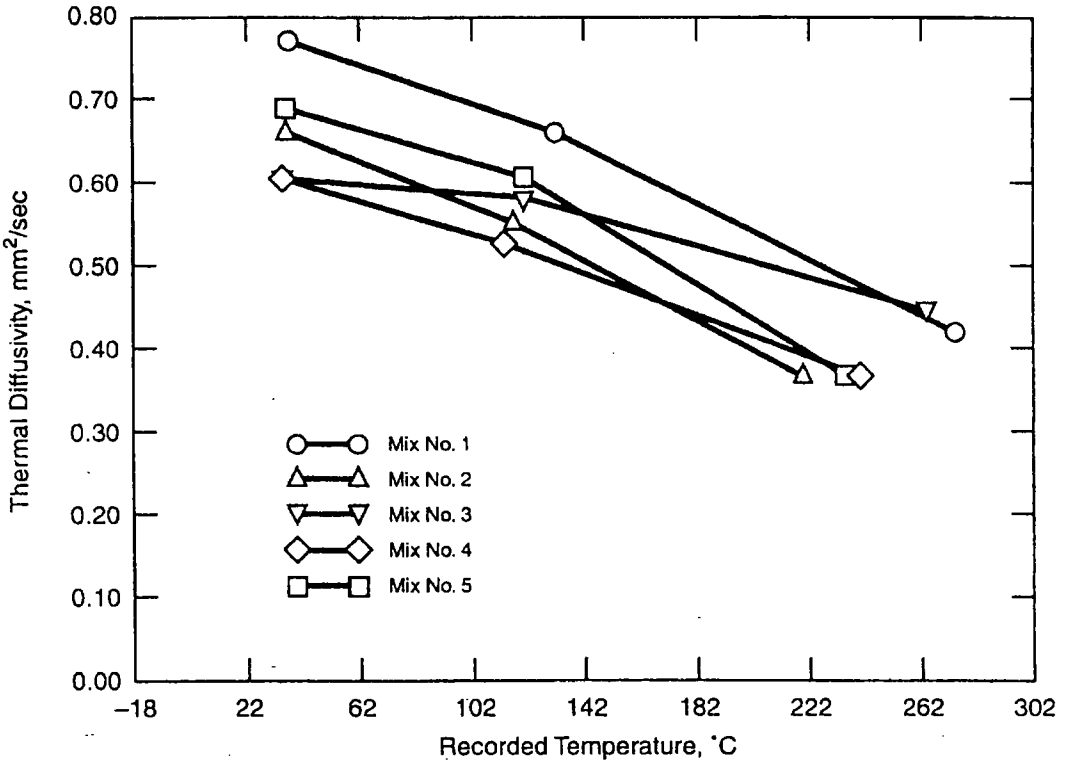

Figure 47. Thermal diffusivity versus temperature for the five high strength concretes described in Table 2 [47-48]

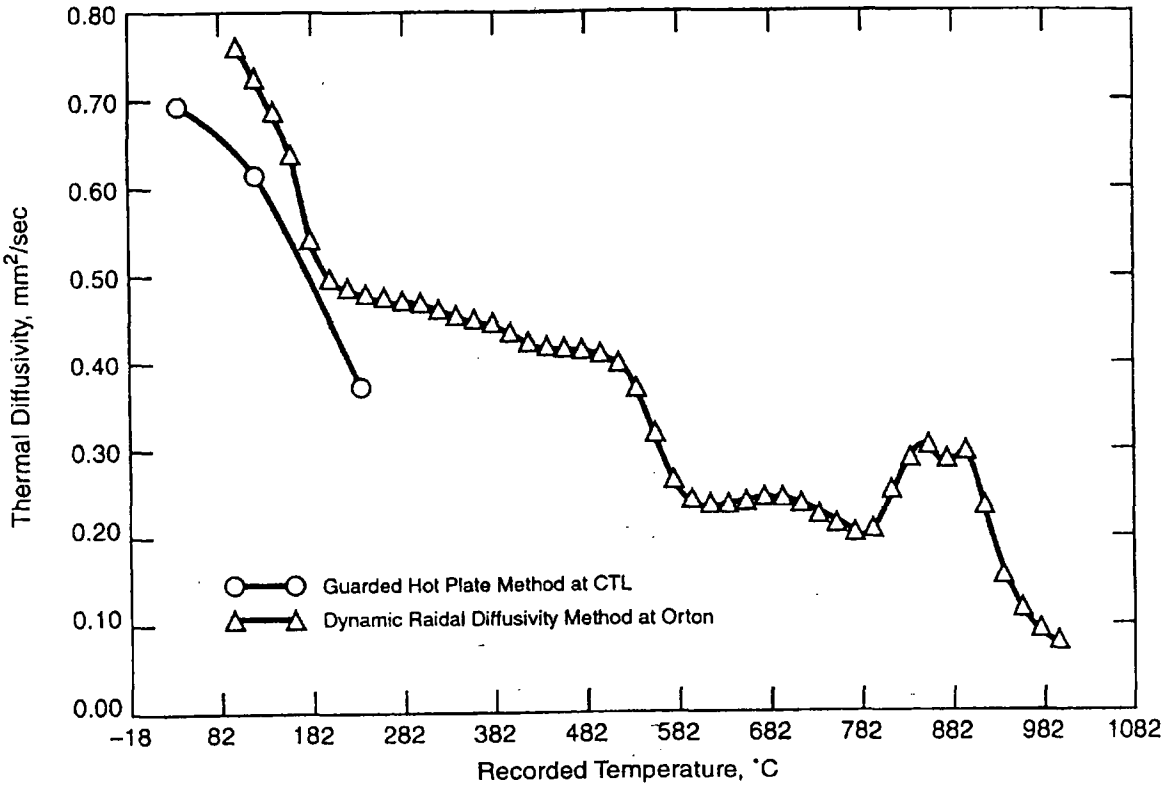

Figure 48. Thermal diffusivity of oven-dried high-strength concrete mix No. 5, as determined by two different techniques [47-48]

4. Correlations and Prediction of Thermal Properties

Concrete is a mixture of cement paste, fine aggregate, and coarse aggregate, with capillary pores and gel pores and some evaporable (as opposed to chemically bound) water. The general approach taken in this section is to examine various equations that can be used to predict a particular property of a mixture from the composition of the mixture and from the (same) property of each of the constituents. Two "mixture rules" are identified below. For the density and the heat capacity of a mixture, these rules reduce to very simple forms that are almost intuitively obvious. For a transport property such as conductivity or diffusivity, that depends upon how the different constituents or components are arranged, the situation gets more complicated, as is discussed in Section 4.3, below.

The simplest mixture rule is that of Bruggeman [61,41] which is

$$\phi^m = \sum_i v_i \phi_i^m \quad , \tag{55}$$

where ϕ is the particular property of interest for the mixture, ϕ_i is the property of the ith component, v_i is the volume fraction [m^3/m^3] of the ith component, and m is a dimensionless constant having a value between -1 and $+1$. The components of a mixture are often stated in terms of the mass fraction ω_i [kg/kg]. The volume fraction and the mass fraction are related to each other by

$$\omega_i = \frac{v_i \rho_i}{\sum_i v_i \rho_i} \quad \text{and} \quad v_i = \frac{\omega_i/\rho_i}{\sum_i \omega_i/\rho_i} \quad , \tag{56}$$

where ρ_i is the density of the ith component, $\sum_i v_i = 1$; and $\sum_i \omega_i = 1$.

A rather versatile mixture rule is that of Hamilton and Crosser [62] who suggest that the property (they were interested in thermal conductivity) of a two-component mixture be expressed as

$$\phi = \phi_1 \left[\frac{\phi_2 + (\eta - 1)\phi_1 - (\eta - 1)v_2(\phi_1 - \phi_2)}{\phi_2 + (\eta - 1)\phi_1 + v_2(\phi_1 - \phi_2)} \right] \quad , \tag{57}$$

where component 1 is the continuous component and η is an empirical constant. Harmathy [41] has rewritten this expression in the form

$$\phi = \frac{v_1\phi_1 + \gamma v_2 \phi_2}{v_1 + \gamma v_2} \quad , \tag{58}$$

where

$$\gamma = \frac{\eta \phi_1}{(\eta - 1)\phi_1 + \phi_2} \tag{59}$$

depends upon η and upon the property value for the two components, but does not depend upon the volume fractions of the components. When $\eta \to \infty$, Eqs. (58) and (59) reduce to the form of Eq. (55) with $m = 1$. When $\eta \to 1$, they reduce to the form of Eq. (55) with $m = -1$. Other limits of these mixture equations are examined in Section 4.3, below.

4.1 Mass, Volume, and Density

The density ρ of a mixture is given simply by Eq. (55) with $m = 1$, which is the same as Eq. (58) with $\gamma = 1$:

$$\rho = \sum_i v_i \rho_i \quad , \tag{60}$$

where ρ_i is the density of the ith component. The overall porosity of a composite solid consisting of several porous components is

$$P = \sum_i v_i P_i \quad , \tag{61}$$

where P_i is the porosity of the ith component.

Harmathy [41, pp. 75-84] states that the bulk density of cement paste can be predicted from the equation

$$\rho = \frac{W_c + W_n}{W_c/\rho_c + W_{wn}/\rho_w} = \frac{1 + (\bar{W}_n/W_c)\zeta}{1/\rho_c + (W_w/W_c)(1 + A)/\rho_w} \quad , \tag{62}$$

where W_c is the mass [kg] of cement in the original cement mixture, W_w is the "effective" [41] mass [kg] of water in the original mixture, W_n is the mass [kg] of non-evaporable water, as determined by drying over dry ice, for the cement paste in its present condition, $W_{wa} = W_w(1 + A)$ is the "adjusted" mass [kg] of water in the original mixture, $\bar{W}_n$ is the mass [kg] of non-evaporable water that would be present on complete hydration of the cement paste, A is the mass [kg/kg] of water, relative to W_w, that would fill the voids created by entrained or entrapped air in the original mixture, $\rho_c \approx 3150$ kg/m^3 is the true density of the solid cement used to make the paste, $\rho_w \approx 1000$ kg/m^3 is the density of free water and capillary water, and ζ [dimensionless] is a measure of the extent of hydration of the cement paste.

Since, for the present project, the room-temperature mass, volume, and bulk density of concrete specimens can easily be determined simply by measuring the mass and volume of a specimen, there is no need to examine further any correlations to attempt to predict these room-temperature values from the composition of the concrete.

The bulk density of a material at elevated temperatures can be computed as

$$\rho(T) = \rho_0 \cdot \frac{W(T)/W_0}{[\,1 + \Delta\ell(T)/\ell_0\,]^3} \quad , \tag{63}$$

where ρ_0 is the room temperature density, $W(T)/W_0$ is the ratio of the mass of a specimen at temperature T to the room temperature mass, usually obtained by thermogravimetry (TG), and $\Delta\ell(T)/\ell_0$ is the linear thermal expansion of a specimen at temperature T, usually obtained by dilatometry. The form of Eq. (63) implicitly includes the assumption that specimens have been at temperature long enough to reach steady-state conditions, i.e., long enough for moisture to be driven off or for chemical reactions, such as dehydration, to come to completion. Otherwise, the density will depend upon the thermal history of the material.

Assuming such steady-state conditions, the mass of the concrete is simply the sum of the masses of its constituents so that $W(T)/W_0$ is easily computed from the corresponding curves for the various constituents -- cement paste, fine aggregate, and coarse aggregate.

The linear-thermal-expansion coefficient is defined, at constant pressure P, as

$$\alpha = \frac{1}{\ell}\left(\frac{\partial \ell}{\partial T}\right)_P , \tag{64}$$

where ℓ is length and T is temperature. The volumetric expansion coefficient is

$$\beta = \frac{1}{V}\left(\frac{\partial V}{\partial T}\right)_P = -\frac{1}{\rho}\left(\frac{\partial \rho}{\partial T}\right)_P , \tag{65}$$

where V is volume and, as before, ρ is density. If the material is isotropic, $\beta = 3\alpha$.

Normally coefficients of thermal expansion are not measured directly but are obtained by differentiation of curves of measured length versus temperature. For example, the observed change in length might be represented by a least-squares-fit power series such as

$$\frac{\Delta\ell}{\ell_0} = \frac{\ell - \ell_0}{\ell_0} = a_0 + a_1 T + a_2 T^2 + a_3 T^3 + \cdots , \tag{66}$$

where ℓ_0 is the length at a reference temperature such as 20 °C. Then the linear thermal expansion coefficient would be computed as

$$\alpha = \frac{a_1 + 2a_2 T + 3a_3 T^2 + \cdots}{1 + a_0 + a_1 T + a_2 T^2 \cdots} . \tag{67}$$

For the present project, it is really not necessary to compute thermal expansion coefficients since the density of concrete can be computed from $\Delta\ell/\ell_0$, as shown in Eq. (63). However, in the literature, correlations for predicting the thermal expansion of mixtures are expressed in terms of expansion coefficients rather than $\Delta\ell$.

Turner [63] recommended that the thermal expansion coefficient of a mixture of isotropic constituents be computed using

$$\alpha = \frac{\sum_i \alpha_i B_i \omega_i / \rho_i}{\sum_i B_i \omega_i / \rho_i} \quad , \tag{68}$$

where α_i, B_i, ω_i, and ρ_i are, respectively, the coefficient of linear thermal expansion [m m^{-1} K^{-1}], the bulk modulus [Pa], the mass fraction [kg/kg], and the density [kg/m^3] of the ith component. This equation implicitly assumes that thermal shear stresses are low enough to be neglected, which may be the case for concrete since cement paste has a low shear modulus. If the bulk moduli are not known but it can be assumed that the various components of the mixture have similar values of Poisson's ratio, the bulk moduli will be nearly proportional to the corresponding Young's moduli and the Young's moduli, rather than bulk moduli, can be used in Eq. (68). If it can be assumed that all of the components of the mixture have very similar bulk moduli, Eq. (68) reduces to

$$\alpha = \sum_i v_i \alpha_i \quad , \tag{69}$$

where v_i is the volume fraction of the ith component. This simple mixing rule corresponds to the Bruggeman rule (Eq. (55) with $m = 1$ and to the Hamilton-Crosser rule (Eqs. (58) and (59)) with $\gamma = 1$ ($\eta \to \infty$). For normal strength or high strength concrete, the curve of thermal expansion versus temperature tends to be rather similar to that of the principal aggregate, which typically occupies roughly 70 percent of the volume of the concrete.

Equations (68) and (69) are known to provide bounds on the thermal expansion coefficient of composite materials. There are other, more complicated, formulae in the technical literature [64-68] that provide somewhat tighter bounds than these two equations. Some of these expressions require knowledge of the shear modulus of each of the constituents, in addition to the bulk modulus. In general, such information will not be available and so these other expressions are of little practical value for the present project. The bulk modulus of different rocks or minerals that might be used as aggregates vary considerably with their origin and their porosity [51] so that even Eq. (68) is of rather limited value unless bulk modulus data are available for the particular lot of aggregate. Since it is much easier to measure high temperature thermal expansion than it is to measure high temperature bulk modulus, Eq. (68) and the other expressions referred to at the beginning of this paragraph are of limited use.

Typical normal strength concretes expand in length by roughly 0.5 to 1.5 percent between room temperature and 1000 °C, corresponding to a decrease in density of roughly 1.5 to 4.5 percent. Thus, for the purposes of this project, it is not necessary to know the thermal expansion of the concrete very accurately. If approximate values for the bulk moduli of the constituents are known, Eq. (68) is probably the most practical formula for predicting the density of the concrete. Otherwise, the simple rule of mixtures, Eq. (69), should provide a fairly reliable estimate.

4.2 Enthalpy, Specific Heat, and Heats of Reaction

The good news is that (1) the enthalpy of a mixture of materials, such as those contained in concrete, can be computed from the masses and enthalpies of the individual components, provided that the

degree of hydration is known or measured; (2) the sensible specific heat will not vary much with changes in type and quantity of aggregate; and (3) the heat of sorption for water will not differ much from the heat of vaporization except for extremely small pores and any difference can be estimated theoretically from the pore size. The bad news is that the rate of heat release or absorption due to chemical reactions will vary with temperature, rate of temperature rise, degree of hydration, absorbed moisture content, and pore pressure.

The specific heat of a mixture does not depend upon how the components are distributed but simply upon the mass fraction and the specific heat of each component:

$$C = \sum_i \omega_i C_i \quad . \tag{70}$$

Harmathy [41] has described a detailed approach to estimating the specific heat of the various constituents of concrete, cement paste, fine aggregate, and coarse aggregate from the estimated chemical composition of each constituent and then computing the specific heat of concrete using Eq. (70). He goes into considerable detail and it does not seem necessary to replicate his work here. It is recommended that this approach be used for the present project, supplemented by experimental verifications.

In Harmathy's method of computing specific heats, he includes the enthalpy associated with release of water of hydration as part of an effective specific heat. In the PCA model for predicting temperatures and pore pressures of concrete exposed to fire conditions, that enthalpy is handled separately from the sensible specific heat of the concrete. Thus care will be required to ensure that the specific heats that are computed treat heats of vaporization, heats of sorption, and heats of dehydration in a manner consistent with that used in the model.

4.3 Thermal Conductivity and Thermal Diffusivity

Heat transfer through a two-component medium, in the absence of large-scale convection, can be considered as having three mechanisms: (a) true thermal conduction through the continuous and discontinuous components, (b) natural thermal convection within the pores or cells of the material, and (c) thermal radiation within the continuous and/or the discontinuous components. These several components of heat transfer are additive but in general are not independent. For a material with reasonably small cells or pores, such as concrete, heat transfer due to natural convection within the pores is small and can either be neglected or can be lumped in with the true conduction component. Large-scale convection, e.g., due to air and water vapor being driven through the concrete by a gradient in pore pressure is not explicitly considered in this section.

Since the sensible portion of the specific heat of concrete will not vary greatly with changes in the type and quantity of aggregate or even with degree of dehydration, the thermal conductivity and the thermal diffusivity will be affected in similar amounts by changes in the concrete. For concrete, both of these thermal transport properties are relatively weak functions of temperature, but they will change quite significantly as functions of porosity, absorbed moisture content, and extent of dehydration. Heating of concrete will result in differential thermal expansion between the cement

paste (which shrinks as it is heated) and the fine and coarse aggregates. Such expansion can greatly affect thermal contact resistance at the interfaces between different components and hence significantly change both thermal conductivity and thermal diffusivity. Pore pressure probably would not directly affect these properties very much but it will affect the extent of dehydration and the absorbed moisture content and thus could indirectly cause significant changes in thermal conductivity and thermal diffusivity.

Thermal conductivity is defined in terms of the ratio of the heat flux to the temperature gradient, in the absence of any mass flow. In general, there is no practical way to stop mass flow from occurring. For materials with low permeability and low mass diffusivity, the diffusive mass flow may be small enough that it should be possible to carry out transient thermal tests to determine thermal conductivity and/or thermal diffusivity before significant mass transfer can occur. However, evaporation and subsequent condensation of moisture can transfer large quantities of heat even for small mass flows so separation of conducted heat from the heat associated with mass transfer can be very difficult and tricky.

For a homogeneous material, thermal conductivity is defined as

$$\lambda = -\frac{q}{\nabla T} \quad , \tag{71}$$

where q is the heat flux and ∇T is the temperature gradient. For a heterogeneous material, this definition is extended to

$$\lambda_{effective} = -\frac{q}{\langle \nabla T \rangle} \quad , \tag{72}$$

where $\langle \nabla T \rangle$ is the average value of the temperature gradient over a region large in comparison with the size of the inhomogeneities. Unless the sample is large in comparison with the inhomogeneities, it is scarcely meaningful to attempt to define an effective thermal conductivity.

In a multi-component material the effective thermal conductivity will depend upon:

1. The thermal conductivity of each component.
2. The proportions of each component.
3. The manner in which the components are distributed; in particular
    a. whether or not the component is continuous in the direction of heat flow,
    b. whether the component distribution is ordered or random,
    c. the size, shape, and orientation of each segment of each component.
4. The nature of the contacts between the different components.
5. The emissive and absorptive properties of the components if there is significant radiative heat transfer through one or more of the components.

The problem of computing the effective thermal conductivity of a mixture from the thermal conductivities of the components is mathematically the same as the problem of computing the electrical conductivity, dielectric constant, or magnetic permeability of a heterogeneous mixture. There exists a large body of pertinent literature, much of which is covered in review articles [69-76].

The following discussion covers a few of the available mathematical relations for correlating the effective thermal conductivity of a mixture with the thermal conductivities of the individual components.

The simplest model for purposes of analysis is that in which the two components are arrayed in alternative parallel layers as shown in Figure 49. If the heat flow is parallel to the layers, the effective thermal conductivity is given by

$$\lambda = f_1 \lambda_1 + f_2 \lambda_2 \quad , \tag{73}$$

where f_1 and f_2 are the volume fractions of the components having thermal conductivities λ_1 and λ_2, respectively; this expression is simply the Bruggeman mixture rule, Eq. (55), with $m = 1$. If the heat flow is perpendicular to the component layers,

$$\lambda = \frac{\lambda_1 \lambda_2}{f_2 \lambda_1 + f_1 \lambda_2} \quad ; \tag{74}$$

this expression is the Bruggeman mixture rule with $m = -1$. Equations (73) and (74) represent the extreme limits of the thermal conductivity of a two-component mixture. These limits are shown in Figure 50 for the case $\lambda_1 = 10\,\lambda_2$. Although both Eq. (73) and (74) predict thermal conductivity values intermediate between the conductivities of the individual components, the conductivity obtained is very different for the two cases. Thus these limits are of relatively little use except for laminated materials.

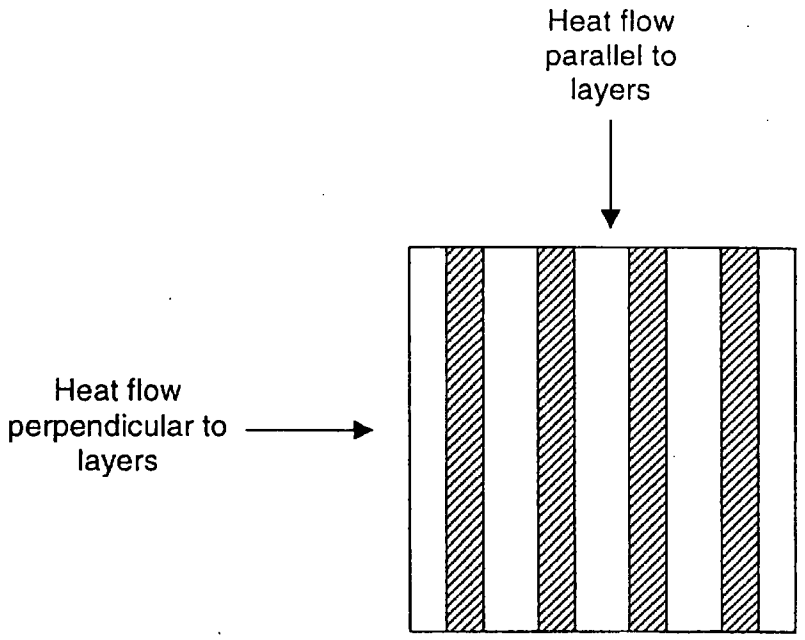

Figure 49. Two-phase material with phases distributed as parallel slabs.

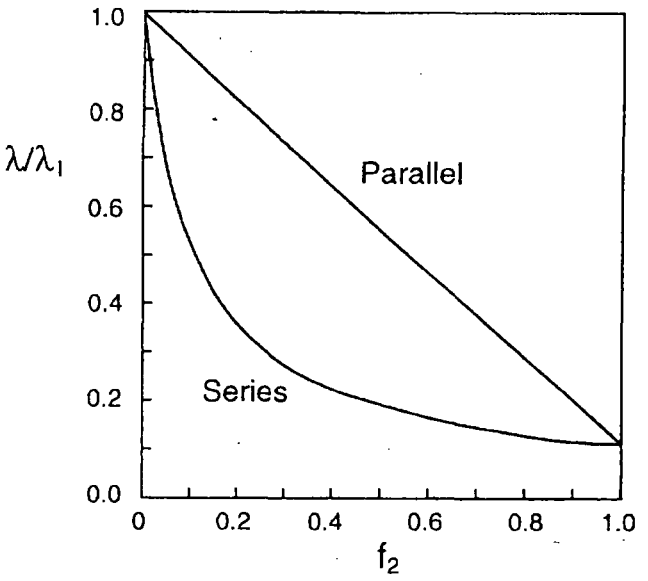

Figure 50. Effective thermal conductivity of a laminated material with heat flow parallel or perpendicular to laminations.

It is possible to obtain tighter limits for the thermal conductivity of a two-component mixture by calculating the apparent effective conductivity by each of two simple methods:

Series Slabs

The material is divided into thin slabs perpendicular to the direction of principal heat flow. The effective conductivity of each slab is computed by assuming that the two components act as conductors in parallel. The effective conductivity of the mixture is then computed by assuming that the slabs act as conductors in series.

Parallel Tubes

The material is divided into thin tubes or rods parallel to the direction of principal heat flow. The effective conductivity of each tube is computed by assuming-a that the two components act as conductors in series. The effective conductivity of the mixture is then computed by assuming that the tubes act as conductors in parallel.

Jackson and Coriell [77] have shown that these two methods provide upper and lower bounds for the true effective conductivity of a mixture. In order to calculate these bounds it is necessary to assume some sort of model representing the manner in which the components are deployed. Several investigators have represented a disperse second component by a cubic array of cubes as shown in Figure 51. The two methods described above can then be used to calculate limits for the effective conductivity of the mixture. Since there is some confusion in the literature on these calculations, it is worthwhile to spell out the steps and assumptions involved.

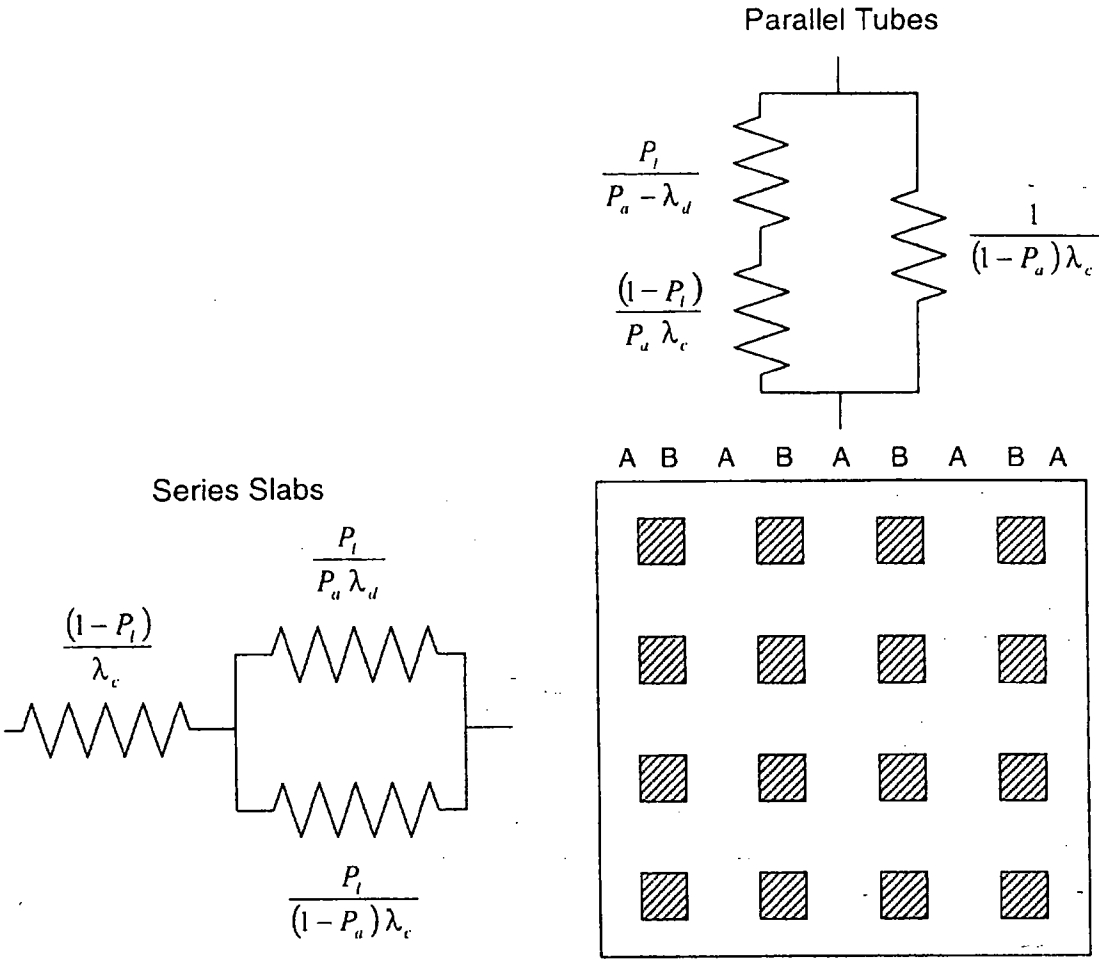

Figure 51. Cross-section of the model in which a disperse second phase is considered to be a cubic array of cubes.

Series Slabs

1. As shown in Figure 51, the mixture is divided into slabs (A) containing no disperse second component and into slabs (B) containing both continuous and disperse components. The effective conductivity of the B-slabs is computed, using Eq. (73), by assuming the disperse and continuous components act as conductors in parallel:

$$\lambda_B = P_a \lambda_d + (1 - P_a) \lambda_c \quad ,$$

where P_a is the fraction of the total area which contains the disperse component of conductivity λ_d and $(1 - P_a)$ is the fraction of the area which contains the continuous component of conductivity λ_c

2. The effective conductivity of the mixture is computed, using Eq. (74), by taking the A-slabs and the B-slabs in series:

$$\lambda = \frac{\lambda_A \lambda_B}{P_\ell \lambda_A + (1 - P_\ell)\lambda_B}$$

where $\lambda_A = \lambda_B$, λ_B was given above, and P_ℓ is the fraction of the total length containing the disperse component. Evaluation of this equation yields

$$\frac{\lambda}{\lambda_c} = \frac{(1 - P_a) + P_a \lambda_d/\lambda_c}{(1 - P_a + P_a P_\ell) + P_a(1 - P_\ell)\lambda_d/\lambda_c} \quad . \tag{75}$$

Parallel Tubes

1. In this approximation, the mixture is divided into parallel "tubes" (A) containing no disperse second component and "tubes" (B) containing, both components.

2. The effective conductivity of the B-tubes is computed, using Eq. (74), by assuming the disperse and continuous components to be in series:

$$\lambda = \frac{\lambda_c \lambda_d}{P_\ell \lambda_c + (1 - P_\ell)\lambda_d}$$

3. The effective conductivity of the mixture is computed, using Eq. (73), by assuming the A-tubes and B-tubes to be in parallel:

$$\lambda = P_a \lambda_B + (1 - P_a)\lambda_A \quad .$$

Evaluation of this equation yields:

$$\frac{\lambda}{\lambda_c} = \frac{P_\ell(1 - P_a) + (1 - P_\ell + P_a P_\ell)\lambda_d/\lambda_c}{P_\ell + (1 + P_\ell)\lambda_d/\lambda_c} \quad . \tag{76}$$

In the above derivations, it was stated that the model was a cubic array of cubes. In fact, it is not necessary to be so restrictive. For Eq. (75) to be valid, it is only necessary that the model can be divided into two types of slabs (perpendicular to the flow of heat)-one containing no disperse component and one having a fraction, P,, of disperse component which can be distributed in any manner. For Eq. (76) to be valid, it is only necessary that the model can be divided into-the two types of "tubes" (parallel to the flow of heat). Thus Eqs. (75) and (76) are, in principle, also applicable to dispersions of, for example, fibers or platelets oriented parallel or perpendicular to the flow of heat. However, these equations will not necessarily bound the true effective conductivity unless both are based on the same component deployment.

For a disperse component in the form of cubes, or in which cubes may be used to approximate an isometric disperse component, equations (75) and (76) may be recast in terms of the volumetric fraction of disperse component, which is designated as f. For the model used, it is easily seen that $P_a = f^{1/3}$ and $P_\ell = f^{2/3}$; with these substitutions, the forms usually seen are obtained:

Series Slabs

$$\frac{\lambda}{\lambda_c} = \frac{(1 - f^{2/3}) + f^{2/3}\,\lambda_d/\lambda_c}{(1 - f^{2/3} + f) + (f^{2/3} - f)\,\lambda_d/\lambda_c} \quad , \tag{77}$$

Parallel Tubes

$$\frac{\lambda}{\lambda_c} = \frac{(f^{1/3} - f) + (1 - f^{1/3} + f)\,\lambda_d/\lambda_c}{f^{1/3} + (1 - f^{1/3})\,\lambda_d/\lambda_c} \quad . \tag{78}$$

Although one would appear to be, on the face of things, considering a fairly complicated model in deriving Eqs. (77) to (78), a little thought reveals that the model reduces to the two simple electrical networks shown in Figure 51. In the series-slabs model, one effectively assumes that the continuous component has an infinite thermal conductivity normal to the principal flow of heat; thus this approach, resulting in Eqs. (75) and (77), always overestimates the effective thermal conductivity. In the parallel-tubes model, one effectively assumes that the continuous component has zero thermal conductivity normal to the principal flow of heat; thus this approach, resulting in Eqs. (76) and (78), always underestimates the effective thermal conductivity.

Maxwell derived an expression for the conductivity of a two-component dispersion of spherical particles of conductivity λ_d, imbedded in a medium of conductivity λ_c. This expression is rigorously valid for dilute dispersions where the average distance between dispersed particles is much larger than the particle size. Maxwell's relation can be written in the form:

$$\frac{\lambda}{\lambda_c} = \frac{2 - 2f + (1 + 2f)\,\lambda_d/\lambda_c}{2 + f + (1 - f)\,\lambda_d/\lambda_c} \quad . \tag{79}$$

The behavior of Eq. (79) for small f is more easily seen by expanding it in the form:

$$\frac{\lambda}{\lambda_c} = 1 - \frac{3f(1 - \lambda_d/\lambda_c)}{2 + \lambda_d/\lambda_c} + \frac{3f^2(1 - \lambda_d/\lambda_c)^2}{(2 + \lambda_d/\lambda_c)^2} - \cdots, \quad f \ll 1 \quad . \tag{80}$$

In Figure 52, the predictions of the series-slabs expression (Eq. (73)), the parallel-tubes expression (Eq. (74)), and the -Maxwell dilute dispersion expression (Eq. (79)) are compared for the case $f = 0.1$. For values of λ_d/λ_c near 1, all three expressions agree. However, if the thermal conductivities of the two components differ significantly, the series-slabs and parallel-tubes expressions disagree with the Maxwell expression, which should be very accurate for $f \leq 0.1$.

To predict the thermal conductivity of a dispersion having less than about 0. 1 volume fraction of isometric dispersed component imbedded in an isotropic continuous component, one should use the

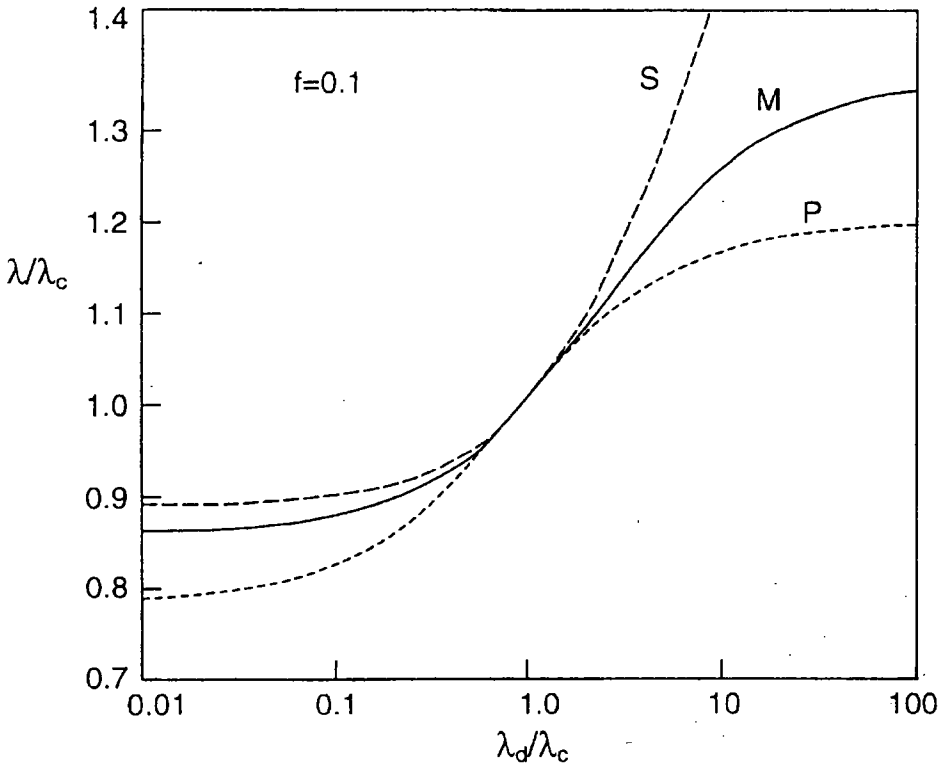

Figure 52. Computed effective conductivity of a dispersion of 0.1 volume fraction of a material of conductivity λ_d in a continuous matrix of material of conductivity λ_c.

S Series-slabs expression, Eq. (77)
P Parallel-tubes expression, Eq. (78)
M Maxwell dilute expression, Eq. (79)

Maxwell dilute dispersion expression, Eq. (79) or (80). The expressions obtained from the cubic array of cubes, Eqs. (75) to (79), should not be used for dilute dispersions in media having an isotropic continuous component. For anisotropic media, the Maxwell expression would have to be modified. For highly anisotropic media, the implicit assumptions of either infinite or zero lateral thermal conductivity of the continuous component might be more nearly met so that one of the series-slabs or the parallel-tubes expressions (Eqs. (75) to (79)) might be more accurate than in isotropic materials. For heat conduction in the poorest conducting direction, the series-slabs expressions, Eqs. (73) and (75), should be more accurate while for heat conduction in the best-conducting direction, the parallel-tubes expressions, Eqs. (74) and (76) should be more accurate.

The two expressions (Eqs. (77) and (78)) derived from the model of a cubic array of cubes disagree seriously with one another in the limiting case of small volume fractions of disperse component. However, for volume fractions of the disperse component approaching unity, Eqs. (77) and (78) converge to a common expression which, quite interestingly, is identical to the Maxwell dilute dispersion expression, Eq. (74).

A special case of interest is the effect of porosity on thermal conductivity. If the thermal conductivity of the continuous material is much greater than the effective conductivity of the pores, $\lambda_d/\lambda_c = 0$ and the above expressions reduce to:

Series-Slabs

$$\frac{\lambda}{\lambda_c} = \frac{1 - f^{2/3}}{1 - f^{2/3} + f} \quad , \quad \lambda_d \ll \lambda_c \quad , \tag{81}$$

which for small f reduces to

$$\frac{\lambda}{\lambda_c} = 1 - f - f^{5/3} + \cdots, \quad \lambda_d \ll \lambda_c \quad . \tag{82}$$

Parallel-Tubes

$$\frac{\lambda}{\lambda_c} = 1 - f^{2/3} \quad , \quad \lambda_d \ll \lambda_c \quad . \tag{83}$$

Maxwell Dilute Dispersion

$$\frac{\lambda}{\lambda_c} = \frac{2 - 2f}{2 + f} \quad , \quad \lambda_d \ll \lambda_c \quad , \tag{84}$$

which for small f reduces to

$$\frac{\lambda}{\lambda_c} = 1 - \frac{3}{2}f + \frac{3}{2}f^2 - \cdots, \quad \lambda_d \ll \lambda_c \quad . \tag{85}$$

In Figure 53 the predictions of Eqs. (81), (83), and (84) are shown for void volume fractions up to 0.1. Over this porosity range the Maxwell equation should be rather accurate if the porosity is in the form of dispersed, disconnected, isometric pores. For cement paste and porous aggregates, this generally will not be the case and Eq. (84) should then serve only as an upper limit for the effective thermal conductivity of a porous material.

For dispersions which are sufficiently dilute for Eq. (79) to be valid, neither the size distribution of the disperse particles nor the manner in which they are deployed are of consequence. However, these factors must be considered if the concentration of the dispersed component is increased. Lord Rayleigh treated the case of uniform spheres arrayed in a cubic lattice distribution. Meredith and Tobias extended Rayleigh's derivation by an additional term and obtained [70]:

$$\frac{\lambda}{\lambda_c} = 1 - \frac{3f}{\dfrac{2 + \lambda_d/\lambda_c}{1 - \lambda_d/\lambda_c} + f - \dfrac{1.315\,(1 - \lambda_d/\lambda_c) f^{10/3}}{4/3 + \lambda_d/\lambda_c + 0.409\,(1 + \lambda_d/\lambda_c) f^{7/3}}} \tag{86}$$

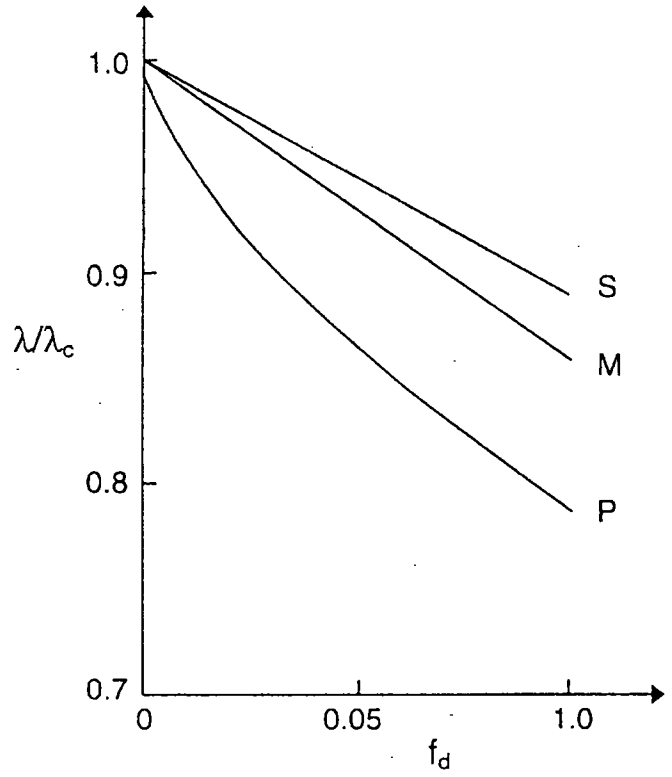

Figure 53. The effect of porosity on thermal conductivity as computed by:

S Series-slabs expression, Eq. (81)
P Parallel-tubes expression, Eq. (83)
M Maxwell dilute expression, Eq. (84)

for the conductivity normal to a side of the cube. If the term involving $f^{10/3}$ in the denominator of the right hand side is dropped, this expression reduces to the Maxwell dilute dispersion expression, Eq. (79). Equation (86) should be more accurate than Eq. (79) for values of f up to $\pi/6 = 0.524$, which is the maximum possible value for a cubic array of spheres.

A rigorous solution for the effective conductivity of a concentrated random array of particles of varying sizes has not been achieved. Several approximations have been developed which are useful in many cases. Bruggeman (see, e.g., [61,69-70]) developed an expression,

$$\frac{\lambda - \lambda_d}{\lambda_c - \lambda_d}\left(\frac{\lambda_c}{\lambda}\right)^{1/3} = 1 - f \ , \qquad (87)$$

which has proved rather effective in predicting the conductivity of a dispersion containing a wide range of particle sizes. For $\lambda_d \to 0$, Eq. (87) reduces to

$$\frac{\lambda}{\lambda_c} = (1 - f)^{3/2} \quad , \quad \lambda_d \ll \lambda_c \quad , \tag{88}$$

while for $\lambda_d \to \infty$,

$$\frac{\lambda}{\lambda_c} = \frac{1}{(1 - f)^3} \quad , \quad \lambda_d \gg \lambda_c \quad , \tag{89}$$

For a concentrated dispersion containing only a narrow range of particle sizes, the Bruggeman variable dispersion expression (Eq. (87)) tends to. overestimate the effect of the disperse component while the Maxwell expression (Eq. (74)) tends to underestimate. Meridith and Tobias [70] suggested an alternative semiempirical expression that predicts conductivity values intermediate between the Bruggeman variable dispersion equation and the Maxwell dilute dispersion equation:

$$\frac{\lambda}{\lambda_c} = \left[\frac{2(\lambda_d/\lambda_c + 2) + 2(\lambda_d/\lambda_c - 1)f}{2(\lambda_d/\lambda_c + 2) - (\lambda_d/\lambda_c - 1)f}\right]\left[\frac{(2 - f)(\lambda_d/\lambda_c + 2) + 2(\lambda_d/\lambda_c - 1)f}{(2 - f)(\lambda_d/\lambda_c + 2) - (\lambda_d/\lambda_c - 1)f}\right] \tag{90}$$

which reduces to:

$$\frac{\lambda}{\lambda_c} = \frac{8(2 - f)(1 - f)}{(4 + f)(4 - f)} \quad , \lambda_d \ll \lambda_c \quad , \tag{91}$$

and

$$\frac{\lambda}{\lambda_c} = \frac{(1 + f)(2 + f)}{(1 - f)(2 - f)} \quad , \quad \lambda_d \gg \lambda_c \quad . \tag{92}$$

Meredith and Tobias [70] contrast the predictions of the various expressions given above. For a given two-component system, all of these expressions predict two different conductivities, dependent on which component is assumed to be disperse. Bruggeman (see [61,69]) derived another approximate expression that should be applicable to mixtures where neither component is necessarily continuous:

$$f_1 \frac{\lambda_1 - \lambda}{\lambda_1 + 2\lambda} + f_2 \frac{\lambda_2 - \lambda}{\lambda_2 + 2\lambda} = 0 \quad . \tag{93}$$

In Figure 54, the predictions of the Bruggeman mixture equations are compared with those from the Maxwell dilute dispersion equation. It is seen that for small values of f_2, the Bruggeman mixture equation is in agreement with a dilute dispersion of particles of conductivity λ_2 in a matrix of conductivity λ_1, while for values of f_2 approaching unity the mixture equation predicts a conductivity due to particles of conductivity λ_1 dispersed in a matrix of conductivity λ_2.

There have not been enough accurate measurements of the thermal conductivity of well-characterized concretes to provide adequate experimental confirmation of any of the above equations. For well-defined systems (such as spheres dispersed in a continuous matrix) which are in good correspondence to the models used in deriving these equations, measurements of electrical

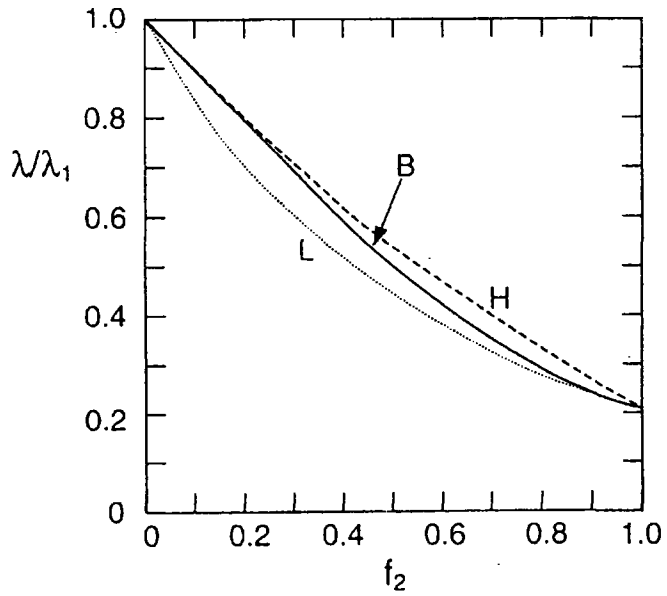

Figure 54. Computed effective thermal conductivity of a mixture.

B Bruggeman mixture expression, Eq. (93)
H Maxwell dilute dispersion expression, Eq. (79), high-conductivity phase continuous
L Maxwell dilute dispersion expression, Eq. (79), low-conductivity phase continuous

conductivity or dielectric constant have shown good agreement with the theoretical predictions of these equations. Concretes, in general, cannot be readily described in terms of a simple model such as spheres dispersed in a uniform medium, and hence in many cases the expressions cited above will indicate qualitatively the effect of an additional component but should not be relied upon for accurate quantitative predictions.

5. Experimental Techniques for Determination of Thermal Properties

5.1 Mass, Volume, and Density

At room temperature, the mass is easily determined by conventional weighing techniques and the volume easily computed from the measured dimensions of a specimen of well-defined geometry. The bulk density of the specimen is then computed from the mass and volume. In this report, the determination of porosity and of "true" density are not addressed.

The change in mass as a specimen is heated is conventionally determined using thermogravimetry (TG or TGA), which is a fancy way of saying that the sample is weighed while it is being heated. There are numerous commercial TGA apparatus available. Typically, a crucible containing the sample material is suspended, inside a vertical tube furnace, from a wire connected to an electronic balance above the furnace. The furnace is equipped with a temperature controller that permits increasing the furnace temperature at a pre-selected constant rate. Provision is made to minimize convection effects on the weighing process and to measure the sample temperature. Usually the furnace is purged with air or some other gas, at a very slow rate, to remove gases that evolve from the test sample. Some TGA apparatus is designed so that the pressure of the gas surrounding the sample can be controlled over a broad range.

Concrete and its components present a few challenges that homogeneous materials do not. Because concrete is a mixture, with the large aggregate typically being 1 to 5 cm in mean diameter, it is either necessary to use a rather large test sample of solid concrete in order to be statistically reliable or else it is necessary to grind up a large sample into a powder, blend it thoroughly, and test a small portion of the powder. Using a large sample of solid concrete presents several difficulties: (1) many TGA apparatus cannot handle a large sample, (2) a large sample will not be isothermal and it is therefore difficult to know what temperature to assign to the test results, and (3) a large sample will retard the evolution of gas – e.g., released water of hydration – from within the sample. Typically, one would expect TGA test results on large solid samples to be dependent upon the sample geometry and size, as well as upon the rate of heating. Using a small powdered sample means that the average temperature of the sample will be close to the temperature of the crucible and that the gas evolving from the sample can easily escape. However, mass loss data taken on a small powdered sample would not be representative of how the concrete would behave under fire conditions.

Rather than carrying out measurements on a solid or powdered sample of concrete, an alternative approach for determining mass change versus temperature is to measure, separately, the mass change of each of the components – cement paste, fine aggregate, and coarse aggregate – and compute the expected mass change for the concrete mixture. Unless fairly large samples can be tested, this latter approach is probably best, not only for mass change but for specific heat and heats of reaction.

As explained in Section 4.1, the change in volume due to heating is usually computed from data on the linear thermal expansion of a suitably large sample. Various techniques for measuring thermal expansion to high temperatures are described in [78-82]. Interferometric techniques, capacitance cells, and X-ray diffraction are more complex and expensive than necessary for engineering materials

such as ceramics or concrete. Thermal expansion measurements can be made using optical techniques, ranging from the use of a cathetometer to measure the change in position of fiducial marks on the specimen, to the use of more sophisticated laser equipment However, the simplest technique, and certainly the most commonly used technique, is push rod dilatometry. In this method the relative expansion of the specimen is transmitted out of the furnace using tubes or rods of some stable material. As described by Kirby [80], there are three variations of push rod dilatometry, with differential dilatometry being the preferred approach whenever possible. In differential dilatometry, the thermal expansion of the test specimen and the thermal expansion of a reference specimen, of nominally the same length, are brought out of the furnace using nominally identical push rods. Since the push rods hopefully experience the same longitudinal temperature distribution, their thermal expansions should be very nearly identical. Thus, the relative motion of the room-temperature ends of the push rods will be due to the relative thermal expansion of the test specimen and the (known) reference specimen.

Most high-temperature dilatometers use specimens no larger than 5 mm in diameter by 50 mm long. Considering that the high-strength concrete of interest to NIST in this project will have coarse aggregate nominally 13 mm in size, thermal expansion specimens of the order of 100 to 200 mm in length should be used if possible. If no other laboratory can handle such large specimens, it would not be too difficult to build a dilatometer at NIST that could handle such sizes.

5.2 Enthalpy, Specific Heat, and Heats of Reaction

There are numerous methods for determining specific heat and heats of reaction[83-93]. Most of the high-temperature techniques that would be suitable for concrete or its constituents are painfully slow and therefore data acquisition is expensive. An exception is differential scanning calorimetry (DSC), which is now the most commonly used procedure for measuring specific heat and for studying reaction kinetics. Most DSC equipment uses very small samples, typically a fraction of a gram in the form of powder, and can only handle measurements up to about 600 °C. For a material such as concrete, it would be very difficult to obtain representative samples of such small size. There are, however, a few commercial instruments that can accommodate large enough samples to be representative of concrete and that can make measurements at temperatures up to 1200 °C or higher. While the sensible heat capacity would not vary significantly with pressure, the reaction kinetics may be seriously affected by the high pore pressures that may occur in concrete exposed to fire conditions. Almost all commercial TGA and DSC equipment operates at atmospheric pressure or below. If commercial equipment can be found that can measure larger samples under controlled pressures, the enthalpy and mass loss measurements should be relatively straightforward. An alternative to using a pressurized system would be to measure on solid specimens of sufficient size that there will be significant internal pore pressures.

5.3 Thermal Conductivity and Thermal Diffusivity

In determining thermal conductivity or thermal diffusivity of concrete, it is important to recognize and deal with the influence of moisture migration. Traditionally, most thermal conductivity

measurements are made under steady-state conditions with thermal conductivity being computed from a geometrical factor, a heat input, and a temperature difference. The apparatus is operated either under conditions of constant heat input, with the resultant temperature difference being measured, or under conditions of constant temperature difference, with the resultant required heat flux being measured. Under such conditions, it may not be possible to measure the thermal conductivity corresponding to a given uniform moisture content in the specimen since the imposed temperature gradient can drive the moisture to the cold side of the specimen where it will collect or escape, depending upon the experimental configuration. Sometimes the moisture migration is sufficiently slow that it appears as if steady-state conditions have been achieved but the data may not yield appropriate thermal conductivity values.

For moist materials, it often is preferable to determine the apparent thermal conductivity or apparent thermal diffusivity under transient or periodic conditions so that data can be acquired without the moisture being driven away. Considerable care and understanding are required to ensure that the technique selected will yield property values that are appropriate for the end-use application. Analysis and interpretation of the results obtained from transient or periodic tests requires caution and an understanding of the limitations of the technique selected. For example, the differential equation that describes conductive heat transfer in an isotropic material of thermal conductivity λ, density ρ, and specific heat C is $\nabla\cdot(\lambda\nabla T) = \rho C(\partial T/\partial t)$, where T is temperature and t is time. If the thermal conductivity is independent of position and of temperature, it may be factored out on the left-hand side, yielding $\nabla^2 T = (1/\kappa)(\partial T/\partial t)$, where $\kappa = \lambda/\rho C$ is the thermal diffusivity. Thermal diffusivity is a questionable parameter if the thermal conductivity is not constant or if there are terms in the differential equation representing other forms of heat transfer, such as radiation or, in the present context, heat transfer associated with moisture migration. Even if an apparent thermal diffusivity is defined for a given test method, analysis would be required to determine whether or not it would be appropriate for use in predicting heat transfer under field use conditions. In general, it is better to use the appropriate analysis of the experimental data to obtain the volumetric specific heat and the apparent thermal conductivity.

The first concern in most techniques for measuring thermal conductivity is to force the heat flow to be unidirectional. Since, under steady-state conditions, heat flow is proportional to a geometric factor, a thermal conductivity, and a temperature difference, the direction of heat flow must be controlled by controlling one or more of these variables. The experimenter's freedom in adjusting these parameters is constrained, sometimes severely, by the often-conflicting requirements of being able to accurately measure total heat flow, geometry, and temperature differences. Very practical considerations, such as available specimen size, frequently constitute severe constraints on apparatus design.

It is not possible to directly measure the heat flow *in* a specimen; one must, rather, measure the heat flow *into* a specimen or *out of* a specimen. This necessitates that not only must transverse heat losses or gains from or to the specimen be prevented or accounted for but, further, there must be no unaccounted-for losses or gains between the specimen and the location at which the heat flow is measured. The most common method of measuring heat flow into a thermal conductivity specimen is to measure the electrical power dissipated in a heater at the hotter end of the specimen. In other "absolute" methods, the heat flow out of a specimen is sometimes measured by a "flow calorimeter,"

with which one observes the temperature rise and flow rate in a circulating liquid of known heat capacity, or by a "boil-off calorimeter," with which one observes the boil-off rate of a fluid of known heat of vaporization. In some types of apparatus, the heat flow is determined from the temperature difference or gradient in another material of hopefully known thermal conductivity that hopefully has the same heat flow; a special case of this type of apparatus would be one using a heat flow meter that is calibrated using one or more specimens of known thermal conductivity. This investigator's bottom line on comparative versus absolute methods is that one should not use comparative methods, including heat flow meter apparatus, unless there are absolute methods available that enable accurate testing of calibration specimens of the same size, and under the same environmental conditions, as are required in the comparison apparatus.

It is not possible to directly measure the temperature *gradient* in a specimen; one must, rather, measure the temperature *difference* between two or more locations and then compute the average temperature gradient. Consider a specimen held between a heat source and a heat sink. If the total thermal resistance of the specimen is large compared with the thermal contact resistances between the source and the specimen and between the specimen and the sink, then the temperature drop across the specimen can be taken as equal to the temperature of the source minus the temperature of the sink and it is not necessary to install temperature sensors in the specimen. However, if the specimen has a low thermal resistance such that thermal contact resistances are not negligible, it is necessary either to correct for these contact resistances or, what is usually done, to install temperature sensors in the specimen.

Measurement techniques, both steady-state and non-steady-state, for determination of thermal conductivity have been extensively reviewed [94,86,87]; for high-temperature measurements, the state-of-the-art has not changed significantly since these reviews were completed. Many of the test methods used for thermal conductivity and thermal diffusivity are described in the proceedings of the International Thermal Conductivity Conference, dating back to 1961.

5.3.1 Steady-State Methods

Most thermal conductivity measurements are made under steady-state conditions, which typically take some hours to achieve. For example, the NIST high-temperature guarded hot plate typically takes 4 to 6 hours to reach steady state. By that time, most of the moisture would be driven out of the specimen, so that the thermal conductivity values achieved would essentially correspond to a dry state.

The vast majority of the various techniques for steady-state measurement of thermal conductivity can be categorized under the headings given below (Types 1 through 7 utilize longitudinal heat flow).

Type 1. Absolute axial heat flow in a rod

This type of apparatus usually use a specimen whose length is very long compared to its diameter, with the specimen held coaxially in a guard cylinder whose inside diameter is typically two to four times the specimen diameter, the space between the specimen and the guard being filled with thermal

insulation. Such apparatus is mainly intended for good thermal conductors, such as metals or high density, high purity ceramics. For materials such as concrete that have quite low thermal conductivity, it would be very difficult to provide adequate guarding, particularly at high temperatures where the thermal conductivity of available insulations is not much lower than that of concretes. In addition, the time to reach thermal equilibrium increases approximately as the square of the specimen length so that long specimens should not be used when it is desired to attain equilibrium before moisture is driven off.

Type 2. Comparative cut-bar apparatus

This type of apparatus typically uses a specimen whose length is comparable (within a factor of, say, 2) with its diameter. The specimen is placed between two rods of known thermal conductivity and the thermal conductivity of the specimen computed from the ratio of the temperature gradients in the known and unknown specimens. As for Type 1 equipment, a coaxial guard and thermal insulation are used to control heat gains or losses. This design avoids the problems of providing the specimen with an attached heater and heat sink. Depending upon the thermal resistance of the specimen, thermocouples may be installed in it or the temperature difference across the unknown specimen may be computed by extrapolation of temperatures measured in the known specimens. For low-thermal-conductivity materials, adequate guarding is difficult. For the thermal conductivity range of concrete, there are not suitable reference materials over the temperature range of interest.

Type 3. Absolute cut-bar apparatus

This type of apparatus can accommodate specimens of similar geometry to those that are used in comparative cut-bar apparatus. However, the apparatus is "absolute," in that the heat flow is determined by measuring the input power to an electrical heater. The only apparatus of this type of which the principal investigator is aware is the one he designed and built at NBS in the early 1960s. By use of sophisticated mathematical analysis and careful experimental procedures, good data were acquired at temperatures up to 1200 °C. In order to make accurate measurements on a material with as low a thermal conductivity as that of concrete, a fairly large (e.g., 10 cm) specimen diameter would be required.

Type 4. Guarded hot plate apparatus

This type of apparatus, intended for use on specimens having relatively low thermal conductivity, utilizes a circular or square specimen whose diameter or edge length is typically an order of magnitude larger than the thickness of the specimen. A guarded hot plate apparatus consists of a heated metering plate, which may be square or circular, separated by a narrow insulating gap from a surrounding coplanar guard plate. Typically, similar specimens are placed on either side of the hot plate; the outside surfaces of the specimen are held between constant temperature cold plates. In operation, the electrical power input to the guard plate is adjusted, usually automatically, so that a multiple-junction differential thermocouple spanning the guard gap has zero output, indicating that there is no temperature difference across the guard gap. Thus the electrically generated heat input to the metering plate flows perpendicularly from both sides of the plate through the specimens to the cold plates. Guarded hot plate apparatus are typically quite reliable at moderate temperatures but

the agreement among different laboratories is not very good at elevated temperatures. The current high-temperature guarded hot plate apparatus at NIST can only be used to about 450 °C. NIST plans to design and build guarded hot plate apparatus for use to about 1200 °C, but that project will require several years. The only commercial high-temperature guarded hot plate apparatus that have been available in recent years are the Holometrix Model GHP-200, which accommodates circular specimens up to 20 cm in diameter, and the Holometrix Model GHP-300, for specimens up to 30 cm square. With the higher-temperature heaters from Holometrix, both models are advertised for use at temperatures up to 650 °C. Anter Laboratories plans to manufacture guarded hot plate apparatus based on the design of equipment developed at the National Physical Laboratory (United Kingdom). All such guarded hot plate apparatus requires a long time to reach equilibrium, thus precluding the possibility of obtaining valid thermal conductivity data before chemical reactions, such as loss of water of hydration, take place.

Type 5. Unguarded hot plate apparatus

This type of apparatus is similar to a guarded hot plate apparatus but the hot plate is made so thin and to have such a low lateral thermal conductance that is effectively self-guarding so that no separate guard is required. The hot plate for such an apparatus has a low thermal capacity so that it can have a fast thermal response, facilitating a rapid approach to thermal equilibrium. The absence of a guard simplifies the design and the operation of this type of apparatus, as well as allows more rapid operation. As will be discussed below under transient methods, an unguarded hot plate apparatus can be operated in either steady-state or transient mode.

Type 6. Guarded flat plate calorimeter

This type of apparatus typically uses a specimen in the form of a flat slab whose thickness is much less than its lateral dimensions. Rather than measure the electrical input to a heat on the hot side of the specimen, a calorimeter is used to measure the heat flow from a central region on the colder side of the specimen. Either a flow calorimeter or a boil-off calorimeter can be used. Since the heat capacities and heats of vaporization of pure fluids are well known, such calorimeters can, at least in principle, be quite accurate. The standardized flow calorimeter apparatus is known to have significant errors for specimens having low thermal conductivity. A disadvantage of either type of guarded flat plate calorimeter is that the colder side of the specimen remains at a temperature not too much greater than that of the calorimetric fluid so that for high hot-side temperatures there is a very large temperature difference across the specimen, making it more difficult to obtain accurate curves of thermal conductivity versus temperature.

Type 7. Heat flow meter apparatus

This type of apparatus also uses a slab-shaped specimen, held between a hot plate and a cold plate. A heat flow meter, which typically consists of a thin sheet of poorly conducting material with provision to measure a signal that is proportional to a temperature difference through the meter, is placed on one or both sides of the specimen. The apparatus is calibrated using specimens of known thermal conductance. Such apparatus is the workhouse of the building insulation industry since it can take data quite rapidly (typically it is operated with the hot and cold plates at fixed temperatures)

and is easy to operate. There do not appear to be any commercial heat flow meters of adequate sensitivity that can cover the temperature range of interest for this project. More critically, there are no suitable reference standards that could be used to calibrate a high-temperature heat flow meter apparatus.

Type 8. Radial heat flow apparatus

This type of apparatus typically uses a specimen in the form of a right circular cylinder, with heat flow radially outward from a heater located in a hole along the axis of the specimen. For solid specimens, it is customary to have temperature sensors located at different radii within the specimen, usually at several angular positions. The apparatus may have end heaters to provide guarding or the specimen may be long enough that it is self-guarding. Such equipment has been used quite successfully on materials ranging from powders to solid ceramics to metals and at temperatures well in excess of what is needed for the present project. Instrumenting the specimens typically is time consuming and the apparatus requires a long time to reach thermal equilibrium.

5.3.2 Transient Methods

Thermal diffusivity, which is a measure of the speed of propagation of heat into a material during changes of temperature with time, is arguably easier to measure than thermal conductivity since it does not require a power or heat flow measurement and since it does not require waiting for thermal equilibrium (steady-state) to occur. For materials and conditions where the only form of energy transport is via heat conduction, under conditions where the thermal conductivity can be assumed to be constant, and when the density and specific heat are very well known from other measurements, it is reasonable to measure thermal diffusivity and compute thermal conductivity values. For the present project, it is essential that **thermal conductivity, not thermal diffusivity**, be measured. Referring back to earlier parts of this report, it is easy to see (p. 5) that Eq. (2) follows from Eq. (1) if the thermal conductivity is constant. However, when there are other modes of energy transfer, thermal diffusivity is not a viable concept. For example, in the energy conservation equation (p. 15, Eq. (53)) for the Ahmed model, all of the material properties are complicated functions of temperature (and possibly of time and pore pressure) so that one cannot combine thermal conductivity and volumetric specific heat as a single property, such as thermal diffusivity. The models that might be used to predict simultaneous heat and mass transfer in porous media require thermal conductivity, not thermal diffusivity as a material property. Accordingly, thermal diffusivity measurements are not further considered in this report.

With one notable exception, there have been relatively few investigations that used transient techniques to obtain thermal conductivity directly (as opposed to measuring thermal diffusivity and computing thermal conductivity). There is a very extensive body of literature on hot-wire or probe methods of measuring thermal conductivity. These techniques have been used extensively for measurements on liquids, where it is important to complete a measurement before significant convection can occur, and for soils and rocks, where it is desired to complete a measurement before there is significant moisture migration. We will also refer to the "transient strip method," which is effectively a variant of the hot-wire method. There have been some studies concerned with thermal

conductivity measurements using one-dimensional transient heat flow through slabs of material; a variant of this approach is considered to be the most viable one for the present project and therefore such techniques are examined in some detail. Note that transient methods of measuring thermal conductivity do require measurement of power or heat flow, which is not the case for thermal diffusivity measurements.

Hot-Wire or Probe Methods

In the so-called hot-wire method, a heater wire is embedded in a specimen, or sandwiched between two slabs. When the heater is turned on, its temperature-time history, or that of a nearby temperature sensor, can be used to compute thermal transport properties. The values thus obtained correspond to a small region of the specimen close to the heater wire and again there are serious questions as to whether or not that small region is representative of a concrete sample with large aggregates. Normally, one would want to have an effective specimen thickness, or effective probing depth, that is roughly an order of magnitude larger than the largest aggregate.

The hot-wire technique and the variant known as or the probe method, both of which are sometimes called the line-heat-source method, were reviewed in 1969 by Pratt [95] and, briefly, by Danielson and Sidles [96]. At that time, the hot-wire method had been used mainly for fluids or for loose-fill or blanket-type insulating material. During the period since these reviews were completed, there has been rather extensive development, particularly in Europe, of the hot-wire method for use on refractory materials, including firebrick. These developments have been reviewed by Davis [97]. Line heat source techniques have, over the past two decades, become the method of choice for most determinations of the thermal conductivity of liquids. The probe method is a variant of the hot-wire technique in which a heater and temperature sensor are packaged in a rigid probe, or needle, that can be inserted into the specimen material. Recently Wechsler [98] reviewed probe methods for use on solids and insulating materials. Flynn has provided a recent extensive bibliography [99] of these methods, which includes abstracts for almost 300 relevant papers and reports. In the early 1980s, another group at NIST carried out an investigation of hot wire techniques for measuring the thermal conductivity of refractory materials at high temperatures [100].

Because of the extensive use of this technique on moist materials, and because of its possible applicability to the present project, a comprehensive discussion of the theoretical basis of this method is included in Appendix A. This discussion includes consideration of the effects of contact resistance between the probe and the specimen and the influence of the finite thermal capacity of the probe on the temperature-versus-time curves that are used to determine thermal conductivity.

There are several variations of the hot-wire method. Sometimes a thermocouple is used to measure the temperature rise of the heater wire with, typically, the thermocouple measuring junction being welded to the heater wire and the thermocouple leads going off perpendicularly to the heater wire. With regard to the present project, this approach has two major disadvantages. First, for a specimen with a fairly low thermal conductivity, the thermocouple leads may carry heat away from the junction, resulting in erroneous temperature measurement. Second, for an inhomogeneous material such as concrete, the temperature along the heater wire may vary with position and the use of a thermocouple at a single location provides very little averaging of that temperature distribution. A

better approach is to use the heater wire as a resistance thermometer to measure its own temperature, thus providing averaging over the region between the potential taps. A probe also may have either one or more discrete temperature sensors or may use the heater as a resistance thermometer. For radial heat flow in cylindrical coordinates, which is the goal with line-heat-source methods, measurement of the temperature-versus-time history of the heat source can provide, at least for homogeneous specimens, accurate data for thermal conductivity but can provide only very limited accuracy for specific heat or for thermal diffusivity. Better accuracy can be obtained for these two properties if the temperature is measured at a known radius from the axis of the heater, either instead of or in addition to the temperature at the axis. Thus, a separate temperature sensor (thermocouple or resistance thermometer), installed at a measured radius from the heater, is sometimes used instead of, or perhaps in addition to, the sensor used to measure the heater temperature.

When the hot-wire technique is used on solid specimens, it is customary to sandwich the heater and temperature sensors between two slabs of the specimen material, with one of them being grooved to accommodate the wire(s). Usually, the heater is turned on and assumed to provide constant power for the duration of the test. It is necessary for the specimens to be large enough that they can be assumed to behave as an infinite body during the duration of the measurements.

Transient Strip and Transient Patch Methods

Gustafsson [101-103] and his colleagues have developed a variant of the hot-wire technique that uses a narrow strip (typically a few millimeters wide) of pure metal as both a heater and a resistance thermometer. Their "transient hot-strip method" has been used with a strip of foil sandwiched between two specimens or by vapor deposition of a heater directly onto the specimen, the latter approach resulting in an extremely thin heater. The authors argue [101] that: "The fraction of the heat that is 'hindered' by the air-filled or oil-filled slots, created at the edges of the strip, when pressing it between the two plane test pieces, is consequently negligible. To achieve a similarly favourable geometrical configuration for the transient hot-wire method would be extremely difficult, or impossible. This fact actually limits the hot-wire method to fluids or to such solids that can be cast satisfactorily around the wire."

Brydsten and Bäckström [104] developed a technique wherein they deposited two metal strips on the specimen, with one strip serving as a heater and the other strip serving as a resistance thermometer, as shown in Figure 55.

The operational procedures for these two transient hot-strip techniques are essentially the same as those for the transient hot-wire or probe methods.

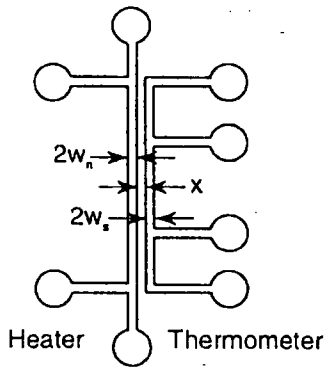

Figure 55. Pattern of copper and nickel strips used by Brydsten and Bäckström [104]. The strip on the left is the heater, and the strip on the right is the thermometer.

Gustaffsson and his colleagues [105-106] also have developed a technique, which they call the "transient plane source technique," in which the heater is a circular or rectangular patch that resembles a resistance strain gage. Since the heater does not cover the entire area of the specimen, as is the case for the methods described below, it seems more appropriate to refer to this technique as a transient patch method. Operationally, this technique is similar to the transient hot-wire and transient hot-strip methods.

Transient Plane Source Methods

In this report, the term "transient plane source methods" is used to designate transient methods in which the heater(s) is(are) nominally the same size, laterally, as the specimens and heat is constrained, by edge insulation or guarding, to flow in one direction, say, parallel to the z-axis, in Cartesian coordinates. Some of the possible boundary conditions for transient plane source methods are shown in Figure 56 [107]. Only the techniques in which the heat input is measured will provide values for thermal conductivity. The techniques with temperature boundary conditions can only provide thermal diffusivity values.

Vernotte [108] suggested that the adiabatic boundary condition required for the boundary conditions shown in Figure 56(a) could be achieved by using mirror images, as shown in Figure 57, where the four slabs in the center of the stack are the specimen material and the ebonite slabs are intended to provide thermal insulation. His assumption was that half of the power provided to each heater would flow toward the center of the stack, resulting in the desired temperature-time history at the mid-plane of the stack.

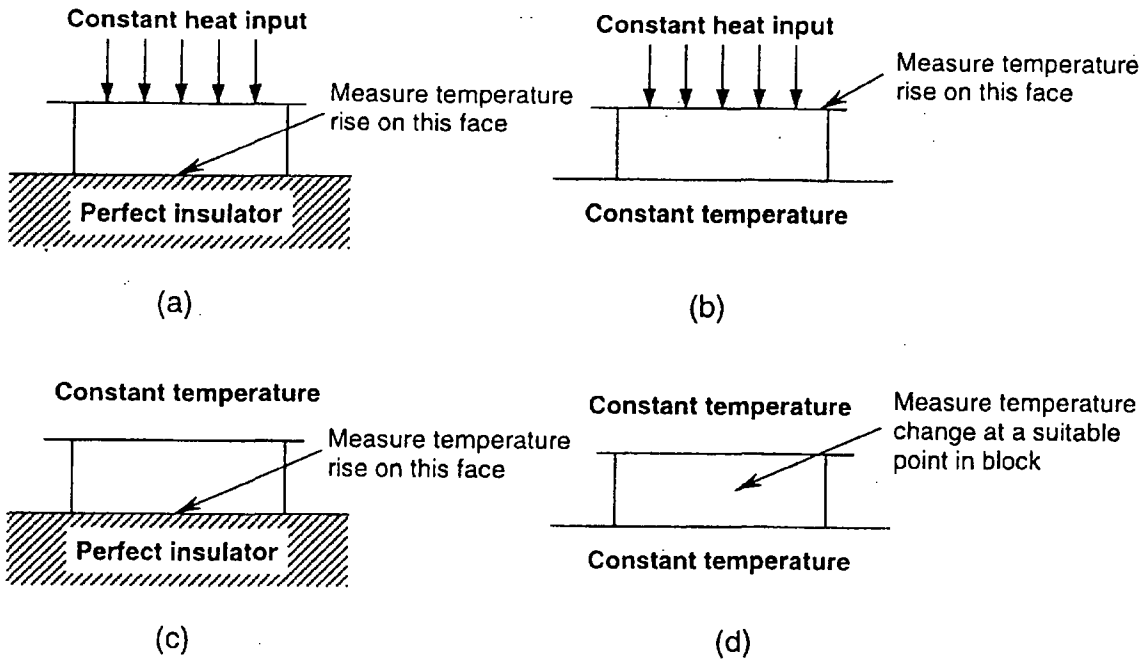

Figure 56. Possible boundary conditions for transient plane source methods for determination of thermal conductivity or thermal diffusivity [107].

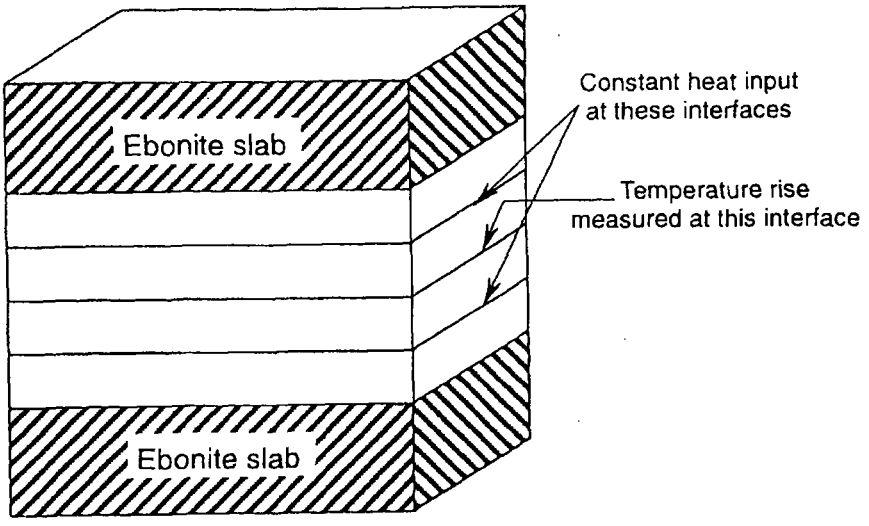

Figure 57. Experimental arrangement suggested by Vernotte [108,107].

Vernotte did not report having made any experimental measurements. When Clarke and Kingston [107,109] implemented the method suggested by Vernotte, they found that, for tests on good insulators, the assumption that half of the heat input flows toward the interface where temperatures are measured was not satisfied. They added additional slabs of specimen material, as shown in Figure 58 in order to provide "a further mirror image." Their heater consisted of a strip of foil interleaved through the stack as shown in Figure 58. In order to minimize the effects of the heat generated in the loops on the heater strip, they provided a "guard pile" of specimen material on either side of the "main pile." Basically this same technique was later used by several other investigators [110-113]. Bastian [113] carried out an extensive set of calculations to ascertain the effects of, among other things, the finite heat capacity of the heaters and thermal contact resistance between the heaters and the specimens.

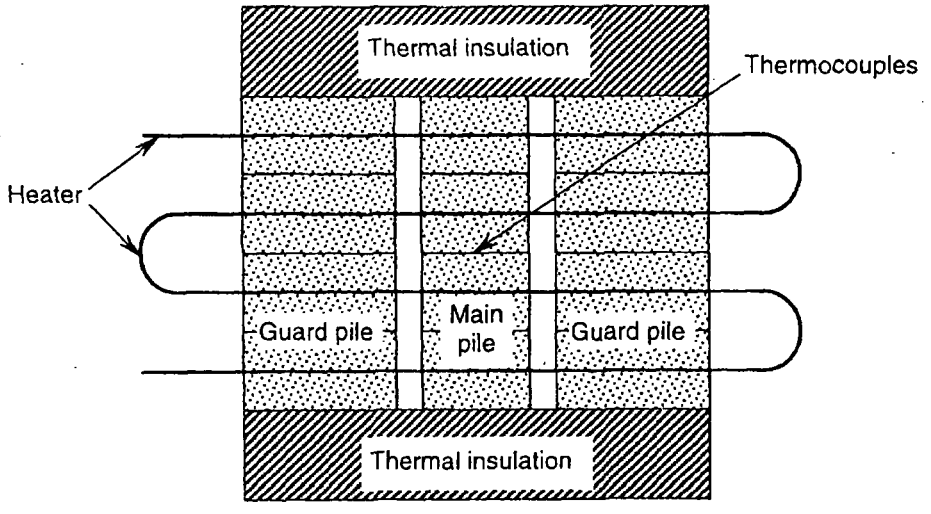

Figure 58. Experimental arrangement used by Clarke and Kingston [107,109].

For the present project, the use of such a thick stack of specimens is not appropriate since it would take so long to bring such a thick mass to a uniform temperature that any chemical reactions, such as loss of water of hydration, would have been completed long before the thermal conductivity test could even begin.

Before discussing other transient techniques, it is useful to make reference to the thin-heater thermal conductivity apparatus developed by Hager [114-120]. While this apparatus is normally allowed to achieve steady-state conditions, the construction of the hot plate is similar to the design that is proposed for the present project, and the Hager apparatus could be operated in a transient mode.

Figure 59 shows the apparatus used by Harmathy [121] to determine the thermal conductivity of concrete and other building materials to high temperatures under transient conditions. The arrangement of the various pieces of specimen material are shown in more clearly in Figure 60. The entire assembly was wrapped in a 1/2-inch layer of ceramic fiber insulation and placed in a furnace so as to minimize heat losses. For high-temperature tests, Harmathy used palladium foil as the heater. Normally, direct current was used to energize this heater. However, Harmathy states:

> For materials which are regarded as electrical insulators at room temperature, there are generally no experimental problems up to about 700°C. Above this temperature serious difficulties may arise, which are associated partly with a gradual increase in the electrical conductivity of such materials, and partly with **a slow charge build up on the metal foil and thermocouple wires following the switching on of the foil heating. This last phenomenon is caused mainly by space-charge polarization, and is less serious when alternating current is used for foil heating**. [emphasis added]

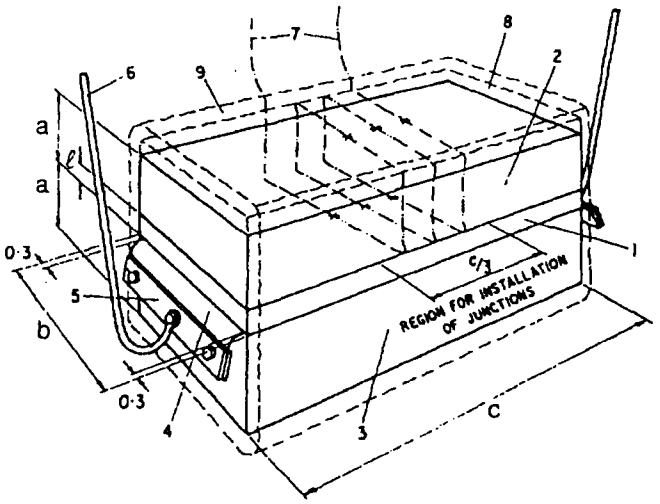

$\ell = \sqrt{262.5\ \kappa}$
a = 4 ℓ
b = 80 to 100 mm
c = 2 b

1 = measuring piece
2 = top piece
3 = bottom piece
4 = palladium foil
5 = Inconel clamps
6 = Alumel lead wire for foil heating
7 = thermocouple wires
8 = Fiberfrax cover
9 = over-all Fiberfax wrapping
X = thermocouple junctions

Figure 59. Isometric view of experimental setup used by Harmathy [121].

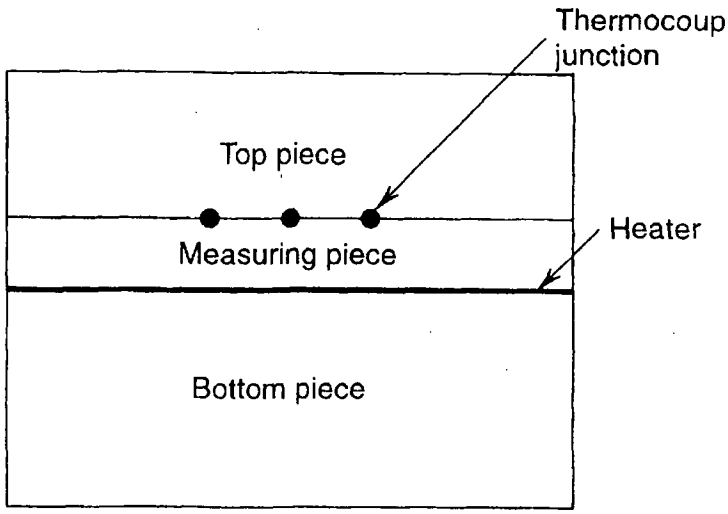

Figure 60. Specimen assembly used by Harmathy [121].

Harmathy used step-function heating, i.e., he turned on the heater and let it remain on until the desired temperature-time history had been recorded. The experiment had to be kept short enough for his assumption that the specimens were effectively of infinite thickness to be met. His mathematical analysis required that the power to the heater be constant, which is not really true for constant-current input to a heater made from a pure metal that has a significant increase in resistance with increasing temperature. His analysis also did not account for the finite heat capacity of the heater, or for contact resistance between the heater and the specimen pieces or between the "top piece" and the "measuring piece." Other investigators who have used Harmathy's method include [122-125]. The experimental setup used by Plummer, *et al.* [126], to measure the thermal diffusivity of ceramics to high temperatures was quite similar to that used by Harmathy although these investigators did not measure the power to the heater and thus could not obtain thermal conductivity.

The most popular method of measuring thermal diffusivity of homogeneous materials is the pulse method, in which the front side of a specimen is irradiated by a short pulse from a laser or a flash lamp and the temperature-versus-time history on the back side is recorded. In such tests it is difficult to measure accurately the energy input by the pulse so that thermal conductivity cannot be obtained directly. A few investigators have used a thin electrical heater to generate a short pulse of energy and measured the energy input so that thermal conductivity could be computed. Dzhavadov [127] used the experimental setup shown in Figure 61, in which three slabs of specimen material, of equal thickness, were sandwiched between two plates that were maintained at constant temperature. The heater at the lower interface was energized for a duration of the order of 0.1 s and the resultant temperature pulse at the upper interface was recorded. From these data the thermal conductivity, specific heat, and thermal diffusivity were computed.

The experimental technique used by Giedd and Onn [128] more closely resembles the classical pulse method in that only one slab of specimen material was used. The heater was a thin film of graphite sprayed onto one side of the specimen. A thermocouple was attached to the back side of the

specimen. A very short pulse was used. The thermal diffusivity was computed from the half rise-time on the back surface and the specific heat was computed from the overall temperature rise of the specimen after it reached thermal equilibrium.

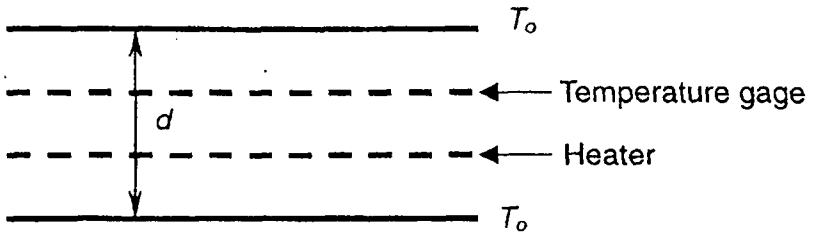

Figure 61. Specimen geometry used by Dzhavadov [127].

In a fairly recent book, Kubičár [129] describes, and references, the rather extensive work that has been carried out at the Institute of Physics of the Slovak Academy of Science, in Slovakia, using electrical pulse methods to determine thermal conductivity, specific heat, and thermal diffusivity. The general experimental approach used at that laboratory is shown in Figure 62. The thermal properties of the specimen are computed from the energy input to the heater, the maximum temperature reached, and the time at which that maximum occurred. These investigators generally used specimens of cylindrical geometry. Kubičár summarizes the procedures that have been developed to deal with the effects of heat loss from the convex surface of the specimens, the finite heat capacity of the heater, and thermal contact resistances between the specimen pieces.

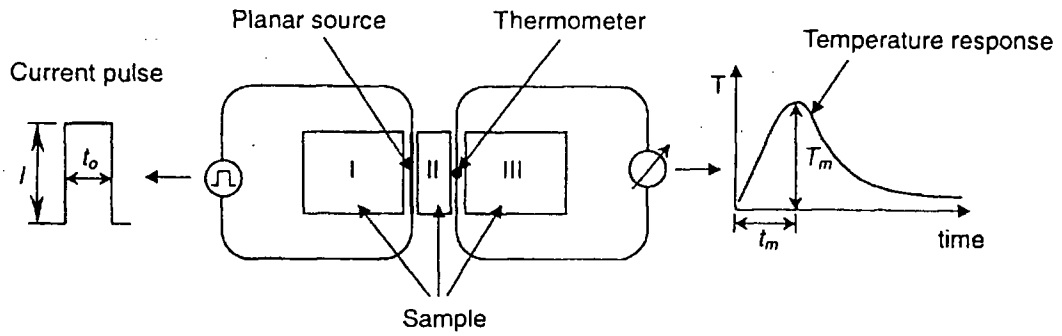

Figure 62. Experimental layout of the pulse method used by Kubičár and colleagues [129].

Piorkowska and Galeski [130-131] describe a transient technique for determining thermal conductivity in which the experimental layout is similar to that of a guarded hot plate apparatus. However, the operational procedure is rather unique. In effect, the "cold plates" are programmed such that their temperature increases linearly with time. Shortly, depending upon the specimen thickness, after this programmed ramp is initiated, the temperature drop across the specimens approaches a quasi-steady-state value. These investigators carried out two runs on the same specimens, with different

power inputs to the heater but with the cold plates increasing at the same rate. By subtracting the measured temperature differences for these two runs, the transient terms cancel out and the thermal conductivity can be obtained, even though true steady-state conditions are never achieved. The subtraction of the two temperature-difference histories also eliminates the influence of heat production or absorption associated with phase transformations. These authors provide extensive mathematical analysis of their method, including allowing the thermal conductivity of the specimen to be temperature dependent.

Some of the analysis procedures used for the above transient plane-source techniques are summarized in Appendix B.

6. Availability of Apparatus and Testing Services

The NIST Building and Fire Research Laboratory does not have in-house capability for carrying out the required thermal property measurements over the temperature range of concern (room temperature to 1200 °C). The NIST Ceramics Division, in the Materials Science and Engineering Laboratory (MSEL), has the capability to carry out measurements of specific heat, heats of reaction, and thermal expansion to temperatures higher than 1200 °C. However, their equipment uses rather small samples. The DTA or DSC measurements would be made on powdered samples of the order of a gram or so. The dilatometer uses a specimen nominally 5 mm in diameter by 25 mm long. The Ceramics Division has no capability to measure thermal conductivity or thermal diffusivity above room temperature. The NIST Metallurgy Division, in MSEL, can measure thermal diffusivity of small specimens only at temperatures above 900 °C.

In order to locate laboratories, outside of NIST, that could provide some or all of the needed measurements the following request was faxed to vendors of thermal property measurement equipment:

> The NIST Building and Fire Research Laboratory is working on a project concerning the response of concrete to fire conditions. My responsibilities include determining what thermal property measurements need to be made and locating laboratories where these measurements can be done reliably.
>
> The materials of interest are normal-strength and high-strength Portland cement concrete, with quartz sand as the fine aggregate and (nominally) 1/2-inch limestone as the coarse aggregate. We are primarily interested in the effective overall thermal properties of the mixture of cement paste, fine aggregate, and coarse aggregate. Thus for properties, such as thermal conductivity and thermal expansion, that depend upon the sizes and deployment of the various phases, the test samples need to be large compared to the size of the coarse aggregate. For properties such as heat capacity, heats of reaction, and mass loss, that only depend upon the mass fraction of the various components, either the test samples need to be large compared to the aggregate size or else it would be necessary to grind and blend rather large pieces of concrete and then take smaller representative samples from the resultant powder. Ideally, we would like to obtain data from room temperature to 1200 C but are interested in laboratories that could obtain data to temperatures above 800 C.
>
> We have not yet determined how many tests will be required for each type of measurement. However, there will be at least four types of concrete and it probably will be appropriate to make measurements at several heating rates. Thus we anticipate that approximately 10 to 12 tests for each property will be required. The thermal properties of interest include:
>
> Heat capacity and heats of reaction (probably DSC measurements)
>
> Mass loss versus temperature (TGA)

Thermal expansion

Thermal conductivity (direct measurements, not from thermal diffusivity)

Thermal diffusivity (?)

At this time, NIST does not wish to buy the instruments to carry out such measurements, but prefers to contract to have the measurements made elsewhere. If you only sell thermal measurement instrumentation and do not provide testing services, please let me know of laboratories that can provide such measurement services, either using your instrumentation or other types of equipment. It also would be helpful if you could indicate which models of your instrumentation would be most appropriate for which types of measurement.

If you do provide testing services, please let me know what types of measurements you can provide, along with the temperature range, estimated accuracy, and required sample size and geometry for each type of measurement. Also, please provide an estimate of the costs of such measurements.

A similar request was faxed to numerous laboratories, but with the next-to-last paragraph omitted.

As of the date of this report, the following vendors and laboratories have been contacted (for foreign vendors, the city of their U.S. subsidiary is given):

Anter Corporation (Pittsburgh, PA)

Ball Aerospace Systems (Boulder, CO)

Cahn Instruments (Madison, WI)

Colorado School of Mines (Golden, CO)

Concurrent Technologies Corporation (Johnstown, PA)

Coors Analytical Company (Golden, CO)

duPont Fibers Analytical Services (Wilmington, DE)

Geoscience Ltd. (San Diego, CA)

Hauser Laboratories (Boulder, CO)

Harrop Industries, Inc. (Columbus, OH)

Hazen Research, Inc. (Golden, CO)

Holometrix, Inc. (Bedford, MA)

Industrial Science & Technology Network, Inc. (York, PA)

Iowa State University (Ames, IA)

Itertek Testing Services (Richardson, TX)

Leach & Garner Technology (North Attleboro, MA)

Linseis Inc. (Princeton Junction, NJ)

Arthur D. Little, Inc. (Cambridge, MA)

Lockheed Martin (Orlando, FL)

Louisiana Productivity Center (Lafayette, LA)

The M&P Lab (Schenectady, NY)

Massachusetts Materials Research (Boylston, MA)

MATECH Associates (Scranton, PA)

Materials Research & Engineering, Inc. (Boulder, CO)

Mettler Toledo Inc. (Hightstown, NJ)

National Physical Laboratory (Teddington, Middlesex, United Kingdom)

Netzsch Instruments, Inc. (Paoli, PA)

Northrop (Rolling Meadows, IL)

Oak Ridge National Laboratory (Oak Ridge, TN)

Orton Ceramic Foundation (Westerville, OH)

Owens Corning Fiberglas Corporation (Granville, OH)

Polymer Solutions Inc. (Blacksburg, VA)

Precision Measurements and Instruments Corporation (Philomath, OR)

Research Triangle Institute (Research Triangle Park, NC)

SETARAM (Grand Prairie, TX)

Shimadzu (Columbia, MD)

Showa Denko America (New York, NY)

TA Instruments (New Castle, DE)

Texas Research Institute (Austin, TX)

Tg Technologies, Inc. (Freehold, NJ)

Theta Industries (Port Washington, NY)

TPRL, Inc. (West Lafayette, IN)

Tulane University (New Orleans, LA)

Ulvac Technologies, Inc. (Methuen, MA)

University of Illinois (Champaign, IL)

As replies from these organizations have come in, there have been numerous suggestions of other laboratories that might be able to carry out some of the measurements. Thus, it is anticipated that there will be further additions to the above list.

While it is too early to select particular laboratories to carry out the needed measurements, it is clear that there will be multiple laboratories with the capability to measure specific heat, heats of reaction, mass loss, and thermal expansion. A few laboratories can measure thermal conductivity (cut-bar method) or thermal diffusivity (flash method) on specimens that are too small to be representative of concrete. Thus far, only one laboratory has indicated that they can measure thermal conductivity using a guarded hot plate apparatus. As discussed earlier in this report, a guarded hot plate apparatus is too slow to allow measurements to be made before chemical reactions go to completion.

7. Design of New Apparatus for High-Temperature Thermal Conductivity Measurements

The cross section of the proposed test setup is shown in Figure 63 – it consists of a thin-foil heater sandwiched between two similar specimens, which are in turn sandwiched between two "cold plates." The specimens will be nominally 200 mm square with thicknesses in the range of 10 to perhaps 50 mm. The cold plates will simply be square, thin sheets of corrosion-resistance metal, such as nichrome or inconel; further analysis may indicate that it would be desirable to provide a guard gap in these cold plates in order to reduce lateral heat flow. NIST has purchased a high-temperature furnace for this project – the outside surfaces of the two cold plates will be exposed to the air in the furnace. The edges of the stack, shown in Figure 63, will be insulated with ceramic fiber insulation.

An expanded view of the thin-foil heater is shown in Figure 64 (not to scale). The heater will consist of a sheet of 0.025 mm platinum foil, folded to make a long, thin U. The interior of the U will be filled by a sheet of ceramic paper, with slots cut into it to accept potential leads to measure the voltage drop across the central portion of the heater. The two arms of the U will be attached to nickel busbars to provide the electrical current for the heater. The platinum heater will also act as a resistance thermometer to read its own temperature. In addition, the space within the U will be provided with Type N thermocouples to provide an independent check on the heater temperature. Several Type N thermocouples will also be attached to each of the two cold plates to provide their temperature.

The type of heaters used, e.g., by Harmathy [121] and by Plummer, *et al.*, are not folded back on themselves as is proposed here. Rather, the current leads for those heaters are at opposite ends of a flat strip heater. That design would be satisfactory if the heater were to be heated by direct current. However, it is proposed that the heater for the NIST apparatus be powered by alternating current, both to minimize the space-charge effects which Harmathy encountered (see the quotation on p.82 of this report) and to enable the use of an integrating digital voltmeter, with excellent ac common mode rejection, to read thermocouple voltages without serious errors due to leakage currents from the heater. With a single-pass heater, such as those used by Harmathy and by Plummer, there would be large inductances in the current loop and in the potential tap loop; such inductances could cause serious measurement errors unless very sophisticated equipment were used to measure the relative phases of the current and voltage signals. The folded heater design that is proposed will have minimal inductance so that the power to the heater is simply the product of the root-mean-square voltage drop across the central portion of the heater times the root-mean-square current through the heater, and the resistance of the heater will be simply the quotient of these two quantities.

Figure 65 shows how the thin-foil heater will be supported. To the right of these drawing can be seen two pieces of nickel angle stock that act as legs to support the right-hand-side of the twin busbars. At the left end of the busbars, they are electrically separated from each other by a thin ceramic washer through which a ceramic pin is inserted to provide a means of supporting that end of the busbars.

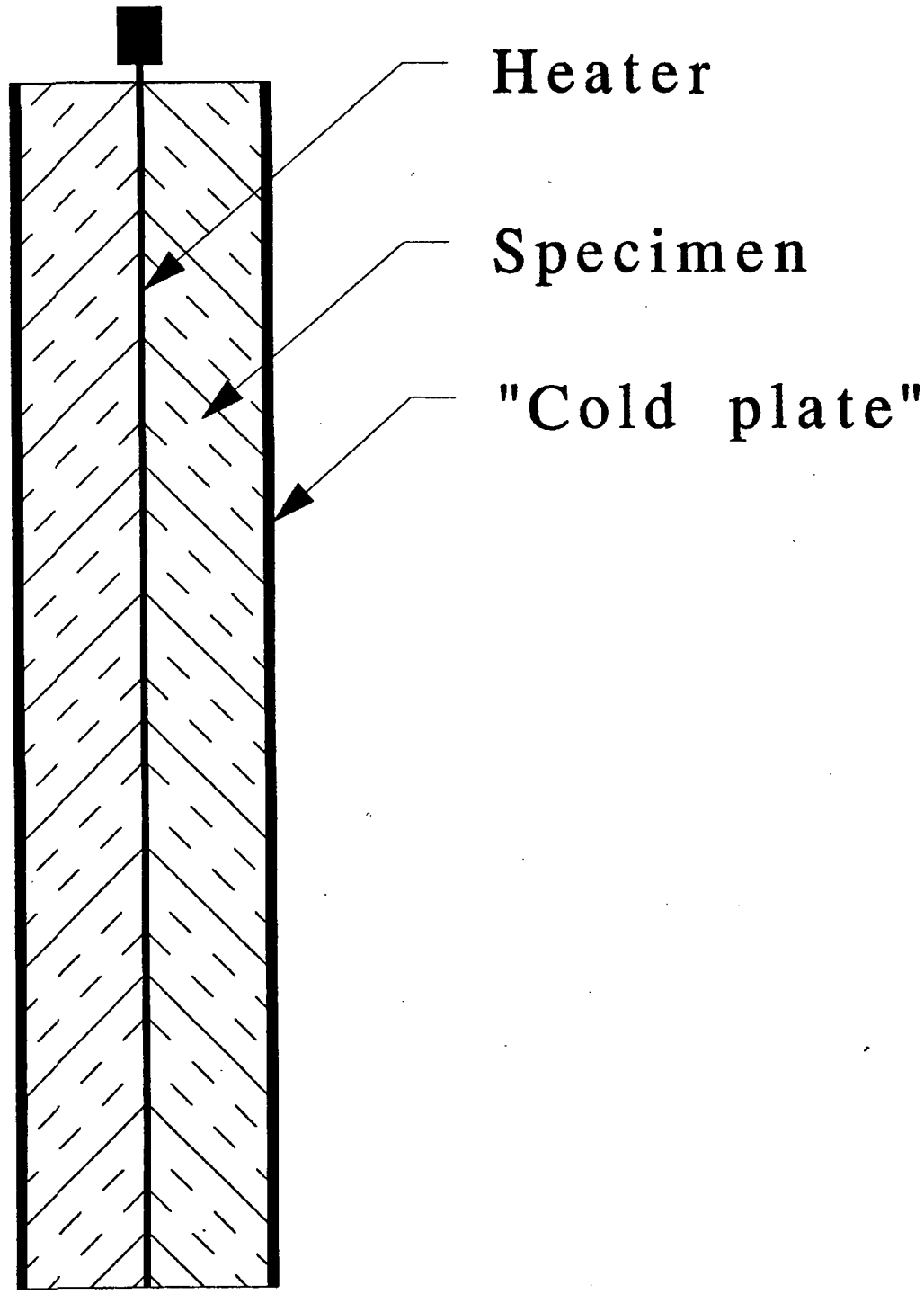

Figure 63. Cross section of proposed apparatus for high-temperature thermal conductivity measurements.

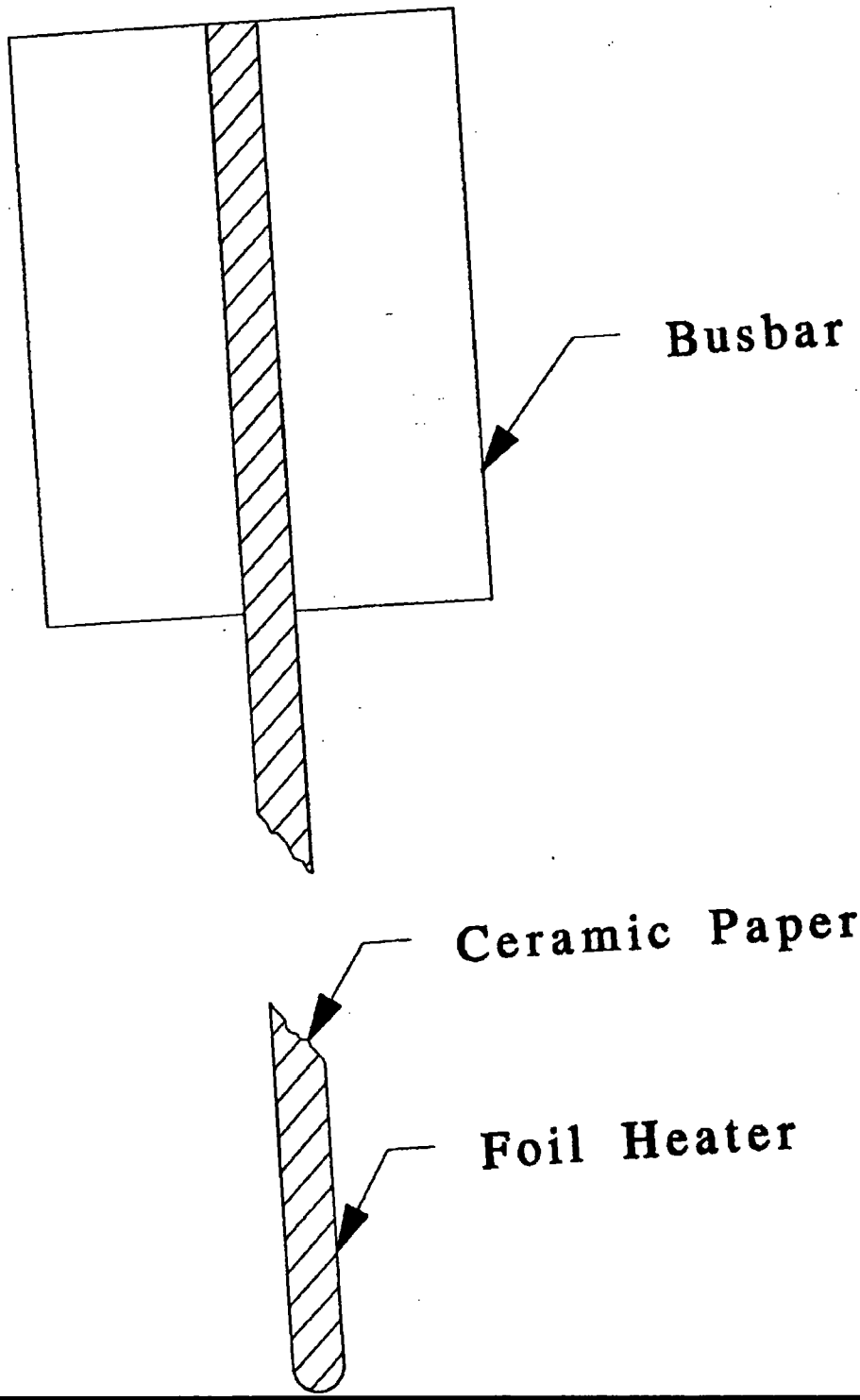
Busbar
Ceramic Paper
Foil Heater

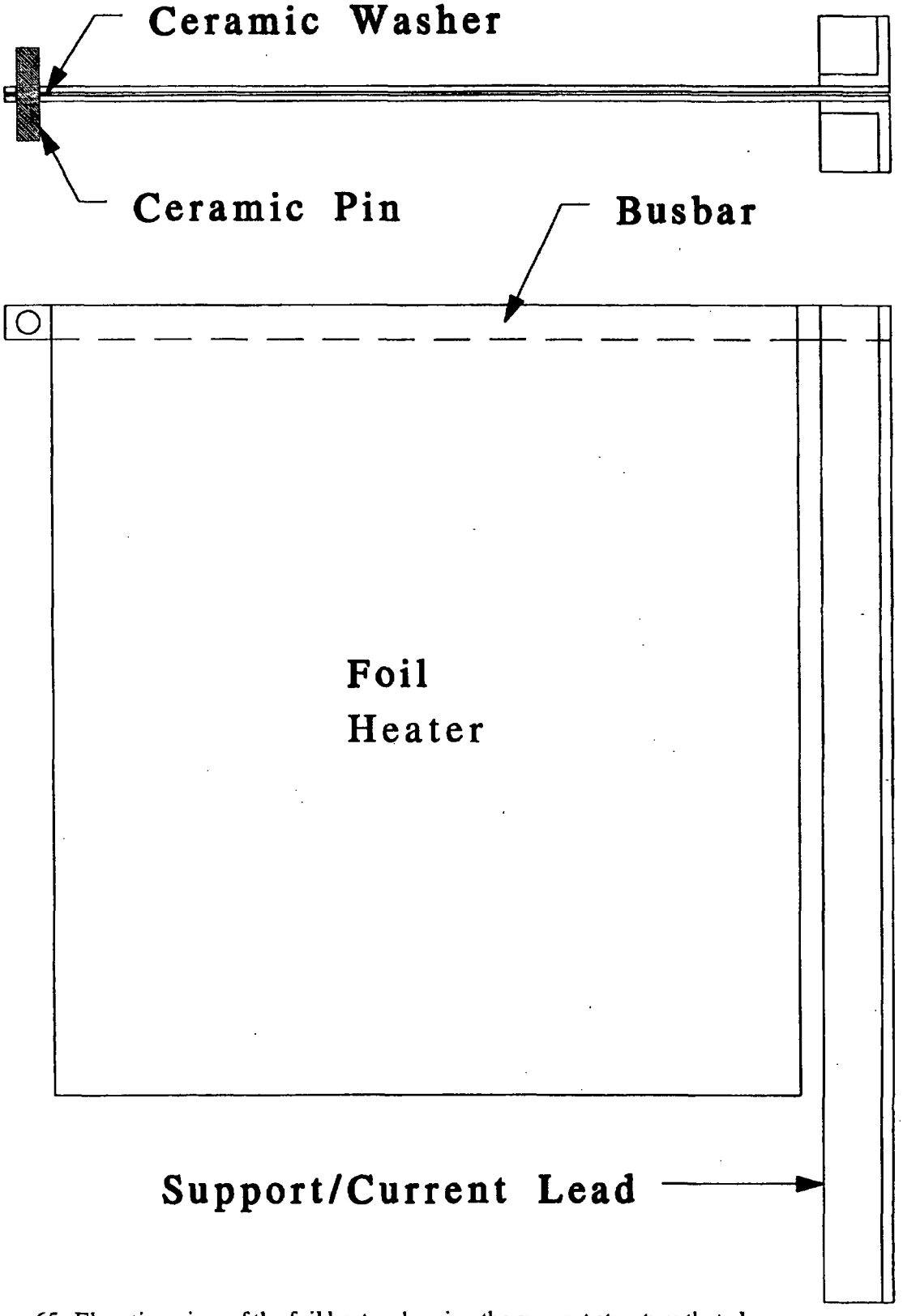

Figure 65. Elevation view of the foil heater showing the support structure that also serves as current leads. The free end of the busbar is supported from the support frame shown in the next figure.

Figure 66 is a conceptual view of the (nichrome or inconel) support frame from which the foil heater, specimens, and cold plates are suspended. The upper drawing is a plan view showing support rails, at each side, from which the components of the specimen assembly are hung. These support rails are held up by four legs, made of angle stock, as shown in the lower elevation view. Halfway up the rear legs a load screw plate is attached. The other load screw is supported from an angled arm attached to a fulcrum. The arrangement for the load screws can better be seen in Figure 67, which shows how a compressive load is applied to the specimen stack (for clarity, the support frame has been omitted in this drawing). Figure 67 represents the case where the weight that provides the compressive load is located inside the furnace. If possible, it would be preferable not too have the weight inside the furnace since it takes up a lot of space, provides a large thermal load for the furnace, and makes it difficult to change the applied force. A far preferable arrangement would be as shown in Figure 68, where the loading force is provided by a weight below the furnace, thus permitting the placement of two identical apparatus inside the furnace. The furnace that has been ordered by NIST is a bottom loading furnace and it may not be practical to have the weights located below the furnace. Figure 69 shows an arrangement whereby the weights can be located above the furnace with a pulley and cable (not shown) to reverse the direction of the force provided by each weight.

The intent is to run the tests in a manner analogous to that used by Piorkowska and Galeski [130-131], as described above on pp. 84-85. Since the changes to the specimens due to chemical reactions will be irreversible, it will not be possible to run tests on the same specimens at two different power levels. Rather, it is planned to run two tests simultaneously on two similar pairs of specimens, one test at a low power (just enough to enable obtaining accurate data for the heater resistance) and one test at a power large enough to cause a temperature drop of, say, 20 to 40 K across the specimens. The calculation procedure used by Piorkowska and Galeski is summarized in Appendix B.

With this apparatus, it also would be possible to carry out runs using Harmathy's method, which is described briefly on pp. 82-83, using his calculation procedure, which is summarized in Appendix B.

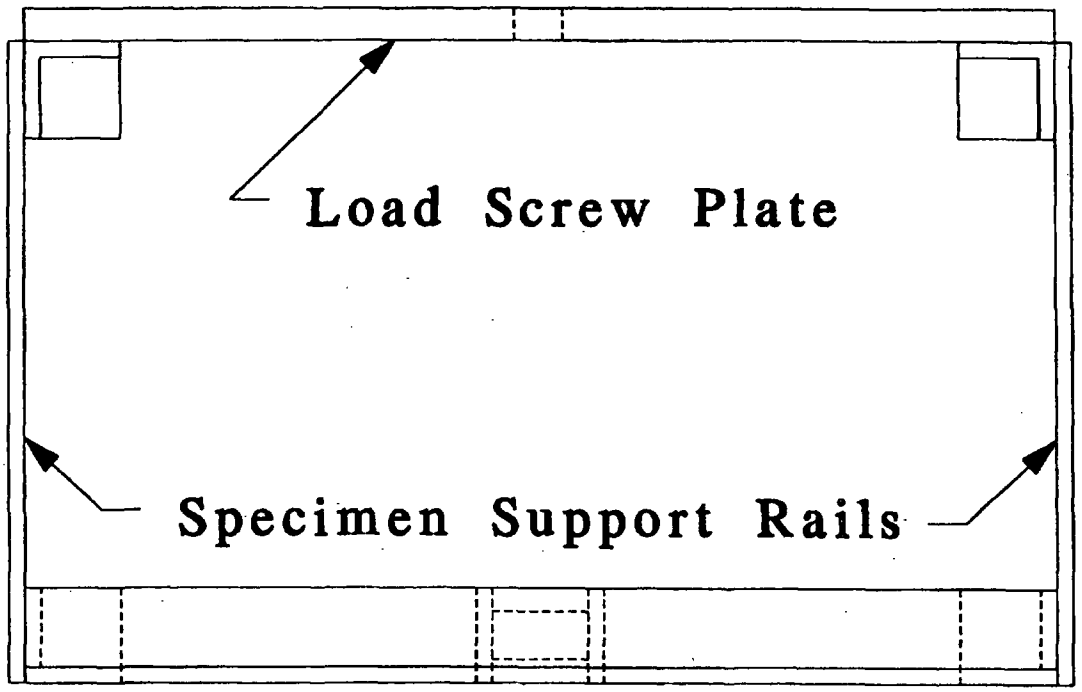

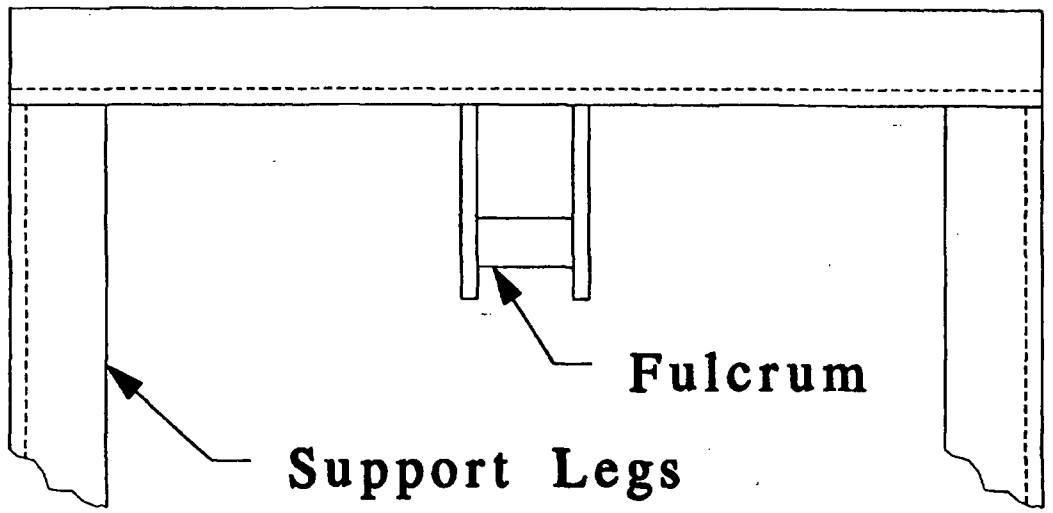

Figure 66. The support frame from which the foil heater, specimens, and cold plates are suspended. The fulcrum position would vary depending upon how the loading force is applied.

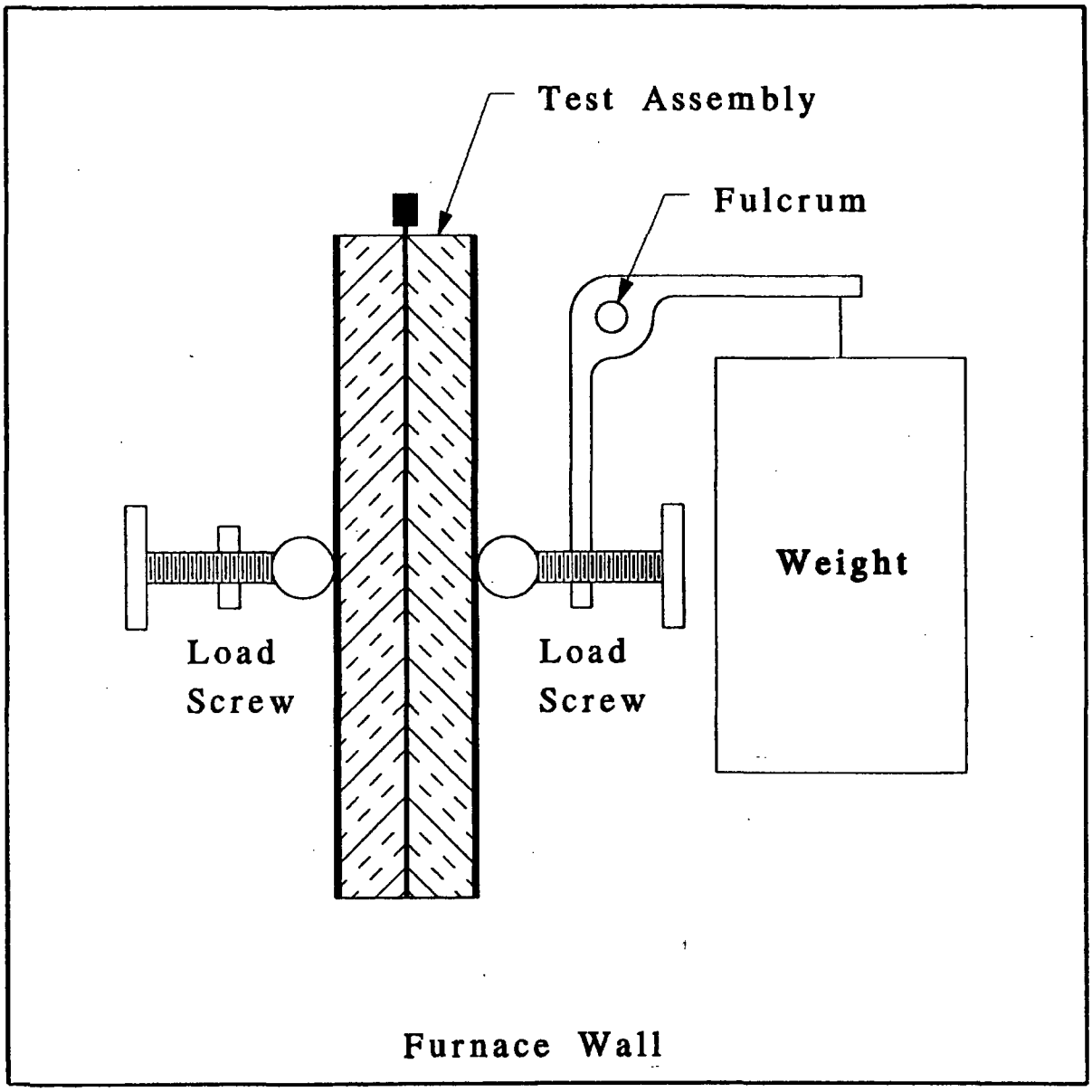

Figure 67. Elevation view of the apparatus if the loading force is provided by a weight inside the furnace.

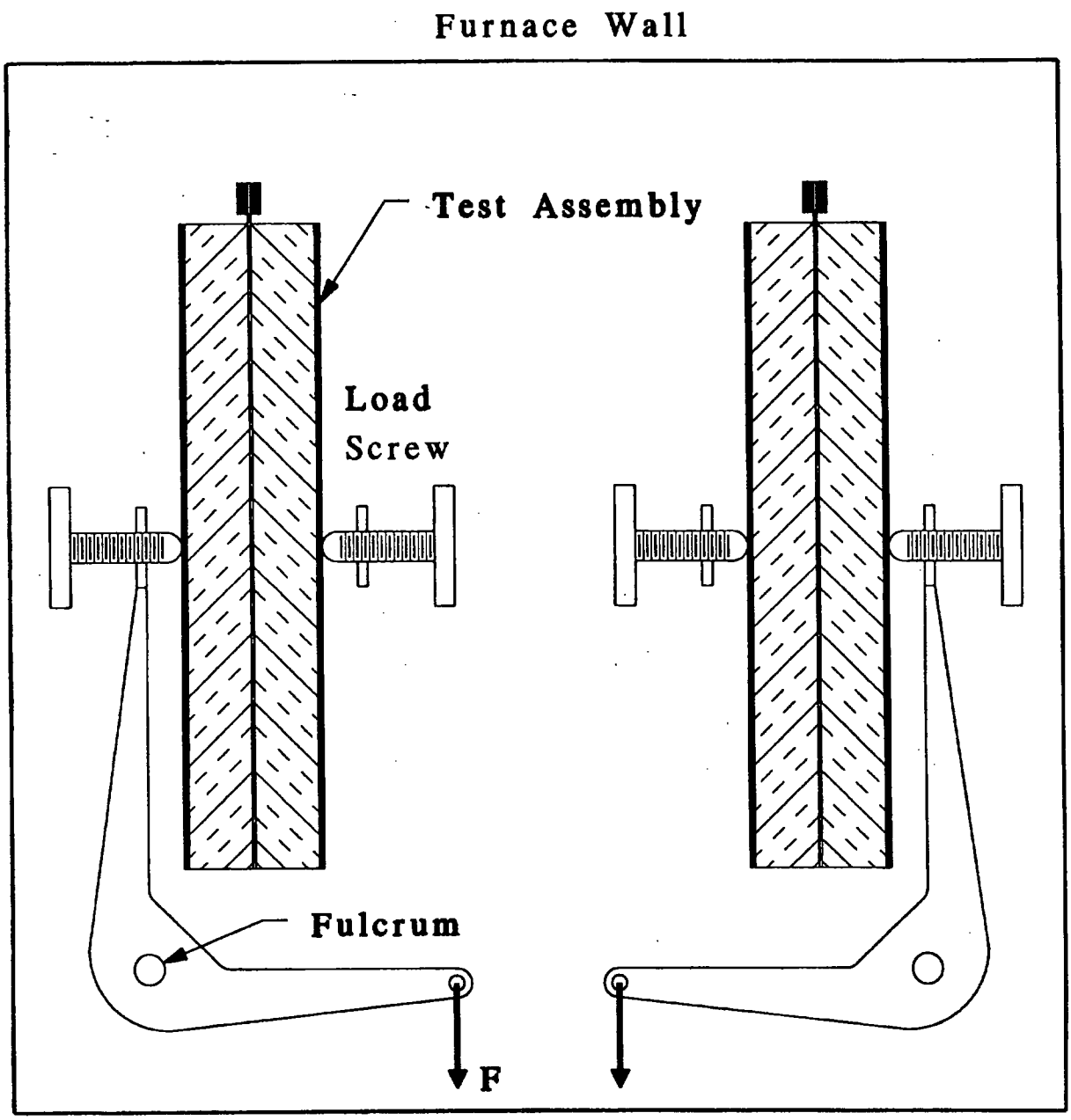

Figure 68. Elevation view of the apparatus if the loading force is provided by a weight below the furnace.

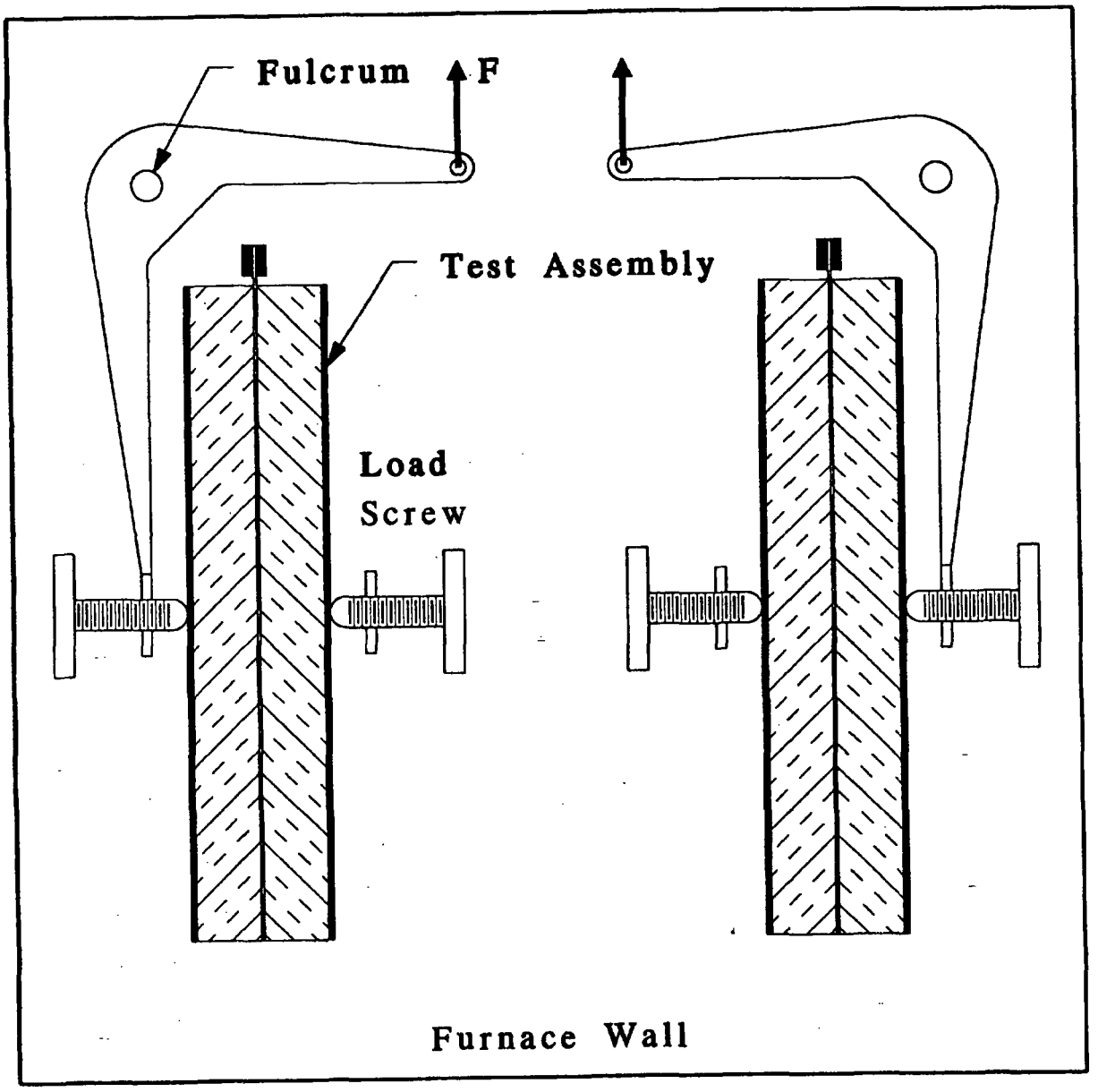

Figure 69. Elevation view of the apparatus if the loading force is provided by a weight and pulley system above the furnace.

8. References

[1] H. B. Callen, "The application of Onsager's reciprocal relations to thermoelectric, thermomagnetic, and galvanomagnetic effects," Phys. Rev. **73**, 1349-58 (1948).

[2] C. A. Domenicali, "Irreversible thermodynamics of thermoelectric effects of homogeneous, anisotropic media," Phys. Rev. **92**, 877-81 (1953).

[3] C. A. Domenicali, "Irreversible thermodynamics of thermoelectricity," Rev. Mod. Phys. **26**, 237-75 (1954).

[4] C. A. Domenicali, "Stationary temperature distribution in an electrically heated conductor," J. Appl. Phys. **25**, 1310-1 (1954).

[5] J. W. Leech, "Irreversible thermodynamics and kinetic theory in the derivation of thermoelectric relations, Canad. J. Phys. **37**, 1044-54 (1959).

[6] S. R. de Groot, "On the thermodynamics of irreversible heat and mass transfer," Intl. J. Heat Mass Transfer **4**, 63-70 (1961).

[7] S. R. de Groot and P. Mazur, *Thermodynamics of Irreversible Processes*, (North-Holland, Amsterdam, 1962).; reprinted by Dover Publications in 1984.

[8] I. Prigogine, *Introduction to Theory of Irreversible Processes* (Interscience Publishers, New York, 1967).

[9] R. Haase, *Thermodynamics of Irreversible Processes* (Addison-Wesley, Reading, MA, 1969); corrected, slightly enlarged edition reprinted by Dover Publications in 1990.

[10] I. Gyarmati, *Non-equilibrium Thermodynamics - Field Theory and Variational Principles* (Springer-Verlag, New York, 1970).

[11] B. H. Lavenda, *Thermodynamics of Irreversible Processes* (Wiley, New York, 1978).

[12] K. S. Forland, T. Forland, and S. K. Ratkje, *Irreversible Thermodynamics: Theory and Applications* (Wiley, Chichester, 1988).

[13] B. C. Eu, *Kinetic Theory and Irreversible Thermodynamics* (Wiley, New York, 1992).

[14] K. Gambár and F. Markus, "On the global symmetry of thermodynamics and Onsager's reciprocity relations," J. Non-Equilib. Thermodyn. **18**, 51-7 (1993).

[15] G. D. C. Kuiken, *Thermodynamics of Irreversible Processes. Applications to Diffusion and Rheology* (Wiley, Chichester, 1994).

[16] D. Jou, J. Casas-Vásquez, and G. Lebon, *Extended Irreversible Thermodynamics, 2nd Ed.* (Springer, New York, 1996).

[17] D. Jou, J. Casas-Vásquez, and G. Lebon, "Recent bibliography on extended irreversible thermodynamics and related topics (1992-95)," J. Non-Equilib. Thermodyn. **21**, 103-121 (1996).

[18] D. A. de Vries, "Simultaneous transfer of heat and moisture in porous media," Trans. Am. Geophys. Union **39**, 909-16 (1958).

[19] D. A. de Vries, "The theory of heat and moisture transfer in porous media revisited," Intl. J. Heat Mass Transfer **30** (7), 1343-50 (1987).

[20] J. R. Philip and D. A. de Vries, "Moisture movement in porous materials under temperature gradients,"Trans. Am. Geophys. Union **38**, 222-32, 594 (1957).

[21] M. Fortes and M. R. Okos, "A nonequilibrium thermodynamics approach to transport phenomena in capillary-porous media," in *Proc. 1st Intl. Symp. on Drying* (McGill Univ., Montreal, 1978).

[22] M. Fortes and M. R. Okos, "Heat and mass transfer in hydroscopic capillary extruded products," AIChE Journal **27**, 255-62 (1981).

[23] A. V. Luikov, *Heat and Mass Transfer in Capillary-porous bodies* (Pergamon, Oxford, 1966).

[24] A. V. Luikov, "Systems of differential equations of heat and mass transfer in capillary-porous bodies," Intl. J. Heat Mass Transfer **18**, 1-14 (1975).

[25] N. G. Zoldners, Thermal Properties of Concrete under Sustained Elevated Temperatures, pp. 1-31 in *Temperature and Concrete, Symposium on Effect of Temperature on Concrete*, ACI Publication SP 25 (American Concrete Institute, 1968).

[26] P. J. Sullivan and M. P. Poucher, The Influence of Temperature on the Physical Properties of Concrete and Mortar in the Range 20 C to 400 C, pp. 103-135 in *Temperature and Concrete, Symposium on Effect of Temperature on Concrete*, ACI Publication SP 25 (American Concrete Institute, 1968).

[27] T. Z. Harmathy, "Thermal properties of concrete at elevated temperatures," J. Matls. **5**, 47-74 (1970).

[28] T. Harada, J. Takeda, S. Yamane, and F. Furumura, Strength, Elasticity, and Thermal Properties of Concrete Subjected to Elevated Temperatures, pp. 377-406 in *Concrete for Nuclear Reactors, Vol. II*, ACI Special Publication SP-34 (American Concrete Institute, 1972).

[29] J. C. Marechal, Thermal Conductivity and Thermal Expansion Coefficients of Concrete as a Function of Temperature and Humidity, pp. 1047-57 in *Concrete for Nuclear Reactors, Vol. II*, ACI Special Publication SP-34 (American Concrete Institute, 1972).

[30] T. Z. Harmathy and L. W. Allen, "Thermal properties of selected masonry unit concretes," Amer. Concrete Inst. J. **70**, 132-42 (1973).

[31] A. M. Neville, *Properties of Concrete* (John Wiley and Sons, New York, 1973).

[32] Y. Anderberg, S. E. Magnusson, O. Pettersson, S. Thelandersson, and U. Wickstrom, An Analytical Approach to Fire Engineering Design of Concrete Structures, pp. 409-38 in Analytical Design of Fire Exposed Concrete Structures (Lund Institute of Technology, Lund, Sweden, 1978).

[33] J. A. Rhodes, Thermal Properties, Chapt. 17 in *Significance of Tests and Properties of Concrete and Concrete-Making Materials*, ASTM Special Technical Publication 169B (American Society for Testing and Materials, Philadelphia, 1978).

[34] C. R. Cruz and M. Gillen, "Thermal expansion of portland cement paste, mortar and concrete at high temperatures," Fire and Matls. **4**, 66-70 (1980).

[35] U. Schneider, *Behavior of Concrete at High Temperatures*, Deutscher Ausschuss für Stahlbeton, Heft 337 (Verlag W. Ernst und sohn, Berlin, 1982).

[36] H. C. Hirth, Jr., M. Polivka, and D. Pirtz, *Final Report on Thermal Properties of Concrete at High Temperatures*, Rept. No. ORNL/BRP-81/1 (Rev. 1) (Oak Ridge Natl. Lab., Oak Ridge, TN, 1984).

[37] U. Schneider (Ed.), *Properties of Materials at High Temperatures – Concrete*, for RILEM Committee 44-PHT (Dept. Civil Eng., Kassel Univ., 1985).

[38] U. Schneider, "Concrete at high temperatures – a general review," Fire Safety J. **13**, 55-69 (1988).

[39] R. Valore, Jr., A. Tuluca, and A. Caputo, *Assessment of the Thermal and Physical Properties of Masonry Block Products*, Rept. No. ORNL/Sub/86-22020/1 (Oak Ridge National Laboratory Oak Ridge, TN, 1988).

[40] P. Morabito, "Measurement of the thermal properties of different concretes," High Temperatures – High Pressures **21**, 51-59 (1989).

[41] T. Z. Harmathy, *Fire Safety Design & Concrete* (Longman Scientific & Technical, Essex, England, 1993).

[42] J. M. Scanlon and J. E. McDonald, Thermal Properties, pp. 229-239 in *Significance of Tests and Properties of Concrete and Concrete-Making Materials*, ASTM Special Technical Publication 169C , P. Klieger and J. F. Lamond, Eds. (American Society for Testing and Materials, Philadelphia, 1994).

[43] P. Smith, Resistance to Fire and High Temperatures, pp. 282-295 in *Significance of Tests and Properties of Concrete and Concrete-Making Materials*, ASTM Special Technical Publication 169C , P. Klieger and J. F. Lamond, Eds. (American Society for Testing and Materials, Philadelphia, 1994).

[44] T. T. Lie and V. K. R. Kodur, "Thermal and mechanical properties of steel-fibre-reinforced concrete at elevated temperatures," Canad. J. Civil Eng. **23**, 511-517 (1996).

[45] Z. P. Bažant and M. F. Kaplan, *Concrete at High Temperatures: Material Properties and Mathematical Models* (Longman (Addison-Wesley), London, 1996).

[46] M. Saad, S. A. Abo-El-Enein, G. B. Hanna, and M. F. Kotkata, "Effect of temperature on physical and mechanical properties of concrete containing silica fume," Cement & Concrete Res. **26**, 669-675 (1996).

[47] M. G. Van Geem, J. Gajda, and K. Dombrowski, *Thermal Properties of Commercially Available High-Strength Concretes*, PCA R&D Serial No. 2031 (Portland Cement Assoc., Skokie, IL, 1996).

[48] M. G. Van Geem, J. Gajda, and K. Dombrowski, "Thermal properties of commercially available high-strength concretes," Cement, Concrete, & Aggregates **19**, 38-53 (1997).

[49] F. Vodák, R. Černý, J. Drchalová, Š. Hošková, O. Kapičková, O. Michalko, P. Semerák, and J. Toman, "Thermophysical properties of concrete for nuclear-safety related structures, Cement & Concrete Res. **27**, 415-426 (1997).

[50] X. Fu and D. D. L. Chung. "Effects of silica fume, latex, methylcellulose, and carbon fibers on the thermal conductivity and specific heat of cement paste," Cement & Concrete Res. **27**, 1799-1804 (1997).

[51] Y. S. Touloukian, W. R. Judd, and R. F. Roy (Eds.), *Physical Properties of Rocks and Minerals*, CINDAS Data Series on Material Properties, Vol. II-2 (Hemisphere Publishing, New York, 1989).

[52] W. L. Sibbitt, J. G. Dodson, and J. W. Tester, Thermal Conductivity of Rocks Associated with Energy Extraction from Hot Dry Rock Geothermal Systems, p. 399 in *Thermal Conductivity 15*, Proc. 15th Intl. Conf. on Thermal Conductivity, V. V. Mirkovich, Ed. (Plenum, New York, 1978).

[53] W. L. Sibbitt, J. G. Dodson, and J. W. Tester, "Thermal conductivity of crystalline rocks associated with energy extraction from hot dry rock geothermal systems,," J. Geophys. Res. **84**, 1117-1124 (1979).

[54] M. T. Morgan and G. A. West, *Thermal Conductivity of the Rocks in the Bureau of Mines Standards Rock Suite*, Rept. No. ORNL/TM-7052 (Oak Ridge Natl. Lab., Oak Ridge, TN, 1980).

[55] M. T. Morgan and G. A. West, The Thermal Conductivity of the Rocks in the Bureau of Mines Standards Rock Suite, pp. 79-90 in *Thermal Conductivity 16*, Proc. 16th Intl. Conf. on Thermal Conductivity, D. C. Larsen, Ed. (Plenum, New York, 1983).

[56] F. E. Heuze, "High-temperature mechanical, physical and thermal properties of granitic rocks – a review," Intl. J. Rock Mech. Min. Sci. & Geomech. Abstr. **20**, 3-10 (1983).

[57] W. B. Durham, V. V. Mirkovich, and H. C. Heard, "Thermal diffusivity of igneous rocks at elevated pressure and temperature," J. Geophys. Res. **92**, 11615-11634 (1987).

[58] W. H. Somerton, *Thermal Properties and Temperature-Related Behavior of Rock/Fluid Systems* (Elsevier, Amsterdam, 1992).

[59] A. Bouguerra, J. P. Laurent, M. S. Goual, and M. Queneudec, "The measurement of the thermal conductivity of solid aggregates using the transient plane source technique," J. Phys. D: Appl. Phys. **30**, 2900-2904 (1997).

[60] N. E. Thompson, "A note of the difficulties of measuring the thermal conductivity of concrete," Mag. Concrete Res. **20**, 45-49 (1968).

[61] D. A. G. Bruggeman, "Über die Geltungsbereiche und die Konstaantenwerte der verscheidenen Mischkörperformeln Lichteneckers," Physikalische Zeit. **37**, 906-XXXX, Chapt. 5 (1936).

[62] R. L. Hamilton and O. K.Crosser, "Thermal conductivity of heterogeneous two-component systems," Ind. Eng. Chem. Fundamentals **1**, 187-91 (1962).

[63] P. S. Turner, "Thermal-expansion stresses in reinforced plastics," J. Research Natl. Bur. Stds. **37**, 239-50 (1946). RP1745

[64] E. H. Kerner, "The elastic and thermo-elastic properties of composite media," Proc. Phys. Soc. **69**, 808-13 (1956).

[65] V. M. Levin, "On the coefficients of thermal expansion of heterogeneous materials," Mech. Solids **2**, 58-61 (1967).

[66] R. A. Schapery, "Thermal expansion coefficients of composite materials based on energy principles," J. Composite Matls. **2**, 380-404 (1968).

[67] B. W. Rosen and Z. Hashin, "Effective thermal expansion coefficients and specific heats of composite materials," Intl. J. Eng. Sci. **8**, 157-173 (1970).

[68] A. A. Fahmy and A. N. Ragai, "Thermal-expansion behavior of two-phase solids," J. Appl. Phys. **41**, 5108-11 (1970).

[69] A. E. Powers, Conductivity in Aggregates, KAPL-2145, Knolls Atomic Power Laboratory (March 1961).

[70] R. E. Meredith and C. W. Tobias, "Conduction in heterogeneous systems," in *Advances in Electrochemistry and Electrochemical Engineering*, C. W. Tobias, Ed. (Wiley, New York, 1962).

[71] H. W. Godbee and W. T. Ziegler, "Thermal conductivities of MgO, Al_2O_3, and ZrO_2 powders to 850 °. II. Theoretical," J. Appl. Phys. **37**, 56-65 (1966).

[72] D. R. Flynn, "Thermal conductivity of ceramics," in *Mechanical and Thermal Properties of Ceramics*, NBS Spec. Pub. 303 (National Bureau of Standards, Gaithersburg MD, 1969).

[73] S. C. Cheng and R. I. Vachon, "A technique for predicting the thermal conductivity of suspensions, emulsions and porous materials," Intl. J. Heat Mass Transfer **13**, 537- (1970).

[74] R. C. Progelhof, J. L. Throne and R. R. Ruetsch, "Methods for predicting the thermal conductivity of composite systems: a review," Polym. Eng. Sci. **16**, 615- (1976).

[75] D. K. Hale, "Review: The physical properties of composite materials," J. Mater. Sci. **11**, 2105- (1976).

[76] R. Landauer, "Electrical conductivity in inhomogeneous media," in *Electrical Transport and Optical Properties of Inhomogeneous Media*, J. C. Garland and D. B. Tanner, Eds. (American Institute of Physics, New York, 1978).

[77] J. L. Jackson and S. R. Coriell, "Transport coefficients of composite materials," J. Appl. Phys. **39**, 2349-54 (1968).

[78] J. Valentich, *Tube Type Dilatometers* (Instrument Society of America, Research Triangle Park, NC, 1981).

[79] G. Ruffino, Thermal Expansion Measurement by Interferometry, pp. 689-706 in Compendium of Thermophysical Property Measurement Methods, Vol. 1 Survey of Measurement Techniques , K.D. Maglić, A. Cezairliyan, and V.E. Peletsky, eds. (Plenum Press, New York, 1984).

[80] R.K. Kirby, Methods of Measuring Thermal Expansion, pp. 549-567 in *Compendium of Thermophysical Property Measurement Methods, Vol. 2 Recommended Measurement Techniques and Practices,* K.D. Maglić, A. Cezairliyan, and V.E. Peletsky, eds. (Plenum Press, New York, 1992).

[81] G. Ruffino, Recent Thermal Expansion Interferometric Measuring Instruments, pp. 569-599 in *Compendium of Thermophysical Property Measurement Methods, Vol. 2 Recommended Measurement Techniques and Practices,* K.D. Maglić, A. Cezairliyan, and V.E. Peletsky, eds. (Plenum Press, New York, 1992).

[82] R. E. Taylor *et al., Thermal Expansion of Solids* (ASM International, Materials Park, OH, 1998).

[83] J. P. McCullough and D.W. Scott, eds., *Experimental Thermodynamics. Volume I Calorimetry of Non-reacting Systems* (Plenum Press, New York, 1968).

[84] A. Cezairliyan, *et al., Specific Heat of Solids* (Hemisphere, New York, 1988).

[85] W. Hemminger, *Calorimetry: Fundamentals and Practice* (Verlag Chemie, Weinheim, 1984).

[86] K.D. Maglić, A. Cezairliyan, and V.E. Peletsky, eds., Compendium of Thermophysical Property Measurement Methods, Vol. 1 Survey of Measurement Techniques (Plenum Press, New York, 1984).

[87] K.D. Maglić, A. Cezairliyan, and V.E. Peletsky, eds., Compendium of Thermophysical Property Measurement Methods, Vol. 2 Recommended Measurement Techniques and Practices (Plenum Press, New York, 1992).

[88] W.W. Wendlandt, *Thermal Analysis* (Wiley, New York, 1986).

[89] M. E. Brown, *Introduction to Thermal Analysis: Techniques and Applications* (Chapman and Hall, New York, 1988).

[90] R.F. Speyer, *Thermal Analysis of Materials* (Marcel Dekker, New York, 1994).

[91] M. J. Richardson, Application of Differential Scanning Calorimetry to the Measurement of Specific Heat, pp. 669-685 in Compendium of Thermophysical Property Measurement Methods, Vol. 1 Survey of Measurement Techniques , K.D. Maglić, A. Cezairliyan, and V.E. Peletsky, eds. (Plenum Press, New York, 1984).

[92] M. J. Richardson, Application of Differential Scanning Calorimetry to the Measurement of Specific Heat, *Compendium of Thermophysical Property Measurement Methods, Vol. 2*

Recommended Measurement Techniques and Practices, K.D. Maglić, A. Cezairliyan, and V.E. Peletsky, eds. (Plenum Press, New York, 1992).

[93] S.C. Mraw, Differential Scanning Calorimetry, pp. 395-435 in, *Specific Heat of Solids*, A. Cezairliyan, ed. (Hemisphere, New York, 1988).

[94] R. P. Tye, ed., *Thermal Conductivity, Vols 1 and 2* (Academic Press, New York, 1969).

[95] A.W. Pratt, Heat Transmission in Low Conductivity Materials, pp. 301-405 in *Thermal Conductivity, Vol. 1*, R.P. Tye, ed. (Academic Press, New York, 1969).

[96] G.C. Danielson and P.H. Sidles, Thermal Diffusivity and Other Non-steady-state Methods, pp. 149-201 in *Thermal Conductivity*, Vol. 2, R.P. Tye, ed. (Academic Press, New York, 1969).

[97] W.R. Davis, Hot-Wire Method for the Measurement of the Thermal Conductivity of Refractory Materials, pp. 231-254 in *Compendium of Thermophysical Property Measurement Methods, Vol. 1 Survey of Measurement Techniques*, K.D. Maglić, A. Cezairliyan, and V.E. Peletsky, eds. (Plenum Press, New York, 1984).

[98] A.E. Wechsler, The Probe Method for Measurement of Thermal Conductivity," pp. 161-185 in *Compendium of Thermophysical Property Measurement Methods, Vol. 2 Recommended Measurement Techniques and Practices*, K.D. Maglić, A. Cezairliyan, and V.E. Peletsky, eds. (Plenum Press, New York, 1992).

[99] D.R. Flynn, *Development of a Measurement System for Field Determination of Thermal Properties of Soils and Rock: 1. Bibliography and Abstracts*, DRF R&D Report No. 97-02-101, April 1997, 110 p.

[100] R.R. Dils, J.D. Allen, J.C. Richmond, and M.B. McNeil, *Hot Wire Thermal Conductivity Measurements in High Temperature Refractories*, U.S. Department of Energy Rept. No. DOE/CS/40442-T1, 1982.

[101] S.E. Gustafsson, E. Karawacki, and M.N. Khan, "Transient hot-strip method for simultaneously measuring thermal conductivity and thermal diffusivity of solids and fluids," J. Phys. D: Appl. Phys. **12**, 1411-1421 (1979).

[102] S.E. Gustafsson and E. Karawacki, "Determination of the thermal-conductivity tensor and the heat capacity of insulating solids with the transient hot-strip method," J. Appl. Phys. **52**, 2596-2600 (1981).

[103] S.E. Gustafsson, K. Ahmed, A.J. Hamdani, and A. Maqsood, "Transient hot-strip method for measuring thermal conductivity and specific heat of solids and fluids: second order theory and approximations for short times," J. Appl. Phys. **53**, 6064-6068 (1982).

[104] U. Brydsten and G. Bäckström, "Hot strip determination of the thermal conductivity tensor and heat capacity of crystals," Int. J. Thermophysics **4**, 369-387 (1983).

[105] S.E. Gustafsson, "Transient plane source techniques for thermal conductivity and thermal diffusivity measurements of solid materials," Rev. Sci. Instrum. **62**, 797-804 (1991).

[106] S.E. Gustafsson, B. Suleiman, N.S. Saxena, and I. ul Haq, "The transient plane source technique: experimental design criteria," High Temperatures – High Pressures **23**, 289-293 (1991).

[107] L.N. Clarke and R.S.T. Kingston, "Equipment for the simultaneous determination of thermal conductivity and diffusivity of insulating materials using a variable-state method," Australian J. Appl. Sci. **1**, 172-187 (1950).

[108] P. Vernotte, "Détermination simultanée de la chaleur spécifique et de la conductiblité thermique des isolants. Method du signal," Comptes Rendus de L'Académie des Sciences **204**, 563-565 (1937).

[109] L.N. Clarke and R.S.T. Kingston, "Further investigation of some errors in a dynamic method for the determination of thermal conductivity and diffusivity of insulating materials," Australian J. Appl. Sci. **2**, 235-242 (1951).

[110] O. Krischer, "Über die Bestimmung der Wärmeleitfähigkeit, der Wärmekapazität und der Wärmeeindringzahl in einem Kurzzeitverfahren," Chemie-Ing.-Techn. **26**, 42-44 (1954).

[111] A.W. Pratt and J.M.E. Ball, "Thermal conductivity of building materials," J. Inst. Heating Ventilating Engrs. **24**, 201-226 (1956).

[112] A.P. Hatton, "Thermal conductivity and diffusivity measurements by an unsteady-state method with application to insulating materials containing moisture and ice," J. Mech. Engng. Sci. **2**, 45-51 (1960).

[113] G. Bastian, "Détermination de caractéristiques thermophysiques de matériaux de construction par la méthode de la source plane en régimes transitoire et asymtotique," Revue Phys. Appl. **22**, 431-444 (1987).

[114] N.E. Hager, Jr., "Miniature thin-heater thermal conductivity apparatus," ISA Trans. **8**, 104-109 (1969).

[115] N.E. Hager, Jr., "Thin-heater thermal conductivity apparatus," Rev. Sci. Instrum. **31**, 177-185 (1960).

[116] N.E. Hager, Jr., "Thin-heater thermal conductivity apparatus," J. Therm. Insul. **9**, 140-159 (1985).

[117] N.E. Hager, Jr., "Recent developments with the thin-heater thermal conductivity apparatus," J. Therm. Insul. **9**, 111-122 (1985).

[118] C.F. Gilbo, "Thermal conductivity measurement using a thin-heater apparatus," J. Therm. Insul. **9**, 92-101 (1985).

[119] G. Sirdeshpande, Thin-heater Thermal Conductivity Apparatus for Measuring Thermal Conductivity of Powdered Insulations, pp. 844-855 in *Thermal Conductivity 22. Proc. Twenty-Second Intl. Conf. On Thermal Conductivity*, T.W. Tong, ed. (Technomic Publishing, Lancaster, PA, 1994).

[120] ASTM C1114-95, Standard Test Method for Steady-State Thermal Transmission Properties by Means of the Thin-Heater Apparatus (Amer. Soc. For Testing and Materials, West Conshohocken, PA, 1995).

[121] T.Z. Harmathy, "Variable-state methods of measuring the thermal properties of solids," J. Appl. Phys. **35**, 1190-1200 (1964).

[122] R.C. Steere, "Thermal properties of thin-film polymers by transient heating," J. Appl. Phys. **37**, 3338-3344 (1966).

[123] A.B. Ng, M.S. Mirza, and T.T. Lie, "Response of direct models of reinforced concrete columns subjected to fire," ACI Structural J. **87**, 313-325 (1990).

[124] P.A. Miles and S.J. Grubits, *Measurement of the Thermal Diffusivity of Masonry. Review of Test Methods*, Report CIB W14/80/40, Experimental Building Station, North Ryde, New South Wales, Australia, 1980, 29 pp.

[125] N.H. Schilmoeller and D. White, Transient System for Measurement of Thermal Properties of Nuclear Fuel Powders of Varying Densities, pp. 857-870 in *Thermal Conductivity. Proc. Eighth Conf.*, C.Y. Ho and R.E. Taylor, eds. (Plenum Press, New York, 1969).

[126] W.A. Plummer, D.E. Campbell, and A.A. Comstock, "Method of Measurement of Thermal Diffusivity to 1000°C," J. Amer. Ceram. Soc. **45**, 310-316 (1962).

[127] L.N. Dzhavadov, "Measurement of thermophysical properties of dielectrics under pressure," High Temperatures – High Pressures **7**, 49-54 (1975).

[128] R.E. Giedd and D.G. Onn, Electronic Flash: A Rapid Method for Measuring the Thermal Conductivity and Specific Heat of Dielectric Materials, pp. 339-346 in *Thermal Conductivity 20. Proc. 20th* Intl. Thermal Conductivity Conf., D.P.H. Hasselman and J.R. Thomas, Jr., eds. (Plenum Press, New York, 1987).

[129] L. Kubičár, *Pulse Method of Measuring Basic Thermophysical Parameters, Part E of Vol. XII, Thermal Analysis, of Wilson and Wilson's Comprehensive Analytical Chemistry*, G. Svehla, ed. (Elsevier, New York, 1990).

[130] E. Piorkowska and A. Galeski, "Measurements of thermal conductivity of materials using a transient technique. I. Theoretical background," J. Appl. Phys. **60**, 485-492 (1986).

[131] E. Piorkowska and A. Galeski, "Measurements of thermal conductivity of materials using a transient technique. II. Description of the apparatus," J. Appl. Phys. **60**, 493-498 (1986).

[redacted]

(This page is blank)

[redacted]

[redacted]

[redacted]

Appendix A. Analysis Procedures for Transient Hot-Wire or Probe Techniques for Thermal Conductivity Measurement

Transient techniques for thermal conductivity measurement have been utilized with planar heat sources, point or spherical heat sources, and cylindrical heat sources, In this appendix, attention is confined to measurement systems utilizing a cylindrical geometry. For most of the analyses discussed below, an infinitely long heat source is assumed. The end effects due to a finite source length are briefly discussed.

A.1 Ideal Line Heat Source

The simplest analysis involves an ideal line heat source (i.e., a source of vanishing diameter) that is turned on at zero time and thereafter produces a constant heat output. Apparatus used for determining the thermal conductivity of liquids and gases usually approximates this ideal line heat source quite closely, the heater wire, which also serves as a resistance thermometer, typically being about 5 to 25 μm in diameter. Thin wire heaters also are frequently used for measuring the thermal conductivity of thermal insulation, including refractory materials. For *in-situ* measurements of, for example, soil thermal properties, a larger, more rugged probe is needed and it is necessary to account for the finite size and thermal capacity of the probe, as well as for thermal contact resistance between the probe and the surrounding medium. It is useful, however, to consider the analysis for an ideal line heat source since that solution serves as a limiting form of the solution for a probe as its diameter decreases and contact resistance becomes smaller.

In some implementations of the line heat source method, the temperature of the heater wire, or slender probe, is measured. In other implementations, the temperature is measured in the surrounding medium at some known radius from the axis of the heater or probe.

Following Carslaw and Jaeger [A1, pp. 261-262], we suppose heat to be released at the continuous rate Q per unit time per unit length along the z-axis. If the heat supply begins at the time $t = 0$, when the medium is isothermal at a temperature $T = 0$, the temperature at a distance r from the z-axis is given by

$$T(r,t) = \frac{Q}{4\pi\lambda} \mathrm{E}_1\left(\frac{r^2}{4\kappa t}\right) \quad , \tag{1}$$

where

$$\mathrm{E}_1(x) = \int_x^\infty \frac{e^{-x}}{x}\, dx \tag{2}$$

is the exponential integral, λ is thermal conductivity, and κ is thermal diffusivity.. For small values of x, corresponding to small values of the radius r or large values of the time t, Eq. (2) reduces to

$$\mathrm{E}_1(x) = -\gamma - \ell n\, x + \frac{x}{1\cdot 1!} - \frac{x^2}{2\cdot 2!} + \frac{x^3}{3\cdot 3!} - \frac{x^4}{4\cdot 4!} - \cdots \quad , \tag{3}$$

where $\gamma = 0.577216...$ is Euler's constant. For values of x sufficiently small that x is negligible compared with $\ell n\ x$, the temperature is given simply by

$$T(r,t) = \frac{Q}{4\pi\lambda}\left(-\gamma + \ln\frac{4\kappa t}{r^2}\right) \quad . \tag{4}$$

For measurements at a fixed value of r,

$$T(a,t) = \frac{Q}{4\pi\lambda}(A + \ln t) \quad , \tag{5}$$

where A is a constant whose value need not be known if only thermal conductivity is needed. Thus the thermal conductivity can be computed from the strength of the heat source and the slope of a plot of temperature versus the logarithm of time. Note that in using Eq. (5) to obtain thermal conductivity, it is not necessary to specify the radius at which the temperature is measured, provided the value of $4\kappa t/r^2$ is large enough for Eqs. (4) and (5) to be valid. If it is desired to use Eq. (4) to compute thermal diffusivity values, it is necessary to know accurately the radius of the heater wire or probe. As pointed out, e.g., by Nieto de Castro [A2-A3], with the very thin probes used for measurements on fluids, and the very short times that are used in order to avoid convection effects, it generally is not possible to obtain thermal diffusivity (or specific heat) values with anywhere near the accuracy that is possible for thermal conductivity values.

For many investigations it is assumed that the line heat source probe is very thin and also very conductive in the radial direction so that the temperature across the probe can be considered to be constant at any given time. Under such conditions the temperature of the probe itself can be used to determine the thermal conductivity, provided the heated section of the probe is also sufficiently long, and of sufficiently low thermal conductance, that all of the power input to the portion of the probe where the temperature is measured can be assumed to flow radially into the surrounding medium whose thermal conductivity is to be determined.

Some investigators have used a two-wire or two-probe method in which the temperature is measured by a sensor located at some distance away from the line heat source. Under such conditions the value of $4\kappa t/r^2$ is usually not large enough for Eq. (5) to be valid so that the thermal conductivity needs to computed using Eq. (1).

A.2 Finite-Diameter Probe

Jaeger [A4; 2, pp. 344-345] has derived a solution for a finite-diameter probe, made of a perfect conductor , with finite thermal contact resistance between the probe and the surrounding medium. As above, the medium is assumed initially to be isothermal at $T = 0$ when the probe is energized at the constant rate Q per unit time per unit length. The temperature of the probe is given by

$$T(t) = \frac{Q}{\lambda} G(\beta, \alpha, \tau) \quad , \tag{6}$$

where

$$G(\beta, \alpha, \tau) = \frac{2\alpha^2}{\pi^3} \int_0^\infty \frac{[\,1 - \exp(-\tau u^2)\,]\, du}{u^3 \Delta(u)} \quad , \tag{7}$$

and J_i and Y_i are the Bessel functions of the first and second kind, respectively, of order I. The dimensionless parameters β, α, and τ are defined as

$$\beta = \frac{\lambda}{bh} \qquad \alpha = \frac{2\pi b^2 \rho C}{S} \qquad \tau = \frac{\kappa t}{b^2} \quad , \tag{9}$$

where the properties of the medium are thermal conductivity, λ [W/m·K], density, ρ [kg/m^3], specific heat, C [J/kg·K], and thermal diffusivity, κ [m^2/s]; the probe is of radius b [m]; S [J/m·K] is the thermal capacity per unit length of the probe; and h [W/m^2·K] is the heat transfer coefficient between the probe and the surrounding medium. The dimensionless parameter β is the ratio of the thermal contact resistance, $1/h$, at the probe-medium interface to the thermal resistance, b/λ, of a layer of the medium of thickness b. The dimensionless parameter α is twice the ratio of the thermal capacity of a cylinder of the medium material of radius b to the thermal capacity of an equal length of the probe. (Note that the probe could actually be a hollow cylinder, rather than a solid cylinder, with S being the thermal capacity of the actual probe material present.) The parameter τ is the usual dimensionless time that is used in transient heat conduction problems, obtained by multiplying the actual time by the ratio of the thermal diffusivity to the square of a characteristic dimension, in this case the radius of the probe (this parameter τ is often referred to as the Fourier number).

The integration shown in Eq. (7) cannot be carried out in closed form so it must be done numerically. For small values of τ, Jaeger [A4] shows that

$$G(\beta, \alpha, \tau) \approx \frac{\alpha}{2\pi}\left[\tau - \frac{\alpha}{2\beta}\tau^2 + \cdots\right] \tag{10}$$

when the heat transfer coefficient h is finite so that $\beta > 0$, and

$$G(\beta, \alpha, \tau) \approx \frac{\alpha}{2\pi}\left[\tau - \frac{4\alpha}{3\sqrt{\pi}}\tau^{3/2} - \cdots\right] \tag{11}$$

when h is infinite (perfect contact) so that $\beta = 0$. For large values of τ, Jaeger [A4] shows that

$$G(\beta, \alpha, \tau) \approx \frac{1}{4\pi}\left[2\beta - \gamma + \ln 4\tau - \frac{4\beta - \alpha}{2\alpha\tau} + \frac{\alpha - 2}{2\alpha\tau}(-\gamma + \ln 4\tau) + \cdots\right] . \quad (12)$$

For values of τ sufficiently large that the last two terms, involving τ^{-1}, can be neglected, Eq. (12) reduces to

$$G(\beta, \alpha, \tau) \approx \frac{1}{4\pi}[2\beta - \gamma + \ln 4\tau + \cdots] . \quad (13)$$

If the probe has a vanishingly small thermal capacity, so that $\beta \to 0$, Eq. (13) reduces to Eq. (4), the expression for an ideal line source. Two features of Eq. (13) are worthy of note. First, for long enough times, the thermal capacity of the probe is no longer a factor. Second, for long enough times, the effect of thermal contact resistance becomes independent of time so that one can compute thermal conductivity from a plot of temperature versus the logarithm of time without having to know either the thermal contact resistance or the thermal capacity of the probe. For a line heat source or a very slender probe such as those used for laboratory measurements on loose-fill materials, it is relatively easy to work in the region where Eq. (13) is valid. However, a probe for *in-situ* measurements of the thermal properties of soils must be rugged enough, and thus large enough in diameter, to be inserted 1 or 2 meters into the ground. Since τ is inversely proportional to the square of the radius of the probe, increasing the probe diameter by, say, an order of magnitude in order to achieve adequate strength, reduces the values of τ by two orders of magnitude. Thus, as is discussed in more detail below, for the probes to be developed for this project, it is necessary to use expressions that are more accurate than Eq. (13) for the values of τ that are of concern.

It also is of interest to examine the behavior of Eq. (7) in the limit when $\alpha \to \infty$. This limit corresponds to the case where the probe is of finite diameter but has negligible thermal capacity. Such a probe could be approximated by a very thin-walled hollow tube. As shown by Jaeger [A4], for $\beta = 0$ and $\alpha \to \infty$,

$$G(0, \infty, \tau) = \frac{2}{\pi^3}\int_0^\infty \frac{[1 - \exp(-\tau u^2)]\,du}{u^3[J_1^2(u) + Y_1^2(u)]} . \quad (14)$$

For finite values of thermal contact resistance (i.e., $\beta > 0$),

$$G(\beta, \infty, \tau) = \frac{\beta}{2\pi} + G(0, \infty, \tau) \quad ; \tag{15}$$

it is seen that β only shows up with respect to the constant temperature drop between the probe and the medium. Thus , for determinations of thermal conductivity, it is not necessary to know or to determine the thermal contact resistance. Equation (14) is the same as the solution for an infinite region with constant heat flux at $r = a$ [A1, p. 338].

Blackwell [A5] derived, with very different notation, the equivalent solution to Es. (6)-(9). In his short-time approximate solution, he included one more term that is given in Eq. (10); in our notation it is

$$G(\beta, \alpha, \tau) \approx \frac{\alpha}{2\pi}\left[\tau - \frac{\alpha}{2\beta}\tau^2 + \frac{8\alpha}{15\sqrt{\pi}\beta}\tau^{5/2} - \cdots\right] . \tag{16}$$

Blackwell's long-time approximation, with appropriate changes in notation agrees with Eq. (12), above. Blackwell [A5] also considered the problem of a hollow cylindrical probe, having a finite thermal conductivity, with heat supplied at the outer surface of the probe and the temperature measured at the inner surface. He obtained large-time and short-time solutions that agreed with Eqs. (12) and (16), above but with the inclusion of correction terms that account for the temperature difference between the inner and outer radii of the probe. As pointed out by Blackwell [A5] and by Wechsler [A6], the corrections in Blackwell's equations are quite small for well-designed probes. Furthermore, in the long-time solution given by Blackwell the correction term for finite probe thermal conductivity varies as τ^{-1} so that, for times long enough that Eq. (13) is valid, it drops out.

De Vries and Peck [A7] derived a long-time solution for a cylindrical probe, of finite thermal conductivity, with an ideal line heat source at its axis. With appropriate change of variables, their solution is identical to Eq. (12), with the addition of a term $(-1/\alpha)(\lambda/\lambda_p)\cdot\tau^{-1}$, where λ_p is the thermal conductivity of the probe material, inside the square brackets. For a homogeneous probe, this term reduces to $(-1/2)(\kappa/\kappa_p)\cdot\tau^{-1}$, where κ_p is the thermal diffusivity of the probe material. As with Blackwell's solution, the correction term for finite probe conductivity is not needed for times long enough that Eq. (13) can be used.

Christoffel and Calhaem [A8] give solutions, analogous to those of Carslaw [A4], for a perfectly conducting probe with no contact resistance, a perfectly conducting probe with contact resistance, and a probe having a finite thermal conductivity but no contact resistance. Although these authors do not indicate where the heat source is, their solution for a probe having a finite thermal conductivity appears to correspond to a probe heated at its outer surface. Their correction for finite probe conductivity is similar to that of Blackwell, whose solution is for a probe with heat supplied at its outer surface.

Bruijn, et al. [A9] used a "modified Jaeger model," which was a homogeneous solid cylindrical probe having the same thermal capacity per unit length as the real probe and an effective thermal contact resistance consisting of the contact resistance between the outer surface of the probe and the surrounding medium and an internal thermal resistance computed between the position of the temperature sensor and the outer radius of the probe. This internal resistance was computed for an idealized probe, with the heater at the axis, surrounded by a hollow cylinder of electrically insulating material (in which the temperature sensor was placed), and an outer metal cylinder. The internal resistance was assumed to be that computed for steady-state radial heat flow in the idealized probe, on the basis that the time constant of the probe is so short compared to the duration of a test that a steady-state temperature profile would be established in the probe.

Bruijn, et al., also give equations for a "four-regions model," consisting of coaxial cylinders: heating wire, insulating material, tube, and medium to be measured. These equations were left in terms of the Laplace-transformed temperatures and therefore are not suitable for use in data analysis.

Lin and Love [A10] give analytical solutions, similar to those of Jeager [A4] and of Blackwell [A5], for a system consisting of a probe, a well casing, and a surrounding medium. The probe and the well casing are assumed to have infinite radial thermal conductivity. They investigate the cases with and without thermal contact resistance at the interfaces and obtain integral solutions, large-time approximate solutions, and small-time approximate solutions. While their results are valuable, the extra complexity of three regions, rather than two, is not needed for the present project.

Bastian and Grosjean [A11] provide analytical solutions for probe consisting of a hollow pipe, open at the ends, with the unique feature that the material being tested in situated both outside and inside the probe.

All of the above theory was based on the assumption that the probe was infinite in length. In a separate paper, Blackwell [A12] examined the errors due to axial heat flow in a finite-length probe and provided guidelines for selecting a suitably long probe to avoid significant errors. Kierkus, et al.,[A13] have examined end effects in conjunction with a line heat source method for fluids.

As indicated previously, most investigators have used a simple large-time solution, such as Eq. (5) or (13), while a few investigators have used a somewhat more involved expression, such as Eq. (12). Very few workers have used an integral expression, such as Eqs. (6)-(9), that is valid over the entire time range.

In conjunction with the Thermal Property Analyzer (TPA) developed for EPRI by workers at Ontario Hydro [A14], a program was written that used a non-linear least squares fit to Blackwell's model [A5] to obtain thermal diffusivity and thermal contact resistance from the temperature versus time data, experimentally determined probe parameters ("effective probe radius" and probe thermal capacity), soil thermal conductivity, and probe power. It is not evident why these investigators elected to compute the thermal conductivity, separately, from the slope of the temperature-versus-time curve, rather than to have the computer program determine thermal conductivity as well. It appears that they computed thermal conductivity from the large-time data, where thermal diffusivity (or heat capacity) of the soil and contact resistance would cause relatively little effect, and then

computed the thermal diffusivity and contact resistance using small-time data. It would be preferable to have the computer use the entire temperature-time history and obtain self-consistent values for thermal conductivity, thermal diffusivity/heat capacity, and contact resistance. With the microprocessors that were available two decades ago, these investigators had to use a simpler approach for the software built into the TPA. They only used the non-linear curve fit program with a mainframe computer.

At about the same time, investigators at Sandia National Laboratories developed equipment and data analysis procedures [A15-A19] for using a probe method to determine the thermal conductivity of powders at high temperatures. These workers used Jaeger's analysis [A4], namely our Eqs. (6)-(9), (11), and (12), as well as finite element or finite difference techniques, to assist in designing their probes. For data analysis, they used a non-linear least squares fit, or parameter estimation technique, based on Jaeger's analysis. There is a significant gap between the range of validity of the small-time solution, Eq. (11), and that of the large-time solution, Eq. (12). There is an intermediate range of τ where neither solution even comes close to providing accurate results. The Sandia workers used the full integral solution, our Eqs. (6)-(9), for small and intermediate values of time and Eq. (12) for large times. They carried out a numerical study to determine what values of τ, for a given β and α, to use for the transition from one solution to the other, so as to obtain good continuity in temperature and its derivative with respect to time. (Discontinuity in either quantity, and particularly in the derivative, can wreck havoc with a non-linear least squares fit.) Koski [A17] indicated that the integral equation, our Eq. (7) proved difficult to integrate in a simple, rapid manner, particularly for larger values of τ, which is the reason they used the approximate solution for larger times.

A.3. Numerical Results

A FORTRAN program was written to compute values of $G(\beta, \alpha, \tau)$, using Eqs. (6)-(9), (14), and (15). Figure A1 shows G plotted versus τ with α as a parameter for $\beta = 0$, i.e., no contact resistance. Considering first the ideal probe with no thermal capacity, i.e., $\alpha \to \infty$, it is seen that, in this semi-log plot, the probe temperature curves rather slowly at small and medium times and asymptotically approaches a straight-line for values of τ greater than about 100, in accordance with Eqs. (5) and (13). Figure A1 includes curves corresponding to $\alpha = \infty$, 100, 50 , 20, 10, 5, 2, 1, 0.5, 0.2, and 0.1 Although the curves for the larger values cannot be distinguished, Figure A2 shows that as the thermal capacity of the probe approaches and then exceeds the thermal capacity of an equivalent volume of the surrounding medium (e.g., soil), a significant time delay is introduced at earlier times. When the contact resistance is zero, as in this case, or relatively small, the time lag due to a probe having a thermal capacity approximately equal to that of the medium (i.e., $\beta \approx 2$) actually results in the curve of temperature versus the logarithm of time approaching a straight line more rapidly than in the case where the probe has a very small thermal capacity. When the thermal capacity of the probe greatly exceeds that of an equivalent volume of the medium, the probe temperature lags behind until values of τ of the order of 1000 are attained. Inspection of Fig. A1 shows that if data over a rather limited range of temperatures, say τ going from 10 to 100, were used, it would be easy to be fooled into thinking the "straight-line region" had been reached but the slope thereby used to compute thermal conductivity could be significantly in error.

Figure A2 shows the same curves as those in Fig. 1, but plotted with a different vertical axis in order to facilitate comparison with the next four figures. Figure A3 shows how the curves change when contact resistance is present, in this case corresponding to $\beta = 1$ (i.e., the contact resistance is equal to the resistance of a plane layer of the surrounding medium having a thickness equal to the radius of the probe). For the case of a very light probe, with $\alpha \to \infty$, the contact resistance simply displaces the temperature-time curve upward, as shown by Eq. (15). For probes having large thermal capacity, the probe temperature cannot "jump" in response to the contact resistance so the temperature of such probes initially increases slowly and then accelerates to "catch up" with the curve for probes having very low thermal capacity. A potentially serious consequence of this behavior is that the curves of temperature versus the logarithm of time can have deceptively linear regions that are much steeper than the true final slope, thus exacerbating the potential error in thermal conductivity. Figures A4, A5, and A6 show the computed temperature-time curves for larger contact resistances, with $\beta = 2$, 3, and 4, respectively. The effects discussed above in this paragraph are exaggerated further as contact resistance increases.

The results shown in these figures clearly illustrate that great caution must be exercised in attempting to use the large-time solutions, such as Eq. (12) or Eq. (13), to determine thermal conductivity. This caution is required because the thermal capacity of the probe and the thermal contact resistance between the probe and the surrounding medium can seriously distort the shape of the temperature-time curve and result in serious measurement errors. The results in these figures also show that, for a given probe, the temperature-time curve is sensitive to the thermal capacity of the medium during the small and medium times but not at long times. Thus, if the heat capacity or the thermal diffusivity of the soil is desired, it is necessary to use information from the early part of the curve; these properties cannot be obtained from large-time data only. Finally, these curves and the above discussion demonstrate the importance of using the complete curve of temperature versus the logarithm of time if it is desired to obtain consistent, accurate values for thermal conductivity, thermal diffusivity, heat capacity, and thermal contact resistance.

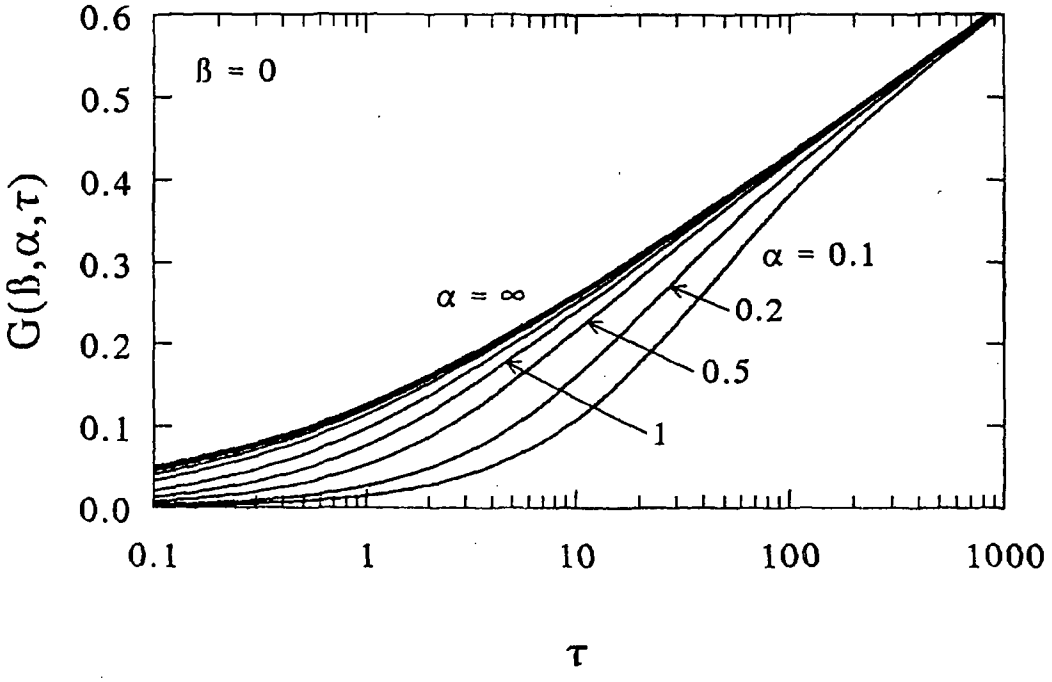

Figure A1. The function $G(\beta, \alpha, \tau)$ versus τ, with α as a parameter, for $\beta = 0$.

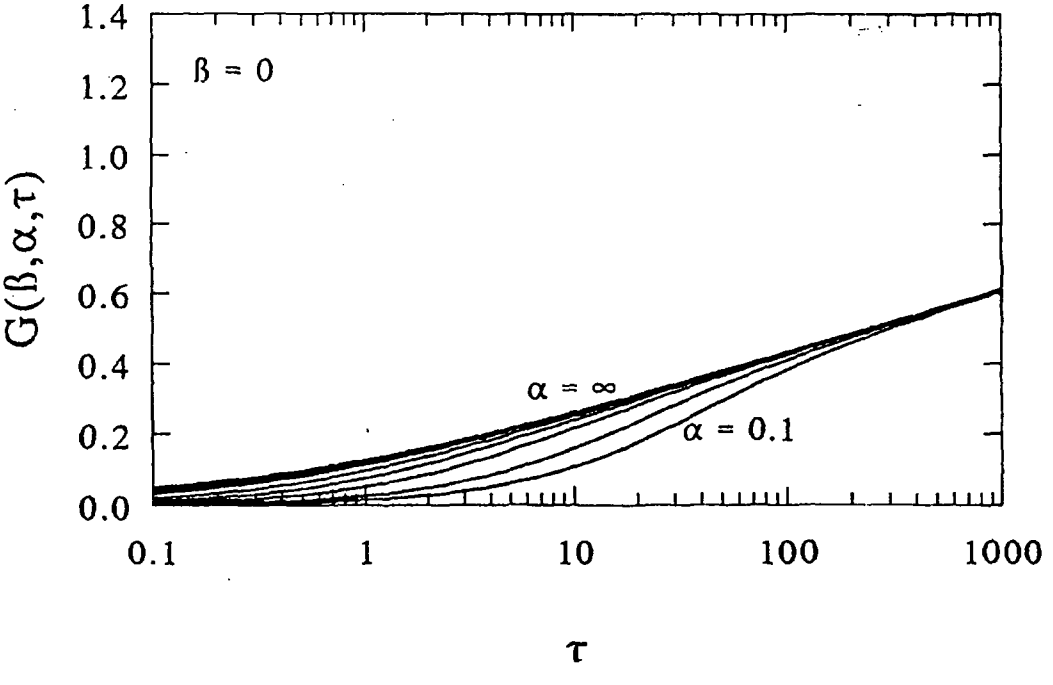

Figure A2. This figure is the same as Figure 1, but with a different vertical scale.

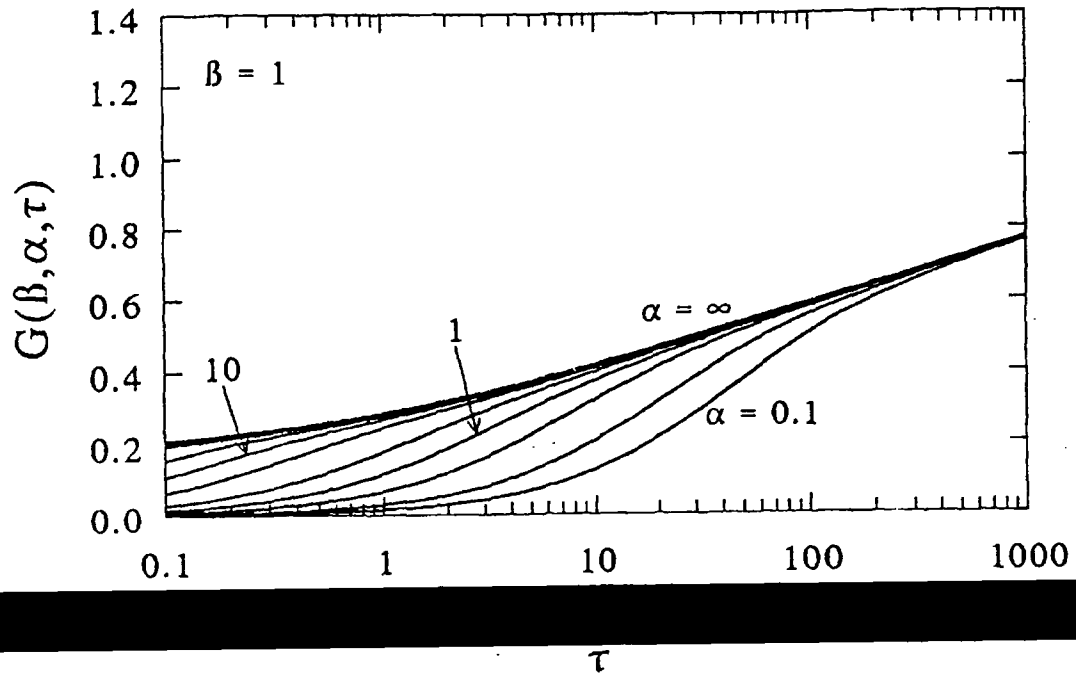

Figure A3. The function $G(\beta, \alpha, \tau)$ versus τ, with α as a parameter, for $\beta = 1$.

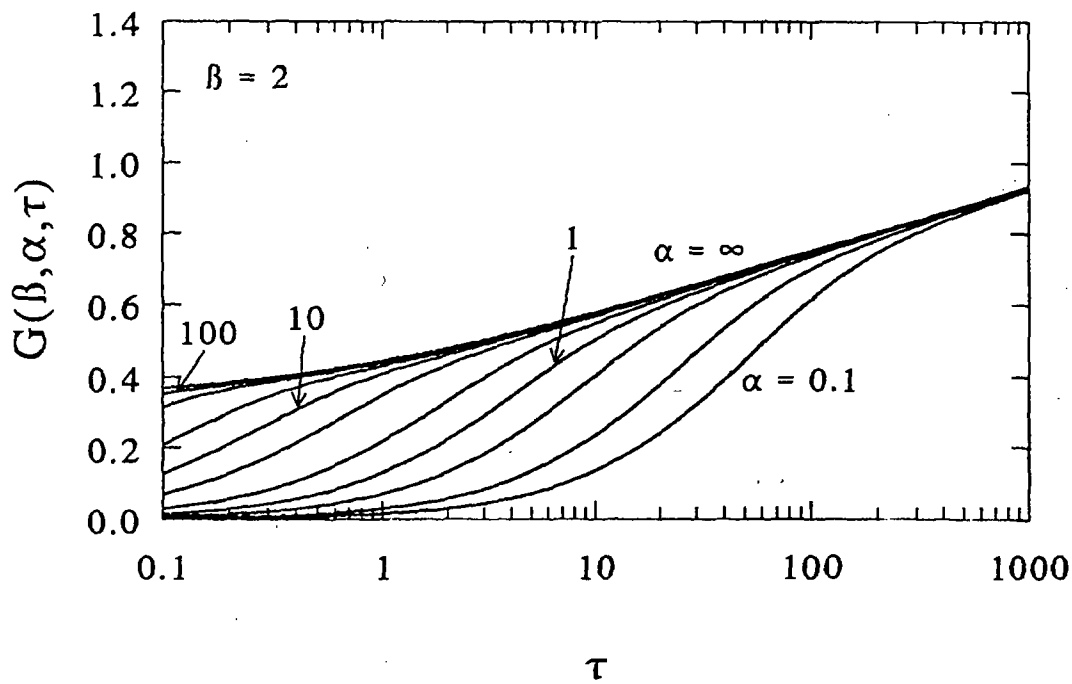

Figure A4. The function $G(\beta, \alpha, \tau)$ versus τ, with α as a parameter, for $\beta = 2$.

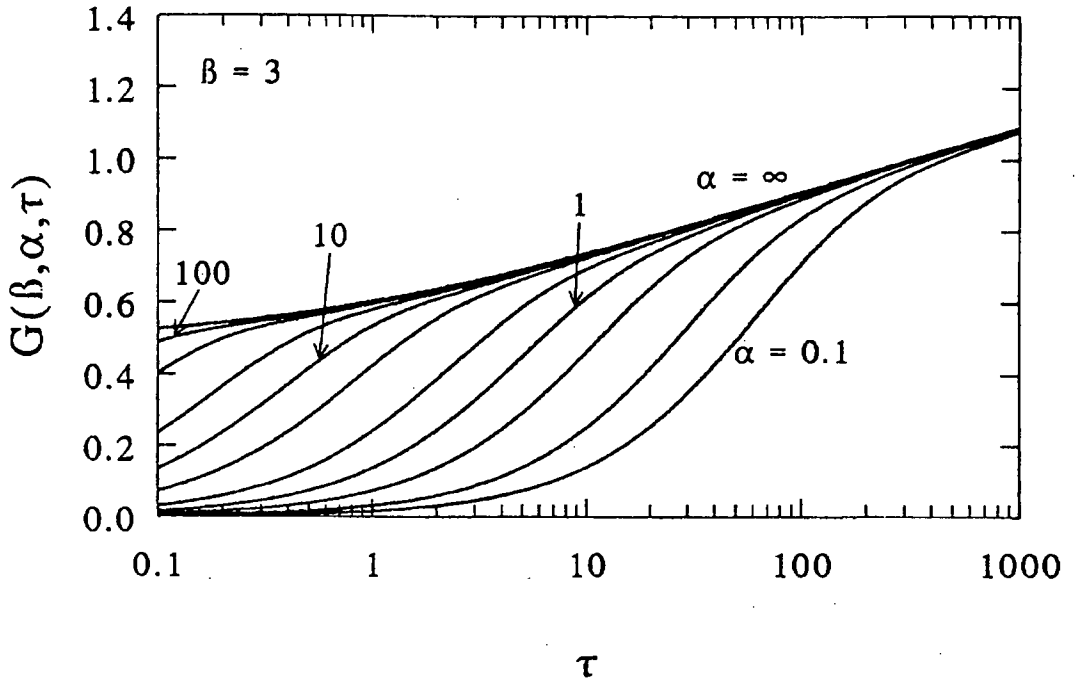

Figure A5. The function $G(\beta, \alpha, \tau)$ versus τ, with α as a parameter, for $\beta = 3$.

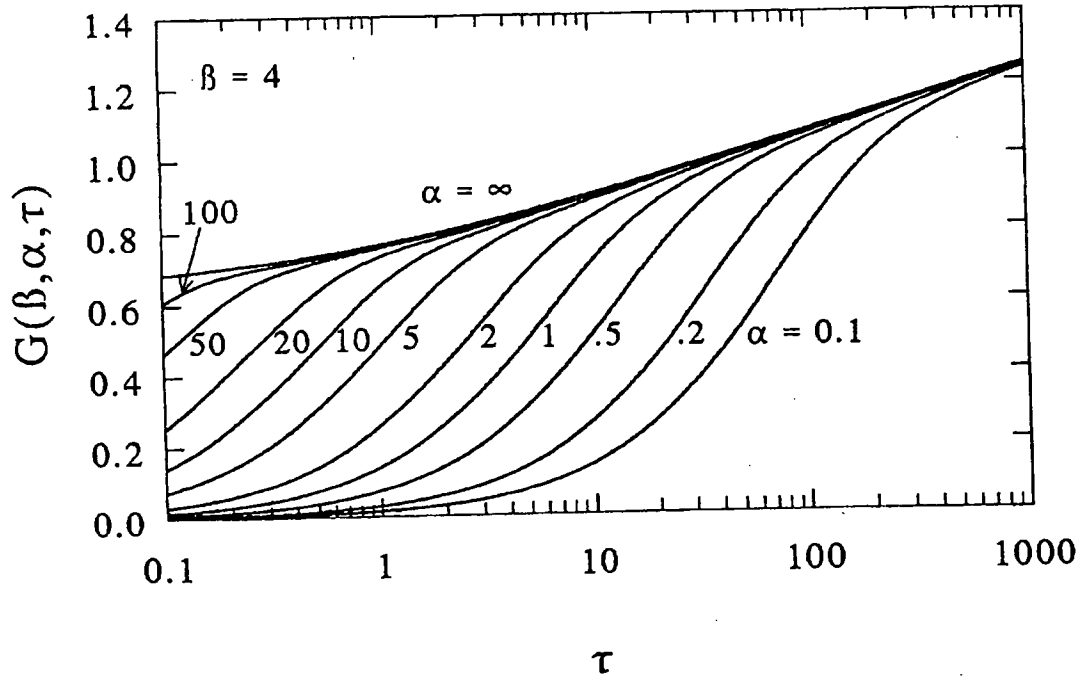

Figure A6. The function $G(\beta, \alpha, \tau)$ versus τ, with α as a parameter, for $\beta = 4$.

A.4. References

[A1] Carslaw, H.S. & Jaeger, J.C. (1959). *Conduction of Heat in Solids (2nd Ed.).* New York, NY: Oxford University Press.

[A2] Nieto de Castro, C.A., Taxis, B., Roder, H.M., and Wakeham, W.A. (1988). Thermal diffusivity measurement by the transient hot-wire technique: a reappraisal. *International Journal of Thermophysics, 9*(3), 293-316.

[A3] Fareleria, J.M.N.A. & Nieta de Castro, C.A. (1989). Simultaneous measurement of the thermal conductivity and thermal diffusivity of fluids. *High Temperatures - High Pressures, 21*(4), 363-371.

[A4] Jaeger, J.C. (1956). Conduction of heat in an infinite region bounded internally by a circular cylinder of a perfect conductor. *Australian Journal of Physics, 9*, 167.

[A5] Blackwell, J. H. (1954). A transient-flow method of determination of thermal constants of insulating materials in bulk. *Journal of Applied Physics, 25*, 137-144.

[A6] Wechsler, A.E. (1992). The probe method for measurement of thermal conductivity. In K. D. Maglic, A. Cezairliyan, and V. E. Peletsky (Eds.), *Compendium of Thermophysical Property Measurement Methods, Recommended Measurement Techniques and Practices* (Vol. 2, pp. 161-185). New York, NY: Plenum Press.

[A7] Vries, D.A. de & Peck, A.J. (1958). On the cylindrical probe method of measuring thermal conductivity with special reference to soils. I. Extension of theory and discussion of probe characteristics. *Australian Journal of Physics, 11*, 255-271.

[A8] Christoffel, D.A. & Calhaem, I.M. (1969). A geothermal heat flow probe for *in situ* measurement of both temperature gradient and thermal conductivity. *Journal of Scientific Instruments (Journal of Physics E), Series 2, 2*, 457-465.

[A9] Bruijn, P.J., van Haneghem, I.A., & Schenk, J. (1983). An improved nonsteady-state probe method for measurements in granular materials: Part I: theory. *High Temperatures - High Pressures, 15*, 359-366.

[A10] Lin, J. D. & Love, T. J. (1985). Analysis of a method of in-situ thermal properties determination for geologic formations. *Journal of Energy Resources Technology, Transactions of the ASME, 107*(1) 122-127.

[A11] Bastian, G. & Grosjean, R. (1991). A hollow cylindrical probe for the measurement of the thermophysical properties of loose materials. *High Temperatures - High Pressures 23*, 271-278.

[A12] Blackwell, J. H. (1956). The axial-flow error in the thermal-conductivity probe. *Canadian Journal of Physics, 34*, 412-417.

[A13] Kierkus, W.T., Mani, N. & Venart, J.E.S. (1973). Radial-axial transient heat conduction in a region bounded internally by a circular cylinder of finite length and appreciable heat capacity. *Canadian Journal of Physics, 51*, 1182-1186.

[A14] Boggs, S. A., Chu, F. Y., Radhakrishna, H. S. & Steinmanis, J. (1980). Measurement of soil thermal properties -- techniques and instrumentation. *IEEE Transactions Power Apparatus Systems PAS-99*(2), 747-752.

[A15] Drotning, W.D. (1983). An automated thermal conductivity probe and applications to powders. In T. Ashworth and D.R. Smith (Eds.) *Thermal Conductivity 18.* New York, NY: Plenum Press.

[A16] Drotning, W.D., Koski, J.A. & Havey, P.E. (1981). *Development of a technique for measurement of the thermal conductivity of powders at high temperatures.* (Report No. NUREG/CR-2287, SAND 81-0631). Albuquerque, NM: Sandia National Laboratories.

[A17] Koski, J.A. (1981). *Analysis of thermal conductivity probes for high temperature applications* (Report No. SAND 81-0106). Albuquerque, NM: Sandia National Labs.

[A18] Koski, J.A. (1982). *CONFIT: a computer code for thermal conductivity probe data reduction with the use of parameter estimation techniques*, (Report No. SAND 82-0741). Albuquerque, NM: Sandia National Labs.

[A19] Koski, J.A. & McVey, D.F. (1983). Application of parameter estimate techniques to thermal conductivity probe data reduction. In J.G. Hust (Ed.), *Thermal Conductivity 17.* New York, NY: Plenum Publishing Corporation.

Appendix B. Analysis Procedures for Transient Plane-Source Techniques for Thermal Conductivity Measurement

The literature concerning analysis procedures for transient plane-source techniques for thermal conductivity measurement is much less extensive than is the case for transient hot-wire or probe techniques. In particular, there is less information available concerning the effects of the heat capacity of the heater and the effects of contact resistance. Accordingly, as part of the development of a suitable apparatus for use at NIST, appropriate mathematical models need to be developed and programmed.

In this appendix, some of the mathematical models from the literature are briefly summarized. The references cited in this appendix are those from Section 8.

Gustafsson's Transient Strip Method [101-103]

Consider a thin strip heater of width $2d$, sandwiched between two slabs of material having density ρ, specific heat C, thermal conductivity λ, and thermal diffusivity $\kappa = \lambda/\rho C$. The assembly is initially isothermal and at time $t = 0$, the heater is energized with a constant electrical current, resulting in a power input Q per unit length. To first order, the voltage drop V across the heater of resistance R varies as

$$\frac{V}{V_0} = 1 + \frac{\alpha Q}{\lambda} \cdot g(\kappa t/d^2) \quad , \tag{1}$$

where V_0 is the voltage drop at $t = 0$ across the heater of resistance R_0, $\alpha = (1/R_0)\, dR/dT$ is the temperature dependence of the heater resistance, and $g(\,)$ is a mathematical function that is given by Gustafsson. When d is very small, Eq. (1) reduces, for reasonable values of t, to an expression equivalent to that given on p. A-2 for an ideal line heat source. The thermal conductivity can be obtained but it is not possible to obtain an accurate value for either the thermal diffusivity or the volumetric specific heat (ρC). When d is very large, Eq. (1) reduces, again for reasonable values of t, to the expression for an infinitely large plane heat source; the quantity known as the "effusivity," $\lambda \rho C = \lambda^2/\kappa$, can be obtained but it is not possible to obtain the individual thermophysical properties. A bit more needs to be said about "reasonable values of t." If d is very small, information about volumetric specific heat or thermal diffusivity could only be obtained for times that are so short that the thermal wave has barely begun to penetrate the test medium and further, so short that it would be difficult to make accurate measurements of the variation in the voltage drop across the heater. If d is very large, information about individual thermophysical properties could only be obtained for times that are so long that the assumptions of an infinitely large medium with negligible heat losses would not be valid. Gustafsson argues that if d is chosen so that, for reasonable times, the maximum argument of $g(\,)$ is approximately unity, it is possible to obtain reliable values for ρC, λ, and κ from a single experiment.

As mentioned above, Eq. (1) is a first-order expression. Gustafsson [103] also has derived a second-order expression for the time dependence of the voltage drop across the heater.

Brydsten and Bäckström Hot Strip Method [104]

As described on p. 79, Brydsten and Bäckström used one strip as a heater and a second strip as a thermometer. Their first-order mathematical analysis results in an expression analogous to Eq. (1) of this appendix, but with a different form for $g(\,)$. The use of a separate thermometer should make it possible to obtain reliable values for ρC, λ, and κ from a single experiment with less restriction on the width of the heater strip than is the case for Gustafsson's method; however, it would be necessary to carry out computations to confirm this supposition.

Gustafsson's Transient Plane Source Method [105-106]

As briefly described on p. 80, this technique uses a rectangular or circular patch heater, resembling a resistance strain gage, that also serves as a thermometer. Again the functional form of the first-order expression for the voltage drop across the heater is similar to Eq. (1) of this appendix, with a different form for $g(\,)$, depending upon the heater geometry.

Vernotte's Method [107-113]

There are several computational techniques presented in these papers. The technique originally used by Clarke and Kingston [107] is similar to that described below for Harmathy's method. Since it is not planned to use Vernotte's method for this project, the various computational techniques are not summarized here.

Harmathy's Method [121-125]

As described on pp. 82-83, Harmathy [121] used a heater that had essentially the same lateral dimensions as the specimen pieces so that, in contrast to Gustafsson's and Brydsten and Bäckström's methods, he obtained essentially one-dimensional heat flow. Neglecting the heat capacity of the heater and neglecting thermal contact resistance, Harmathy used a standard formula for the temperature rise, T, at position z in an infinite solid with constant heat flux in the $z = 0$ plane,

$$T = \frac{Pz}{\lambda} \cdot \left(\frac{\kappa t}{z^2} \right)^{\frac{1}{2}} \cdot \text{ierfc} \, \frac{1}{2} \left(\frac{z^2}{\kappa t} \right)^{\frac{1}{2}} \quad , \tag{2}$$

where $P/2$ is the heat flux into one specimen, of the pair, and ierfc( ) is the integrated complimentary error function. If the temperature rise at the heater were to be measured, Eq. (2) would reduce to

$$T = \frac{P}{\lambda} \cdot \left(\frac{\kappa t}{\pi} \right)^{\frac{1}{2}} = P \cdot \left(\frac{t}{\pi \lambda \rho C} \right)^{\frac{1}{2}} \quad , \tag{3}$$

and, as discussed following Eq. (1), it is only possible to determine the effusivity and not any of the normally defined thermophysical properties. This problem does not arise, however, if the temperature is measured at a sufficiently large distance from the location of the heater. Harmathy

let $z = \ell$, the thickness of the "measuring piece," as shown in Figures 59 and 60 of this report, wrote two equations of the form of Eq. (2), one at time t and the other at time $2t$, and formed the ratio

$$\frac{T(2t)}{T(t)} = \frac{\sqrt{2}\ \text{ierfc}\ \frac{1}{2}\left(\frac{\ell^2}{2\kappa t}\right)^{\frac{1}{2}}}{\text{ierfc}\ \frac{1}{2}\left(\frac{\ell^2}{\kappa t}\right)^{\frac{1}{2}}} \quad . \tag{4}$$

He computed this function and compared it to the experimental data in order to obtain κ and then inserted that value of κ into Eq. (2) to compute λ. With modern computers, it would probably be simpler to use non-linear parameter estimation techniques.

Pulse Methods [127-129]

For an instantaneous planar heat pulse in an infinite body, the resultant temperature at a distance ℓ from the heat source is given by [129]

$$T = \frac{H}{2\rho C\sqrt{\pi\kappa t}} \cdot \exp\left(-\frac{\ell^2}{4\kappa t}\right) \quad , \tag{5}$$

where H is the energy per unit area provided by the heater. This function has the form shown on the right-hand-side of Figure 62, on p. 84. The maximum temperature T_m occurs at the time t_m when $\kappa t/\ell^2 = 1/2$, and thus κ can be computed from

$$\kappa = \frac{\ell^2}{2t_m} \quad . \tag{6}$$

Substituting $\kappa t/\ell^2 = 1/2$ into Eq. (5), the value of the maximum temperature is given by

$$T_m = \frac{H}{\sqrt{2\pi e}\ \ell\rho C} \tag{7}$$

so that the volumetric heat capacity can be computed from

$$\rho C = \frac{1}{\sqrt{2\pi e}} \cdot \frac{H}{\ell T_m} = 0.2420 \cdot \frac{H}{\ell T_m} \quad . \tag{8}$$

The thermal conductivity is then computed from $\lambda = \kappa\rho C$.

If the pulse length is not short compared to t_m, it is necessary to use a more complicated expression, than Eq.(5), that properly accounts for the pulse shape and duration. Kubičár [129] addresses this issue as well as the effects of the heat capacity of the heater, thermal contact resistances, and heat losses from the edge of the specimen.

Dzhavadov [127] obtains expressions analogous to those above. However, his specimens were not treated as infinite bodies (see Figure 61, on p. 84 of this report) and the pulse width was not negligible.

Giedd and Onn [128] used thin specimens and assumed that there was no heat loss from these specimens. Thus their theoretical temperature-time histories do not go through a maximum but rather asymptotically approach a constant value. They compute thermal diffusivity from the time required for the backside temperature to reach half of its final value. Specific heat is computed from the overall rise in temperature of the specimen when it reaches its final isothermal equilibrium value.

Piorkowska and Galeski's Continuous Ramp Method [130-131]

Since it is proposed to use a variant of this method for the high-strength concrete project, it is worthwhile to provide some detail as to the analysis procedure used by Piorkowska and Galeski. Consider a pair of specimens, each of thickness ℓ, with a thin heater between them at $z = \ell$. The heater is assumed to have negligible heat capacity and there is assumed to be no thermal contact resistance between the heater and the specimens. At the beginning of a test, it is assumed that the outside surfaces of the specimens, $z = 0$ and $z = 2\ell$ are at a temperature $T = 0$ and that the heater has been providing a constant heat flux P for a sufficiently long time that steady-state conditions have been achieved. Thus the initial conditions are

$$T(z,0) = \frac{Pz}{2\lambda} \quad \text{for } 0 \le z \le \ell$$
$$\text{and} \qquad T(z,0) = \frac{P(2\ell - z)}{2\lambda} \quad \text{for } \ell \le z \le 2\ell \quad . \tag{9}$$

At time $t = 0$, the outer surfaces of the specimens are programmed to change in temperature according to

$$T(0,t) = T(2\ell,t) = vt \quad , \tag{10}$$

where v is the constant rate of change of temperature with time. As shown by Piorkowska and Galeski, the resultant temperature distribution within the lower specimen, $0 \le z \le \ell$, will be

$$T(x,t) = \frac{Pz}{2\lambda} + vt - vF(x,t) \quad , \tag{11}$$

with a similar expression for the other specimen, except that the leading term is replaced by the second line of Eq. (9). The function $F(x,t)$ is given by

$$F(x,t) = \frac{16\ell^2}{\kappa\pi^3}\sum_{n=0}^{\infty}\frac{1}{(2n+1)^3}\sin\left(\frac{(2n+1)\pi z}{2\ell}\right)\left[1 - \exp\left(-\frac{(2n+1)^2\pi^2\kappa t}{4\ell^2}\right)\right] . \quad (12)$$

Evaluating Eq. (11) at $z = 0$ and $z = \ell$, the temperature difference across each of the samples is

$$\Delta T(t) = \frac{P\ell}{2\lambda} - \frac{v\ell^2}{2\kappa} + \frac{16v\ell^2}{\kappa\pi^3}\sum_{n=0}^{\infty}\frac{(-1)^n}{(2n+1)^3}\exp\left(-\frac{(2n+1)^2\pi^2\kappa t}{4\ell^2}\right) . \quad (13)$$

Note that only the first term in this equation involves the power to the heater. Thus if two tests are run with the same value for v but different values for P, say P_1 and P_2, and the corresponding values of the temperature difference across the specimen, ΔT_1 and ΔT_2, are subtracted from each other, the second and third terms cancel leaving simply

$$\Delta T_1(t) - \Delta T_2(t) = \frac{(P_1 - P_2)\ell}{2\lambda} = \text{a constant} . \quad (14)$$

Thus the thermal conductivity can be computed from

$$\lambda = \frac{(P_1 - P_2)\ell}{2[\Delta T_1(t) - \Delta T_2(t)]} . \quad (15)$$

Piorkowska and Galeski also show that Eqs. (14) and (15) are valid when the thermal conductivity and thermal diffusivity are functions of temperature.

Although Piorkowska and Galeski do not discuss the determination of thermal diffusivity, it also is straightforward to compute. The simplest case would be to consider Eq. (13) at times long enough that the transient third term has died out enough to be negligible. The thermal diffusivity is then given by

$$\kappa = \frac{v\ell^2}{2\left(\frac{P\ell}{2\lambda} - \Delta T(t)\right)} , \quad (16)$$

where the value of λ computed from Eq. (15) can be substituted. However, for a test with no power to the heater, κ is given simply by

$$\kappa = -\frac{v\ell^2}{2\,\Delta T(t)} , \quad (17)$$

where $\Delta T(t)$ is simply the amount that the temperature at the heater lags the temperature at the two outer surfaces of the specimens when they are heated according to $T = vt$.

NIST-114
(REV. 6-93)
ADMAN 4.09

U.S. DEPARTMENT OF COMMERCE
NATIONAL INSTITUTE OF STANDARDS AND TECHNOLOGY

MANUSCRIPT REVIEW AND APPROVAL

(ERB USE ONLY)	
ERB CONTROL NUMBER	DIVISION
PUBLICATION REPORT NUMBER: NIST GCR 99-767	CATEGORY CODE
PUBLICATION DATE: March 1999	NUMBER PRINTED PAGES

INSTRUCTIONS: ATTACH ORIGINAL OF THIS FORM TO ONE (1) COPY OF MANUSCRIPT AND SEND TO THE SECRETARY, APPROPRIATE EDITORIAL REVIEW BOARD

TITLE AND SUBTITLE (CITE IN FULL)

Response of High Performance Concrete to Fire Conditions

CONTRACT OR GRANT NUMBER: 43-NANB-809607

TYPE OF REPORT AND/OR PERIOD COVERED: METSys Report No. 98-01-101, December 1998

AUTHOR(S) (LAST NAME, FIRST INITIAL, SECOND INITIAL)

Flynn, D.R.
MetSys Corporation, Millwood, VA 22646-0317

PERFORMING ORGANIZATION (CHECK (X) ONE BOX)
- [ ] NIST/GAITHERSBURG
- [ ] NIST/BOULDER
- [ ] JILA/BOULDER

LABORATORY AND DIVISION NAMES (FIRST NIST AUTHOR ONLY)

SPONSORING ORGANIZATION NAME AND COMPLETE ADDRESS (STREET, CITY, STATE, ZIP)

U.S. Department of Commerce
National Institute of Standards and Technology, Gaithersburg, MD 20899

PROPOSED FOR NIST PUBLICATION

[ ] JOURNAL OF RESEARCH (NIST JRES)	[ ] MONOGRAPH (NIST MN)	[ ] LETTER CIRCULAR
[ ] J. PHYS. & CHEM. REF. DATA (JPCRD)	[ ] NATL. STD. REF. DATA SERIES (NIST NSRDS)	[ ] BUILDING SCIENCE SERIES
[ ] HANDBOOK (NIST HB)	[ ] FEDERAL INF. PROCESS. STDS. (NIST FIPS)	[ ] PRODUCT STANDARDS
[ ] SPECIAL PUBLICATION (NIST SP)	[ ] LIST OF PUBLICATIONS (NIST LP)	[x] OTHER NIST GCR
[ ] TECHNICAL NOTE (NIST TN)	[ ] NIST INTERAGENCY/INTERNAL REPORT (NISTIR)	

PROPOSED FOR NON-NIST PUBLICATION (CITE FULLY) [ ] U.S. [ ] FOREIGN

PUBLISHING MEDIUM
- [ ] PAPER
- [ ] CD-ROM
- [ ] DISKETTE (SPECIFY)
- [ ] OTHER (SPECIFY)

SUPPLEMENTARY NOTES

ABSTRACT (A 2000-CHARACTER OR LESS FACTUAL SUMMARY OF MOST SIGNIFICANT INFORMATION. IF DOCUMENT INCLUDES A SIGNIFICANT BIBLIOGRAPHY OR LITERATURE SURVEY, CITE IT HERE. SPELL OUT ACRONYMS ON FIRST REFERENCE.) (CONTINUE ON SEPARATE PAGE, IF NECESSARY.)

The NIST Building and Fire Research Laboratory (BFRL) has undertaken a project concerning the effect of fire on high strength concrete. Heating concrete to sufficiently high temperatures results in water of hydration being driven off, with a resultant irreversible loss of concrete strength. In addition, it has been observed that rapid heating of high strength concrete can result in spalling of the concrete. Computer models for prediction of temperature and pore pressure distributions in heated concrete typically include consideration of (1) mass transfer of air and water by diffusion and by forced convection, conversion of liquid water to vapor, and release of water of hydration and (2) heat transfer by conduction, mass diffusion, and forced convection. In order to make valid predictions, the computer models require reliable data as to the physical properties of the concrete. Mass transport properties are being investigated by the Building Materials Division. Thermal transport properties, the subject of this report, are being investigated by the Building Environment Division. The present report addresses (1) identification of materials properties critical to prediction of heat and mass transfer in high strength concrete at high temperatures, (2) variation of the thermal properties with temperature, pressure, and thermal history, (3) examination of correlations between concrete composition and thermal properties.

KEY WORDS (MAXIMUM OF 9; 28 CHARACTERS AND SPACES EACH; SEPARATE WITH SEMICOLONS; ALPHABETIC ORDER; CAPITALIZE ONLY PROPER NAMES)

computer models; concretes; fire tests; heat transfer; literature reviews; mass transfer; spalling; temperature

AVAILABILITY
- [x] UNLIMITED
- [ ] FOR OFFICIAL DISTRIBUTION - DO NOT RELEASE TO NTIS
- [ ] ORDER FROM SUPERINTENDENT OF DOCUMENTS, U.S. GPO, WASHINGTON, DC 20402
- [x] ORDER FROM NTIS, SPRINGFIELD, VA 22161

NOTE TO AUTHOR(S): IF YOU DO NOT WISH THIS MANUSCRIPT ANNOUNCED BEFORE PUBLICATION, PLEASE CHECK HERE. [ ]

WORDPERFECT

WVMP SAR Reference 3-20

"Lightweight Insulating Concrete for Floors and Roof Decks,"
R. W. Steiger and M. K. Hurd, Concrete Construction,
23(7), 1978.

Lightweight insulating concrete for floors and roof decks

By R. W. Steiger, Designer, and
M. K. Hurd, Consultant
Farmington, Michigan

The cost of energy production and the consequences of its indiscriminate use impel us to thoughts of conservation and the construction technologies that make it possible. Just as the human head loses a disproportionate amount of heat when not properly insulated with a covering, so a building can manifest a disproportionately high level of thermal transfer through its roof to the outside atmosphere if it lacks adequate insulation. Designers, builders and owners today as never before must become aware of the energy-saving potential of lightweight concrete used as insulating fill for floors and roofs.

This article is restricted primarily to the thermal insulation qualities of lightweight concretes, although many of these concretes serve capably for other insulation purposes. The insulating lightweight concretes may be considered according to composition in three groups:

I—Concretes made with expanded perlite or vermiculite aggregate or expanded polystyrene pellets. Oven-dry weight ranges from 15 to 60 pounds per cubic foot.

II—Cellular concretes made by incorporating air voids in a cement paste or cement-sand mortar, through use of either preformed or formed-in-place foam. These concretes weigh from 15 to 90 pounds per cubic foot.

III—Concretes made with aggregates prepared by calcining, sintering, or expanding such products as slag, clay, fly ash, shale or slate; also made with aggregates processed from natural materials such as scoria, pumice, or tuff. Concretes in this group range in weight from 45 to 90 pounds per cubic foot.

Data are given here for Groups I and II, because generally the most effective thermal insulation is found in the lower density ranges of these groups. However, attractive combinations of insulating and strength properties may be achieved with Group III concretes, and the reader is alerted to these possibilities (see box).

Design considerations

Looking at the broad spectrum of lightweight concretes now available (Figure 1), we find an almost infinite variety of mixes and a wide range of densities. It is diffi-

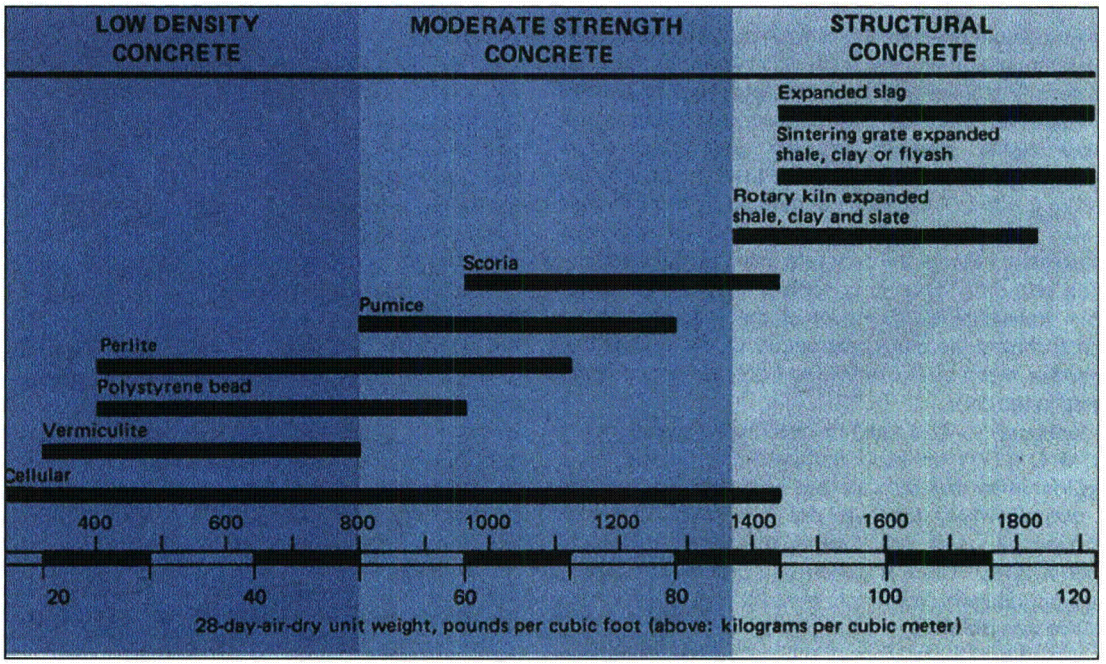

Figure 1. The full spectrum of lightweight concretes. Low density mixes discussed in this article (shaded band at left) offer best insulating properties. Chart adapted from ACI 213 report "Guide for Structural Lightweight Aggregate Concrete," *Journal of the American Concrete Institute*, August 1967, pages 433-469.

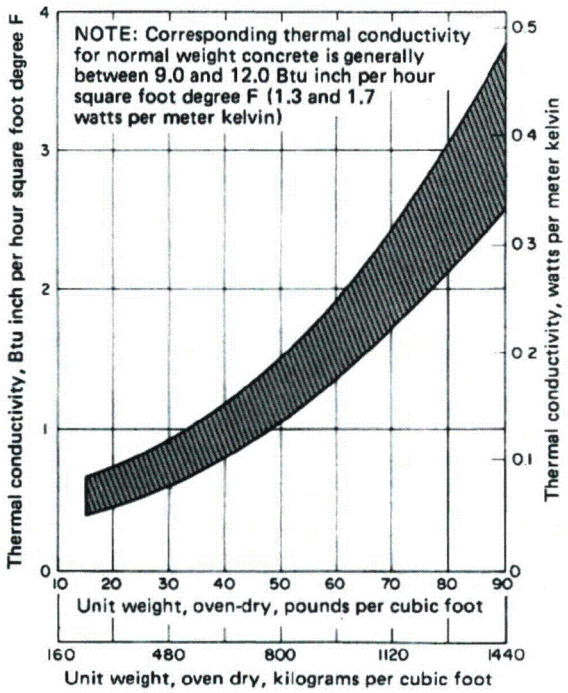

Figure 2. Approximate relationship between oven-dry unit weight and thermal conductivity of lightweight insulating concretes. From Special Types of Concrete, Portland Cement Association, Skokie, Illinois, Publication IS183T, 6 pages, 1977.

cult to draw a sharp line between structural and nonstructural capabilities, or to say at just what density a given type of concrete ceases to provide effective insulation. Generally, the heavier concretes in the group have higher strength and are less effective as insulation. The lightest concretes provide the best insulation—k-values from 0.4 to 0.7 Btu inch per hour square foot degree F—but very little strength. The designer must consider not only the insulating value of the concrete material, but also how it combines with other flooring or roofing materials and what the thermal transmittance (U-value) of the total system is. Trade and technical literature referenced at the end of this article provides much useful detail, and only general properties are mentioned here.

Thermal conductivity—This must be determined by laboratory test (ASTM C 177†) for each concrete mix design. As a general guide when test data are not available, the k-values (thermal conductivities) for oven-dry concretes shown in Figure 2 may be used. Moisture in the concrete affects thermal conductivity. There is generally a 5 percent increase in thermal conductivity for each percent increase in unit weight due to free moisture.

Compressive strength—As shown in Figure 3, compressive strength increases with increasing unit weight. Design requirements depend primarily on the installation. A compressive strength of 100 psi or even less may be quite acceptable for insulating underground steam lines; however, roof and floor fill requires enough early strength to withstand the traffic of workmen. Strengths of 100 to 200 psi are usually adequate, although up to 500 psi is sometimes specified.

Drying shrinkage—Shrinkage is not usually critical for low density fill or insulating concretes, although excessive shrinkage can cause curling. Moist cured cellular concretes made without aggregates do have high shrinkage.

Resistance to freezing and thawing—Lightweight insulating concrete is usually covered by roofing material such as hot mopped asphalt or pitch, and therefore not exposed directly to the elements. As for normal weight concretes, resistance to damage by freezing and thawing depends on the entrained air content of the mix.

Expansion joints: to use or not to use?– Follow the aggregate producers' recommendations. Some recommend insertion of a 1-inch expansion joint at the juncture of all roof projections and the concrete. Transverse expansion joints are used at a maximum spacing of 100

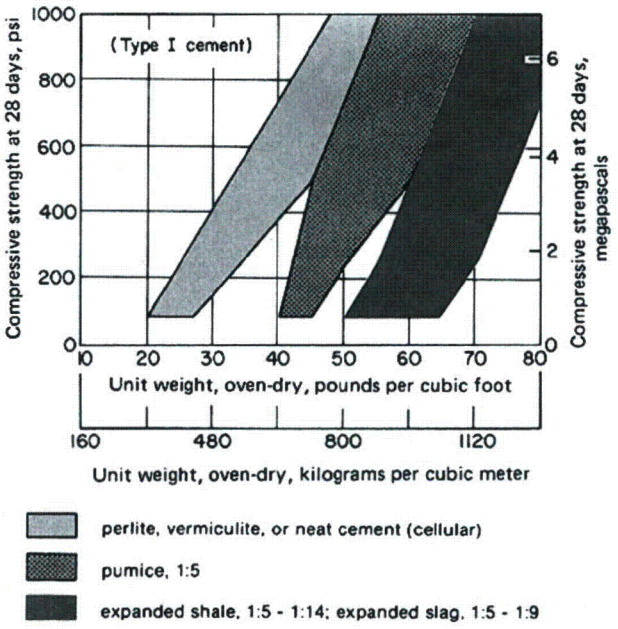

Figure 3. Approximate relationship between oven-dry unit weight and compressive strength of lightweight insulating concretes tested in air-dry conditions.
Note: mix **proportions for perlite and vermiculite concretes range from 1:3 to 1:10 by volume. From Special** Types of Concrete, **Portland Cement Association, Skokie, Illinois, Publication IS183T, 6 pages, 1977.**

† Standard Test Method for Seady-State Thermal Transmission Properties by Means of the Guarded Hot Plate.

feet in any direction to allow for a thermal expansion of 1 inch per 100 lineal feet. A joint material that will compress to one-half its thickness under a stress of 25 psi is generally used. With other aggregates, expansion joints may not be necessary because the initial shrinkage of the concrete is greater than any combination of thermal, moisture or freezing expansion that will occur in a roof deck.

Construction practices

Whether low density concrete is used as a floor fill or part of a roof deck, the form which supports it generally becomes a permanent part of the in-place construction. Typical forming or support systems include:

- Corrugated, galvanized sheet metal, appropriately vented and designed to carry the roof load.
- Insulating acoustical form board supported on flanges of steel subpurlins, with woven wire mesh reinforcement draped over the subpurlins to lie in the lower part of the concrete.
- Lath and mesh systems, where the concrete is placed on either paper backed wire mesh or a ribbed, expanded metal lath.
- Structural precast concrete or wood floors or roofs, where concrete serves as either leveling or insulating fill.

All of these systems require adequate venting in accordance with the recommendations of manufacturers and the National Roofing Contractors Association.

Mixing, placing and finishing—Proper consistency and uniform distribution of materials are necessary to achieve the required unit weight and can only be accomplished by mechanical means. Excessive mixing and handling can break down aggregate particles and should be avoided. Insulating concretes should be placed immediately after mixing by qualified technicians. Conventional placement methods can be used, but pumping is ideal and customarily used due to the normal consistency of lightweight insulating concrete.

Low density concrete should not be placed during rain or snow, nor should it be placed on a deck or form where standing water, snow or ice are present.

Workability—Insulating concretes have excellent workability because of their high air content. Appearance of the mix may be the most reliable indication of consistency. Slumps of 5 to 7 inches are usually quite satisfactory, and the mixtures are highly plastic and homogeneous.

Bleeding and segregation problems will not ordinarily be present. These mixtures can usually be placed simply by pouring and screeding, without further consolidation. This is particularly true with the cellular concretes which can be handled as liquids.

Curing and weather conditions—The surface of freshly smoothed low density concrete should be prevented from drying for not less than 3 days. If temperatures are above 40°F during the first 24 hours after placing, standard curing practices may be used. When temperatures during the first 24 hours are predicted to be from 30 to 40°F, high-early-strength cement and heated mixing water are recommended. Low density concrete should not be placed during freezing weather unless special cold weather procedures are followed.

Perlite concrete

Perlite, derived from the French word perle, resembles tiny clusters of pearls when viewed under the microscope. Perlite is a type of lava mined in large open pits in the western United States, and then crushed to sand sized particles for shipment to processing plants in 32 states. A small amount of water is locked inside the tiny particles and when heated to between 1500 and 2000° F the particles "pop" or expand, just like popcorn. The crude rock expands to about ten times its original volume.

Expanded perlite weighs only 7 1/2 to 10 pounds per cubic foot, approximately one-twelfth as much as sand. During the popping process, it changes to almost pure white from gray or black. The tiny perlite particles are composed of many minute glass-sealed dead air cells. The thermal conductivity of expanded perlite itself is 0.34 Btu inch per hour square foot degree F when graded for use as a concrete aggregate, which explains its excellent insulating value.

Perlite insulating concrete consists of a mixture of expanded perlite, portland cement, water and an air-entraining agent. The dry concrete weighs from 20 to 50 pounds per cubic foot, depending on the mix design selected. Perlite concrete can be placed monolithically on flat, uneven, curved or sloping surfaces. On flat roofs, the thickness of perlite concrete can be varied to provide specified drainage slopes.

The designer must select the strength and insulating value that he considers most appropriate to his project. The physical properties of perlite concrete are controlled by its dry density which is the principal factor in its specification. An ideal balance between reduced dead load, adequate compression and indentation strengths and good insulating value can be achieved with a density of 24 to 28 pounds per cubic foot. Greater densities can be specified if higher strengths or better nail holding capacity are more important than insulating value. For insulated floor slabs on grade, a density of 20 to 24 pounds per cubic foot is recommended.

Perlite roofs may have polystyrene insulation board sandwiched between layers of perlite concrete and supported on a metal deck. This system is capable of achieving U-values as low as 0.04 Btu per hour square foot degree F with a 2-hour fire rating.

Perlite concrete should meet the specified physical properties at the point of placement. It should be deposited and screeded in a continuous operation until the placing of a panel or section is completed. The 1-inch

expansion joints mentioned earlier should be installed through the full depth of the concrete around the perimeter of the roof deck and at the juncture of all roof projections (skylights, penthouses, ventilators, parapet walls) and perlite concrete.

The built-up roofing should be applied as soon as the perlite insulating concrete can carry construction traffic and is dry enough to develop adhesion with hot asphalt or pitch. Normally the perlite concrete should be permitted to cure at least three days.

For greater strength and corresponding higher density, blends of perlite and medium weight aggregates may be used. However, due to varying characteristics of naturally occurring aggregates in different parts of the country, the local perlite aggregate manufacturer should be consulted before specifying blends.

Vermiculite concrete

Vermiculite is a soft, laminated, mica-like material in its raw form. It is found in twelve states and mined commercially in seven. Vermiculite is a mineral that has few uses in its natural state but when heated and exfoliated becomes a lightweight aggregate of great value for fill and insulating concrete. The crude vermiculite is crushed, cleaned, dried and sized, and the resulting concentrate is shipped to processing centers, where it is heated in furnaces at temperatures of 1800 to 2000°F. Water molecules trapped in the flakes of vermiculite ore turn to steam and force the micaceous plates of the material to expand or exfoliate in an accordion-like fashion. Each individual granule is expanded to 10 to 15 times its original size. Air spaces thus formed convert the vermiculite into an aggregate that provides excellent insulating properties. Usually light brown or golden in color, the expanded product weighs from 6 to 10 pounds per cubic foot.

The components of vermiculite insulating concrete are expanded vermiculite aggregate, air-entraining admixture, portland cement, and water, all mixed and applied according to precise procedures. The ratio of cement to aggregate determines the density, strength and insulating value of the finished concrete. As used in the average roof deck, the ratio ranges from 1:4 to 1:8 by volume.

The resulting concrete mixture is usually pumped to the roof site and screeded into place over the structural base. Vermiculite concrete is installed in thicknesses of 2 inches and greater, depending on design needs and strength requirements. It weighs from 20 to 40 pounds per cubic foot, with compressive strengths from 90 to 500 psi.

Vermiculite roof deck assemblies have been developed using a slotted or perforated corrugated metal deck. These positive vented decks offer up to 3 percent open area in the steel form at no penalty or loss in structural performance. The openings help to speed up ventilating and drying of the insulating concrete. Insulation values are therefore quickly reached. In the event of subsequent roofing membrane leaks, the point of leakage is easily located on the underside of the metal decking.

Vermiculite concrete roof insulation, like perlite, can also be cast around a layer of polystyrene insulation board. A slotted opening pattern in the polystyrene permits vertical vapor flow through the board, in order to promote faster, more complete drying and venting of the concrete. The slots also ensure the positive locking and keying of the polystyrene board to the vermiculite concrete to enhance the shear strength of the insulation sandwich and provide a strong, composite roof insulation system. This system provides insulation with a U-value of 0.10 Btu per hour square foot degree F or less and a 1 1/2-hour fire rating.

Vermiculite lightweight concrete is best mixed and placed by experienced, licensed contractors. Current technology now permits contractors to pour quality decks in marginal weather, down to 32°F and even lower in certain cases.

Expanded polystyrene bead concrete

Expanded polystyrene, processed to a nominal density of 1 pound per cubic foot, serves as a stable, nonabsorptive aggregate in lightweight insulating concrete. Polystyrene, unlike perlite and vermiculite aggregate raw materials which are found in nature, is a polymer of styrene which is created by an involved chemical process from a liquid unsaturated hydrocarbon. The polystyrene is foamed to produce a lightweight aggregate. The polystyrene can be pre-expanded or supplied in an unexpanded form and foamed on the site by application of steam. During this process it expands to approximately 50 times its original size. Each closed cell aggregate particle contains prepackaged air and is

HEAVIER, STRONGER CONCRETES ALSO INSULATE

Low density concrete—50 pounds per cubic foot or less—provides the best insulation, but has limited strength. The user who needs greater strength without sacrificing all insulating properties should consider both aggregate and cellular concretes in the moderate density range. For information, consult the comprehensive (and encyclopedically titled) report of ACI Committee 523, "Guide for Cellular Concretes Above 50 pcf, and for Aggregate Concretes Above 50 pcf with Compressive Strengths Less Than 2500 psi." This report was published in the February 1975 issue of the Journal of the American Concrete Institute, pages 51-66, and is reprinted in Part 3 of the ACI Manual of Concrete Practice.

* Standard Method of Fire Tests of Building Construction and Materials

spherical in shape.

Typically, polystyrene bead lightweight insulating concrete consists of Type I or Type II portland cement, polystyrene aggregate expanded to a nominal density of 1 pound per cubic foot, air-entraining agent and water.

To enhance specific physical properties for a given application, additional mix components such as sand, limestone or pozzolans may be used. Depending upon the conditions of application, tensile stresses may be met by using mesh reinforcement, special bead aggregate coatings or a combination of the two.

Insulating roof fill of polystyrene bead concrete usually has a dry density of 26 to 30 pounds per cubic foot. Densities are available from 25 to 60 pounds per cubic foot. Fire resistance, verified by small scale ASTM E 119* fire tests conducted by the Portland Cement Association on 46-pound-per-cubic-foot-density concrete, resulted in the following ratings: 2 1/2-inch slab, 2 hours; 5-inch slab, 6 hours; 7-inch slab, 11 hours.

Polystyrene beads tend to resist absorption of water and are not readily wetted by water. Accordingly, cement paste or mortar does not adhere very well to them. Furthermore, their extremely low density makes them tend to segregate by floating out of the mix. To overcome this, the manufacturers have developed a number of bond-improving additives. Epoxy resin or an aqueous dispersion of polyvinyl propionate are recommended.

Shrinkage and swelling strains are high compared to dense concretes, and allowance must be made for this in the design. Polystyrene bead concrete has good workability, is quite pumpable, and requires minimum vibration in placement. Frost resistance is enhanced by entrained air, ranging from 5 to 10 percent of the matrix by volume.

As with all special types of concrete a technical consultant specializing in polystyrene lightweight concrete should be contacted for detailed recommendations covering formulations and mixing/placing techniques for your application.

Cellular concrete

Cellular insulating lightweight concrete owes its distinctive properties to a multitude of macroscopic, discrete air cells uniformly distributed throughout the mix. These cells may account for up to 80 percent of the total volume. Weight of the concrete may range from 12 to 90 pounds per cubic foot. Density and strength can be controlled to meet specific design requirements by varying the amount of air.

Numerous proprietary methods and agents are used to produce cellular concrete but essentially they can be considered in two groups, those using a preformed foam and those using formed-in-place foam. Formed-in-place foam is generated by special high speed mixing of water, foaming agent, cement and aggregates (if any) to allow foam to form in the mixer. Initially large air bubbles are reduced to a reasonably uniform size as mixing proceeds.

By the other method, a uniform preformed aqueous foam is blended with a portland cement and water slurry using only enough water to ensure proper hydration of the cement and facilitate the placing operation. The portland cement used may be Type I, II, III or portland blast-furnace slag cement, Type IS. The foam itself is made by blending a foam concentrate, water and compressed air in predetermined proportions in a foam generator calibrated for discharge rate. The concrete mix is blended in a mortar mixer or in a specially designed continuous blender. Each bubble of air in the foam is surrounded by a tough protein membrane which ensures stability during mixing and handling. However, since this membrane will eventually break down it is recommended that mixing and placing be completed within one hour. Use of high-early-strength cement (Type III) further ensures rapid setting and stability of cellular concrete, although good results are also obtained with regular portland cement (Type I) plus 2 percent calcium chloride, by weight of cement, as an accelerator.

As with other lightweight insulating concrete, the strength and thermal conductivity depend on density. The material can be made so light (down to 12 pounds per cubic foot) that its strength is only sufficient for it to retain its shape during handling. Thermal conductivities range from 0.51 Btu inch per hour square foot degree F for a density of 20 pounds per cubic foot to 2.3 Btu inch per hour square foot degree F for a density of 90 pounds per cubic foot.

Cellular concrete is totally incombustible (8 inches of concrete represents a fire rating of about 8 hours); yet it can be worked much like wood. Where prolonged working is likely, long-life tools are advised. These and other properties enhance the attractiveness of cellular concretes for floor and roof deck fill and insulation.

For more information

Obviously, subtle differences exist between the various lightweight insulating concretes available, which may recommend one type over another to satisfy some specific design objective. Costs and availability in the local market must also be considered.

Each type of insulating concrete, if mixed properly with high quality materials and placed and finished properly, will do an excellent job. Further research and study may reveal just the right characteristic that suits your need. A list of references for further information is given below.

REFERENCES

1. *Special Types of Concrete,* IS183T, Portland Cement Association, Skokie, Illinois, 1977, 8 pages.

2. Valore, R. C., Jr., "Insulating Concretes," *Journal of the American Concrete Institute,* November 1956, pages 509-532.

3. ACI Committee 523, *Guide for Cast-in-Place Low Density Concrete, American Concrete Institute,* Detroit, Michigan, 1967, 8 pages.

4. *The Roof Deck,* National Roofing Contractors Association, 1515 North Harlem Avenue, Oak Park, Illinois 60302.

5. "Vermiculite Roof Deck and Insulating Concrete," *Concrete Construction,* March 1961, pages 66-67.

6. "Perlite Roof Deck and Insulating Concrete," *Concrete Construction,* April 1961, pages 95-97.

7. "Perlite Insulating Concrete," 3.4d/Per, Perlite Institute Inc., 45 West 45th Street, New York, New York 10036.

8. Cook, D. J., "Polystyrene Aggregates," *Constructional Review* (Sidney, Australia), August 1972, pages 52-53.

9. *Cellular Concrete for Insulated Roof Decks,* Cellular Concrete Association Inc., 715 Boylston Street, Boston, Massachusetts 02116.

10. "Cellular Concrete," *Concrete Construction,* January 1963, pages 5-8.

11. Valore, Rudolph C. Jr., "Cellular Concretes, Parts 1 and 2," *Journal of the American Concrete Institute,* May and June 1954, pages 773-796 and 817-836.

PUBLICATION #C780411

WVMP SAR Reference 3-22

Fire Tests of Precast Cellular Concrete Floors and Roofs, NBS Monograph 45, J. V. Ryan and E. W. Bender, April 1962.

NBS MONOGRAPH 45

Fire Tests of Precast Cellular Concrete Floors and Roofs

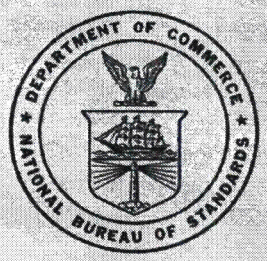

U.S. DEPARTMENT OF COMMERCE
NATIONAL BUREAU OF STANDARDS

THE NATIONAL BUREAU OF STANDARDS

Functions and Activities

The functions of the National Bureau of Standards are set forth in the Act of Congress, March 3, 1901, as amended by Congress in Public Law 619, 1950. These include the development and maintenance of the national standards of measurement and the provision of means and methods for making measurements consistent with these standards; the determination of physical constants and properties of materials; the development of methods and instruments for testing materials, devices, and structures; advisory services to government agencies on scientific and technical problems; invention and development of devices to service special needs of the Government; and the development of standard practices, codes, and specifications. The work includes basic and applied research, development, engineering, instrumentation, testing, evaluation, calibration services, and various consultation and information services. Research projects are also performed for other government agencies when the work relates to and supplements the basic program of the Bureau or when the Bureau's unique competence is required. The scope of activities is suggested by the listing of divisions and sections on the inside of the back cover.

Publications

The results of the Bureau's research are published either in the Bureau's own series of publications or in the journals of professional and scientific societies. The Bureau itself publishes three periodicals available from the Government Printing Office: The Journal of Research, published in four separate sections, presents complete scientific and technical papers; the Technical News Bulletin presents summary and preliminary reports on work in progress; and Basic Radio Propagation Predictions provides data for determining the best frequencies to use for radio communications throughout the world. There are also five series of nonperiodical publications: Monographs, Applied Mathematics Series, Handbooks, Miscellaneous Publications, and Technical Notes.

A complete listing of the Bureau's publications can be found in National Bureau of Standards Circular 460, Publications of the National Bureau of Standards, 1901 to June 1947 ($1.25), and the Supplement to National Bureau of Standards Circular 460, July 1947 to June 1957 ($1.50), and Miscellaneous Publication 240, July 1957 to June 1960 (Includes Titles of Papers Published in Outside Journals 1950 to 1959) ($2.25); available from the Superintendent of Documents, Government Printing Office, Washington 25, D.C.

UNITED STATES DEPARTMENT OF COMMERCE • Luther H. Hodges, *Secretary*

NATIONAL BUREAU OF STANDARDS • A. V. Astin, *Director*

Fire Tests of Precast Cellular Concrete Floors and Roofs

J. V. Ryan and E. W. Bender

National Bureau of Standards Monograph 45

Issued April 12, 1962

For sale by the Superintendent of Documents, U.S. Government Printing Office
Washington 25, D.C. - Price 15 cents

Contents

Fire Tests of Precast Cellular Concrete Floors and Roofs

J. V. Ryan and E. W. Bender

The results of an investigation of lightweight, precast cellular concrete planks are given. Fire tests were made of two floor and five roof specimens made up of these planks. Variables included density of the cellular concrete, thickness and span of the planks, reinforcement, and cover for the latter. A steel beam encased in blocks of cellular concrete was included in one floor specimen. The flexural strengths of 14 individual planks were determined. The investigation showed fire endurances up to 2 hr for 6-in. thick slabs tested under load and up to 4 hr for other slabs not loaded. Estimates were made of the probable results to be expected for slabs of thicknesses other than those actually tested.

1. Introduction

The framework and foundations of a building represent a large part of the total cost in multistory construction. They must carry both the live loads imposed by occupancy and the dead load of the finished building. Significant economies can be achieved in the cost of buildings by reducing the loads to be carried, and thereby permitting less expensive framework and foundation. Since reduction in allowable live load limits the usefulness of the building, research has been aimed at reducing the dead weight of building elements and materials.

Research aimed at the reduction of the dead weight of concrete structures led to development of lightweight aggregates as substitutes for dense natural aggregates, and to development of cell-forming processes for producing cellular concretes. The cell-forming processes included the use of aluminum powder and other gas-forming agents, the addition of preformed foam into the mixer, the addition of chemicals that form and retain air bubbles produced during mixing, and the use of excess water. Although known as "gas concrete," "foam concrete," or "aerated concrete," according to the particular process employed, all are included in the more general term "cellular concretes" [1].*

Cellular concretes have been developed that have densities as low as 20 lb/ft^3, are sawable, and workable with general carpentry tools. Such cellular concretes are being manufactured commercially and used to produce prefabricated blocks and panels for floor, roof, and wall assemblies.

The economies achieved through the use of cellular concretes are not limited to those associated with dead-weight reduction. Because of their cellular structure, they have significantly lower thermal conductivities than conventional dense concretes. Therefore, the use of cellular concretes often permits the elimination of additional insulating materials that would otherwise be necessary.

A research program was carried out on floor and roof slabs assembled from precast planks of a gas-formed cellular concrete to determine the fire endurances of representative specimens and the effects thereon of variables such as amount of cover for the reinforcing bars, overall thickness, amount and distribution of reinforcement, and density of the concrete. Five standard fire-endurance tests of roof assemblies and two of floor assemblies were conducted in a large floor furnace. Each specimen consisted of several planks grouted together. A steel I-beam, protected by cellular concrete blocks, was tested in conjunction with one of the floor specimens.

2. Test Specimens

2.1. General Description

The floor and roof panel specimens were made up of planks of cellular concrete specially cast in the necessary lengths for this study by a manufacturer. They were representative of commercially produced planks used in floor and roof construction. The mix constituents and ratios used in their production were not revealed. However, the particular cellular concrete is understood to be of the gas-formed type.

The planks were 18 in. wide and had a length of either 13 ft 5 in. (to span the short dimension of the furnace opening), or 17 ft 11 in. (to span the long dimension of the furnace opening). They were supplied in thicknesses of 5, 6, and 8 in., representative of the range of normal production. The nominal density of the planks for floor use was 44 lb/ft^3, and that of the roof planks was 31 lb/ft^3. The measured densities ranged from 42.6 to 46.5 lb/ft^3 for the floor planks, and from 35.8 to 42.2 lb/ft^3 for the roof planks.

For four of the seven standard tests, the specimen panels were made up of twelve 6-in.

*Figures in brackets indicate the literature references on page 11.

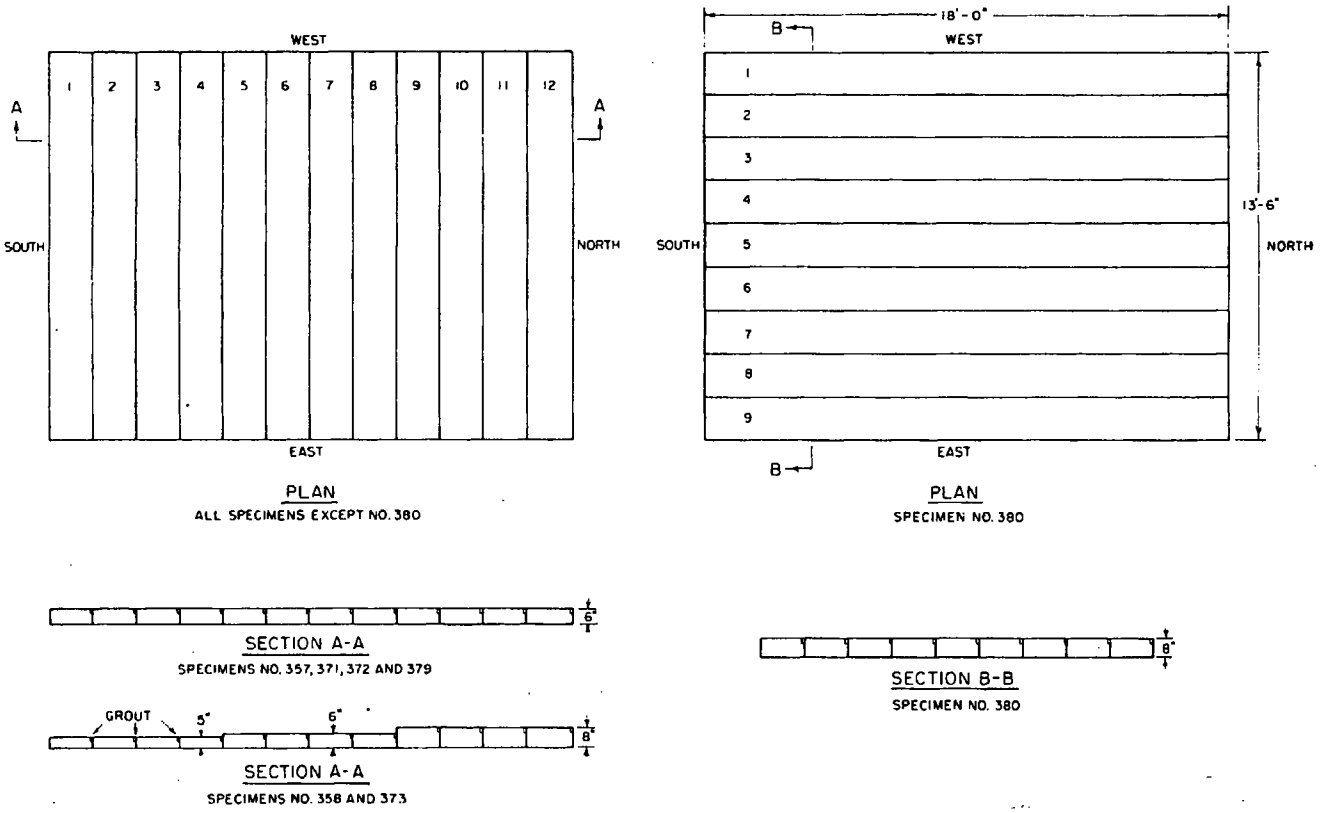

FIGURE 1. *Arrangement of planks within the furnace opening.*

The individual plank numbers are as used in section 8, appendix.

planks laid across the furnace. Three specimens of this group were roof panels and differed either in the reinforcement design of the planks or in the load applied during the test; the fourth was a floor panel. One other roof panel was made up of nine 8-in. planks laid along the length of the furnace opening. For the remaining two full-scale tests (one floor and one roof), four planks of each of the three thicknesses supplied, 5, 6, and 8 in., were laid across the furnace opening, with the 6-in. section in the center. Figure 1 shows the different assemblies.

After an exploratory test in a small furnace to determine the feasibility of the procedure, a structural steel I-beam protected by cellular concrete blocks was tested along with the floor panel of graduated thickness. The beam was a 10-in. I-beam weighing 25.4 lb/ft, of 17 ft 7¾ in. length to span the long dimension of the furnace. The floor panel (with planks crosswise of the furnace) rested on the top of the beam. The sides and bottom, or soffit, of the beam were encased in precast blocks to provide a cellular concrete cover of 2⅞ in. on the bottom and $1\frac{15}{16}$ in. on the sides.

Flexural strength tests were made on several individual planks, which had not been exposed to fire.

2.2. Reinforcement and Cover

The term *cover* refers to the thickness of concrete between a steel reinforcing bar and the nearest surface of the reinforced concrete assembly, or to the thickness of protective material encasing a structural steel member. The cover of greatest interest in connection with reinforced concrete flexural members is that between the bottom tensile reinforcement and the surface exposed to fire.

The reinforcement in the specimens consisted of nominally round, hot-rolled, plain steel bars, in various patterns or combinations of number and size. The basic pattern of reinforcement consisted of longitudinal bars at two levels (one in the tensile zone and one in the compressive zone), plus crossbars, anchor bars, and spacers. The crossbars maintained the spacing between longitudinal bars at a single level and positioned them in the form. The anchor bars provided anchorage for the ends of the lower level, or tension bars. The spacers, which were formed of sheet metal, maintained the spacing between levels as determined by the overall thickness and cover. The longitudinal reinforcing bars were located and spaced so that those of the upper level had the same cover from the top surface as did those of the lower level from the bottom surface. The amount of cover was varied among the specimens. The variations within the basic pattern of reinforcement are illustrated in figure 2 and the cover for each specimen is given in table 1.

TABLE 1. *Summary of specimen details and results*

No.	Type	Thickness	Clear span	Reinforcement	Concrete: Cover	Concrete: Density, Nominal	Concrete: Density, Measured	Applied load	Computed tensile steel stress	Time to initial end point	Limiting condition
		in.	*ft in.*	[a]	*in.*	*lb/ft*³	*lb/ft*³	*lb/ft*²	*lb/in.*²	*hr: min*	
357	Roof	6	13 5	A_1	¾	31	35.8	74	17,800	0:57	Load failure.
				B_1	[b] 1¼			74	37,300		
371	Roof	6	13 5	A_1	¾	31	35.8	56	14,300	0:53	Load failure.
379	Roof	6	13 5	[c] A_1	¾	31	42.2	56	14,900	1:29	Max surf. temp.
380	Roof	8	17 4	E	¾	31	36	70	16,100	1:13	Ignite waste.
358	Roof	5	13 5	B_2	1¾	31	36	None		3:13	Ignite waste.
		6	13 5	B_1	1¾	31	36	None		4:07	Max surf. temp.
		8	13 5	B_1	1¼	31	36	None			
372	Floor	6	13 5	A_2	¾	44	44.5	70	12,600	1:40	Max surf. temp.
373	Floor	5	13 5	D	1¾	44	46.5	None		4:20	Max surf. temp.
		6	13 5	B_3	1¾	44	45.4	None			
		8	13 5	C	1¾	44	42.6	None			
373	I-Beam	9⅞	17 8		[d] 1 15/16 [d] 2⅞		36.7	[e] 17,700	20,000	2:22	Load failure.

[a] See figure 2 for details of reinforcement.
[b] Following the test, the cover in three planks was found to have been 1¼ in., rather than the intended ¾ in.
[c] Contained shear reinforcement; see text for description.
[d] Thickness of side and soffit blocks used to protect steel beam.
[e] Load equally divided among four application points.

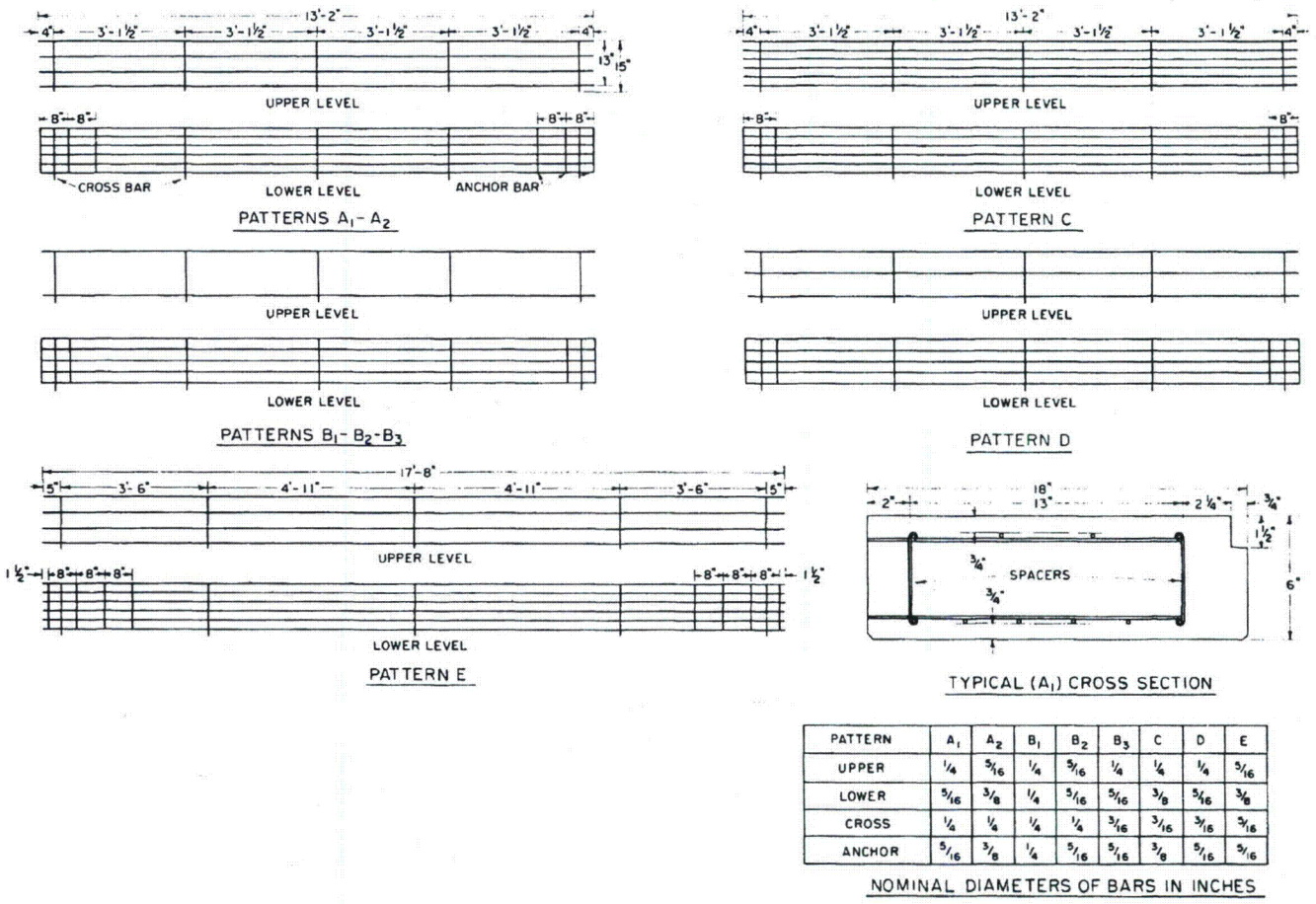

PATTERN	A_1	A_2	B_1	B_2	B_3	C	D	E
UPPER	1/4	5/16	1/4	5/16	1/4	1/4	1/4	5/16
LOWER	5/16	3/8	1/4	5/16	5/16	3/8	5/16	3/8
CROSS	1/4	1/4	1/4	1/4	3/16	3/16	3/16	3/16
ANCHOR	5/16	3/8	1/4	5/16	5/16	3/8	5/16	5/16

NOMINAL DIAMETERS OF BARS IN INCHES

FIGURE 2. *Reinforcement details.*

In the planks used for one of the 6-in. roof panels (test No. 379), shear reinforcement was provided in addition to the reinforcement already described. The shear reinforcement consisted of ⅛-in.-diam rod bent in a multiple-V shape, each V section thus formed being about 4½ in. deep and 5¼ in. long. A continuous length of this shear reinforcement was placed along each side of the assembly of reinforcement bars and wire tied to the upper and lower bars nearest each side of the plank. The

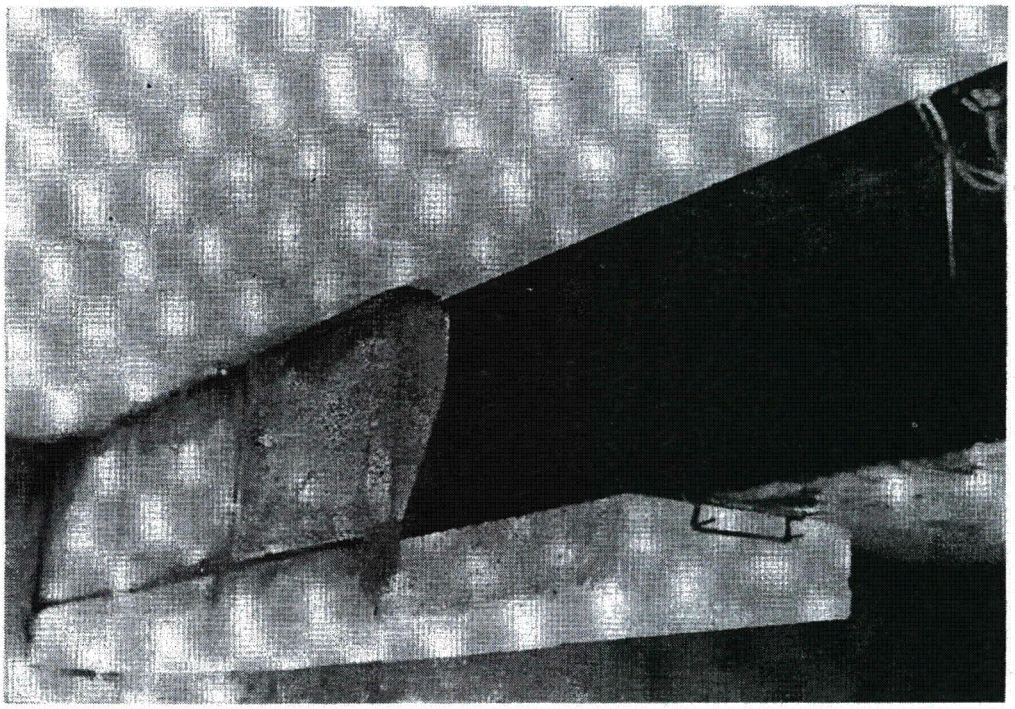

FIGURE 3. *Steel beam partly encased.*

ties were single strands of 0.027-in. wire and varied as to spacing, some being 5¼ in. and others 10½ in. apart. In these planks the sheet metal spacing clips were supplemented by ¼-in. diam steel rods welded to the upper and lower bars nearest the sides of the plank, 3 in. from their ends.

2.3. Construction of Specimens

In making up the test panels in the furnace, the planks were placed in contact with one another, and a grout consisting of 3 parts portland cement to 1 part sand, by weight, was poured between the panel and the furnace restraining frame and into the groove formed along each joint between planks by a kerf ¾ in. wide by 1½ in. deep along one edge of each plank. The kerfs and adjoining edges of the planks were wet down immediately before pouring the grout, and periodically for a week or ten days thereafter, to prevent unduly rapid drying of the grout, and thereby to improve the bond. An electric heater was placed in the furnace, and for the week immediately preceding each test a temperature of 125 to 150 °F was maintained in an attempt to remove excess moisture from the assembly.

The steel I-beam, tested in conjunction with the floor panel of graduated thickness, was placed along the longitudinal center line of the furnace and attached at both ends to steel plates by means of standard AISC B2 connectors [2]. These plates, in turn, were bolted to the furnace frame in such a way that the beam was supported, restrained against rotation of the ends, but could expand longitudinally. The beam was encased in precast blocks of cellular concrete, after the floor planks were in place. The soffit blocks (9 in. wide, 17 13/16 in. long, and 2⅞ in. thick) were attached to the beam by means of formed wire clips. Transverse wires of the clips were driven into the ends of the blocks, holding them in good to fair contact with the beam. The soffit blocks extended about 2¼ in. beyond the beam flange on each side. The joints between blocks were filled with mortar consisting of 1 part lime, 1 part portland cement, and 5 parts crushed cellular concrete by volume. A bed of this mortar was placed on the upper surface of the soffit blocks, and the side blocks (9 in. wide, 18 in. long, and 1 15/16 in. thick) were placed thereon. The vertical joints between blocks and the spaces between blocks and floor planks were filled with mortar. The joints were wetted before the application of the mortar and periodically thereafter for the next 10 days to prevent excessively rapid drying. Throughout the following week, an electric heater was kept in the furnace chamber and temperatures in the range of 125 to 150 °F were maintained in an attempt to remove some of the excess moisture. Figure 3 shows the beam partly encased.

3. Test Method and Equipment

The tests were conducted in accordance with the accepted standard test methods (ASTM designation E119) [3]. Not all the tests were stopped when the initial end-point criterion was reached, but some were continued in order to obtain more information about the behavior of the specimen.

This practice deviated from the standard test method, under which tests are stopped when the initial end point is reached and the specimens are subjected to the hose-stream and the double-reloading tests.[1] Inasmuch as the results would not have been indicative of the true performance of the specimens, because of their extended fire exposure, neither the hose-stream nor the double-reloading test was performed on any of the specimens. The fire-endurance limits were determined by the initial end point and are therefore in accordance with the standard test method, even though the fire exposure was continued.

The specimens were tested in the furnaces at the National Bureau of Standards designed for the purpose of testing floor and roof specimens. The small furnace, used for the exploratory test, took specimens 2 ft by 2 ft in size, while the large furnace, used for the standard tests, was constructed in such a manner as to accommodate a specimen 18 ft long by 13½ ft wide. Both furnaces were box-shaped, open at the top, so that the bottom face of the specimen was exposed to the flames.

To measure the temperature in the chamber of the large floor furnace, twelve thermocouples, encased in porcelain insulators and enclosed in iron pipes sealed at one end, were placed in the furnace so that the junctions of the thermocouples were approximately 1 ft below the exposed surface of the specimen. In the small furnace, four thermocouples were used. They were of the same type and were placed in the same manner as those in the large furnace. The furnace fires were controlled to approximate as nearly as feasible the temperatures set forth in the standard test method, which include 1,000 °F at 5 min, 1,300 °F at 10 min, 1,550 °F at 30 min, 1,700 °F at 1 hr, 1,850 °F at 2 hr, 2,000 °F at 4 hr, and 2,300 °F at 8 hr and longer.

The fire-exposure severity, which is defined as the ratio of the area under the curve of average furnace temperature to the area under the standard time temperature curve, is required to be between 90 and 110 percent for tests of 1 hr or less; between 92.5 and 107.5 percent for tests over 1 hr but not over 2 hr, and between 95 and 105 percent for tests longer than 2 hr.

In order to obtain temperature data on the unexposed surfaces of the specimens, a total of 12 chromel-alumel thermocouples whose junctions were in contact with the unexposed surface of the specimen were used in each test. They were distributed over the surface in a symmetrical pattern, with junctions and short lengths of the thermocouple wire coiled under standard felted asbestos pads 6 in. square by 0.4 in. thick.

Temperatures of the reinforcing bars in the specimens were measured by means of chromel-alumel thermocouples tied to the bars of some planks, at the time of fabrication. There were 5 thermocouples on the lower bars, and 3 on the upper bars, of each of the selected planks. Planks with thermocouples were located in positions 3, 6, and 9 (see fig. 1) of specimens 357, 371, and 372; positions 3, 5, and 7 of specimen 380; and positions 3, 4, 5, 7, 9, and 10 of specimens 358 and 373. No planks with thermocouples were provided for specimen 379.

The temperatures on the I-beams in the exploratory and full-scale tests were measured by chromel-alumel thermocouples which had their junctions peened in small holes drilled into the beams. Twenty-four thermocouples were used on the beam in the full-scale test (373). The thermocouples were located in four groups of six, the groups being spaced 42 to 43 in. on centers. Two of the thermocouples of each group on the beam were placed on the bottom of the top flange, one on each side of the web, and two on the top of the lower flange.

The recommendations of the manufacturer who produced the cellular concrete planks were followed in loading the specimens. The superimposed loads were applied by means of hydraulic jacks and were distributed evenly over the specimens. The manufacturer indicated that the "normal" loads were based on a design tensile stress of 18,000 lb/in.^{2} in the lower reinforcing steel. However, some specimens were tested at loads other than normal, to provide an indication of the effect of extent of loading on fire endurance. Values of the stresses in the lower reinforcing bars, as computed on the basis of simple beam theory, are given in table 1.

The four-point load applied to the steel I-beam was transmitted through four planks of the graduated floor specimen, thereby partially loading the latter. No other external load was applied to either of the graduated specimens.

The beam was loaded with a live load intended to produce a steel stress of 20,000 lb/in.^{2} The deflections were measured by a system of wires attached to the specimen and passed over pulleys to a scale, where riders on the wires indicated the amount of change from the initial level.

3.1. Moisture-Content Determinations

Samples were taken from the specimens in the furnace a day before each test in the study, except the first, and from extra planks. The samples were cylindrical cores, cut from the full thickness of the individual slabs. They were taken from near the corners of the specimens in the furnace. The holes were filled with the mixture used to grout the planks together.

Moisture determinations were made by drying specimens at 105 °C (221 °F). The specimens were the cylindrical cores in some cases, and thin wafers cut from the cores in others. Some were from planks as received, others as tested (after heating of the furnace chamber) and others from

[1] Both these supplementary tests have been deleted from the Standard E119 since the study reported herein was started.

planks stored at 50 percent relative humidity. Some of the specimens were conditioned in various ways, after removal from the planks, others were not. One group of wafer specimens were placed in 50 percent relative humidity after having been dried at 105 °C in order to permit measurement of the moisture regain. The results of these measurements are summarized in table 2.

It is doubtful that the moisture contents for the fire-test specimens can be related to the observed fire endurances, or to behavior in the fire tests. The moisture-content specimens were taken from near the edges of the fire-test specimens. Their moisture contents may therefore show somewhat higher values than those of planks nearer the center of the exposed area.

TABLE 2. *Moisture content data determined by oven-drying, at 105 °C for 24 to 72 hr, cores removed from planks heated after assembly into fire test specimens*

Test	Age	Duration of heating in furnace	Number of specimens	Mean moisture content by weight
	mos	*Days*		*%*
358	2½	7	1	5.4
371	7½	10	4	8.1
372	8	8	2	1.9
373	9	6	2	2.2
379	11½	7	2	14.6
380	10	6	2	2.5

Additional tests with cores, and thin wafers from cores, indicated equilibrium moisture content of about 2 percent when stored at 50 percent relative humidity, both for specimens as received and oven-dried. It required much more than 30 days for equilibrium to be reached throughout a 6-in. plank.

4. End-Point Criteria

The previously mentioned standard test methods state that the endurance of a specimen is the earliest time when any one of the following end-point criteria is reached or observed:

(a) The specimen shall no longer sustain its design load;

(b) The average temperature on the unexposed surface rises 250 °F above the initial temperature;

(c) The maximum one-point temperature on the unexposed surface rises 325 °F above the initial temperature;

(d) Cracks or openings shall develop in such a manner as to allow the passage of flames or gases hot enough to ignite cotton waste.

Although not included in the test methods as criteria for failure, the following data are considered to be of general interest and are tabulated, in part, in this report.

(e) The times at which steel structural members or reinforcement attained an average temperature of 1,000 °F at any appropriate level or section.

(f) The times at which steel structural members or reinforcement attained a temperature of 1,200 °F at any one point.

It should be noted here that while criteria (b), (c), and (d) are quite specific in defining failure, (a) is not, and it is sometimes difficult to judge when load failure occurs.

5. Results and Discussion

However, an objective method of determining this end point has been developed which defines a critical deflection and a critical rate of deflection. The method has been shown to give results reasonably consistent with those determined by an experienced operator in charge of test [4]. The critical deflection is defined as $D=L^2/800d$, and the critical rate of deflection as $R=L^2/150d$ per hour, where L is the span, or length of the specimen between supports, and d is the depth [2] of the specimen. The time when both of these critical values has been reached is reported in this study as the time of load failure.

The principal results of the tests made in the large furnace are given in table 1, and representative time-temperature and time-deflection curves are shown in figures 4 and 5. The observations of the behaviors of the individual specimens, made during the tests, are summarized in the test logs in the appendix. The results of flexural strength tests on individual planks are summarized in table 3.

TABLE 3. *Results of flexural tests*

Individual planks placed on supports at 12 ft spacing and subjected to load at center only. The failures of the 13 ft 5 in. planks were judged due to yielding of the steel; those of the 17 ft 11 in. planks to shear in the concrete.

Thickness	Length	Reinf. pattern [a]	Nominal density of concrete	Test No. [b]	Max. load [c]	Deflection at max. load
in.	*ft:in.*		*lb/ft³*		*lb*	*in.*
6	13:5	B_1	31	358	2440	1.83
6	13:5	A_2	44	372	4275	1.90
8	13:5	B_1	31	358	1900	1.72
8	13:5	C	44	373	4590	1.40
8	17:11	E	31	380	5790	[d] 1.30

[a] See figure 2.
[b] Number of test in which other similar planks were exposed to fire.
[c] Mean of 2 to 5 specimens.
[d] Sudden failure, deflection reading not possible for 4 out of 5.

Of the five panels tested under load, the performances of two were limited by load failure, two by unexposed surface temperature rise, and one by ignition of cotton waste over a crack. The only criterion applicable to a beam tested under load is load failure; this was reached on the one I-beam tested. The two panels assembled of 5-, 6-, and 8-in. planks were not subject to the limiting condition of load failure; other limiting conditions were reached on the 5-in. section of each specimen and on the 6-in. section of one. For these two specimens, the attainment of the defined

[2] "Depth" is determined by the type of construction: for reinforced concrete slabs it is measured from the top of the slab to the bottom of the main reinforcement. This differs from "effective depth," which is measured to the centroid of tension reinforcement and which was used to compute the steel stresses given in table 1.

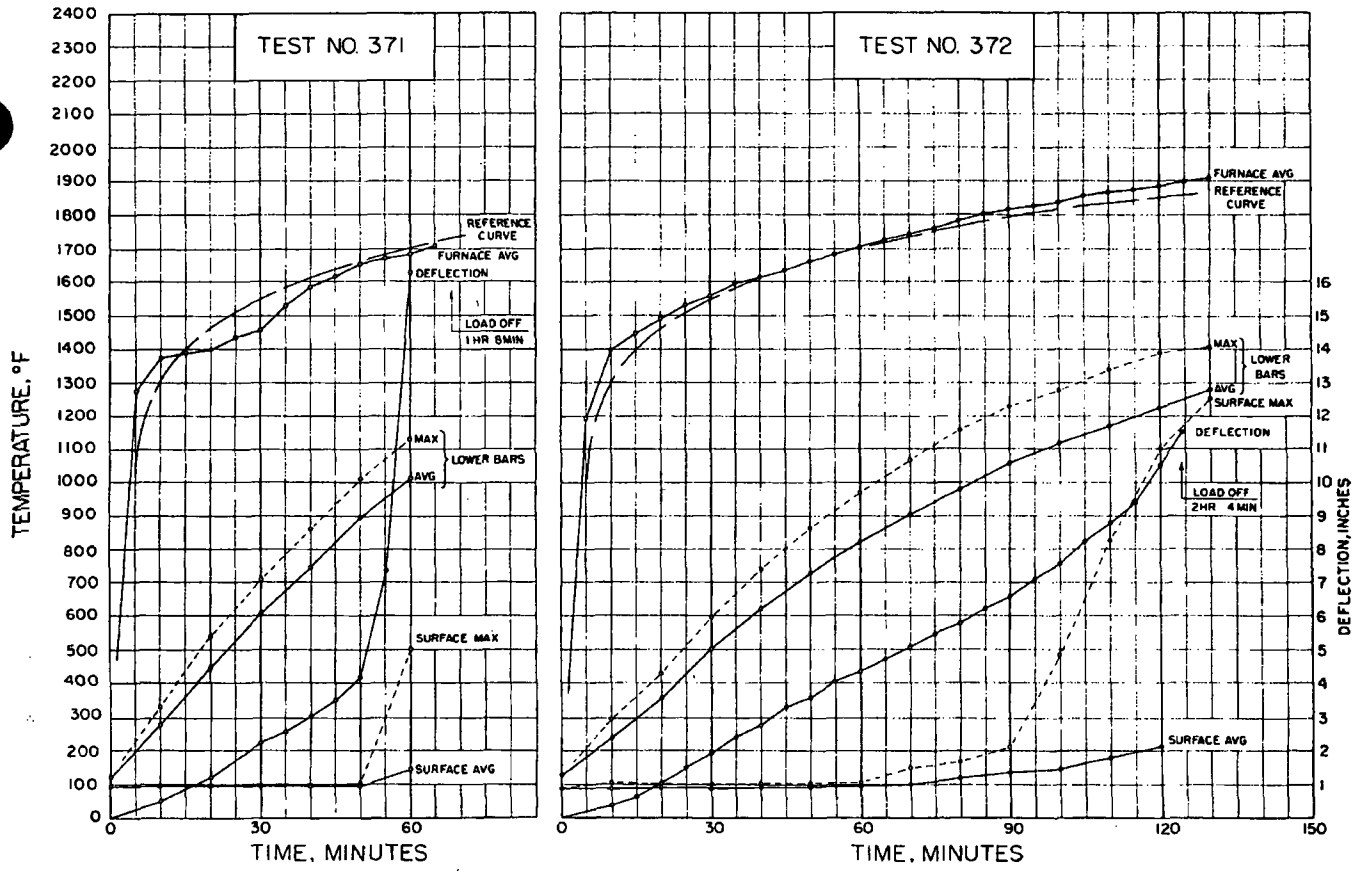

FIGURE 4. *Time-temperature and time-deflection curves for 6-in. roof (371) and floor (372) specimens.*

criteria was secondary in importance to the development of information on the effect of thickness. Although the ignition of cotton waste occurred in one of these tests, it is not considered useful data for comparisons.

During the test (373) of the floor without load, flames issued from the exposed surface of one of the 5-in. planks, possibly from burning of plastic tape used with the thermocouples. This was an exception to the general behavior observed in this study. The temperatures of the reinforcing bars in one of the 5-in. planks in this specimen rose much more rapidly than those for the other, presumably due to the flaming. Since the flaming was not representative, and in fact cannot be definitely explained, the data from this plank have been disregarded.

5.1. Plank Thickness and Cover

Each of the two graduated specimens, tests 358 and 373, provides a basis for comparisons of performance of planks of different thickness. Except for the 8-in. roof planks in test 358, all planks had the same cover. Within each test, all the individual planks were of the same nominal density There were differences in the number and size of reinforcing bars, but only those resulting from design on the basis of span, thickness, and other variables.

Among the roof planks (358), the limiting temperature rises on the unexposed surface were reached on the 5-in. planks at 3 hr 39 min for the average and 3 hr 37 min for the maximum, and at 4 hr 10 min and 4 hr 7 min respectively on the 6-in. planks, but were not reached on the 8-in. planks. Temperatures of 1,000 °F average and 1,200 °F maximum respectively were reached on the lower level reinforcing bars at 2 hr 9 min and 2 hr 14 min respectively for the 5-in. planks, and 2 hr 6 min and 2 hr 17 min for the 6-in. planks. The data for temperatures of the reinforcing bars in the 8-in. planks were not applicable in evaluation of the effect of thickness because the amount of cover used differed from that for the 5- and 6-in. planks.

In order to avoid complete collapse of the I-beam, test 373 was stopped immediately after the 3 hr 50 min data readings, although no limiting condition applicable to floor slabs had been attained. It was estimated by extraploation of the data obtained that the limiting maximum temperature rise would have been reached on the 5-in. planks at 4 hr 20 min. Temperatures of 1,000 °F average and 1,200 °F maximum were reached at 2 hr 50 min and 3 hr 6 min respectively on the

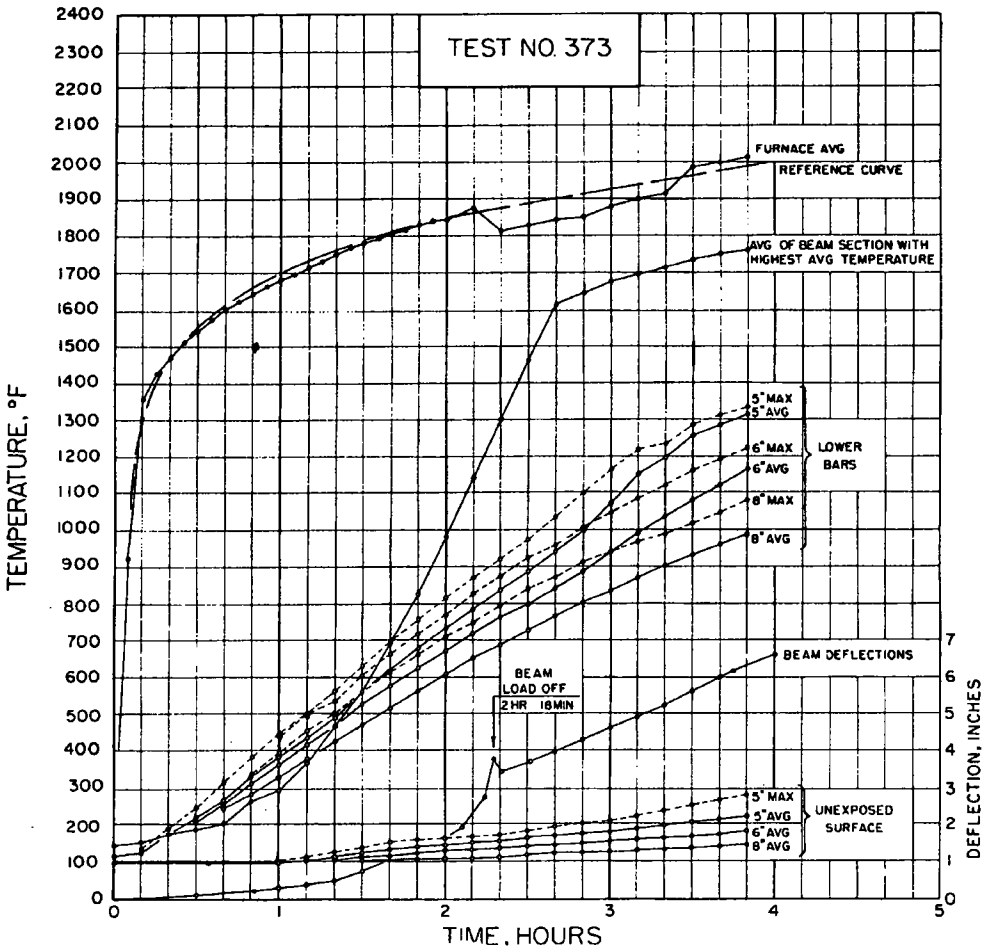

FIGURE 5. *Time-temperature and time-deflection curves for steel beam and floor slab made up of 5-, 6-, and 8-inch thick planks.*

The load was concentrated on planks directly over the beam and was removed when the latter failed.

lower-level reinforcing bars of the 5-in. planks, and at 3 hr 12 min and 3 hr 40 min for the 6-in. planks. It was estimated that the 1,000 °F average would have been reached at 3 hr 52 min for the 8-in. planks; the 1,200 °F maximum was not reached.

The steel temperatures chosen are generally associated with loss of steel strenghth such that load failure is imminent for reinforced concrete structural elements designed with a safety factor of two for the reinforcing bars. Since neither of the two graduated specimens were subjected to loads appropriate to the plank designs, the times at which the reinforcing bar temperatures reached 1,000 °F average and 1,200 °F maximum may differ appreciably from those that would have been observed in tests of similar planks loaded in accordance with accepted design practices. Under such load the development of cracks and the sloughing or spalling of concrete cover may differ from and lead to earlier and more rapid steel-temperature rise than would be observed under comparatively light load. However, the times observed in these tests should be valid indications of the relative performances to be expected for the various thicknesses.

The effect of cover was not easy to evaluate because all specimens with ¾-in. cover were tested under load and all those with 1¾-in. cover were tested without load. However, it was discovered after test 357 that three planks with 1¼-in. cover had been supplied inadvertently along with the nine planks with the intended ¾-in. cover. Moreover, the former had only half as much reinforcement as the latter. Therefore, another test, 371, was conducted essentially duplicating the earlier specimen except that all planks had ¾-in. cover and the applied load was reduced by 25 percent. Despite the reduced load in the latter test, the specimen failed under load at 53 min, compared with 57 min in the earlier test. Therefore the greater cover gave appreciably longer fire endurance to the assembly.

The method of varying cover by changing the effective depth of the reinforcing bars would change the allowable load, the steel stress, or require a change in the amount of reinforcing steel. Ordinarily all of these would be held constant and change of cover would be accomplished by change of overall thickness. The unusual procedure in this study resulted in the

effect of cover variation's not being masked by the effect of thickness.

5.2. Reinforcement

Longitudinal reinforcing bars having nominal diameters of ¼, 5/16, and ⅜ in. were used in the specimens. Shear reinforcement was also used in one specimen. For the most part, the number and size of reinforcing bars incorporated in the test specimens were such as to satisfy design criteria related to span, load, and stress in the steel. In general, the number and size of bars were the same among planks having the same thickness, span, concrete density, and cover for the bars. However, there was an exception to this general rule, as can be seen from comparison of reinforcement in specimens 372 and 379. The spans, thickness, concrete density, number of reinforcing bars, and cover were equal (within practical limits) for these specimens, but the former had ⅜-in. lower level and 5/16-in. upper-level bars, whereas the latter had 5/16-in. lower and ¼-in. upper bars plus full-length shear reinforcement. The specimen in test 372 was subjected to an applied load equal to 1¼ that applied in test 379. The initial limiting criterion in each test was unexposed surface temperature rise, that in test 372 having been reached at 1 hr 40 min and that in test 379 at 1 hr 30 min.

The deflection data would be more indicative of the effect of variation of the reinforcement than would be the surface-temperature data. Unfortunately, these tests were not continued to load failure. The available deflection data do indicate that load failure, for the specimen in test 372, would have been about 40 min later than that for the specimen in test 379. From this, it appears that the 1/16-in. increase in bar diameter was much more effective than the addition of shear reinforcement.

5.3. Concrete Density

The nominal density of the cellular concrete specified for floors was 44 lb/ft³, whereas that for roofs was 31 lb/ft³. The actual densities of the concretes as received were obtained from full-sized planks, with correction for the weight and volume of the reinforcement, or from cores removed from planks; these were within ±2.5 lb/ft³ of the nominal densities for the floor planks and were about 5 lb/ft³ high for the roof planks, with one exception (test 379). In this specimen the average density of the cellular concrete, based on the total weight of two extra planks, was found to be 42.2 lb/ft³ although they were marked as roof planks. Even after correction for moisture content, the densities of the roof planks were in the range of 33 to 37 lb/ft³.

The specimens of tests 371 and 379 were very similar, differing only as to concrete density, and the presence of shear reinforcement in the latter. Each was subjected to the same applied load. Each was limited by temperature rise on the unexposed surface, reached at 1 hr in test 371 (density 35.8 lb/ft³) and at 1 hr 30 min in test 379 (density 42.2 lb/ft³). The times at which 1,000 °F average and 1,200 °F maximum temperatures were reached on the lower level reinforcing bars were 59 min and 1 hr 4 min, respectively, in the former test, and over 1 hr 30 min in the latter. Similar comparisons of the effect of concrete density may be made from the unexposed surface temperature data of the 5-in. planks in tests 358 and 373 as well as from the temperature data for the reinforcing bars of the 5-in. and 6-in. planks of the same tests.

These data indicate that, within the ranges of density and other variables covered in this study, the cellular concrete will provide increased resistance to heat penetration at higher densities.

Such behavior agrees with that to be expected if the thermal diffusivity of the concrete decreased as the density increased. Thermal diffusivity α is defined as $\alpha = k/\rho c$, where k is thermal conductivity, ρ is density, and c is specific heat. Since the cellulur concretes of various densities may be presumed not to vary greatly as to chemical composition, the values of specific heat should be reasonably constant. Although the values of thermal conductivity tend to increase with density, apparently the net effect for the cellular concrete in the particular range of densities investigated is one of lower diffusivity for that of high density than for that of low density. This is in agreement with previously published data [5]. However, the same data indicate that this trend is reversed at densities of about 60 lb/ft³ and that diffusivity increases with increased density above that level.

5.4. Estimates of Fire Endurance

Data from standard fire tests are often used as the basis for estimates of the probable fire endurances of similar constructions not actually tested. The usefulness of such estimates is dependent on the amount of test data available on similar constructions, the simplicity of the basic construction, and the degree of similarity between the constructions actually tested and those for which estimates are made. Another important factor is the basis for the method employed in making the estimates.

A method has been developed on the basis of many years of experience in tests of solid, essentially homogeneous walls [6]. It relates fire endurance to the 5/3 power of the thickness. Since the cellular concrete floors and roofs approximated homogeneity very closely, it was believed that a similar relationship might hold for them, although probably with the thickness raised to a different power than that for walls. A plot of the data confirmed this assumption. Data for load failure, unexposed surface temperature limiting rise, and 1,000 °F average and 1,200 °F maximum temperatures on the lower-level reinforcement were plotted and lines faired through the points. The exponents for the various lines were in the range 0.64 to 0.80.

Specimens were tested at 5-, 6-, and 8-in. thicknesses. The lines developed from the data plots were extended from 3 to 10 in., representing extrapolation over 2 in. of thickness at each end. The times at which the aforementioned load and temperature conditions might be expected were picked off the lines and are given in table 4. This table gives only the values from the lines; hence the values at 5, 6, and 8 in. do not agree in all cases with those given in table 1, the actual values for the particular specimens tested. The data from table 4 were analyzed to determine which failure criterion would be reached first; the resulting estimated fire endurances are given in table 5. Although fire endurance ordinarily is stated to the nearest minute, the estimates obtained from table 4 were rounded off to the nearest 5 min up to 2 hr and to the nearest 10 min for longer times. This was done because the uncertainties in the estimates in table 5, due to the combined effects of uncertainty in each data point, in fairing the lines through the data, and in rounding off the figures, are dependent on the extent of extrapolation and the time. An estimate of about 6 hr for a 10-in. nonloaded roof slab is probably within 30 min of the true value whereas for a 10-in. loaded roof slab the estimate of 1 hr 30 min is probably within 10 min. For 3-in. slabs, the uncertainty would be about 10 min in 2 hr and 5 min in 30 min.

The times at which the high temperatures of the reinforcing bars were reached were not considered in developing table 5, since the reinforcement temperature is not a defined limiting condition in the standard test method [3]. Since no specimens with 1¾-in. cover were tested under load, load-failure estimates were not made for them in table 4. However, the tabulated estimates for 1,000 °F average and 1,200 °F maximum may be taken as rough indications of when such failure might occur, provided that the specimens were loaded to develop the design stress in the steel.

The ignition of cotton waste on the unexposed surface is an applicable end point, and occurred twice in the study reported herein. It always occurs at a local failure, such as a crack or spall. Such local failures often indicate a point not representative of the overall specimen; therefore they are difficult to predict. Consequently, no attempt was made to estimate times for this failure in drawing up tables 4 and 5.

TABLE 4. *Estimated times to various conditions*

The estimates were obtained from lines faired through data in the range of 5 to 8 in. and extrapolated at both ends.

Overall thickness	Unexposed surf. temperature rise		Load failure	Lower reinf. bar temperature	
	250 avg	325 max		1,000 avg	1,200 max
	Roofs, loaded, ¾ in. cover				
in.	*hr : min*	*hr : min*	*hr : min*	*hr : min*	*hr : min*
3	0:50	0:42	0:36	0:36	0:37
4	1:01	0:52	0:44	0:44	0:45
5	1:11	1:00	0:51	0:51	0:52
6	1:20	1:08	0:58	0:58	0:59
7	1:29	1:16	1:04	1:04	1:05
8	1:37	1:23	1:10	1:10	1:11
9	1:45	1:30	1:16	1:16	1:17
10	1:53	1:36	1:22	1:22	1:22
	Roofs, nonloaded, 1¾ in. cover				
3	2:35	2:33	----------	1:27	1:30
4	3:08	3:06	----------	1:45	1:50
5	3:39	3:37	----------	2:02	2:09
6	4:08	4:06	----------	2:18	2:26
7	4:35	4:33	----------	2:33	2:43
8	5:01	4:58	----------	2:47	2:59
9	5:26	5:23	----------	3:01	3:15
10	5:50	5:47	----------	3:14	3:30

TABLE 5. *Estimated fire endurances of cellular concrete roofs*

These were derived from table 4, rounding off as described in the text.

Thickness	Loaded [1]		Nonloaded [2]	
	Time	Limiting criterion	Time	Limiting [3] criterion
in.	*h : m*		*h : m*	
3	0:35	Load	2:30	ST
4	0:45	Load	3:10	ST
5	0:50	Load	3:40	ST
6	1:00	Load	4:10	ST
7	1:05	Load	4:30	325
8	1:10	Load	5:00	ST
9	1:15	Load	5:20	325
10	1:20	Load	5:50	ST

[1] With ¾-in. cover, reinforcement appropriate for span, and load based on design stress of 15,000 lb/in.² for roofs.

[2] With 1¾-in. cover, reinforcement at least 60 percent of that design live load of 56 lb/ft².

[3] Limiting conditions: Load = load failure, 250 = average surface temperature rise, 325 = maximum surface temperature rise; ST = both 250 and 325 degree temperature rises at same time.

Practical considerations made it obvious that estimates on nonloaded floors were of no value, and might be misleading. Only one floor specimen was tested under load and this was not deemed an adequate basis for estimates. Therefore, tables 4 and 5 were confined to estimates on roofs.

6. Conclusions

The results of the tests clearly indicate that cellular concrete slabs, made up of precast planks similar to those employed in this study, can be designed to provide fire endurances of 1 to 2 hr, and probably up to 4 hr.

The use of greater cover for the reinforcing bars, in the range of ¾ to 1¼ in., even without increasing the total thickness will result in longer fire endurance. In practice, this fact must be balanced against the effect on the load-carrying capacity under normal conditions. In normal practice, a slab is designed to have a particular load-carrying capacity. Once a combination of percent reinforcement and effective depth have been determined to satisfy this requirement, they would be held constant and increased cover would be achieved by increased overall thickness. Such procedure would lead to longer fire endurance

corresponding to the increased cover and overall thickness.

Within the density range of 35 to 50 lb/ft^3, slabs made of higher density concrete will provide longer fire endurance than will those of lower density, both in terms of heat transfer through the slab and in terms of continued structural stability.

Although slabs of greater thickness may be expected to provide longer fire endurance than those of lesser thickness on the same span, no simple conclusion can be drawn from this study for the case of greater thickness made necessary by the provision of longer span members having load-carrying capacities equal to those of shorter spans.

The use of reinforcing bars of larger diameter and consequently of greater ratio of reinforcement results in longer fire endurance than the combination of smaller bars plus shear reinforcement employed in this study.

7. References

[1] R. C. Valore, Jr., Cellular concretes, J. Am. Concrete Inst. 25 (May and June 1954).

[2] Steel Construction, Am. Inst. Steel Construction.

[3] Standard Methods of Fire Tests of Building Construction and Materials, ASTM, Designation E 119.

[4] J. V. Ryan and A. F. Robertson, Proposed criteria for defining load failure of beams, floors, and roof constructions during fire tests, J. Research NBS 63c, (Eng. and Instr.) No. 2, 121–124 (1959).

[5] Lightweight Aggregate Concretes, HHFA, U.S. Government Printing Office, Washington 25, D.C. (1942).

[6] Fire resistance classifications of building constructions, Appendix B, NBS BMS 92, U.S. Government Printing Office, Washington 25, D.C. (1942).

8. Appendix

Information presented here includes the more important observations from the test logs, statements of the various end points, and the times at which they were reached. These times have been corrected for deviation, if any, of the furnace time-temperature curves from that defined in ASTM E 119 [3]. The correction formula is given in the same standard. Representative plots of time-temperature and deflection data, plus tabulation of end-point and other data, have been given in the body of this report.

The planks were numbered from the south end of the furnace in all but Test 380. In that test they were numbered from the west. This was done to facilitate the recording of observations and has been carried over in the following summaries of the test logs.

Roof Test 357—At 11 min, furnace and specimen luminous; 17 min, light smoke issued from joints between slabs; 41 min, diagonal cracks in unexposed surface across four corners of specimen running across two or three planks, also planks 1, 4, 10, 11, 12 were cracked longitudinally; 48 min, cracks much wider, heavy smoke from crack in plank 10; 53½ min, deflection about 7.7 in. and was increasing at the rate of 67 in./hr, causing loading pressure to fall off rapidly; 55 min, planks 7–10 broke 3 ft from west end, but reinforcement prevented complete collapse; load off; 1 hr, gas off.

The initial limiting condition in this test was load failure; it occurred at 57 min (corrected) when the deflection and rate of deflection became excessive. The limiting temperatures were not reached on the unexposed surface; but 1,200 °F maximum was reached on the reinforcing bars at 54 min and 1,000 °F average at 56 min.

Roof Test 371—At 9 min, fine crack across southwest corner of plank 2, slight separation between filler grout and furnace along south and east sides; 21 min, transverse cracks at west end of plank 1 and east end of planks 7, 8, 9, 10, longitudinal crack in center of plank 12, all in unexposed surface; 39 min, crack in plank 12 extended full length of plank, sides of crack in west end of plank 2 offset ⅜ in.; 51 min, two parallel cracks 8 in. apart extended almost full length of specimen about 3 to 4 ft from east side, heavy smoke rose from cracks; 57 min, planks buckled along transverse cracks which extended through to exposed surface; 1 hr 8 min, pressure in loading system unstable, partial collapse of specimen, load off, gas off.

The initial limiting condition in this test was load failure at 53 min. The maximum one-point rise of 325 °F on the unexposed surface occurred at 1 hr, and, by 1 hr 5 min, it was 700 °F. At 59 min, the 1,000 °F avg. on the lower reinforcing bars was reached. At the end of the test it appeared that all of the planks except 1, 2, 11, 12 were broken 3 to 4 ft from the east end.

Roof Test 379—At 37 min, planks 1 and 12 cracked diagonally 3 ft from each end and longitudinally near center, all cracks in unexposed surface; 58 min, planks 2, 10, 11 had short fine cracks at ends; 1 hr 11 min, planks 1 and 12 had fine but moderately long cracks, plank 2 had fine cracks 3 ft from west end; 1 hr 22 min, joints between planks 3 and 4, 4 and 5, and 9 and 10 cracked, smoke was seeping out, plank 3 cracked longitudinally, and considerable amount of smoke issued forth; 1 hr 31 min, maximum deflection 9.4 in., load off, gas off.

The initial limiting condition in this test was the maximum one-point temperature rise of 325 °F on the unexposed surface. This occurred at 1 hr 29 min near the crack in plank 3. By 1 hr 31 min, it was obvious that load failure was imminent. At this time, the maximum temperature on the unexposed surface was 650 °F. Cotton waste was placed over the crack in plank 3 at 1 hr 24½ min. This waste did not ignite immediately. However, observations after the test showed that it had been charred to a great extent.

Roof Test 380—At 33 min, a few cracks 1 to 3 ft long in joints and across planks near edge of unexposed surface, plank 4 cracked longitudinally 8½ to 9 ft long; 52 min, 15-ft-long crack in plank 4. Plank 8 had crack 10 ft long, plank 2 had crack 3 ft long in south end, maximum deflection 6.0 in.; 58 min, deflection 7.5 in.; 1 hr 12 min, sides of crack in plank 8 offset 4 in., joint between planks 8 and 9 offset 6 in., planks 2 through 6 bowed up at about 3 ft from south end, plank 9 cracked across exposed surface at center span; maximum deflection 11.4 in.; 1 hr 13 min, cotton waste placed over crack in plank 8 and ignited; 1 hr 16 min, load off, maximum deflection exceeded 12 in.; 1 hr 17 min, gas off.

The initial limiting condition in this test was the ignition of cotton waste over the crack in plank 8 at 1 hr 13 min. The 1,200 °F maximum temperature on the reinforcing bars was reached at 1 hr 11 min; the 1,000 °F average temperature was reached at 1 hr 10 min. Load failure was imminent at 1 hr 16 min, at which time

the center span came into contact with the furnace structure 1 ft below the initial level of the specimen.

Roof Test 358, planks 5, 6, and 8 in. thick—At 12 min, wisps of smoke issued from joint between planks 2 and 3; 52 min, separation between planks and furnace, ends of planks raised ⅛ in.; 1 hr 7 min, cracks at east end of planks 3, 4, and 8, and at west end of plank 4; 1 hr 15 min, 6-in. planks (5–8) bowed up ⅜ in. at ends, 5- and 6-in. planks visibly dished; 1 hr 49 min, all planks had dished appearance, plank 4 had ¼-in.-wide transverse crack near east end; planks 2, 3, 4, and 8 had fine transverse cracks near east end, planks 2, 3, 4, 9, 10 and 12 had fine transverse cracks at west end, all cracks in unexposed surface; 2 hr 12 min, longitudinal crack 2 ft long in west end of plank 4, plank 10 raised 1⅛ in. at west end, plank 12 broken 3 to 4 ft from west end; 2 hr 29 min, plank 5 raised 1½ in. at west end, glow of furnace visible through crack in end of plank 10, 2 hr 55 min; transverse cracks in exposed surfaces of three planks 3 ft from east end, also several short cracks in planks 3 and 4; 3 hr 13 min, plank 4 cracked so that cotton rag ignited after few seconds, planks 3 and 4 sagged at each side of center; 3 hr 15 min, several pieces of concrete 1- to 4-in. diam fell from plank 4; 3 hr 40 min, flames passing through joint between planks 4 and 5, plank 4 offset 3 to 4 in. below plank 5 at centerspan; 3 hr 40 min, furnace glow visible from crack in plank 3 at 2 to 3 in. from east end; 3 hr 45 min, gas off.

After the specimen had cooled, examination showed that the exposed surface of the 5-in. planks had vitrified to a depth of 2 in., the 6-in. planks to a depth of ¾ in., and the 8-in. planks only on a thin surface layer. The 1,000 °F average occurred on the reinforcing bars of the 5-in. plank at 2 hr 9 min, the 6-in. plank at 2 hr 6 min, and the 8-in. plank at 2 hr 53 min. The 1,200 °F maximum occurred in the 5-in. planks at 2 hr 14 min, in the 6-in. planks at 2 hr 17 min and in the 8-in. planks at 3 hr 4 min. The maximum one-point rise of 325 °F on the unexposed surface was reached on the 5-in. planks at 3 hr 37 min and the average rise of 250 °F was reached at 3 hr 39 min. These limits were not reached on the 6-in. planks nor on the 8-in. planks. A cotton rag was ignited over a crack through a 5-in. plank at 3 hr 13 min, and, at 3 hr 40 min, flames were passing through the joint between planks 5 and 6. However, the times to limiting conditions resulting from cracking should not be taken as representative of nor compared with those observed in the tests of specimens of uniform thickness under design load.

Floor Test 372—At 25 min, crack along joint between planks 1 and 2; 37 min, plank 1 cracked along south side where supported by furnace frame, 55 min; blister of about 6 in. diam formed; 1 hr 8 min, plank 3 had 7-in. crack along center, maximum deflection (at south quarter point) 5.0 in.; 1 hr 21 min, sides of crack in plank 3 offset ¼ in.; 1 hr 39 min, maximum deflection 7.5 in.; 1 hr 59 min, maximum deflection exceeded 10 in. and was increasing very rapidly; 2 hr 4½ min, load off; 2 hr 12 min, gas off.

The initial limiting condition in this test occurred at 1 hr 40 min when the maximum allowable one-point temperature rise of 325 °F on the unexposed surface was reached. Load failure was reached at 2 hr 2 min. The average temperature on the reinforcing bars reached 1,000 °F at 1 hr 24 min, and the maximum temperature reached 1,200 °F at 1 hr 28 min.

Test 373—Floor planks 5 in., 6 in., and 8 in. thick. Note: the observations for the steel I-beam in this test are given separately. At 7 min, smoke issued from joints between planks 8 and 9 and between 9 and 10; 14 min, flames (possibly from encasing material of thermocouples) issued into furnace from southeast corner, continuing until after 40 min; 1 hr, cracks 1/16 in. wide between specimen and furnace frame along east and west edges; 1 hr 15 min, short cracks in extreme west ends of planks 3 and 4 on unexposed surface; 2 hrs, two diagonal cracks across center of plank 12, 8-in. planks raised ½ to 1 in. at each end; 2 hr 23 min, long crack in middle of plank 11, diagonal cracks in southeast and southwest corners extending across planks 1 through 4; 3 hr 8 min, 8-in. planks raised 1 to 1½ in., 6-in. planks raised ⅝ in., separations between planks and furnace increased, some joints between planks cracked; 3 hr 44 min, considerable smoke issued from joint between planks 2 and 3; 3 hr 50 min, gas off.

The 1,000 °F average on the lower reinforcing bars was reached at 2 hr 50 min for the 5-in. planks and at 3 hr 12 min for the 6-in. planks. The maximum of 1,200 °F was reached at 3 hr 6 min for the 5-in. planks and at 3 hr 40 min for the 6-in. planks. Neither of these temperatures were reached in the 8-in. planks, but it was estimated that 1,000 °F average would have been reached at 3 hr 52 min. Again, this test was not intended to represent a single sample of construction and was not uniformly loaded. Consequently, there were no definite criteria which could be used to determine the limiting conditions of the specimen.

Test 373—Steel I-beam encased in blocks. At 37 min, horizontal and vertical hairline cracks in several joints between blocks, vertical cracks across 2 blocks near center of east face; 1 hr, more cracks in joints; vertical cracks across block in west face; 1 hr 41 min, one soffit block cracked through and was sagging; 2 hr 11 min, third soffit block from south cracked and was sagging in 3-in. deep V, side block on west face above this dropped about 1 in., 2 hr 15 min, cracked soffit block and three blocks from each side fell; 2 hr 22 min, load off; 2 hr 23 min, soffit and side blocks from half of beam fallen, 2 hr 26 min, separation of ½ to 1 in. between beam and floor planks; 2 hr 51 min, only beam protection still in place were blocks in south 1½ ft and blocks in north 2 to 3 ft, test continued to obtain data on floor planks.

The limiting condition was load failure at 2 hr 22 min. The average temperature of 1,000 °F on the beam was first reached on one section of the beam at 2 hr 1 min. The maximum one-point temperature of 1,200 °F was reached at 2 hr 9 min. By 2 hr 30 min, the average temperatures of all 4 sections of the beam were well above 1,000 °F; the highest section average was over 2,000 °F. The temperature of the steel does not constitute a limiting factor in tests of beams carrying design loads.

U.S. GOVERNMENT PRINTING OFFICE: 1962